Observer-Based Monitors and Distributed Wave Controllers for Electromechanical Disturbances in Power Systems

by

Ernst Scholtz

B. Eng. (Electrical Engineering), University of Pretoria (1997)
M. Eng. (Electronic Engineering), University of Pretoria (1999)

Submitted to the Department of Electrical Engineering and Computer Science
in partial fulfillment of the requirements for the degree of

Doctor of Philosophy

at the

Massachusetts Institute of Technology

September 2004

Author _____
Department of Electrical Engineering and Computer Science
August 23, 2004

Certified by _____
George C. Verghese
Professor, Department of Electrical Engineering and Computer Science
Thesis Supervisor

Certified by _____
Bernard C. Lesieutre
Staff Scientist, Lawrence Berkeley National Laboratory
Thesis Supervisor

Accepted by _____
Arthur C. Smith
Chairman, Departmental Committee on Graduate Students

Observer-Based Monitors and Distributed Wave Controllers for Electromechanical Disturbances in Power Systems

by

Ernst Scholtz

Submitted to the Department of Electrical Engineering and Computer Science
on August 23, 2004, in partial fulfillment of the
requirements for the degree of
Doctor of Philosophy

Abstract

The thesis deals with monitoring and control of system-wide electromechanical (or "swing") dynamics in power systems. The first part of the thesis is devoted to observer-based monitoring, while the second part introduces novel decentralized controllers that exploit the wave nature of the swing disturbances in order to manipulate their propagation.

Power system monitors can be used to estimate the full state of the system as well as identify and isolate a number of events (e.g., faults) using only sparse local measurements, all in the presence of various system disturbances. The thesis analyzes different observer realizations for the Differential Algebraic Equation (DAE) swing model of a power system, and highlights the advantages of designing singular observers (versus state-space observers) for DAE models. We investigate various design approaches, and introduce a novel graphical design approach using a directed graph that reflects system structure. Investigations into the type, number and placement of measurements are conducted. Design examples on small- (9 bus) and large-scale (179 bus) power systems are discussed for both type of monitors.

The second part of the thesis develops and exploits a spatio-temporally integrated view of electromechanical dynamics. This contrasts with the traditional approach of either studying temporal variations at fixed spatial points or investigating spatial variations of specified temporal behavior. We use a continuum model of the swing dynamics to expose the wave-like propagation of electromechanical disturbances and to gain insight for the design of controls. We develop strategies for decentralized control of these electromechanical waves, drawing on prototype controllers found in electromagnetic transmission line theory (e.g., matched-impedance terminations) and active vibration damping (e.g., energy-absorbing controllers and vibration isolators). Finally, we propose various controllers to realize quenching or confining-and-quenching strategies, and test these in simulations of a 179-bus reduced-order representations of the WSCC network.

Thesis Supervisor: George C. Verghese
Title: Professor, Department of Electrical Engineering and Computer Science

Thesis Supervisor: Bernard C. Lesieutre
Title: Staff Scientist, Lawrence Berkeley National Laboratory

Dedication

To Amanda,

and my Family

Acknowledgements

First and foremost I would like to thank my excellent advisors, George Verghese and Bernie Lesieutre, for their help and guidance during the past five years. I immensely enjoyed working with them. Without their guidance and support I would not have been able to reach this milestone in my life.

George is a top-rate advisor (and boss). What is even more amazing is that he is an exceptional person. He is one of the most generous persons I know and he has always been there for me on an academic and personal level. Comparing my interactions and experiences with George to the same type of experiences that some of my colleagues had with their advisors, I concluded that I had the best advisor, period. I want to thank George for his excellent academic leadership, careful editing of this document and for teaching me a range of trades. He guided me to embrace new ideas and definitely helped in breaking some of my bad habits! I have come to appreciate his approach of thinking through a problem before running to a computer to simulate it!

Bernie has been my co-supervisor since day one. I have always been impressed with his creative ideas and his good nature. It was one of his ideas that led to one part of this thesis. Bernie's enthusiasm and love for the power system field reassured me that I can have a rewarding career in power (as I originally set out to do). Lastly, I want to thank him for taking time out of his schedule, to help with the fine tuning of this document.

I would also like to thank the members of my committee, Jeff Lang and Alex Stankovic for reading and critiquing this document. Thank you to Jeff for all his insights pertaining to our wave investigations. I appreciated your enthusiasm for our controller work, and if

time allowed for it, I would have wanted to explore this topic even further. I want to thank Alex for his interest, and suggesting that we investigate an aggregated 179-bus version of the Western States Coordinating Council (WSCC) network. This suggestion has helped us to present our work in a striking fashion. I also want to thank Alex for the invitation he extended towards us for me to present our wave control work at the 2004 IEEE Power Engineering Society's General Meeting. I relished this opportunity!

The ideas presented in this thesis were tested on this WSCC system graciously supplied to us by Professor Arun G. Phadke at VPISU and Professor V. Vittal at Iowa State University; we are very grateful.

I would like to thank my friends and collegeages at the Laboratory for Electromagnetic and Electronic Systems, affectionately known as LEES. I would like to thank John Kassakian for his interest in my work and his help in setting up a summer internship (in 2002) for me at ISO-NE. Many thanks go out to all in LEES (past and present) and in particular: Vivian Mizuno, Lodewyk Steyn (my Afrikaner-partner in crime), Joshua Phinney, James Hockenberry, Tim Neugebauer, Tushar Parlikar, Sandip Roy, Ivan Celanovic, Juan Rivas, Babak Ayazifar, Vahe Caliskan, Ian Lorilla, Chris Laughman, Rob Jensen, Rob Cox, Sauparna Das, Karin Janson-Strasswimmer and Kiyomi Boyd. If I forgot to mention anybody, please do not be offended.

I would also like to thank the MIT-South African braai team, Thomas Jones and Mauritz van Schalkwyk, for tasty meat, good wine and excellent company over the past few years.

The bulk of the work in this thesis was completed while I was supported under the AFOSR DoD URI F49620-01-1-0365: "Architectures for Secure and Robust Distributed Infrastructures" (led by Stanford University). I am very appreciative of their support, which has allowed me to work on my thesis without the added worry of funding.

Special thanks goes to the Skye Foundation Charitable Trust, for their generous fellowship gift, which helped in making my studies at MIT a reality. I also want to thank the National

Research Foundation of South Africa for the one year scholarship I received during my first year at MIT.

I would also like to thank my MEng advisor from the University of Pretoria South Africa, Professor Ian Craig (SM'87). He has been an excellent role model to me, as well as a great friend. He showed me that it was possible to study outside of South Africa by paving the way to MIT. I appreciate all the support he has given me and I want to thank him for the life and academic lessons he taught me over the years. He was instrumental in my decision to continue my education, at a time when it appeared more attractive to move onto industry. I am glad I persevered and I am grateful for his guidance in my formative years.

I also want to thank Professor Willhelm Leuschner from the University of Pretoria for his support and his help in clearing obstacles on my way to MIT.

Last, but not least, I'd like to thank my family. My parents have always supported me and made sure that they provide me with ample opportunities. I thank my late mother for instilling a good work ethic in me, and for nudging me in a direction to complete a Masters degree. I am sure she would have been proud that I surpassed her initial milestone for me. I want to thank my dad for always being very supportive and teaching me how to approach formal writing, even though it was in Afrikaans! I would also like to thank my brother and sister-in-law as well as my grandparents for all their love and support over the years. I also want to thank Ray and Tamra Hollenbaugh for their love and support and spurring me on along the way. And very last but definitely most important, I would like to thank Amanda, who has had to deal the last year an a half with a lot of uncertainty and be content with being neglected on a regular basis (not to mention the lack of a honeymoon!) as I tried to finish this thesis. I could not have asked for a more supportive and lovely wife!

I would like to conclude with a few words in Afrikaans.

Dit was lekker, maar ek is bly dit is nou verby! Dankie en Babaai!

Contents

1 Introduction **13**

1.1 Scope and Contributions of this Thesis 14

1.1.1 Power System Monitors 15

1.1.2 Power System Control 22

1.2 Organization of Thesis 24

2 Power System Models **26**

2.1 Power Systems 26

2.2 Active and Reactive Power Flow on the Network 27

2.3 Swing Models 29

2.4 Power System Measurements 32

2.5 Linearized Swing Model 33

2.6 Parametric Model Uncertainty 37

2.7 Electromechanical Perturbations Experienced by Power Networks 38

2.7.1 Modeling of Load and Generation Changes 39

2.7.2 Modeling Generator Outages 39

2.7.3 Modeling of Line Flow Perturbations 40

2.8 Conclusion 40

I Power System Monitors using Model-Based Observers 42

3 System-Wide State Estimation using Observers 43

3.1 Nonlinear Observer 45

3.1.1 Linear Parameter Varying Observer for Nonlinear State Estimation . 46

3.1.2 Arcak-Kokotović Nonlinear Observer 49

3.1.3 Hybrid Nonlinear versus Linear Observers Using the Same Linearly Designed Gain 51

3.2 DAE or State-Space Observer Synthesis 53

3.2.1 DAE versus State-Space Example 56

3.3 Observability Notions for DAE Models 57

3.4 H_∞ Observer Synthesis 58

3.4.1 DAE Systems 60

3.4.2 State-Space Models 62

3.4.3 Comparison Example: Nine-Bus Power System 63

3.4.4 Robust H_∞ Estimation 66

3.4.5 Measurement Placement and Type 66

3.5 Conclusion 67

4 Graphical Observer Design for Large-Scale Systems 69

4.1 Directed Graphs Associated with Linear Structured Systems 73

4.2 Graphical Observer Design 75

4.2.1 Motivating Examples 75

4.2.2 Design Approach 78

4.3 Measurement Placement, Type and Number 87

4.3.1 Measurement Placement 87

4.3.2 Measurement Type 95

4.3.3 Number of Measurements 103

4.3.4 Illustrative Nine-Bus Example 105

4.4 State Estimation of Large-Scale System: WSCC 179-Bus 107

4.5 Conclusion 114

5 Power System Monitors: Fault Detection and Isolation 116

5.1 Model-Based Fault Detection and Isolation 117

5.1.1 FDI via Residual Generation 120

5.1.1.1 Brief Problem Description 120

5.1.1.2 Residual Generator Examples 123

5.2 Fault Detection and Isolation for a Large-Scale System: WSCC 179-Bus System 135

5.3 Conclusions 137

II Decentralized Controllers for Electromechanical Waves in Power Networks 139

6 Decentralized Electromechanical Wave Controllers 140

6.1 Electromechanical Wave Theory 144

6.1.1 The Continuum Model 144

6.1.2 One-Dimensional Wave Phenomena on a String-of-Generators 147

6.1.3 Inserting a Lumped Electromechanical Impedance Between Two Strings 152

6.2 Electromechanical Wave Controllers 157

6.2.1 Zero Reflection Control 157

6.2.2 Zero Transmission Control 167

6.2.3 Perturbation Quenching Control 172

6.2.4 Transmission Doubling Control 175

6.3 Electromechanical Wave Controllers Realized at Hub Nodes 176

6.3.1 Zero Reflection Control at Hub Nodes 178

6.3.2 Zero Transmission Control at Hub Nodes 179

6.3.3 Perturbation Quenching Control at Hub Nodes 180

6.3.4 Some Thoughts on Control Strategies 181

6.4 Conclusion 181

7 Applications of EWC's to General Networks **183**

7.1 WSCC 179-Bus Aggregated Model 184

7.2 Uncontrolled Response 187

7.2.1 Estimation of Electromechanical Waves Using Observers 190

7.3 Quenching Control Strategy 191

7.4 Confining and Quenching Control Strategy 199

7.5 Conclusion 202

8 Conclusions and Future Work **206**

8.1 Summary and Conclusions 207

8.2 Future Work 216

8.2.1 Power System Monitors 216

8.2.2 Decentralized Electromechanical Wave Controllers 218

8.2.3 An Integrated Monitoring and Control Framework 219

A Linear Matrix Inequalities **220**

B Robust H_∞ Estimation **223**

C Towards Implementing an EWC through an AVR **235**

Chapter 1

Introduction

Electrification of the industrialized world has been labeled as the greatest engineering accomplishment of the 20^{th} century by the National Academy of Engineering of the United States[1]. The power system infrastructure (i.e., the generation plants as well as transmission and distribution networks) comprises complex engineered systems and spans vast geographical areas. With the onset of deregulation of the energy industry, profit has emerged as an important driving factor in the operation of the power grid. During the past regulated era these power systems were conservatively designed for robustness purposes, and were also operated in such a manner as to have ample reserve capacity. In the current deregulated industry environment, power grids are being operated closer to their limits, and this new operation paradigm and inadequate investment in the power grid infrastructure make these grids prone to failure as well as more difficult to control.

The importance of 'keeping the lights on' was recently emphasized by the spate of large-scale blackouts, all occurring during 2003, in the north-east of the USA, Sweden, Italy and in London. Various factors that contributed to the final collapse of the north-eastern US power grid are outlined in [1]. Key events in the buildup to this blackout were the "unnoticed" tripping of lines in Ohio — unnoticed because one of the big Mid-Western power utility's alarm system had failed. Also, the monitoring tools (with limited capabilities) used by the Midwest Independent System Operator (MISO) were disabled for a brief period due to human error and thus not functioning correctly. The lack of information regarding the state of the Mid-Western grid contributed to MISO operators not being able to take timely

[1]See URL — http://www.greatachievements.org/greatachievements/

corrective actions. These blackout events suggest that a reevaluation of current monitoring and control schemes for power systems may be needed.

The research that forms the basis of this thesis started taking shape even before the recent blackouts, but turns out to be aligned with recommendations of the joint U.S.-Canada Power System Outage Task Force (investigating the north-east US blackout of 2003) made in [1]: that better real-time tools for operators and reliability coordinators should be adopted (recommendation #23); that the use of time-synchronized data recorders should be required (recommendation #28); and that controls should be implemented to manage system health, network monitoring, and incident management (recommendation #35). The explorations reported in this thesis have overlap with all of the above recommendations and we are hopeful that this work will resonate with some in the power system community.

Even though this writing is intended for a high-voltage power transmission grid audience, some of the ideas in this thesis can also be applied to smaller scale power systems such as those found on ships and possibly buildings.

1.1 Scope and Contributions of this Thesis

System-wide studies are fundamental to power system engineering, and in this thesis alternative approaches to power system monitoring (e.g., state estimation, fault detection and isolation) and control of power networks are investigated.

Our focus is on the electromechanical transients of power networks in response to load, supply or other perturbations. These transients can be studied using a dynamical model describing the swing motions of the network. We mainly focus on the swing model of power networks and neglect voltage dynamics. Extensions to more general power system models can be built on these results.

1.1.1 Power System Monitors

Traditional power system state estimation schemes are aimed at providing best estimates of *quasi-static* variables (voltage magnitudes and angles at network buses) using a set of *redundant* (but typically inconsistent) measurements. In this thesis a *dynamic* state estimation scheme will be discussed, which is concerned with estimating the swing states (i.e., bus voltage angles, and generator speed deviations[2]) of a power network from *sparse* measurements by using observers. The nonlinear dynamic observer model, accumulates over time and interpolates over space (i.e., over the entire network) the information contained in measurements (possibly sampled), obtained from a limited — i.e., highly *non*-redundant — set of sensors. The role of the dynamic model is to relate measurements taken at any given time to those taken at other times, and to relate measured variables at the sensor locations to unmeasured variables throughout the network. In this way, sufficiently redundant information about the entire system is built up over time. Appropriate processing of this information then yields the desired estimates of the system state. These observers can be employed in model-based fault detection and identification schemes.

Fault detection and identification play an important role in modern day complex controlled processes. If the system under consideration should stay operable even in the presence of faults, being able to isolate and identify a fault in time will be extremely valuable. This information helps a supervising entity to determine whether the fault can lead to a catastrophic failure or whether the system might recover and what type of control action is needed. In the case when the system might recover, no action might be needed. However, for the case where the system is heading towards a catastrophic failure, it is imperative that control action be taken.

We will now discuss the two sections of this thesis in more detail. We begin by discussing

[2]Modeling reactive power on the network might enable us to estimate bus voltage magnitudes as well, but the quality of such estimation using a limited set of sensors can be poor. This possibility is attributed to not using a dynamic model of the voltage states. In this case, we are merely executing a traditional power system state estimation for the bus voltage magnitudes using a few measurements.

the two subsections associated with our power system monitor work. First, we focus on swing state estimation and observer design in general. Next we discuss the possibility to apply observer-based fault detection and isolation schemes to power systems.

After the above discussions, we will discuss our work on power system control in more detail.

State Estimation

State estimation in power systems has mainly focused on static estimation from redundant measurements [2]. There is a literature on dynamic state estimation (DSE), which deals with: either recursive processing of measurements, but with no dynamics in the state [3, 4]; or with slow-speed state dynamics induced by load variations, so the dynamics referred to is that of the load, and these dynamics are estimated on-line in various ways using load forecasting ideas [3, 5, 6].

In this thesis we will continue with our earlier work presented in [7], where we investigated the use of a few (rather than redundant) measurements for observer-based dynamic state estimation, while focussing on the faster dynamics associated with the swing motions of a power system. Control centers run contingency analyses using very detailed models of power systems, and with the favorable state of current computation capability, it may be argued that real-time simulators of the swing dynamics of the system are feasible. What makes observer-based approaches attractive, is that one can use these real time simulators and feed the measurements through an appropriate gain matrix to realize an observer. Hence, implementing observers seems conceptually straightforward.

Observer-based dynamic estimation of the swing state of a power network was investigated in [7, 8, 9, 10, 11]. Swing-state estimation, as defined in [7], involves estimating the bus angles and generator speeds and not the bus-voltage magnitudes. In [9] the single-machine, infinite-bus case is treated using a nonlinear gain-scheduled observer. In [7] a mixture of generator and load buses were modeled via a nonlinear Differential Algebraic Equation (DAE) swing model, in contrast to a linear collapsed all-generator network investigated by Stolz in [8]. He

realized Linear Quadratic Estimators (LQE) for an all generator network (i.e, state-space model) using only angle measurements. Stolz introduced a "hybrid" observer that uses the LQE designed gain matrix in the intuitive nonlinear extension of the Luenberger observer.

Modir et al. [10, 11] used *linear* Kalman filters to perform swing-state estimation. The models used in the estimator were linearized versions of the network model and generator model; and a Markov model was used to represent the process load. The filters were employed in a modular setup to enhance traditional state-estimation schemes (voltage magnitudes and the steady-state of the bus angles were updated by a traditional power system state estimation scheme).

Phadke [12] states that one of the biggest developments in real-time monitoring of power systems has been the advent of Synchronized Phasor Measurement Units (PMU). These PMUs provide real-time measurements of voltages and currents (on the three-phase element level) at substations. Typical scan rates of these devices are 1 cycle of the fundamental frequency, and the measurements can be repeated as often as 2-5 cycles [12]. Samples are time stamped and processed at a suitable location in order to build up an integrated picture of the state of the power system. Executing dynamic state estimation as proposed in this thesis, using PMU's sparsely located across the whole network, will provide us with a more detailed system-wide picture of the dynamic state of the power system. If one wanted a similar system-wide picture using only these PMU's, numerous devices would have to be placed, which would be costly.

In [12], it is further remarked that there is a lack of tools to accurately evaluate the condition of the network in real time. This lack of adequate information of the system state can lead to false trips in the power network. We believe that observer-based system wide dynamic state estimation can help with the mitigation of these false trips. However, investigating the performance of our observer-based state estimators, for a false-trip case-study, falls outside the scope of our exploratory work. A study of this nature is left for future research.

An additional application of the proposed state estimation work in this thesis might be

adaptive relaying. Adaptive relaying entails an assessment of the state of the power system and automatically making adjustments to the protection system so that the settings of these devices are correct for the current operating conditions [12]. Illustrating how we could use our observer-based state estimators in the realization of an enhanced adaptive relaying scheme, is also left for future research.

Recent investigations [13] have been conducted by members of the Power System Engineering Research Center into power system state estimation and optimal measurement placement for a distributed multi-utility industry. This research investigates optimal design of metering systems (particularly to maintain full system observability during switching actions), distribution of data and computational burdens of state estimation among participating control areas, and methods for estimating controller and system parameters as well as state variables. Note that this type of state estimation follows the traditional power system state estimation framework, hence the state variables are bus voltage magnitudes and angles that are estimated using a redundant set of measurements.

In a deregulated environment a local power company may want to employ dynamic swing state estimator, in order to gauge the actions of their competition (as well as the state of the network). This estimator/monitor can use a non-redundant set of measurements (possibly provided by an Independent System Operator (ISO) or their own sparsely deployed field devices). Assessing the economic benefit of following such an approach falls outside the scope of this thesis.

Fault Detection and Isolation

The swing-model observers that will be investigated in this thesis can also be used in the realization of model-based fault detection and identification schemes. An unexpected change in system function is seen as a fault [14]. From this general definition it can be concluded that a fault does not necessarily represent a physical failure or a breakdown. Detection and identification of incipient (slowly developing) faults are important; undetected in due time, these might lead to a catastrophic outcome. The steps that a fault detection and isolation

system executes are [14, 15]: fault detection (a binary decision of either that something happened); fault isolation (determining the location of the fault); and fault identification (gauging the size, type, and nature of the fault).

Types of power system faults and disturbances that will be investigated in this thesis are: prime mover input power/torque changes; load changes; balanced line-flow faults (e.g., line outages). Other type of faults that can be considered (but not in this thesis) are generator inertia uncertainty/changes, damping uncertainty/changes as well as sensor failures. Preliminary work investigating the detection and identification of inertia uncertainty and sensor failures was reported in [16], where information from multiple observers (running in parallel) was used in a parameter estimation scheme.

In order for controlled systems to continue operating acceptably during the occurrence of a fault, information about the fault is important. There may be some acceptable performance degradation for a fault-tolerant system operating under a faulty condition. However, the primary objective is to maintain system operation and give the operating entity reasonable time to repair the system or employ alternative measures in order to avoid a catastrophe. Fault diagnosis plays an important role in a fault-tolerant control system, because before any control law can be reconfigured the fault ought to be reliably detected, isolated, identified and the necessary information should be communicated to a supervision entity [14].

Limit checking (checking a variable or a trend and taking action once it reaches a certain threshold) is an easy way of implementing a fault diagnosis system [14]. The drawbacks of limit checking are: false alarms originating from input variations and change of the operating point; and a single fault can cause many system signals to exceed their limits and hence it appears as multiple faults.

Examples in the power system context, where power flow limit checking by relays led to catastrophic black-outs when the limits were set incorrectly, are discussed in [12]. Limit checking can also lead to a false trip of a generator when the transient swing the machine is experiencing will return to a stable operating point, but is falsely perceived as unstable.

Currently, in order to curb the number of false trips of generators, out-of-step relaying is advocated [12]. Conditions when a group of machines (or a portion of the power system) is about to lose synchronism with the rest of the network are detected by the out-of-step relaying scheme. This scheme should then disconnect the appropriate machines from the rest of the network in order to avoid a catastrophic failure. If the swings are stable, system separation might still occur if some relay zones are entered. Phadke [12], furthermore states that often the actual power system state is different from which had been simulated for determining the relay-zone settings. This discrepancy results in the out-of-step relays seldom being very reliable in their decision making. Current proposed solutions include the use of time synchronized phasor measurements of the machines experiencing the swing. By communicating between the relevant relays, the outcome of the swing that is in progress can be assessed using the equal-area criterion. Observer-based dynamic state estimation and fault detection might prove beneficial (and cheaper — because fewer PMU's need to be employed) in mitigating these false trips of generators.

Hardware Redundancy and Analytical Redundancy are ways the reliability of a system can be increased [14]. The former implies having multiple parallel units of hardware. The drawbacks of this method are: the cost of extra equipment (that may be sitting idly); maintenance cost; additional space to accommodate equipment. This appears to be the route that power system operators have been following in the past.

On the other hand, Analytical Redundancy uses cross-checking of dissimilar measured variables to generate residual signals used for FDI [14]. Model-based approaches use a mathematical model of the process; consistency checking is done between the measured variables and their estimates. The benefit of this approach is that no additional hardware faults are introduced, but this comes at the cost of developing better mathematical models and increased computational requirements when the scheme is realized in software.

One of the new adaptive relaying protection concepts discussed in [12], will use multiple protection schemes running in parallel. It is proposed that a voting scheme (which is a

considered a suitable approach for processing information) should be used to decide whether a certain piece of equipment should be tripped. Our aim is to illustrate that the state estimation and FDI frameworks, developed in this thesis, can provide alternative and more flexible ways in realizing adaptive relaying protection schemes. The realization of such adaptive schemes will not be discussed in this thesis.

Model-based FDI includes observer-based and parameter estimation approaches [17, 18]. FDI can be achieved by designing residual generators (realized using observers) that are sensitive to predefined faults and robust to predefined disturbances [14, 19]. For parameter estimation methods model parameters are tracked and changes in these parameters serve as the basis for detecting and isolating faults [18]. Model-based approaches are attractive in the power system setting, because power system models are well understood and taken to be quite accurate descriptions of the dynamics.

In [20], a modular method for fast fault detection and classification in power systems is presented. Model-free and model-based fault detection approaches are discussed, and for the model-free case signal processing and wavelet theory are used to create fast and sensitive fault indicators. For the model-based case the authors remark (and do not examine) that residual generation schemes can be used to generate fault indicators. The indicators can then be analyzed by standard statistical hypothesis testing or artificial neural networks to create intelligent decision rules. The creation of intelligent decision rules fall outside the scope of this thesis, but investigations into generation of residuals as fault indicators in the power system context will be one of the contributions of this thesis.

The authors of [20], also conducted a survey of fault-detection methods in the power system environment. They stated that the problem of detecting high-impedance faults (i.e., line outages) was unresolved. They briefly mentioned different approaches explored, but this survey appeared not-extensive and might be a bit dated.

In [21, 22] members of the Power System Engineering Research Center investigated a fault location algorithm applied to transmission networks using modeling, simulation and limited

field recorded data. The idea behind the algorithm is to match the recorded waveforms (captured using digital relays) and simulated waveforms to determine the most probable fault location. The simulated waveforms are obtained by running a short circuit program, using an accurate model of the system under consideration.

It is worthwhile pointing out that most of the fault detection and isolation literature in the power system context focuses on the three-phase element level (i.e., investigates balanced and unbalanced faults), whereas in this thesis we will focus more on a higher level system description. Thus, the line faults that we will investigate will be of the balanced type.

It can be argued that the global view of system stability gets lost by using detailed "local" element-level fault detection/location algorithms. The proposed FDI investigations in this thesis will focus on the system-wide level and aim to provide a "big picture" to power system operators.

1.1.2 Power System Control

The faults that occur in the system excite various dynamics, including the electromechanical dynamics of the system. The last topic that will be addressed in this thesis, focuses on the control of electromechanical transients associated with the acceleration and deceleration of generator rotors that are coupled through an electric power grid. The notion of electromechanical disturbances in power systems propagating as traveling waves appears in a paper by Semlyen in 1974 [23], which presented partial differential equations describing the idealized continuum limit of a swing-equation model. Cresap and Hauer [24] used a continuum model while analyzing the Western Power System in 1981, in order to explain the emergence of a new swing mode. More recently, electromechanical waves in power systems were similarly modeled by Thorp, Seyler and Phadke [25], as a way to understand angle observations from phasor measurement units in the field. These electromechanical waves are manifested in the mechanical shaft dynamics of electrically-coupled generators.

Accepting that electromechanical disturbances spread as traveling waves, one can design a controller to extinguish these transients in a manner analogous to impedance matching for suppression of electro*magnetic* waves on transmission lines. We developed such a controller that approximately achieved an impedance matching objective and reported it in [26]. In that paper we demonstrate that such a "zero-reflection" controller (ZRC) will effectively quench electromechanical traveling waves at the boundary of the network.

It is important to emphasize that this approach to system control design is very different than traditional methods. Typical tuning of governor and power system stabilizer controls uses linearized models and modal analysis [27]. Usually this is accomplished with a detailed model of the generator(s) to be tuned and a simplified representation for the remainder of the system. The only spatial information that is used in the design is embedded in information about mode shapes, and is therefore quite indirect. In cases when a detailed representation over a wide geographical area is used one identifies critical modes of oscillations and their mode shapes, and tunes the controller accordingly [27]. This approach is analogous to representing the dynamics as a superposition of standing waves rather than as a traveling wave.

This thesis reviews and extends work reported in [26]. As mentioned above, in that paper we demonstrated the effectiveness of a ZRC in quenching electromechanical traveling waves at the boundary of the network. We also showed that this control strategy appears to be robust to wide variations in parameter values. However, in that work mostly regular grids of generators were considered. This thesis investigates the performance of these ZRC controllers (as well as other Electromechanical Wave Controllers — EWC's — we will develop) in more practical settings (i.e., irregular grids and networks consisting of generators and loads).

Only being able to negate the electromechanical disturbance at the boundary of a network might expose heavily loaded parts of the network to traveling electromechanical disturbances, making these stressed parts prone to failures. This situation is not desirable and it

is beneficial for overall system stability and reliability if we are able to confine these disturbances to local areas and eventually extinguish them locally. In order to create a confining and quenching control strategy, we will develop zero-transmission controllers (ZTC) and perturbation quenching extinguishers (PQC).

In this thesis, we will demonstrate practical uses of these electromechanical wave controllers, by realizing various control strategies and implementing them on models of aggregated real world networks.

1.2 Organization of Thesis

In Chapter 2 models for line-flows on the network are given. The swing model, describing the electromechanical behavior of a power network, is also introduced in this chapter. Model uncertainty is discussed and possible electromechanical perturbations the system can experience are introduced.

Part one of this thesis is concerned with the development of power system monitors. In Chapters 3 and 4 various observer design approaches are tested in order to efficiently and effectively design power system monitors. Chapter 3, follows more of a traditional approach to observer design, whereas in Chapter 4 a novel graphical observer design technique is proposed that is suitable for large-scale systems.

In Chapter 5, the observer framework developed in the two previous chapters are used in fault detection and isolation schemes. The graphical-observer-design approach introduced in Chapter 4 is preferred to realize the observers studied in Chapter 5.

The second part of this thesis focuses on decentralized control of electromechanical transient disturbances in power networks. In Chapter 6, the notion of electromechanical transient motions traveling as electromechanical wave motions, is introduced and discussed. We develop a theory to study the interconnection of electromechanical 'transmission lines' (also

referred to as strings-of-generators) with lumped electromechanical elements. We use this theory to suggest various controllers that will be able to manipulate 'wave' reflection and transmission on lumped parameter networks.

In Chapter 7, we apply these decentralized controllers to general network models, such as the model of the 179-bus aggregated Western States Coordinating Council (WSCC) model. In Appendix C we present a brief write up highlighting some of the issues involved when we move beyond the swing model and we want to implement a one of our decentralized controllers through the voltage loop of a generator.

In Chapter 8, we give a summary, with intertwined conclusions, of the thesis work. We end this journey by pointing to possible future research directions.

Chapter 2

Power System Models

Dynamic modeling of power systems can be described as a mature field, as the numerous textbooks on the subject can attest [28, 29, 30, 31, 32]. Most of our attention will be focused on the swing model (also referred to as the classical model) for power systems. This electromechanical model accounts for generator mechanical shaft dynamics and their relation to the conversion of mechanical power to electric power to supply the needs of the power system. These rotating machines are electrically coupled through transmission lines. A helpful analog is to think of this system as a spring-mass system where: the strength of a particular spring is related to the electrical power flow on the associated electrical transmission line; and the masses are the rotational inertias of the generators. This chapter presents various versions of the nonlinear swing model, which is the most basic dynamical model of a power system.

2.1 Power Systems

Power systems consists of generation equipment, transmission lines, distribution networks and loads. These power system networks may span vast geographical areas, and in this thesis we will be focussing on system-wide (i.e., wide-area) studies of the dynamics of these systems.

Power systems can be modeled for our purposes as nonlinear lumped parameter circuits. We assume balanced three-phase operation, with quasi-sinusoidal current and voltage signals.

A voltage time signal is expressed as $v(t) = V(t)\cos(\omega_s t + \delta(t))$, where $V(t)$ is a slowly varying amplitude and $\delta(t)$ a slowly varying phase (slow relative to ω_s). Of importance to us are the time-varying magnitude $V(t)$ and phase $\delta(t)$ of this sinusoidal signal. We can gather these variables to form a phasor, which for this voltage signal is the voltage phasor $\widehat{V}(t) = V(t)\angle\delta(t)$.

Our emphasis in this thesis will be on *system-wide* dynamic investigations. Of particular interest are how:

(a) the transient response to an electromechanical perturbation (generator and line outages, load changes, etc.) can be estimated using observers;

(b) electromechanical perturbations propagate in both space and time on a power network;

(c) an occurrence of an electromechanical perturbation can be detected.

In the next section, we will introduce the swing model of a power system.

2.2 Active and Reactive Power Flow on the Network

For a power network we can construct a graph whose nodes correspond to buses in the network, and whose edges correspond to the transmission lines or transformers between these network buses.

Let θ denote the vector of bus angles (measured in radians), V the vector of per-unit voltage bus magnitudes, $P(\theta, V)$ and $Q(\theta, V)$ the vectors of directed active and reactive power flows on the transmission lines (measured in per-unit, see [29, 32] for a discussion on the per-unit system, abbreviated as *p.u.*) which can be written in the following convenient matrix-vector

forms,

$$P(\theta, V) = -\Upsilon\mathcal{B}\sin(F'\theta) - \Upsilon\mathcal{G}\cos(F'\theta) + \tfrac{1}{2}\mathcal{G}(F' - |F|') \circ V^2, \tag{2.1}$$

$$Q(\theta, V) = \Upsilon\mathcal{B}\cos(F'\theta) - \Upsilon\mathcal{G}\sin(F'\theta) + \tfrac{1}{2}(\mathcal{B})(F' - |F|') \circ V^2. \tag{2.2}$$

where: F is the directed bus-line incidence matrix of the network graph (the orientation of line h can be picked arbitrarily, and $F_{s,h} = 1$, $F_{t,h} = -1$ if this directed line goes from bus s to bus t); $'$ denotes matrix transposition; depending on the context, diag$(\cdot)$ extracts the diagonal of its matrix argument and forms a column vector, or forms a diagonal matrix by placing its vector argument on the diagonal; $\sin(\cdot)$ and $\cos(\cdot)$ imply taking elementwise sine or cosine of their corresponding vector arguments; $\circ$ implies elementwise multiplication of two vectors; V^2 implies the elementwise square of the vector V; $\mathcal{B}$ and $\mathcal{G}$ are diagonal matrices with line susceptances and conductances as diagonal elements; g_h and b_h are the conductance and susceptance of line h respectively. The network θ can be ordered as: $\theta = [\ \theta_g' \quad \theta_l'\ ]'$, where subscripts g and l indicate generator and load buses respectively. Let n_g be the number of generator buses; and n_l be the number of load buses. If the orientation picked for edge h when defining F goes *from* node s *to* node t then $P_{st}(\theta, V)$ is simply the h^{th} component of $P(\theta, V)$ above.

Let $P^{nw}(\theta, V)$ denote the active power flowing into the network, and $Q^{nw}(\theta, V)$ the reactive power flowing into the network. We obtain the powerflow equations of the network by aggregating (using F — the divergence operator) the line flows at the buses, and these equations are expressed as follows:

$$P^{nw}(\theta, V) = -F\Upsilon\mathcal{B}\sin(F'\theta) - |F|\Upsilon\mathcal{G}\cos(F'\theta) + \text{diag}(F\mathcal{G}F') \circ V^2; \tag{2.3}$$

$$Q^{nw}(\theta, V) = -F\Upsilon\mathcal{G}\sin(F'\theta) + |F|\Upsilon\mathcal{B}\cos(F'\theta) - [\text{diag}(F\mathcal{B}F') + \text{diag}(B_{sh})] \circ V^2; \tag{2.4}$$

$$\Upsilon = \text{diag}(\exp(|F|'\ln(V))); \tag{2.5}$$

where B_{sh} is a vector of the shunt susceptances at each bus (contributed by capacitive elements in the network). In (2.3) $F'\theta$ yields a vector of angle differences across branches

of the network; diag($F\mathcal{G}F'$) and diag($F\mathcal{B}F'$) are n-dimensional vectors whose elements are the sums of the conductances and susceptances of edges emanating from the corresponding nodes respectively.

To illustrate these expressions, let us look at an example where we want to find the powerflow expressions between two buses s and t. We assume that the network consists of one transmission line between buses s and t. For this edge we have $F' = \begin{bmatrix} 1 & -1 \end{bmatrix}$ and the associated susceptance b and conductance g. We can show that:

$$P^{nw} = \begin{bmatrix} P_{st}(= P(\theta, V)) \\ P_{ts} \end{bmatrix} = \begin{bmatrix} -V_s V_t b \sin(\theta_s - \theta_t) - V_s V_t g \cos(\theta_s - \theta_t) + g V_s^2 \\ -V_s V_t b \sin(\theta_t - \theta_s) - V_s V_t g \cos(\theta_t - \theta_s) + g V_t^2 \end{bmatrix} \quad (2.6)$$

$$Q^{nw} = \begin{bmatrix} Q_{st}(= Q(\theta, V)) \\ Q_{ts} \end{bmatrix} = \begin{bmatrix} V_s V_t b \cos(\theta_s - \theta_t) - V_s V_t g \sin(\theta_s - \theta_t) - b V_s^2 \\ V_s V_t b \cos(\theta_t - \theta_s) - V_s V_t g \sin(\theta_t - \theta_s) - b V_t^2 \end{bmatrix} \quad (2.7)$$

which agrees with the expressions given on page 72 in [2].

2.3 Swing Models

Three variations of the swing model will be introduced in this section. In the first version the source impedances of the network generators are taken into account and consequently the generator bus angles and internal angles of the generators are different from one another when nonzero power is delivered by the generator. We also assume for this model that the bus voltage magnitudes are not tightly controlled and hence we will consider reactive power on the network.

The second variation is obtained when we neglect the machine source impedance. In this scenario, one can assume that the internal angles of the generators are equal to the generator bus angles. We still assume that the bus voltage magnitudes are not tightly controlled.

The third variation is obtained by assuming that the bus voltage magnitudes are tightly

regulated at the specified operating point. This assumption reduces the size of the model, since reactive power in the network is neglected.

The swing model is merely Newton's second law in rotational form. For a generator in the network, a mismatch between the prime-mover input torque/power (i.e., mechanical input power to the generator) and the electrical power supplied to the electrical network will either accelerate or decelerate the generator. We will focus on transmission-level power system models in this thesis, and assume that loads do not exhibit dynamics on the time-scales of interest. On the transmission level, the loads represent aggregated load areas or distribution networks from lower voltage levels; an instantaneous load change might correspond to load shedding. It is commonly assumed that these loads are functions of frequency and voltage levels.

The first version of the swing model mentioned above takes the following nonlinear Differential-Algebraic Equation[1] (DAE) form (using (2.3 and (2.4)):

$$\underbrace{\left[\begin{array}{cc|cc} I & 0 & 0 & 0 \\ 0 & M_g & 0 & 0 \\ \hline 0 & 0 & 0 & 0 \\ 0 & 0 & 0 & 0 \end{array}\right]}_{M} \underbrace{\left(\begin{array}{c} \dot{\delta} \\ \dot{\omega} \\ \hline \dot{\theta} \\ \dot{V} \end{array}\right)}_{\dot{x}} = \underbrace{\left(\begin{array}{c} \omega \\ \hline P_g^e - P_{elec}(\delta,\theta,V,E_g) - D_g\omega \\ \left(\begin{array}{c} P_{elec}(\delta,\theta,V,E_g) \\ P_l^e \end{array}\right) - P^{nw}(\theta,V) \\ \left(\begin{array}{c} Q_{elec}(\delta,\theta,V,E_g) \\ Q_l^e \end{array}\right) - Q^{nw}(\theta,V) \end{array}\right)}_{f(x,u,w)}; \tag{2.8}$$

where ω is a vector of generator speed deviations from synchronous, measured in rad/s and x denotes the internal variables of the DAE description. The dimension of the singular system is $n(= 4n_g + 2n_l)$. Note that δ_g and ω are state variables ($x_d = \left[\begin{array}{cc} \delta_g' & \omega' \end{array}\right]'$), while θ

[1] Also called descriptor, singular or generalized systems. DAE systems appear in the fields of robotics, economics and circuits to name a few. The increasing complexity of systems requires more modular modeling, which can be achieved by interconnecting subsystems. This concept of subsystem modeling leads to the use of redundant coordinates in the description of the complex system. Generally the behavior of these subsystems are described by differential equations, and their coupling by algebraic equations [33].

and V are composed of algebraic variables (x_a). The vector P_l^e denotes power injected at the load buses (and hence typically has negative entries), while P_g^e is the net power injected at the generator buses (typically mechanical power input to a generator if we neglect losses in the generator). We can combine these two vectors into vector P^e (the vector of external bus power injections). These injections may be partly or completely known; the known parts are gathered in the vector u, while the unknown parts (perhaps 'process noise', faults or any other unknown-inputs) are gathered in w. D_g and M_g are diagonal matrices whose nonzero entries consist of the damping coefficients and the (normalized) inertias of the generators respectively. P_{elec} and Q_{elec} are respectively the active and reactive power, provided by the generators to the network, and are expressed as:

$$P_{elec,i} = \frac{E_{g,i}V_{g,i}}{X'_{d,i}} \sin(\delta_i - \theta_{g,i}); \tag{2.9}$$

$$Q_{elec,i} = \frac{V_{g,i}^2}{X'_{d,i}} - \frac{E_{g,i}V_{g,i}}{X'_{d^i}} \cos(\delta_i - \theta_{g,i}). \tag{2.10}$$

where $E_{g,i}$ is the constant source voltage, δ_i is the phase angle of the source, and $X'_{d,i}$ is the source impedance.

The second version of the swing model is obtained when the source reactances (X'_d) are omitted and as a consequence we set $\delta = \theta_g$, and the following nonlinear DAE swing model is obtained:

$$\underbrace{\left[\begin{array}{cc|cc} I & 0 & 0 & 0 \\ 0 & M_g & 0 & 0 \\ \hline 0 & 0 & 0 & 0 \\ 0 & 0 & 0 & 0 \end{array}\right]}_{M} \underbrace{\left(\begin{array}{c} \dot{\delta} \\ \dot{\omega} \\ \hline \dot{\theta}_l \\ \dot{V} \end{array}\right)}_{\dot{x}} = \underbrace{\left(\begin{array}{c} \omega \\ P_g^e - P_g^{nw}(\theta, V) - D_g\omega \\ \hline P_l^e - P_l^{nw}(\theta, V) \\ Q^e - Q(\theta, V) \end{array}\right)}_{f(x,u,w)}, \tag{2.11}$$

where all the variables have been previously defined. The dimension of this singular system is now $n(= 3n_g + 2n_l)$.

Assuming that the bus voltages are tightly regulated around their operating set-points (they

appear stiff), the third variation of the swing model is obtained. Without loss of generality, we can assume that the network voltages stay constant at $V = 1p.u.$ The nonlinear DAE swing model for this case will only feature the active power flowing in the network and is expressed as:

$$\underbrace{\left[\begin{array}{cc|c} I & 0 & 0 \\ 0 & M_g & 0 \\ \hline 0 & 0 & 0 \end{array}\right]}_{M} \underbrace{\left(\begin{array}{c} \dot{\delta} \\ \dot{\omega} \\ \hline \dot{\theta}_l \end{array}\right)}_{\dot{x}} = \underbrace{\left(\begin{array}{c} \omega \\ \hline P_g^e - P_g^{nw}(\theta, V=1) - D_g\omega \\ \hline P_l^e - P_l^{nw}(\theta, V=1) \end{array}\right)}_{f(x,u,w)}, \tag{2.12}$$

where all the variables were as previously defined. The dimension of this singular system is $n = 2n_g + n_l$, which for a large scale power network can be almost a factor of 2 smaller than for the model in (2.11).

For most of this thesis, we will work with (2.12).

2.4 Power System Measurements

The measurements $y = g(x)$ available to an observer greatly influences the performance of the realized state estimator. In this thesis, we will investigate the number, nature and placement of measurements needed in order to realize observers for large-scale power systems. In [7], an initial investigation of this sort was launched for a small-scale example.

Focusing on the swing model (2.12), five types of measurements are available for observer design. The measurements available at selected buses or lines are those of bus angles, generator speeds, power injected into the network at the buses, power flow on the lines, and angle differences across lines. Thus, the i^{th} measurement (in the absence of noise), can take

on one of the following forms (assuming $V = 1p.u.$):

$$g(x)_i = \begin{cases} \theta_j,\, j \in \{1, \cdots, n\} \\ \omega_j,\, j \in \{1, \cdots, n_g\} \\ P_j^{nw}(\theta),\, j \in \{1, \cdots, n\} \\ P_{st}(\theta),\, s,t \in \{1, \cdots, n\}]|(s,t) \text{ an edge} \\ \delta_{st}(\theta),\, s,t \in \{1, \cdots, n\}]|(s,t) \text{ an edge} \end{cases}, \tag{2.13}$$

where θ_j is the bus angle associated with bus j, ω_j is the speed deviation from synchronous associated with generator j, $P_j^{nw}(\theta)$ is the net power at bus j flowing into the network (this is simply the j^{th} element of (2.3)) and $P_{st}(\theta)$ is the power injected at s onto the line h to bus t. $P_{st}(\theta)$ is obtained by taking the h^{th} entry of (2.1) (where we kept V fixed).

In [8] only direct angle measurement were considered and in [10] the authors investigated the employment of only frequency measurements at generator buses (i.e., generator speed measurements). The measurement set we investigate in this thesis is in accordance with measurements used for traditional power system state estimation schemes, as discussed in [2].

2.5 Linearized Swing Model

Linearized versions of the swing models introduced in the previous section are frequently studied by power engineers. A vector in the nonlinear system can be expressed as $\zeta(t) = \overline{\zeta} + \widetilde{\zeta}(t)$, where $\overline{\zeta}$ is the steady-state vector and $\widetilde{\zeta}(t)$ is the vector of deviations from this steady-state (assumed small when deriving the linearized model). In order to simplify notation, the time dependence of the variables will be suppressed.

The different nonlinear DAE swing models introduced in the previous section can be linearized around the steady state (loadflow) solution $\delta = \overline{\delta}$, $\theta = \overline{\theta}$, $V = \overline{V}$ and $\omega = \overline{\omega} = 0$. The Jacobian matrices: $P^\theta \triangleq \left[\frac{\partial P^{nw}}{\partial \theta}\right]_{\overline{\theta},\overline{V}}$; $Q^\theta \triangleq \left[\frac{\partial Q^{nw}}{\partial \theta}\right]_{\overline{\theta},\overline{V}}$; $P^V \triangleq \left[\frac{\partial P^{nw}}{\partial V}\right]_{\overline{\theta},\overline{V}}$; and $Q^V \triangleq$

$\left[\frac{\partial Q^{nw}}{\partial V}\right]_{\overline{\theta},\overline{V}}$, feature in the linearized versions of swing models (2.8), (2.11) and (2.12) and are expressed as:

$$P^{\theta} = \left[-F\overline{\Upsilon}\mathcal{B}\,\mathrm{diag}(\cos(F'\overline{\theta})) + |F|\overline{\Upsilon}\mathcal{G}\,\mathrm{diag}(\sin(F'\overline{\theta}))\right]F' \tag{2.14}$$

$$Q^{\theta} = \left[-|F|\overline{\Upsilon}\mathcal{B}\,\mathrm{diag}(\sin(F'\overline{\theta})) - F\overline{\Upsilon}\mathcal{G}\,\mathrm{diag}(\cos(F'\overline{\theta}))\right]F' \tag{2.15}$$

$$P^{V} = 2G\overline{V} - \left[F\overline{\Upsilon}\mathcal{B}\,\mathrm{diag}(\sin(F'\overline{\theta})) + |F|\overline{\Upsilon}\mathcal{G}\,\mathrm{diag}(\cos(F'\overline{\theta}))\right]F'\,\mathrm{diag}(\overline{V})^{-1} \tag{2.16}$$

$$Q^{V} = \left[\!\left[F|\overline{\Upsilon}\mathcal{B}\,\mathrm{diag}(\cos(F'\overline{\theta})) - F\overline{\Upsilon}\mathcal{G}\,\mathrm{diag}(\sin(F'\overline{\theta}))\right]\!\right]F'\,\mathrm{diag}(\overline{V})^{-1} - 2B\overline{V} \tag{2.17}$$

where $G = \mathrm{diag}(\mathrm{diag}(F\mathcal{G}F'))$, $B = \mathrm{diag}(\mathrm{diag}(F\mathcal{B}F') + B_{sh})$ and B_{sh} are the shunt susceptance branches from buses to ground (contributed by capacitor banks). A matrix of the form FWF' is called the edge-weighted Laplacian of a graph, and we note that for a lossless power network (i.e., $\mathcal{G} = 0$) P^{θ} is an edge-weighted Laplacian of the graph associated with the power network. Interesting statements can be made about the relation between the graph spectra of Laplacian matrices and their relation to the modal dynamics of oscillatory networks (see [34] for a detailed study on this subject applied to linearized power system swing models).

The Jacobian matrices (2.14) – (2.17) can be partitioned into four submatrices by distinguishing between generator and load buses. For instance, we can partition P^{θ} as follows:

$$P^{\theta} = \left[\begin{array}{c|c} P^{\theta}_{g,g} & P^{\theta}_{g,l} \\ \hline P^{\theta}_{l,g} & P^{\theta}_{l,l} \end{array}\right]. \tag{2.18}$$

Neglecting higher-order deviation terms in the linearization of (2.12), a linearized DAE swing model of the following form can be written:

$$\underbrace{\left[\begin{array}{cc|c} I & 0 & 0 \\ 0 & M_g & 0 \\ \hline 0 & 0 & 0 \end{array}\right]}_{M}\underbrace{\left(\begin{array}{c} \dot{\widetilde{\delta}} \\ \dot{\omega} \\ \hline \dot{\widetilde{\theta}}_l \end{array}\right)}_{\dot{\widetilde{x}}} = \underbrace{\left(\begin{array}{c} 0 \\ B_g \\ \hline B_l \end{array}\right)\widetilde{P}^{e}}_{B\widetilde{u}+Ew} - \underbrace{\left[\begin{array}{cc|c} 0 & -I & 0 \\ P^{\theta}_{g,g} & D & P^{\theta}_{g,l} \\ \hline P^{\theta}_{l,g} & 0 & P^{\theta}_{l,l} \end{array}\right]}_{-A}\underbrace{\left(\begin{array}{c} \widetilde{\delta} \\ \omega \\ \hline \widetilde{\theta}_l \end{array}\right)}_{\widetilde{x}}, \tag{2.19}$$

where $\begin{bmatrix} 0 & B'_g & B'_l \end{bmatrix}' = \left[\frac{\partial f}{\partial P^e}\right]_{\overline{P}^e}$. We only show the linearized version of (2.12), but using Equations (2.14) – (2.17), linearized versions of (2.8) and (2.11) can also be obtained.

Gathering the differential and algebraic variables and partitioning the vectors and matrices in the linearized models (of which (2.19) is an example) accordingly (for this example the partitioning is indicated by solid lines in (2.19)), the linearized DAE swing model can be written in the following form:

$$\begin{bmatrix} M_d & 0 \\ 0 & 0 \end{bmatrix} \begin{pmatrix} \dot{\widetilde{x}}_d \\ \dot{\widetilde{x}}_a \end{pmatrix} = \begin{bmatrix} A_{dd} & A_{da} \\ A_{ad} & A_{aa} \end{bmatrix} \begin{pmatrix} \widetilde{x}_d \\ \widetilde{x}_a \end{pmatrix} + \begin{bmatrix} B_d & E_d \\ B_a & E_a \end{bmatrix} \begin{pmatrix} \widetilde{u} \\ w \end{pmatrix} \tag{2.20}$$

where $\widetilde{x}_d$ are the differential and $\widetilde{x}_a$ are the algebraic variables of the DAE description.

DAE models associated with the swing model of a power system are regular and of index one, which means that $|\lambda M - A| \neq 0$ and that A_{aa} is invertible respectively. The condition of regularity ensures that the characteristic polynomial for the system does not vanish identically. The index of a DAE system measures the type of singularity, and it gives the number of times the algebraic equations of a DAE system have to be differentiated in order to get a full set of differential equations for all the variables of x [33]. For thorough treatments of the DAE systems the interested readers are referred to [33, 35, 36].

Seeing that the swing DAE model is of index one, we can express it with an equivalent state-space model by "collapsing" the DAE model down using a Ward reduction. Essentially all we do is to express algebraic variables in terms of differential variables. The original structure of the system is lost when we collapse the system. Sparse system matrices in the DAE description are then replaced by full matrices in the state-space description. The structure effectively becomes hidden when we carry out such a transformation.

A natural question is why one would be interested in investigating and simulating the structure-preserving DAE linear model, when it has an equivalent state-space formulation? Reasons for this are discussed in [37]. From a numerical point of view, such a transformation

causes difficulties. The authors of [37] suggest that if accurate results are sought, one should work with the index-one DAE system rather than with its reduced-order state-space system. In Section 3.2, this issue will arise again in the context of observer design.

Let us collapse (2.19) into a state space model. First we express the algebraic variables as a function of the differential variables and inputs:

$$\widetilde{x}_a = -A_{aa}^{-1}(A_{ad}\widetilde{x}_d + B_a u + E_a w). \tag{2.21}$$

Next, we substitute this expression into the differential equation block of the differential variables to obtain:

$$\dot{\widetilde{x}}_d = A_s\widetilde{x}_d + B_s\widetilde{u} + E_s w, \tag{2.22}$$

$$\text{where } A_s = M_d^{-1}(A_{dd} - A_{da}A_{aa}^{-1}A_{ad}), \tag{2.23}$$

$$B_s = M_d^{-1}(B_d - A_{da}A_{aa}^{-1}B_a), \tag{2.24}$$

$$E_s = M_d^{-1}(E_d - A_{da}A_{aa}^{-1}E_a). \tag{2.25}$$

The linearized system output (measurements) of the DAE model, $\widetilde{y} = C\widetilde{x}$ (where $\widetilde{y}$ is the linearized version of $y = g(x)$ and $C \triangleq \left[\frac{\partial g(x)}{\partial x}\right]_{\overline{x}}$), can be expressed in terms of the state-space variables as follows:

$$\widetilde{y} = C_s\widetilde{x}_d + D_s\widetilde{u} + J_s w; \tag{2.26}$$

$$C_s = (C_d - C_a A_{aa}^{-1}A_{ad}); \tag{2.27}$$

$$D_s = -C_a A_{aa}^{-1}B_a; \tag{2.28}$$

$$J_s = -C_a A_{aa}^{-1}E_a. \tag{2.29}$$

2.6 Parametric Model Uncertainty

The parameters in the models influence the behavior of the state trajectories. Possible uncertain parameters for the models presented thus far are the line parameters (i.e., line susceptances and conductances), inertias of the machines, load or generation changes, and internal impedances of generators. In the next chapter we will be concerned with the design of observers that can track the system state even in the presence of these parametric model uncertainties. In functional form the linearized swing model (2.20) with model uncertainty is expressed as

$$(\overline{M} - \widetilde{M})\dot{\widetilde{x}} = (\overline{A} + \widetilde{A})\widetilde{x} + \overline{B}\widetilde{u} + Ew, \tag{2.30}$$

$$\widetilde{y} = (C + \widetilde{C})\widetilde{x}, \tag{2.31}$$

where $\widetilde{M}$ represents uncertainty of machine inertias; $\widetilde{A}$ represents uncertain line parameters, uncertain generator impedances, and the uncertainty of the damping coefficient for generator shaft dynamics; and $\widetilde{C}$ might represent uncertain line parameters for corresponding power flow measurements on lines, or inaccuracy associated with the measurement device.

Suppose that the parameters of each line are only known to a given accuracy. Moreover, let the line susceptance and conductance of a line h be expressed as $b_h = \overline{b}_h + \widetilde{b}_h$ and $g_h = \overline{g}_h + \widetilde{g}_h$ respectively, where overbar signifies the known part and overtilde refers to the uncertain part. We can gather all the known susceptances and conductances into the diagonal matrices $\overline{\mathcal{B}}$ and $\overline{\mathcal{G}}$ respectively. The uncertain parts can similarly be gathered into diagonal matrices $\widetilde{\mathcal{B}}$ and $\widetilde{\mathcal{G}}$. Investigating how these uncertain parameters feed into the linearized swing model, we can, for instance, write their contribution to (2.14) as:

$$\widetilde{P}^{\theta} = \sum_{h=1}^{n_e} \left[\underbrace{-\widetilde{b}_h \cos(F_h'\overline{\theta})}_{\beta_h} F_h + \underbrace{\widetilde{g}_h \sin(F_h'\overline{\theta})}_{\alpha_h} |F_h| \right] F_h', \tag{2.32}$$

where $\widetilde{b}_h$ or $\widetilde{g}_h$ can be zero for any line; and n_e signifies the number of lines in our network.

The matrices $F_h F_h'$ and $|F_h|F_h'$ are rank-one perturbation matrices. Similar expressions can be developed for the contributions of the uncertain parameters to Equations (2.15) – (2.17).

Concentrating on the linearized version (with parametric model uncertainty) of the swing model (2.12) expressed in functional form in (2.30), we can make the contributions of (2.32) to $\widetilde{A}$ explicit as follows:

$$\widetilde{A}_h^b = \begin{bmatrix} 0 & 0 & 0 \\ \beta_h F_{h,g} F_{h,g}' & 0 & \beta_h F_{h,g} F_{h,l}' \\ \beta_h F_{h,l} F_{h,g}' & 0 & \beta_h F_{h,l} F_{h,l}' \end{bmatrix}; \tag{2.33}$$

$$\widetilde{A}_h^g = \begin{bmatrix} 0 & 0 & 0 \\ \alpha_h |F_{h,g}| F_{h,g}' & 0 & \alpha_h |F_{h,g}| F_{h,l}' \\ \alpha_h |F_{h,l}| F_{h,g}' & 0 & \alpha_h |F_{h,l}| F_{h,l}' \end{bmatrix}. \tag{2.34}$$

The contributions of uncertainty in the damping coefficients is given by $\widetilde{A}^d$ and is given by:

$$\widetilde{A}^d = \begin{bmatrix} 0 & 0 & 0 \\ 0 & -\widetilde{D}_g & 0 \\ 0 & 0 & 0 \end{bmatrix}. \tag{2.35}$$

Finally we evaluate $\widetilde{A}$ as follows:

$$\widetilde{A} = \widetilde{A}^d + \sum_{h=1}^{n_e} \left(\widetilde{A}_h^b + \widetilde{A}_h^g \right). \tag{2.36}$$

2.7 Electromechanical Perturbations Experienced by Power Networks

The electromechanical perturbations that we will investigate in this thesis are load or generation changes, generator outages, line flow perturbations (e.g., line outages or short circuits).

All faults are assumed to be of a balanced nature, i.e., all three phases of the power system are affected equally.

The above perturbations generally will be unknown to the system operator (except maybe scheduled generation changes). In this thesis, we want to investigate how one can monitor the state of the system in the presence of these unknown perturbations. Moreover, we will be concerned with observer design in order to yield satisfactory state-estimates in the presence of these input perturbations (referred to as 'unknown inputs') to our system. In the next few subsections we will discuss how to model these perturbations.

2.7.1 Modeling of Load and Generation Changes

Modeling external perturbations in the form of load and generation changes is straightforward, because these changes are accounted for by changing the appropriate entry in either P_g^e or P_l^e defined in (2.8).

2.7.2 Modeling Generator Outages

The loss of a generating facility is a potential large perturbation that the system can experience. A total generator outage can be modeled by changing the generation amount to zero and removing the mass and damping terms associated with the generator from the swing model (M will drop rank — see (2.12)). This total loss of generation and the removal of the generator from the network will change the defined structure of the network, because a generator bus is converted to a load bus. The differential and algebraic variables associated with the generator bus in the DAE description will coalesce into algebraic variables associated with the new load bus. This change in classification has to be taken into consideration when such an event is simulated.

Partial generation outages are easier to model in our swing model setup. Assume that

originally a number of generators were running in parallel, and a fraction of these parallel generators suddenly go off-line. Thus, at the generator bus (as seen from the network side), we will see a mass and damping change of the aggregated generator along with a change in generated power ($M_{g,i}$, $D_{g,i}$ and $P^e_{g,i}$ — defined in (2.12) — will change). These changes can easily be done during the course of a simulation.

2.7.3 Modeling of Line Flow Perturbations

We mainly consider the case of a line outage. We investigate this effect using the linearized version of (2.19) and, as previously indicated in Section 2.6, a change in the line-parameters corresponding to rank-one perturbations in A. An unknown line outage occurring on line h (directed from bus s to bus t) can thus be modeled as:

$$Ew = \begin{array}{c} \vdots \\ s \rightarrow \\ \vdots \\ t \rightarrow \\ \vdots \end{array} \begin{bmatrix} 0 \\ \kappa_1 \\ 0 \\ \kappa_2 \\ 0 \end{bmatrix} \underbrace{\zeta F'_h \widetilde{x}}_{w}, \tag{2.37}$$

where $\kappa_1 = -\overline{b}_h \cos(F'_h\overline{\theta}) + \overline{g}_h \sin(F'_h\overline{\theta})$; $\kappa_2 = +\overline{b}_h \cos(F'_h\overline{\theta}) + \overline{g}_h \sin(F'_h\overline{\theta})$; w is the unknown-input; and ζ reflects the percentage fraction of the outage. For a complete line outage, one will have $\zeta = -1$.

2.8 Conclusion

In this chapter we did the groundwork and introduced different types of swing models that one can look at. However, the work pertaining to power system monitors in the following chapters can be extended to models that incorporate voltage dynamics.

Nonlinear and linearized versions of the swing models were given, and a matrix-vector equation was written that displays the network structure. We showed what type of model uncertainty one might expect for these models. We also discussed the different types of measurements available for us in order to create power system monitors. Lastly, we discussed different types of electromechanical perturbations that may occur in a power system.

In the following two chapters we will focus on swing-observer design for power systems and illustrate how we can apply these observers to realize power system monitors.

Part I

Power System Monitors using Model-Based Observers

Chapter 3

System-Wide State Estimation using Observers

In this chapter we will develop the model-based observer framework that can be used for the realization of power system monitors. Two types of monitors will be considered: first, a monitor concerned with dynamic state estimation; and second, the realization of fault detection and isolation filters.

Traditional state estimation in power systems has mainly focused on *static* estimation from *redundant* measurements [2]. There exists literature on dynamic state estimation (DSE), which deals with either: *recursive* processing of measurements, but with *no dynamics* in the state [3, 4]; or *slow-speed* state dynamics induced by *load* variations, so the dynamics referred to are that of the load, and these dynamics are estimated on-line in various ways using load forecasting ideas [3, 5, 6]. Traditional power system state estimation will not be addressed further in this thesis. The interested reader is referred to the authorative text by Monticelli [2].

Observer-based dynamic estimation of the swing state of a power network was investigated in [7, 8, 9]. In [9] the single-machine, infinite-bus case is examined. Swing-state estimation, as defined in [7], involves estimating the bus angles and generator speeds, but not the bus-voltage magnitudes. In [7] a mixture of generator and load buses was modeled via a nonlinear Differential Algebraic Equation (DAE) swing model, in comparison to the linear collapsed all-generator network investigated in [8].

A dynamic model of the system is used in the realization of an observer to accumulate over time, and interpolate over space (i.e., over the entire network), the information contained in measurements obtained from a limited — i.e., highly *non*-redundant — set of sensors. The role of the dynamic model is to relate measurements taken at any given time to those taken at other times, and to relate measured variables at the sensor locations to unmeasured variables throughout the network. In this way, sufficiently redundant information about the entire system is built up over time. Appropriate processing of this information then yields the desired estimates of the system state.

It should be pointed out that even though our investigations relating to observer design are essentially confined to the swing model, the methodologies proposed should be extendable to the case where we want to incorporate the voltage variables associated with the power network. For this one might represent the generators using two-axis models (see [32] for a description of this model) and model reactive power flowing on the network (see (2.4)). In this thesis, examples of this sort will not be presented.

Initial work on swing-state estimation has been reported in [7]. The following items distinguish the work discussed in this thesis from this paper:

- We investigate other possible nonlinear observers, and motivate our choice of retaining the observer form introduced in [7].
- We investigate different synthesis methods that yield superior state tracking performance. Moreover, we illustrate that designing observers using DAE design techniques has some added benefit relative to state-space observer design techniques.
- We investigate the performance of the observers in a noisy setting.
- We illustrate how one can design observers that are robust to model uncertainty, which was not done in [7].
- We introduce a novel graphical observer design approach in the next chapter, borrowing ideas from the theory of linear structured systems [38]. We furthermore illustrate that

this design technique is attractive for large-scale systems.

Linear observers can be designed for the linearized swing model (2.19), and these observers may be expected to do a reasonable job of tracking deviations of the nonlinear swing model (2.12) from steady state, provided these deviations are small enough to be reasonably captured by the linearized model. In this thesis, we are interested in tracking large deviations from nominal, and with this in mind, we will realize nonlinear observers.

The measurement set available to an observer greatly influences the performance of the realized state estimator. The placement and the number of measurements available to an observer is an important problem that will be addressed in this chapter. Increasing the measurement set might enhance the performance of the observer-based state estimator, because of the extra information contained in the larger set of measurements. A method for deciding the number, nature and placement of measurements needs to be investigated. In [7] an initial investigation of this sort was launched for a small scale example. In this chapter we will revisit this problem.

3.1 Nonlinear Observer

The nonlinear swing model (2.12) (in which we neglected machine reactances and took all bus voltages to be constant) can be rewritten as:

$$M\dot{x} = A_0 x + Bu + N\Phi(Rx), \tag{3.1}$$

$$A_0 = \begin{bmatrix} 0 & I & 0 \\ 0 & -D_g & 0 \\ 0 & 0 & 0 \end{bmatrix}, \tag{3.2}$$

where $\Phi(Rx)$ contains all the nonlinear terms associated with $P^{nw}(\theta)$ given in (2.3). For the time being let us assume that the network is lossless, i.e. $\mathcal{G} = 0$, resulting in $N = \begin{bmatrix} 0 \\ F\mathcal{B}\Upsilon \end{bmatrix}$

and $\Phi(Rx) = \sin(Rx)$ where $Rx = F'\theta$. Each of these nonlinear elements $\phi_i(R_i x)$ of $\Phi(Rx)$, corresponding to line i and with R_i being the i^{th} row of R, is Lipschitz continuous. Note that the nonlinear terms are due to the active power transfer laws across the transmission lines of the power network, and are therefore sinusoidal.

A possible nonlinear observer for this system might be:

$$M\dot{\widehat{x}} = A_0\widehat{x} + Bu + k(\widehat{x}, y - \widehat{y}), \tag{3.3}$$

where $\widehat{x}$ denotes the internal (differential and algebraic) variables of the observer system, $y = g(x)$ is the measured output (where element i of $g(x)$ can take on any of the possibilities shown in (2.13)), $\widehat{y} = g(\widehat{x})$ is the observer's estimate of y, and $k(\cdot,\cdot)$ is a yet-undetermined nonlinear function.

Defining the error vector $e = x - \widehat{x}$, we obtain the dynamic equations for the error system as follows:

$$M\dot{e} = A_0 e + N(\Phi(Rx)) - k(\widehat{x}, y - \widehat{y}). \tag{3.4}$$

In the next few subsections, we will explore different possible functions $k(\cdot,\cdot)$. However, this exploration will not be extensive, and the interested reader is referred to [39] in which a summary on nonlinear observer design is given.

3.1.1 Linear Parameter Varying Observer for Nonlinear State Estimation

The most intuitive choice of $k(\widehat{x}, y-\widehat{y})$, that is in accordance with the observer we proposed in [7], is:

$$k(\widehat{x}, y - \widehat{y}) \quad = \quad N\Phi(R\widehat{x}) + L(y - \widehat{y}), \tag{3.5}$$

which leads to the observer having the nonlinear form

$$M\dot{\widehat{x}} \;=\; A_0\widehat{x} + Bu + N\Phi(R\widehat{x}) + L(y - \widehat{y}), \tag{3.6}$$

where L is the observer gain and the last term is a linear correction term proportional to the discrepancy between the measured y and the observer's estimate $\widehat{y}$ of y. This type of observer is in accordance with that used by Rajamani in [40] for the state-space case.

Substituting (3.5) into (3.4) we obtain the nonlinear DAE error system associated with observer (3.6):

$$M\dot{e} = A_0 e + N(\Phi(Rx) - \Phi(R\widehat{x})) - L(y - \widehat{y}). \tag{3.7}$$

Global asymptotic observer design for state-space systems (i.e., when M is invertible and without loss of generality we take $M = I$) of the form (3.1), with $y = Cx$, has been studied by Rajamani [40]. The observer that he proposes is of the form (3.6) (with $M = I$) and with $\widehat{y} = C\widehat{x}$. He proves that for (A_0, C) observable, and $\Phi(Rx)$ Lipschitz with a constant γ, the state-space error dynamics (i.e., (3.7) with $M = I$) is globally asymptotically stable as long as we can design L such that: $(A_0 - LC)$ is stable, and that the minimum singular value over all positive frequency values of $(A_0 - LC - j\omega I)$ is greater than γ. This result ties in with the small gain theorem for the interconnection of the linear dynamics with the static state-dependent nonlinear block.

For the swing model, the A_0 matrix in (3.2) is so sparse, that in order to guarantee a similar notion of observability for the DAE system, we will need an extensive measurement set; we would essentially need to measure all load angles. However, in this thesis we want to confine our attention to scenarios where we have a limited set of sensors.

Using the relationship $x = \widehat{x} + e$ we can rewrite the nonlinear part in (3.7) as:

$$\Phi(Rx) - \Phi(R\widehat{x}) = \left[\tfrac{\partial\Phi}{\partial R\widehat{x}}\right] Re + \xi(\widehat{x}, e), \tag{3.8}$$

where $\left[\frac{\partial \Phi}{\partial R\widehat{x}}\right]$ denotes the Jacobian of $\Phi(\cdot)$ with respect to $R\widehat{x}$, and ξ contains higher order terms associated with this linearization. The i^{th} element of the vector ξ is found to be

$$\xi_i(\widehat{x}_i, e_i) = \cos(R_i\widehat{x})(\sin(R_ie) - R_ie) + \sin(R_i\widehat{x})(\cos(R_ie) - 1). \tag{3.9}$$

Substituting (3.8) into (3.7) we obtain the following DAE error system:

$$M\dot{e} = (A_0 + N\left[\frac{\partial \Phi}{\partial R\widehat{x}}\right]R)e - L(y - \widehat{y}) - N\xi(\widehat{x}, e), \tag{3.10}$$

from which we define $A(\widehat{x}) = (A_0 + N\left[\frac{\partial \Phi}{\partial R\widehat{x}}\right]R)$.

The error system (3.10) is recognized as a Linear Parameter Varying (LPV) [41] system with parameter $\widehat{x}$, and in recent years research attention has been focused on designing controllers for such state-space systems [42]. What appears to be common in these designs are that a family of gains is designed, and using gain-scheduling, the appropriate gain is used as the parameters vary. For the observer case the varying parameter is $\widehat{x}$ and one possibility in the observer realization is to redesign the gain along the trajectory of $\widehat{x}$. However, this approach can be computationally intensive (depending on the synthesis method) if this gain $L(\widehat{x})$ is redesigned in real-time as the $\widehat{x}$ trajectory changes significantly. A possible trade-off might be to design the gain L at a specific operating point and use L for a wide range of $R\widehat{x}$.

The beauty of writing the error system as an LPV system, is that a linear design technique can be used to design a stabilizing $L(\widehat{x})$ for the error system. The existence of such an $L(\widehat{x})$ depends on the 'observability' of $(M, A(\widehat{x}), C)$ [43], where $A(\widehat{x})$ is less sparse than A_0. The observability of $(M, A(\widehat{x}), C)$ does not require an extensive measurement set, as we discuss in Section 3.3, and we can thus investigate limited measurement sets.

Let us investigate the stability of the error system by considering the following Lyapanov

candidate function for this DAE system [44][1]:

$$\mathcal{V} = e'M'Xe, \tag{3.11}$$

$$\text{with } M'X = X'M \geq 0. \tag{3.12}$$

Taking the time derivative of $\mathcal{V}$ we find:

$$\dot{\mathcal{V}} = \underbrace{e'((A(\widehat{x}) - L(\widehat{x})C)'X + X'(A(\widehat{x}) - L(\widehat{x})C))e}_{\dot{\mathcal{V}}_l} + \underbrace{2e'X'N\xi(\widehat{x}, e)}_{\dot{\mathcal{V}}_{nl}}. \tag{3.13}$$

We have abandoned the idea of finding a global stabilizing gain L for the error dynamical system, instead we are interested in finding a local stabilizing gain $L(\widehat{x})$. First, let us consider the behavior of $\dot{\mathcal{V}}_{nl}$ in the neighborhood of $e = 0$. In this local neighborhood e remains small, and from (3.9) we notice that $\xi_i(\widehat{x}, e) \to 0$ and hence $\dot{\mathcal{V}}_{nl} \to 0$. Thus we only need to focus on the linear system $(M, A(\widehat{x}) - L(\widehat{x})C)$ for which we can use a linear synthesis technique to design stable error dynamics. For such a system we know that we can find a X that will satisfy (3.12) and also have $\dot{\mathcal{V}}_l < 0$. Thus in the neighborhood of $e = 0$ we have that $\dot{\mathcal{V}} \to \dot{\mathcal{V}}_l < 0$ and $\mathcal{V} \geq 0$ hence $\mathcal{V}$ is a valid Lyapanov function and the DAE-LPV error system will be local asymptotically stable around $e = 0$ if $(M, A(\widehat{x}) - L(\widehat{x})C)$ is stable, even if $\widehat{x}$ evolves (granted that $L(\widehat{x})$ is updated as $\widehat{x}$ evolves).

3.1.2 Arcak-Kokotović Nonlinear Observer

Recently Arcak and Kokotović [45] introduced a novel nonlinear observer for state-space models of the form (3.1) with $M = I$. They assume that each nonlinear term is monotonically nondecreasing. In [46] the same authors suggests how one can recast a problem with Lipschitz nonlinearities to a problem with nondecreasing nonlinearities, allowing us to investigate their observer design method for our swing-models. The state-space observer presented in [45, 46, 47] can be generalized to include the DAE case. This DAE Arcak-

[1] We assume that the original system (2.12) is local asymptotical stable.

Kokotović observer has the following form in the case of linear measurements $y = Cx$:

$$M\dot{\widehat{x}} = A_0\widehat{x} + N\Phi(R\widehat{x} + K(y - \widehat{y})) + L(y - \widehat{y}), \tag{3.14}$$

$$\widehat{y} = C\widehat{x}, \tag{3.15}$$

Defining $e = x - \widehat{x}$, the error dynamics are obtained as:

$$M\dot{e} = (A_0 - LC)e + N\Psi(z), \tag{3.16}$$

$$\Psi(z) = (\Phi(Rx) - \Phi(R\widehat{x} + K(y - \widehat{y}))), \tag{3.17}$$

$$z = (R - KC)e, \tag{3.18}$$

where z is the modified output of the linear DAE system $(M, A_0 - LC, R - KC)$. This linear system is then interconnected in a feedback fashion with a multivariable sector nonlinearity $\Psi(\cdot)$. The output of this nonlinear block provides us with the driving input of the linear DAE system.

In [45] a state-space observer (i.e., $M = I$) of the form in (3.14) is shown to have globally exponential stable error dynamics when a specific Linear Matrix Inequality (LMI) problem is feasible. (See Appendix A for a brief introduction on LMI's.) The design method relies on a circle criterion argument and the extension of their proof of stability for the state-space observer to the DAE case can be done. In this extension, their original LMI condition given in [45] is augmented by the additional LMI (3.12). The nonlinearities in the swing model are not monotonic nondecreasing, but in [46], the authors illustrate how global Lipschitz nonlinearities can be transformed to monotonic nondecreasing nonlinearities. In [47] an initial treatment of the analytical tests for the existence of such an observer was given; however in most of the papers by these authors, the feasibility of the conditions for the existence of such observers relied on the feasibility of the set of LMIs they had proposed.

Rather than giving an extensive analysis of an Arcak-Kokotović observer, let us investigate the added benefit of having the extra feedback $K(y - \widehat{y})$ available. Focusing on the nonlinear

part we see that:

$$\begin{aligned}\phi_i(R_i x) - \phi_i(R_i\widehat{x} + K_i C e) &= \sin(R_i\widehat{x})\left[\cos(R_i e) - \cos(K_i C e)\right] \\ &\quad + \cos(R_i\widehat{x})\left[\sin(R_i e) - \sin(K_i C e)\right], \end{aligned} \tag{3.19}$$

from this we see that we have the opportunity to cancel the i^{th} nonlinear component of $\Phi(Rx)$ from the DAE error system. This cancellation is achievable (i.e. there exists such a K_i) when $\ker(R_i) \supseteq \ker(C)$. What this implies is that the structure of C helps in the distribution of the elements of K_i (a design matrix) such that we are able to cancel the nonzero entries of R_i. The added benefit of having KCe feeding back into the nonlinear term of the observer is not apparent if the latter condition for each i^{th} component does not hold. If we force this condition to hold for every i^{th} component we will need an extensive measurement set (i.e., the nullspace of C would become smaller ultimately tending to the empty set, which is in the nullspace of each R_i). Studies using extensive measurement sets fall outside the scope of our work where we only want to focus on limited measurement sets.

3.1.3 Hybrid Nonlinear versus Linear Observers Using the Same Linearly Designed Gain

From the two previous subsections one can conclude that designing an LPV observer might yield the best state estimator for the nonlinear system. (One can think of this estimator as a special case of the Extended Kalman Filter.) However, implementing this LPV observer in real-time can be very computationally intensive (depending on the design method used to find $L(\widehat{x})$) for a large-scale power network. Thus, in the ensuing studies, we will not realize LPV observers in our simulations in order to save on computational requirements, although the design approaches we will introduce could be used when LPV observers are to be implemented.

In this section we will introduce our hybrid observer that uses an observer gain that is

designed using a linearized model (at $\overline{x}$ and $\overline{u}$) in the realization of

$$M\dot{\widehat{x}} = f(\widehat{x}, u = \overline{u}, w = 0) + L(y - \widehat{y}), \tag{3.20}$$

where M, f, u, w are as defined in (2.12), $y = g(x) + v$ is the measured data, and $\widehat{y} = g(\widehat{x})$ is the output predicted by the observer.

The error dynamics associated with this observer is written as

$$M\dot{e} = f(x, u = \overline{u}, w) - f(\widehat{x}, u = \overline{u}, w = 0) - L(y - \widehat{y}), \tag{3.21}$$

which can be written as the LPV system

$$M\dot{e} = (A(\widehat{x}) - LC(\widehat{x}))e + \xi(e, \widehat{x}) + Ew - Lv, \tag{3.22}$$

where $A(\widehat{x}) = \left[\frac{\partial f}{\partial \widehat{x}}\right]$, $C(\widehat{x}) = \left[\frac{\partial g}{\partial \widehat{x}}\right]$ and $E = \left[\frac{\partial f}{\partial w}\right]$.

We can rewrite the above error dynamics as

$$M\dot{e} = (A(\overline{x}) - LC(\overline{x}))e + \beta(e, \widehat{x}, \overline{x}) + Ew - Lv, \tag{3.23}$$

where $\beta(e, \widehat{x}, \overline{x}) = [A(\widehat{x}) - A(\overline{x}) - LC(\widehat{x}) + LC(\overline{x})]e + \xi(e, \widehat{x})$. In Section 3.1.1 we showed that $\xi(e, \widehat{x}) \to 0$ in a local neighborhood of $e = 0$. In order to have $\beta(e, \widehat{x}, \overline{x}) \to 0$ in this neighborhood of e, we need that $\widehat{x}$ be close to $\overline{x}$.

Placing this extra restriction of $\widehat{x}$ being close to $\overline{x}$, might urge us to investigate linear observers of the form

$$M\dot{\widetilde{\widehat{x}}} = A(\overline{x})\widetilde{\widehat{x}} + L(\widetilde{y} - \widetilde{\widehat{y}}), \tag{3.24}$$

where $\widetilde{y} = C(\overline{x})\widetilde{x} + v$ is the linearized version of y with measurement noise v, and $\widetilde{\widehat{y}} = C(\overline{x})\widetilde{\widehat{x}}$ is the estimate of $\widetilde{y}$. Defining $\widetilde{e} = \widetilde{x} - \widetilde{\widehat{x}}$, the following linear error dynamical system is

obtained

$$M\dot{\widetilde{e}} = (A(\overline{x}) - LC(\overline{x}))\widetilde{e} + Ew - Lv, \tag{3.25}$$

which is similar to (3.23).

One might expect that the linear observer may do a reasonable job of tracking deviations of the swing dynamics from steady state, provided these deviations are small enough to be reasonably captured by the linearized model. On the other hand, we would expect that the hybrid nonlinear observer (3.20) can track larger deviations from nominal.

We anticipate that this nonlinear observer will tend to perform better than a linear observer. For instance, assume no modeling errors and that the linear and nonlinear observers have initial conditions equal to the state of the system. When the state and the state moves away from the linearization point, the linear observer can have an internal model that differs wildly from the model of the plant. Thus, discrepancies will arise and the error will start to increase. The nonlinear observer, on the other hand, will track the state.

Experimentally it was found that for the examples we considered in this thesis, the discrepancies between the performances of the linear and nonlinear observers were marginal. An illustration of these discrepancies will not be shown at this juncture.

3.2 DAE or State-Space Observer Synthesis

The question we want to address in this section is whether we should design the observer gain L using DAE or state-space observer design techniques. Before we discuss available synthesis methods let us investigate the relation between DAE and state-space observer design.

The question of whether to design observers using state-space design or DAE observer

design techniques was briefly mentioned in [33]. The author preferred to design state-space observers for the known-input state-estimation problem; however, he did not elaborate on the perceived benefits of using a state-space design approach.

Recently various researchers have investigated DAE observer design. Some of the papers address observer design for very general DAE models, such as rectangular (as compared to square) DAE systems and higher-index DAE systems. Such general investigations fall outside the scope of this thesis, seeing that the DAE model of the swing dynamics is square and of index one.

We start off by assuming that an L exists that stabilizes the error system. The conditions that the DAE model needs to satisfy in order to guarantee the existence of such L will be addressed in the following section.

We can express (3.25) in the the following form (where we assumed the absence of model uncertainty):

$$\begin{bmatrix} M_d & 0 \\ 0 & 0 \end{bmatrix} \begin{pmatrix} \dot{\widetilde{e}}_d \\ \dot{\widetilde{e}}_a \end{pmatrix} = \begin{bmatrix} A_{dd} - L_d C_d & A_{da} - L_d C_a \\ A_{ad} - L_a C_d & A_{aa} - L_a C_a \end{bmatrix} \begin{pmatrix} \widetilde{e}_d \\ \widetilde{e}_a \end{pmatrix} + \begin{bmatrix} L_d & E_d \\ L_a & E_a \end{bmatrix} \begin{pmatrix} -v \\ w \end{pmatrix}. \tag{3.26}$$

$\widetilde{e}_d$ is the vector of dynamical variables (also referred to as the slow variables); $\widetilde{e}_a$ is the vector of algebraic variables; v is the vector of measurement corruption signals (and in the standard setup is referred to as measurement noise); and w is the vector of unknown inputs driving the error dynamical system.

In order to answer the question of this section, it is instructive to collapse (3.26) to form a state-space model (see Section 2.5, where the steps associated with collapsing a DAE model to its equivalent state-space model are illustrated). Collapsing (3.26) we obtain the

state-space equivalent model as:

$$\begin{aligned} M_d\dot{e}_d &= \left[A_{dd} - L_dC_d - (A_{da} - L_dC_a)\,(A_{aa} - L_aC_a)^{-1}\,(A_{ad} - L_aC_d)\right] e_d \\ &\quad +(E_d - (A_{da} - L_dC_a)(A_{aa} - L_aC_a)^{-1}E_a)w \\ &\quad -(L_d - (A_{da} - L_dC_a)(A_{aa} - L_aC_a)^{-1}L_a)v, \qquad (3.27) \\ e &= \begin{bmatrix} I_{ng} \\ -(A_{aa} - L_aC_a)^{-1}(A_{ad} - L_aC_d) \end{bmatrix} e_d \\ &\quad - \begin{bmatrix} 0 \\ (A_{aa} - L_aC_a)^{-1} \end{bmatrix} (E_aw - L_av)\,. \qquad (3.28) \end{aligned}$$

Equation (3.27) confirms that we are faced with a tricky design, if we were to use state-space techniques, because of the presence of the gain block L_a. Setting $L_a = 0$ simplifies the observer design and we find that (3.27) reduces to,

$$\begin{aligned} M_d\dot{e}_d &= \left[A_{dd} - L_dC_d - (A_{da} - L_dC_a)\,(A_{aa})^{-1}\,(A_{ad})\right] e_d \\ &\quad +(E_d - (A_{da} - L_dC_a)(A_{aa})^{-1}E_a)w - L_dv, \qquad (3.29) \end{aligned}$$

which can be conveniently expressed using the collapsed state-space matrices of the original system (see Equations (2.22) – (2.29)). Thus (3.29) can be expressed as

$$\begin{aligned} \dot{e}_d &= (A_s - L_sC_s)e_d + E_sw - L_sv, \qquad (3.30) \\ e &= \begin{bmatrix} I_{ng} \\ -A_{aa}^{-1}A_{ad} \end{bmatrix} e_d - \begin{bmatrix} 0 \\ A_{aa}^{-1} \end{bmatrix} E_aw \qquad (3.31) \end{aligned}$$

where $L_s = M_d^{-1}L_d$. We recognize that by setting $L_a = 0$ we can design the gain of the nonlinear DAE observer, $L = \begin{bmatrix} L_d' & L_a'(=0) \end{bmatrix}'$, by designing a state-space observer gain L_d.

A natural question to ask is whether we lost degrees of freedom in the design stage by taking $L_a = 0$. What are the benefits of having the additional gain block L_a? The answer to this

question is best demonstrated by the following small example.

3.2.1 DAE versus State-Space Example

In this example we will consider the DAE system corresponding to a linearized swing model of a generator connected to a load. The system matrices are given by:

$$A = \begin{bmatrix} 0 & 1 & 0 \\ -b & -d & b \\ b & 0 & -b \end{bmatrix}, E = \begin{bmatrix} 0 \\ 0 \\ 1 \end{bmatrix}, M = \begin{bmatrix} 1 & 0 & 0 \\ 0 & 1 & 0 \\ 0 & 0 & 0 \end{bmatrix}, C' = \begin{bmatrix} 0 \\ 0 \\ 1 \end{bmatrix}, L = \begin{bmatrix} l_1 \\ l_2 \\ l_3 \end{bmatrix}.$$

The collapsed state-space system $(A_s, E_{sw}, C_s, D_{sw})$ can be computed using Equations (2.22) – (2.23).

Consider realizing a DAE observer of the form (3.24) for which the error dynamics are of the form (3.26). Our aim is to design observers that will attenuate the effect of the unknown-input. Thus, we want the steady-state error in response to an unknown step input to be attenuated. The expression of the steady-state error for this system is given by:

$$G_{ew}(s=0) = (sM - A + LC)^{-1}E|_{s=0} = \begin{bmatrix} \frac{b-dl_1-l_2}{b(dl_1+l_2+l_3)} \\ \frac{l_1}{dl_1+l_2+l_3} \\ \frac{1}{dl_1+l_2+l_3} \end{bmatrix}.$$

Choosing $l_1 = 0$, $l_2 = b$ and l_3, large the steady-state error $G_{ew}(s=0) \to 0$. We used the three available design parameters to achieve 'ideal' unknown-input attenuation. There are no extra design parameters available in order to independently move the poles of the closed loop error dynamical system. For this design these closed-loop poles are at $(\frac{1}{2}(-d \pm \sqrt{-4b+d^2}))$, which is different from the open-loop poles $(0, -d)$ of the system.

Now let us consider the state-space design case where we need to find the elements of $L_s = \begin{bmatrix} l_{s1} & l_{s2} \end{bmatrix}'$. The expression of the steady-state error for the state-space designed

closed-loop error dynamical system in response to an unknown step input is given by:

$$G_{ew}(s=0) = C_{fs}(sI - A_s + L_sC_s)^{-1}(E_s - L_sD_s)|_{s=0} + D_{fs} = \begin{bmatrix} \frac{b-dl_{s1}-l_{s2}}{b(dl_{s1}+l_{s2})} \\ \frac{l_{s1}}{dl_{s1}+l_{s2}} \\ \frac{1}{dl_{s1}+l_{s2}} \end{bmatrix}$$

It is evident that for this case one cannot achieve 'ideal' unknown-input attenuation. Setting $l_{s1} = 0$ and $l_{s2} = b$, only two of the three steady-state errors can be set to zero ($G_{ew}(s = 0) = \begin{bmatrix} 0 & 0 & \frac{1}{b} \end{bmatrix}$), and the poles are also at ($\frac{1}{2}(-d \pm \sqrt{-4b + d^2})$). Thus, by setting $L_a = 0$ we have eliminated one of our degrees of design freedom.

In the presence of measurement noise it will not be advisable to let l_3 be too large, but a suitable trade-off can be achieved.

In Section 4.2.2 the benefit of having L_a nonzero will be highlighted again, using a different motivation. Another benefit of having L_a nonzero in (3.26) is that the extra degrees of freedom come in handy when directional fault detectors (where the occurrence of a fault yields a unique output direction, aiding in fault isolation) are realized.

DAE observer design is currently an active research field and literature exists where various state-space synthesis techniques are extended in order to realize full-order DAE observers [36, 43, 48, 49, 50, 51]. We will not investigate all of these techniques, but rather focus on H_∞ estimation problem for DAE systems. A very recent recent paper [50] (2003) reported on H_∞ filtering for DAE systems, treating a more general class of problems than the H_∞ observer design problem that we limit ourselves to here.

3.3 Observability Notions for DAE Models

In Section 2.4 different types of measurements available for swing-observer design were introduced. In this section we will discuss what kind of observability guarantees the exis-

tence of L in (3.24). Various researchers have asked this question [36, 48, 43]. In [36] the requirement for the existence of a stabilizing L for an index-one DAE system is given as:

- System (2.19) has a singular observer (i.e., L exists) if and only if it is detectable (Theorem 4-1.2, page 105 in [36]).
- System (2.19) is detectable if and only if $rank \begin{bmatrix} sM - A \\ C \end{bmatrix} = n, \forall s \in \overline{\mathbb{C}}^{+}, s$ finite.

The requirement of detectability limits the set of measurements that can be employed, and translates to detectability of the equivalent state-space system.

A subtle issue emerges when we consider swing-observer design utilizing a single speed measurement. Using a measurement of this form results in the system not being detectable. The reason is that the mode at $s = 0$ is unobservable, i.e. the matrix $\begin{bmatrix} A \\ C \end{bmatrix}$ has rank less than n. This reflects the fact that *absolute* angles cannot be estimated using just speed measurements, only *relative* angles can. However, relative angles are ultimately all that we require in our application. It suffices for us to modify the above rank test for detectability by checking for rank n at all *nonzero* $s \in \mathbb{C}^{+}$, implying that single speed measurements are allowed.

3.4 H_∞ Observer Synthesis

Kalman Filtering (of which Linear Quadratic Estimation is a special case) was used to design [7, 9, 10, 11] swing-state observers for power systems. Kalman Filtering is one of the more popular ways to deal with state estimation [52]. Kalman Filtering is generally based on the assumption that the system under consideration and the statistics of stationary white noise processes w and v. The Kalman filter provides an optimal estimate of the desired system state that minimizes the covariance of the estimation error. In the case when the

noise statistics are not exactly known, one can use the describing parameters of the noise processes as tuning parameters in the design process. Mangoubi [53] incorporated model uncertainty in the Kalman filter framework, but a detailed discussion of these extensions fall outside the scope of this thesis.

At the beginning of the 1990's researchers introduced H_∞ filtering to bypass the requirement of exact knowledge of the statistics of the system noise processes. In the H_∞ framework we assume that the unknown input signals w (which can be process noise or large deviations due to faults on the system) and the measurement corruption signals v (which can be a noise process or a momentarily offset in the measurement) have bounded energy.

In this thesis we will introduce and discuss the H_∞ filtering problem using a Linear Matrix Inequality (LMI) setup. A brief explanation of LMIs is given in Appendix A and the interested reader is referred to the textbook [54] and the course notes by Scherer and Weiland [55]. It is reasonable to ask why we opted to investigate the H_∞ problem using the LMI framework, and not the traditional Algebraic Riccati Equation setup. The reason is the ease with which we could test the difference between DAE observer and state-space observer design. Incorporating extra constraints (possibly performance related) on the problem is also handled with more ease in the LMI setup. Another bonus is that the Matlab LMI toolbox [56] can be used to solve the H_∞ optimization problem subjected to LMIs.

In section 3.2 we illustrated the extra degrees of freedom afforded by designing a DAE observer versus a state-space observer design. Unfortunately, for practical power networks the number of non-generator buses is substantially greater than the number of generator buses. Thus, the size of the DAE model can potentially be orders larger than the equivalent state-space system. The number of decision variables associated with the DAE H_∞ LMI filtering problem can potentially be very large compared to the number of decision variables associated with the H_∞ filtering problem for the equivalent state-space system. In the following two subsections we will investigate estimation for the descriptor case and the state-space case. In practice, the scenario might arise that the DAE H_∞ filter might not

be feasible when we take the computational issues into consideration.

3.4.1 DAE Systems

The H_∞ observer design setup is a direct application of the generalized bounded real lemma [50]. The generalized bounded real lemma for the following DAE system

$$M\dot{x} = Ax + Bu \tag{3.32}$$

$$y = Cx + Du, \tag{3.33}$$

for which we use the shorthand (M, A, B, C, D) can be stated as follows.

LEMMA 3.1

The transfer function matrix

$$G_{yu} = C(sM - A)^{-1}B + D \tag{3.34}$$

associated with system (M, A, B, C, D) *have* $\|G_{yu}\|_\infty < \gamma^2$*, if and only if there exists a matrix* X *such that*

$$M'X = X'M \geq 0 \tag{3.35}$$

$$\begin{bmatrix} A'X + X'A + C'C & X'B + C'D \\ B'X + D'C & D'D - \gamma^2 I \end{bmatrix} < 0 \tag{3.36}$$

From the constraint $M'X = X'M \geq 0$ one can show for our diagonal singular M that $X = \begin{bmatrix} X_{dd} & 0 \\ X_{ad} & X_{aa} \end{bmatrix}$ with $M_d' X_{dd} = X_{dd}' M_d$. Thus, due to the structure of M some of the decision variables (elements of X) are eliminated.

The H_∞ observer synthesis LMIs are obtained by substituting $(M, A - LC, E, Q = I, D = 0)$

corresponding to the system given in Equation (3.25) for (M, A, B, C, D) in Lemma 3.1. Hence, the H_∞ filter exists if the following LMIs with decision variables X, $Y'(= -X'L)$, γ^2 are feasible:

$$M'X = X'M \geq 0 \tag{3.37}$$

$$\begin{bmatrix} A'X + X'A + Y'C + C'Y + C_e'C_e & X'E \\ E'X & -\gamma^2 I \end{bmatrix} < 0. \tag{3.38}$$

The premise of the design is to minimize γ^2 subject to the constraints (3.37) and (3.38). The introduction of Y into the problem ensures that the problem stays linear because LMI solvers cannot solve the LMI feasibility problem with decision variables X, L and γ^2. The latter problem would involve matrix terms of the form $X'L$, which is nonlinear in the decision variables.

The presence of the measurement corruption signals v can adversely influence the performance of an observer. The level of trust the LQE/Kalman filter places in these corrupted measurements is weighted according to the description of the noise processes associated with the measurements. We have assumed in the H_∞ filter design discussed thus far that the measurement signal is uncorrupted, and we will have to take possible measurement corruption into account.

One possible way of including the effect of measurement noise is to append v to w and $-L$ to B_w, thus effectively redefining w. However, it was found that the realized observers were conservative and performed poorly in the presence of unknown load/generation changes. Following this approach one implicitly assumes that $\|v\|_2$ and $\|w\|_2$ are comparable, which might not be the case.

Another possible approach to account for v is to investigate a multi-objective design problem [55], i.e., $\|G_{ew}(s)\|_\infty < \gamma^2$ and $\|G_{ev}(s)\|_\infty < \nu^2$. Unfortunately, multi-objective design problems are typically intractable in state-space, so these problems are frequently converted to a mixed design problem [55]. In this thesis we will investigate the mixed design problem,

which requires us to also satisfy the additional (in conjunction with (3.37) and (3.38)) LMI constraint:

$$\begin{bmatrix} A'X + X'A + Y'C + C'Y + C_e'C_e & Y' \\ Y & -\nu^2 I \end{bmatrix} < 0, \tag{3.39}$$

where we substituted the system $(M, A - LC, -L, C_e, 0)$ into Lemma 3.1. The main difference between mixed and multi-objective design is that for the mixed design problem we want to find X and Y that satisfy constraints (3.37) – (3.39), whereas for the multi-objective design problem we want to find X_1 and Y_1 (satisfying (3.37) and (3.38)) as well as X_2 and Y_2 (satisfying (3.37) and (3.39)). The existence of distinct Xs and Ys makes it difficult to obtain L in the multi-objective case.

In designing an observer using the mixed design approach that will be able to guarantee a certain level of unknown-input and measurement corruption attenuation, we would want to minimize $\gamma^2 + \alpha_\nu \nu^2$, where α_ν is fixed. Initial choices for α_ν might be $\alpha_\nu = \frac{\|v\|_2}{\|w\|_2}$. The larger α_ν becomes, the less the observer will trust the measurements and consequently will rely more on the internal model of the observer.

We will now briefly state the LMI-based H_∞ filtering problem for state-space systems. We will then move on to an example where we will pit H_∞ DAE designed observers versus H_∞ state-space designed observers.

3.4.2 State-Space Models

The bounded real lemma for state-space systems is obtained from Lemma 3.1 simply by setting $M = I$.

Following the same route as the DAE case, the LMI constraints of the state-space H_∞ filtering problem are given by the following, where we use the matrix notation from (2.22)

– (2.27) and also define $C_{fs} = \begin{bmatrix} I \\ -A_{aa}^{-1}A_{ad} \end{bmatrix}$ and $D_{fs} = \begin{bmatrix} 0 \\ -A_{aa}^{-1}E_a \end{bmatrix}$:

$$X = X' > 0; \tag{3.40}$$

$$\begin{bmatrix} A_s'X + X'A_s + Y'C_s + C_s'Y + C_{fs}'C_{fs} & X'E_s + Y'D_s + C_{fs}'D_{fs} \\ E_s'X + D_s'Y + D_{fs}'C_{fs} & D_{fs}'D_{fs} - \gamma^2 I \end{bmatrix} < 0; \tag{3.41}$$

$$\begin{bmatrix} A_s'X + X'A_s + Y'C_s + C_s'Y + C_{fs}'C_{fs} & Y' \\ Y & -\nu^2 I \end{bmatrix} < 0. \tag{3.42}$$

The mixed-design state-space H_∞ filter is obtained by minimizing $\gamma^2 + \alpha_v^2$ subject to the above constraints.

3.4.3 Comparison Example: Nine-Bus Power System

The following example will serve a dual purpose. Firstly, we will illustrate the performance difference between DAE-designed H_∞ filters and state-space-designed H_∞ filters. Secondly, we will illustrate the performance of these observers in a noisy setting (we assume measurement noise and process noise on all the load buses), and establish that the DAE H_∞ optimization problem did not let L_a become too large (to minimize $\|A_{22} - L_2C_2\|$), otherwise the response of the DAE-designed observer would be too sensitive to possible measurement corruption signals.

The power system example we will be considering is a classical nine-bus example (see Figure 3.1) adopted from [32]. For this system we assume that there are three unknown-input in total (at bus 5, 6, and 8). We assume that both observers have the same measurements available, and these are of the form of direct angle measurements taken at buses 4, 7 and 9.

During the course of the simulation we will apply a discrete event in the form of a $2p.u.$ unknown load change in the real power load at bus 8. We will assume the system and the observer were initially in their respective steady states for both simulations. The applicable

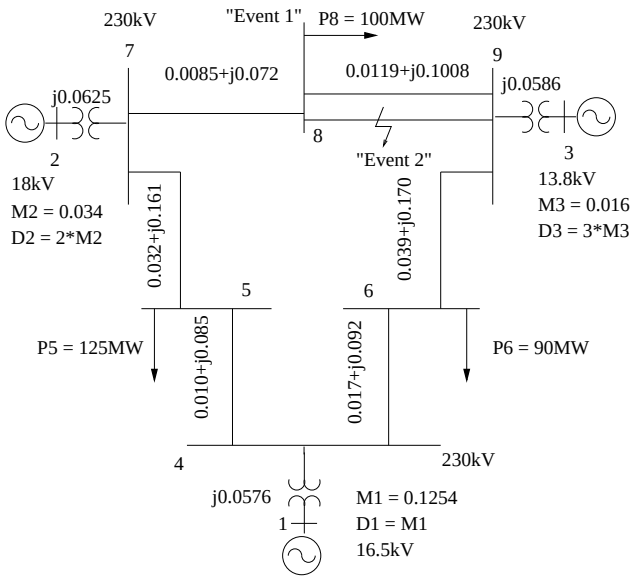

Figure 3.1: Classical 9-bus example used in this this section (and other sections to follow). The line parameters are shown as impedances.

event occurs during $0.001s \leq t \leq 4.001s$ in each simulation. For the ensuing discussion we will examine the angle at a bus relative to the center-of-inertia angle movement θ_{coi} that is computed as:

$$\theta_{coi} = \sum_{i=1}^{n_g} \frac{M_i}{M_{total}} \theta_i, \tag{3.43}$$

and we define $\theta_{ic} = \theta_i - \theta_{coi}$ and $\widehat{\theta}_{ic} = \widehat{\theta}_i - \widehat{\theta}_{coi}$ where $i \in \{2, \cdots, n\}$.

In Figures 3.2 – 3.4 the performance of the DAE-designed H_∞ filter is contrasted to the performance of the state-space designed H_∞ filter. From these figures we can conclude that the DAE-designed filter indeed does a better job than the state-space-designed filter. (One can define a metric on e for both of these observers to get a quantitative feel of performance difference.)

Note that there are no direct speed measurements taken at bus 3, or in fact anywhere in the network, so the dynamic model plays a key role in providing the speed estimate shown in Figure 3.4(b).

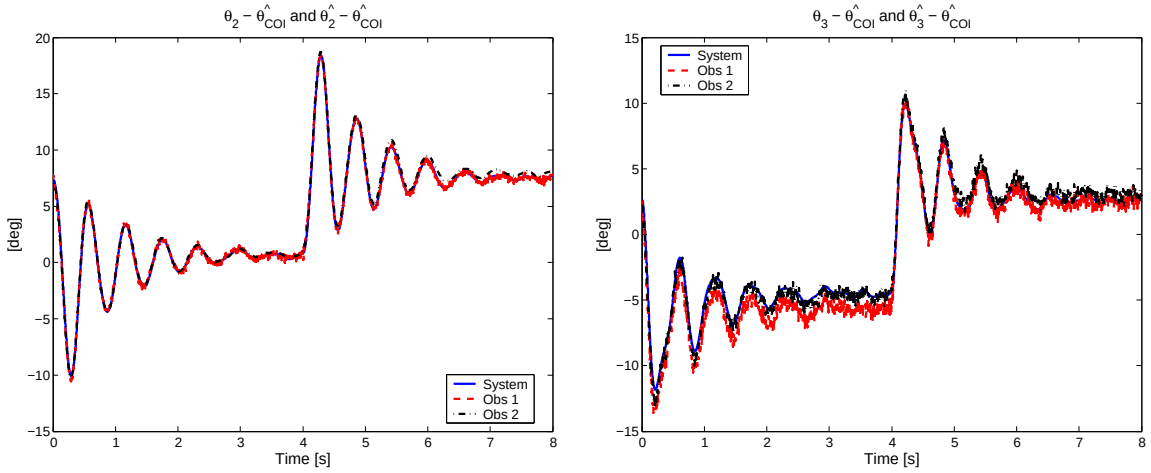

(a) θ_{2c} (b) θ_{3c}

Figure 3.2: Time plots of the system response (solid line); DAE-designed H_∞ filter (dashed line — Obs1) and state-space-designed H_∞ filter (dashed-dot line — Obs2) in response to a $2p.u.$ load change at bus 8.

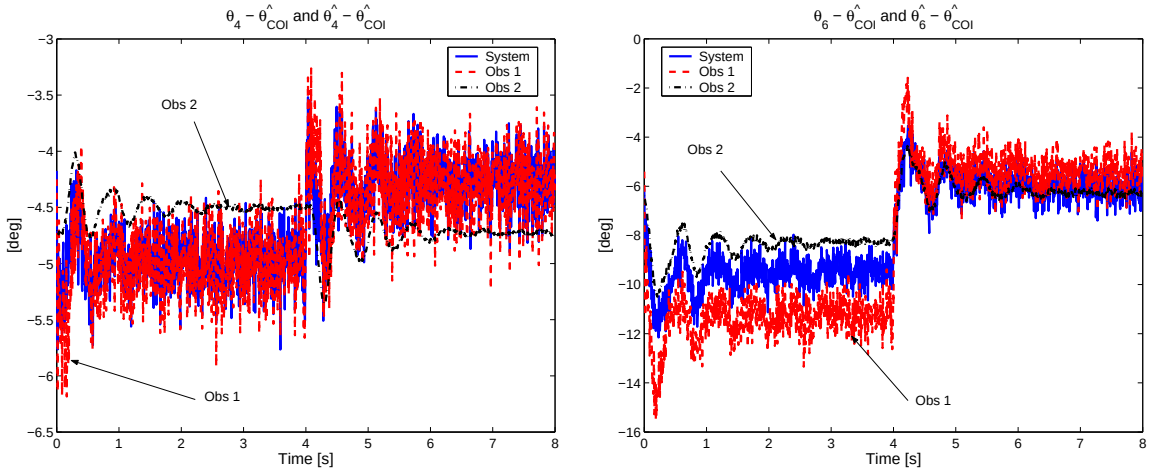

(a) θ_{4c} (b) θ_{6c}

Figure 3.3: Time plots of the system response (solid line); DAE-designed H_∞ filter (dashed line — Obs1) and state-space-designed H_∞ filter (dashed-dot line — Obs2) in response to a $2p.u.$ load change at bus 8.

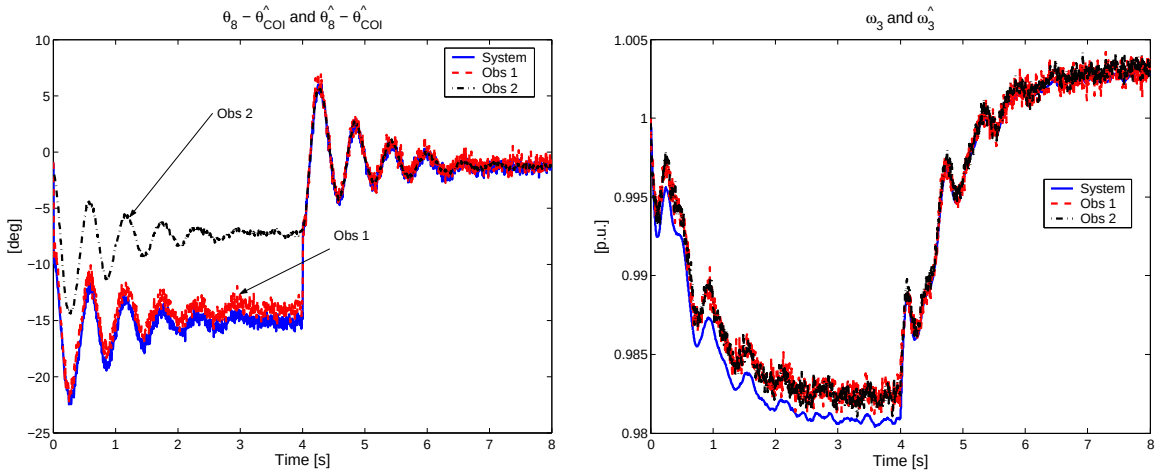

(a) θ_{8c} (b) ω_3

Figure 3.4: Time plots of the system response (solid line); DAE-designed H_∞ filter (dashed line — Obs1) and state-space-designed H_∞ filter (dashed-dot line — Obs2) in response to a $2p.u.$ load change at bus 8.

3.4.4 Robust H_∞ Estimation

In Section 2.6 we discussed possible uncertain parameters in our swing models. This parametric model uncertainty has not been accounted for during the observer design stage, and in Appendix B we account for these uncertainties in the observer design problem. We will not build on this technical material, but the interested reader is referred to the appendix.

3.4.5 Measurement Placement and Type

A possible measurement placement and type exploration algorithm can be devised by sequentially working through the list of possible measurements. A similar strategy was proposed in [7] using the LQE observer synthesis method. However, employing a similar approach, but utilizing H_∞ DAE filtering, will be too unwieldy for practical power networks. A possible cost function for this approach might be a combination of the error convergence rate and γ. Due to the computational burden such a sequential search will evoke, we will

not report on the initial results obtained using this algorithm.

As an alternative one can use H_∞ state-space filter design algorithms that use Algebraic Riccati Equation solvers. The computational requirements of this approach will be more viable, but will place restrictions on out our measurement set as discussed in Section 3.3.

3.5 Conclusion

In this chapter we investigated observer design for swing models. We briefly touched on nonlinear observer possibilities. We concluded that a viable approach for realizing an observer for the nonlinear swing model would be to design a linear parameter varying observer gain (the parameters in question are the estimates of the system state variables).

This possibility presented us with the opportunity to design an observer gain using linear techniques. The next question that arose was whether we should design these gains using state-space techniques or DAE design techniques. We concluded that when unknown-input attenuation is of importance we should design the observer gain using a DAE synthesis technique. This approach provides us with more degrees of freedom in order to attenuate the effect of the unknown input on the estimation problem.

We then discussed the conditions under which we can find these observer gains. From there we investigated the realization of robust H_∞ filters for the DAE and state-space design case. The state-space case is considered for computational reasons. Unfortunately, a DAE system associated with a practical power network can be large. The number of algebraic variables can be much larger than the number of differential variables, increasing the number of decision variables in the LMI-based H_∞ optimization problem significantly. From these studies we concluded that if computational power is limited, LMI-based H_∞ DAE filter design is presently not realistic.

In the next chapter we will introduce a novel observer design approach, that is suited for

on-line design for large-scale systems.

Chapter 4

Graphical Observer Design for Large-Scale Systems

A linear state-space system is considered structured when each entry of the state-space system matrices, (A, B, C, D), is either a fixed zero, a free parameter, or a fixed nonzero parameter. The survey paper [38] presents a good introduction to these types of systems and summarizes representative results in the field. The background section presented here is a brief summary of the survey [38]. The reader should keep in mind, however, that our main interest will be in structured systems with fixed zeros and fixed (nominally known) parameters, but *not* free parameters.

The structure in the system is mainly derived from the fixed-zero entries in the system matrices. The fixed non-zero parameters of these matrices represent the specific role that certain variables play in the system. Examples of these fixed parameters are: a system comprising a composition of subsystems (e.g., a series connection); and fixed algebraic relations between variables (e.g., one state variable being the derivative of another state variable — this results in having $1s$ in the system matrices). The absence of relations between variables gives rise to the fixed-zero entries in the system matrices. For these fixed zeros one can conclude that some variables have no direct action on others. The locations of these fixed zeros pin down the structure of the system.

Several approaches can be followed in studying the properties and the possibility of control/estimation for such systems [38]. The most widely used approach (and the approach followed in the sections preceding this one) is to obtain values of the physical parameters

and incorporate them into a standard state-space representation with numerical data, to which we can apply the techniques of state-space theory. Numerous results have been published attesting to the success of such an approach. However, the authors in [38] state that knowledge on the structure of the system is typically lost or not used. The zero entries of the system matrices have a strong meaning (showing no direct actions between certain variables), and in standard state-space design approaches these zeroes are treated as numerical values like any other, and not exploited.

In the survey paper [38] the authors report on investigations of system-theoretic properties (also called generic properties) associated with these structured systems that are true for almost any value of the free parameters. They also illustrate how these generic properties can be checked by means of directed graphs that can be associated with a structured system. The vertices of this graph correspond to the variables in the system description (i.e., input, state and output variables), and there exists a directed edge from vertex i to vertex j if there is a nonzero parameter quantifying the direct dependence of the variable associated with vertex j on the variable associated with vertex i. Some of the generic results the authors discuss in [38] are: controllability; solvability of the disturbance-rejection problem; and input-output decoupling of structured systems expressed in graph-theoretic terms. The authors also point out some drawbacks of investigating structured systems and their associated directed graphs. Some of the drawbacks are:

- Aspects of the structure that may influence the properties of the system are completely ignored. For example, knowledge of the nonzero fixed entries is not used.
- There are properties (for instance stability) which cannot be handled with this model. Neither stability nor instability is a structural property.
- This model is based on a state-space model with a given order. All the parametric variations of the system that we accept are limited within this order.

In [19] the same authors investigate the generic solvability of the fault detection and iso-

lation problem for state-space systems. In this paper they provide necessary and sufficient conditions under which this problem has a solution for almost any values of the free parameters. These conditions are expressed in terms of input-output paths of the directed graph associated with the original LTI system (not the closed-loop LTI system associated with the residual error dynamical system). Investigating this directed graph provides good insight into the problem. We will discuss this paper further in Section 5.1.1.2, and later on in this section.

In both [38, 19] the authors stress that investigating the directed graph of the linear structured system is a useful modeling and analysis tool. They emphasize that this modeling technique allows one to get a number of important results based only on poor information of the system. Graph-theoretic conditions are furthermore intuitive and easy to check, by hand for small systems, and by means of well-known polynomially bounded combinatorial techniques for larger systems. These polynomial-bounded algorithms can be regarded as special, since in general, checking graph conditions can be NP-hard. The computational burden is thus low and allows us to deal with large-scale systems, especially when the system matrices are very sparse.

Our interest is in the use of graphical techniques to display system structure. Results on generic properties are of less interest, since our models don't typically have free parameters in the sense of [38, 19].

In [38, 19] the authors focus on state-space systems, but the swing model we have been studying is in DAE-form. One can follow the approach of expressing the DAE system in its equivalent state-space form, however, by doing so the structure in our problem is hidden and on top of this we lose degrees of design freedom when we design the observers using this equivalent state-space model (as we discussed in Section 3.2). We thus want to work with the structure-preserving DAE form, and by doing this we will also be able to establish connections between the structure of the network and the directed graph of the linear structured system.

Reinschke [57] investigated generic controllability of linear structured DAE systems and from his work it is evident that additional arcs are associated with entries in the M matrix. For the swing model considered in this thesis, these additional arcs help us to distinguish between differential and algebraic variables, but do not provide us with additional insight during the observer design process. We will elaborate on this observation when we introduce an example. Reinschke also illustrated the usefulness of using graphical design methods for multivariable control problems in his book [58].

In the next few sections we will show how one can design unknown-input observers by creating a desired directed graph of the linear structured error dynamics associated with the observer. What makes this observer design approach so attractive is the fact that the designed L can easily be updated by *extracting* certain values from linearized system matrices. This extraction from linear matrices, which can be accomplished by linearizing at each point along the system trajectory, makes this approach feasible for on-line, LPV-observer realization.

What we will illustrate is that one can design the observer gain elements by following a few simple rules and taking the network structure into consideration. The intuitive design approach makes it feasible to realize observers (not just for a swing model) on large-scale power systems without running into computational issues that are normally associated with the design of H_∞ filters for large DAE power-system models. Using this graphical observer-design approach, the observer can furthermore be made adaptable and can easily be reconfigured when measurements are lost (due to failures or bad data detection) or new measurements are incorporated. Because of these advantages, we advocate this type of observer design as a viable approach for large-scale power systems that operate at different operating points.

The design approach discussed in this section appears to be novel, to the best of the author's knowledge. Similar investigations for the dual problem, i.e., input-output decoupling and disturbance rejection for the control problem, have been covered by Reinschke in [58].

On the downside, this observer design approach will not provide us with performance guarantees in the presence of unmodeled dynamics and model uncertainty. If the latter two scenarios are encountered, it might be beneficial to use robust observer design theory such as H_∞ filtering, discussed earlier.

What sets our approach apart from the investigations in [19] is that when we discuss observer design in the following sections, we will draw the directed graph of the error dynamical system rather than the original system. The authors of [19] are concerned with analysis of the fault detection problem given a specific structured model, and are attempting to determine whether the FDI problem is solvable by merely investigating the directed graph of the original system (M, A, E, C). We on the other hand, want to solve a design problem.

4.1 Directed Graphs Associated with Linear Structured Systems

For the convenience of the reader we will briefly repeat the observer-based state estimation problem. The following system

$$M\dot{x} = Ax + Bu + Ew \tag{4.1}$$

$$y = Cx, \tag{4.2}$$

with: internal variables x; measurements y; and subject to unknown inputs (w), can be estimated using an observer of the form

$$M\dot{\widehat{x}} = A\widehat{x} + Bu + L(y - \widehat{y}) \tag{4.3}$$

$$\widehat{y} = C\widehat{x}, \tag{4.4}$$

where $\widehat{x}$ is the estimate of x, L is the designed-observer gain, and $\widehat{y}$ is the estimated version of y. Defining $e = x - \widehat{x}$ the resulting DAE-error system for this estimation problem has

the form

$$M\dot{e} = (A - LC)e + Ew \tag{4.5}$$

$$r = Qe, \tag{4.6}$$

where r is defined as residuals and we use $(M, A - LC, E, Q, D = 0)$ as shorthand notation for this DAE-error system. (We will drop $D = 0$ from the above shorthand for the rest of this thesis.)

We can associate a directed graph $\mathbf{G}(\mathbf{V}, \mathbf{Z})$ with the linearized version of the error dynamics given by Equation (3.26). For this system we have n internal variables in the DAE description; m unknown inputs (that can be divided into faults and disturbances); and p residuals (also the number of measurements of the original system). $\mathbf{V}$ denotes the set of vertices, and is obtained by forming $\mathbf{V} = \mathbf{E} \cup \mathbf{W} \cup \mathbf{R}$ where $\mathbf{E}, \mathbf{W}, \mathbf{R}$ are the error, unknown input and the residual variable sets denoted by $\{e_1, e_2, \cdots, e_n\}$, $\{w_1, w_2, \cdots, w_m\}$, $\{r_1, r_2, \cdots, r_p\}$. Thus the variables of the system description form the vertices of the directed graph.

The arc set $\mathbf{Z}$ is obtained by forming the union of $\mathcal{E}_b = \{(w_i, e_j)|E_{ji} \neq 0\}$, $\mathcal{E}_a = \{(e_i, e_j)|A_{ji} \neq 0\}$, $\mathcal{E}_m = \{(e_i, e_j)|M_{ji} \neq 0\}$, $\mathcal{E}_r = \{(e_i, r_j)|Q_{ji} \neq 0\}$, and $\mathcal{E}_{lc} = \{(e_i, e_j)|L_{j,:}C_{:,i} \neq 0\}$ (where $L_{j,:}$ represents row j of L and $C_{:,i}$ represents column i of C). The latter arc set comprises the so called feed-back arcs. We see that the associated edge weights can be obtained from the system matrices and are a function of the operating (linearization) point. In the studies discussed in [38], the authors are not concerned with these edge weights, whereas in this thesis we will use these values during observer design.

Due to the diagonal structure of M the set $\mathcal{E}_m$ will consists of self-cycles at the differential variable vertices. These additional loops do not provide us with extra insight into observer design and will be omitted in the directed graph examples shown in the following few sections. Also, whenever $Q = I$ we will not explicitly draw the $\mathcal{E}_r$ arcs.

4.2 Graphical Observer Design

4.2.1 Motivating Examples

We start this section by investigating the elementary example we introduced in Section 3.2. The underlying power system consists of one generator and one load, and the system matrices are given as:

$$A = \begin{bmatrix} 0 & 1 & 0 \\ -b & -d & b \\ b & 0 & -b \end{bmatrix}, E = \begin{bmatrix} 0 \\ 0 \\ 1 \end{bmatrix}, M = \begin{bmatrix} 1 & 0 & 0 \\ 0 & 1 & 0 \\ 0 & 0 & 0 \end{bmatrix}, C' = \begin{bmatrix} 0 \\ 0 \\ 1 \end{bmatrix}, L = \begin{bmatrix} l_1 \\ l_2 \\ l_3 \end{bmatrix}.$$

In Figure 4.1(a) the directed graph of the linear structured error-dynamical system $(M, A - LC, E, I)$ is shown, before values of L are assigned. In this figure $e_1 = \theta_1 - \widehat{\theta}_1$, $e_2 = \omega_1 - \widehat{\omega}_1$, and $e_3 = \theta_2 - \widehat{\theta}_2$. For this example we algebraically designed an observer gain in order to force a maximal number of zero entries in the transfer function matrix $G_{ew}(s)$, i.e., the transfer function from unknown inputs w to errors e to become zero. Substituting the elements of this DAE-designed L into Figure 4.1(a), we obtain Figure 4.1(b). From this figure we note that there are no forward paths from w to e_1 or e_2. We further note that there is a high-gain self-cycle at e_3, which gives us the ability to attenuate the unknown input to a desired level. In Figure 4.1(c) the state-space-designed observer case is considered. From this directed graph we notice that there are also no forward paths from w to e_1 or e_2; however the effect of the unknown input on e_3 cannot be attenuated to a desired level because $l_3 = 0$, as prescribed by state-space observer design.

Our second example is a little more complicated. Let us investigate a three-bus power system example, shown in Figure 4.2(a). The power system consists of one generator and two loads (2 differential variables — x_1, x_2 — and two algebraic variables — x_3, x_4). The directed graph of the linear-structured DAE model (M, A, E, I), is shown in Figure 4.2(b), and the system matrices are:

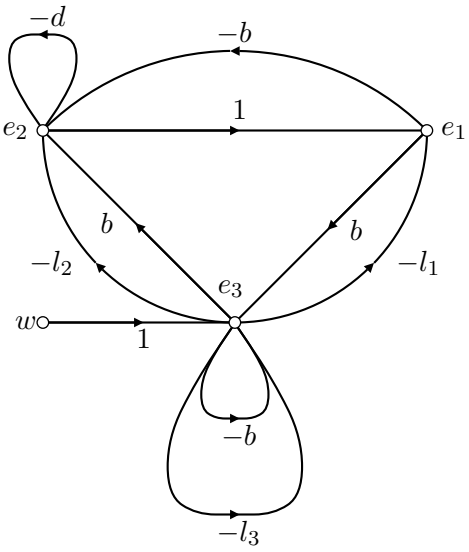

(a) Directed graph of structured error dynamics, with observer feedback arcs overlaid.

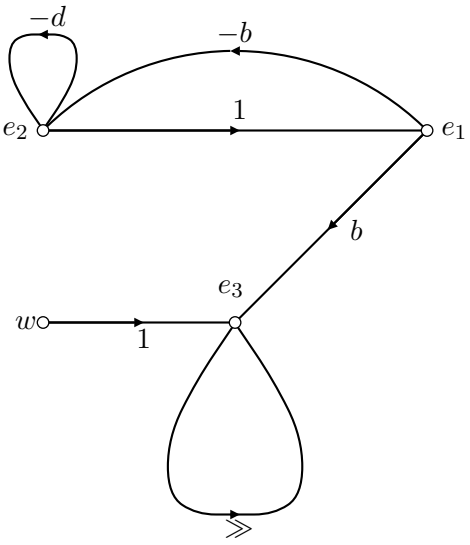

(b) Directed graph of DAE-designed structured error dynamics. ($l_1 = 0$, $l_2 = b$, $l_3 \gg$)

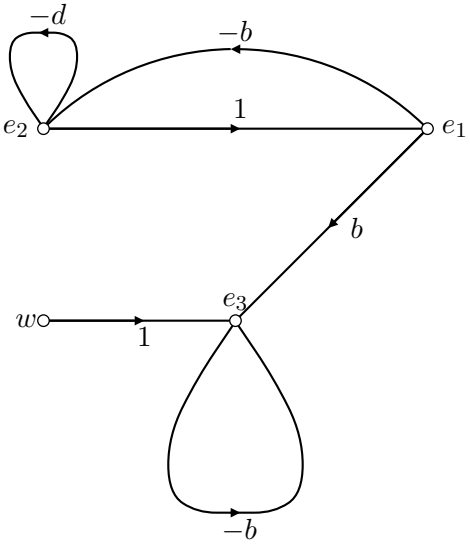

(c) Directed graph of state-space-designed structured error dynamics. ($l_1 = 0$, $l_2 = b$, $l_3 = 0$)

Figure 4.1: Design steps associated with observer design for unknown-input attenuation discussed in Example 3.2.1.

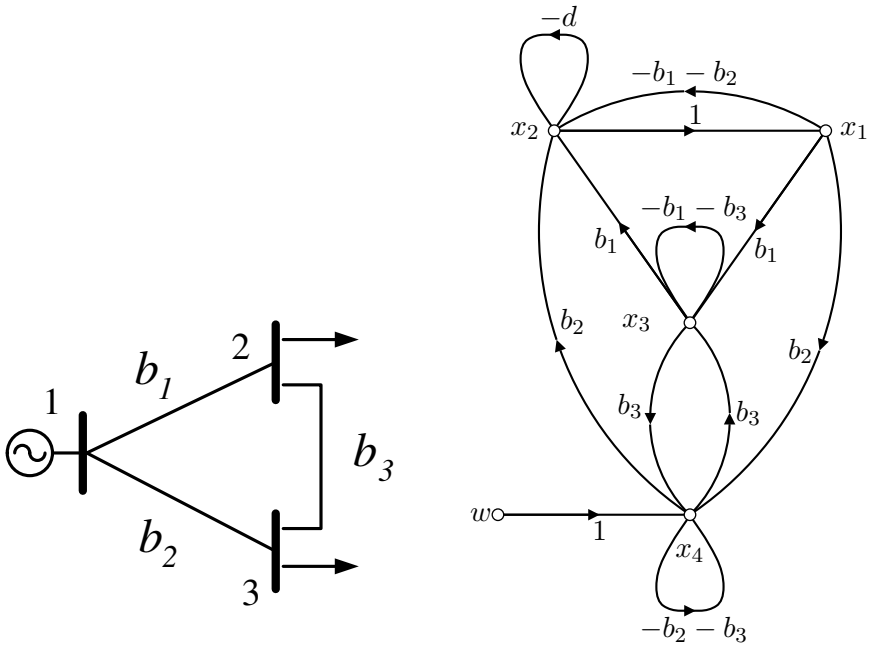

(a) Three-Bus power system.

(b) Directed graph of the structured DAE model.

Figure 4.2: Three-bus system and the associated directed graph of the linear structured system.

$$A = \begin{bmatrix} 0 & 1 & 0 & 0 \\ -b_1-b_2 & -d & b_1 & b_2 \\ b_1 & 0 & -b_1-b_3 & b_3 \\ b_2 & 0 & b_3 & -b_2-b_3 \end{bmatrix},\ E = \begin{bmatrix} 0 \\ 0 \\ 0 \\ 1 \end{bmatrix},\ M = \begin{bmatrix} 1 & 0 & 0 & 0 \\ 0 & 1 & 0 & 0 \\ 0 & 0 & 0 & 0 \\ 0 & 0 & 0 & 0 \end{bmatrix}.$$

For this example we place an angle measurement at bus 2, resulting in $C = \begin{bmatrix} 0 & 0 & 1 & 0 \end{bmatrix}$. The observer-design graph is shown in Figure 4.3(a), which depicts the directed graph $(M, A-LC, E, I)$ where $e_1 = \theta_1 - \widehat{\theta}_1$, $e_2 = \omega_1 - \widehat{\omega}_1$, $e_3 = \theta_2 - \widehat{\theta}_2$, and $e_4 = \theta_3 - \widehat{\theta}_3$. Our aim is to force as many entries as possible to zero in $G_{ew}(s)$ by an adequate choice of L. A sufficient choice is $L = \begin{bmatrix} 0 & b_1 & (-b_1-b_3) & l_4 \end{bmatrix}'$, and consequently $G_{ew}(s) = \begin{bmatrix} 0 & 0 & \frac{1}{l_4-b_3} & 0 \end{bmatrix}'$. The design result is shown in Figure 4.3(b).

From Figure 4.1(b) and Figure 4.3(b) we notice that in both instances signal flow paths in the respective $(M, A-LC, E, I)$-graphs were eliminated. We also ended up with a desirable

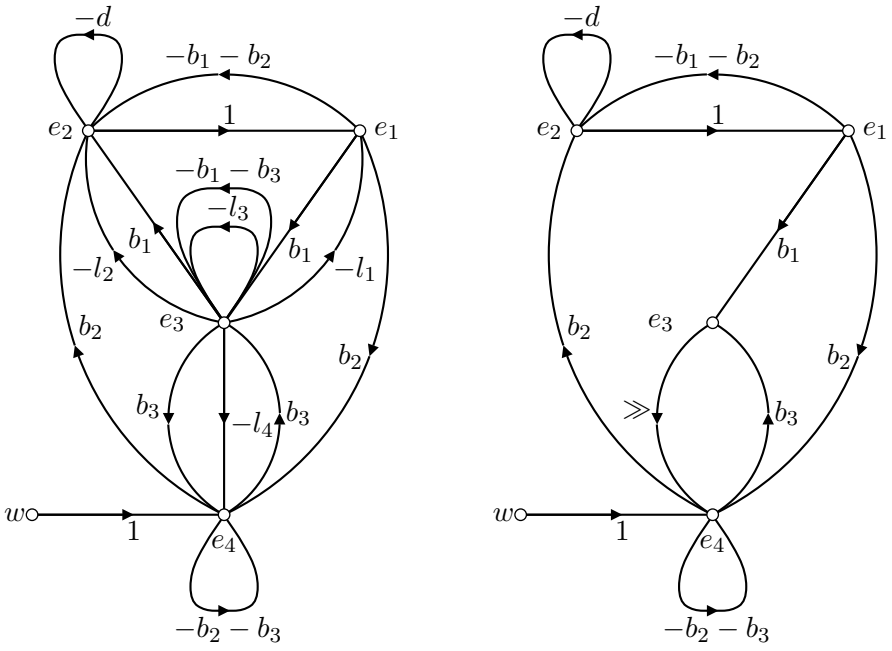

(a) Design Setup

(b) Designed Structured Error Dynamics

Figure 4.3: Graphical Observer Design with $C = \begin{bmatrix} 0 & 0 & 1 & 0 \end{bmatrix}$.

scenario of being able to achieve a designed level of attenuation of the driving w on all e-variables.

4.2.2 Design Approach

The two examples in the previous section hint that there might be more to the approach of eliminating forward paths in the directed graph of $(M, A - LC, E, I)$. Abstracting from these single-disturbance single-measurement examples, we might suggest the following design steps:

(a) Draw $\mathbf{G}(\mathbf{V}, \mathbf{W})$ for the error dynamical system $(M, A-LC, E, I)$ (the internal-variable vertex set of the DAE system is denoted by the set $\{e\}$);

(b) By assigning values of L, eliminate forward paths in $\mathbf{G}(\mathbf{V}, \mathbf{W})$ from the e-vertex where

the feedback arcs (i.e., $-LC$) originate (i.e., the measured state variables), except the forward paths to the e-vertices directly impacted by w (i.e., one hop away).

(c) Increase the edge weights of these latter forward paths to form high-gain arcs from the measurement site to the e-vertices directly influenced by the disturbance (i.e., one hop away from w).

The above design approach does not cover all possible cases. For instance, when we are dealing with a line-flow perturbation (i.e., two e vertices are dependently affected by the same perturbation), the two high-gain arcs we insert between the measurement site and these two e-vertices will necessarily end up being related to one another. One such example will be considered at the end of this section.

Next we will state a more general result than what the above design approach and examples suggest. The dual problem, disturbance rejection using full-state feedback control, is discussed by Reinschke on pages 82-87 of [58]. The theorem we will present in this section is not the dual extension of Reinscke's work, although his work served as inspiration.

Assumptions

We will first consider the case where the number of measurements, p, is larger than the number of unknown inputs, m, (i.e., $p \geq m$). We assume that the e-vertices of system are enumerated in order to yield $E = \begin{bmatrix} 0 \\ F \end{bmatrix}$, where $F \in \mathbb{R}^{q \times m}$ and q is defined as the number of e-vertices that are one hop away from an unknown input. Initially we assume that $q \geq m$. The case where $q < m$ will be discussed in Section 4.3.3. We will focus on systems for

which C may be written as $C = \left[\begin{array}{c} C_E \\ \hline C_\lambda \end{array}\right] = \left[\begin{array}{ccc} 0 & C_{E,b} & 0 \\ \hline C_{\lambda,a} & C_{\lambda,b} & C_{\lambda,c} \end{array}\right]$, where $C_E \in \mathbb{R}^{m\times n}$ and $C_\lambda \in \mathbb{R}^{(p-m)\times n}$. We have that $\left[\begin{array}{cc} C_{\lambda,a} & C_{\lambda,c} \end{array}\right] \in \mathbb{R}^{(p-m)\times(n-m)}$ and $C_{E,b} \in \mathbb{R}^{m\times m}$. The observer gain matrix is given by $L = \left[\begin{array}{c|c} L_E & L_\lambda \end{array}\right] = \left[\begin{array}{c|c} L_{0,E} & L_{0,\lambda} \\ \hline L_{1,E} & L_{1,\lambda} \end{array}\right]$, where $L_E \in \mathbb{R}^{n\times m}$, $L_\lambda \in \mathbb{R}^{n\times(p-m)}$, $L_{0,E} \in \mathbb{R}^{(n-q)\times m}$, $L_{1,E} \in \mathbb{R}^{q\times m}$, $L_{0,\lambda} \in \mathbb{R}^{(n-q)\times(p-m)}$, and $L_{1,\lambda} \in \mathbb{R}^{q\times(p-m)}$.

Let $\mathcal{A} = sM - A + LC$, which we split up into $\mathcal{A} = \mathcal{A}_E + \mathcal{A}_\lambda$. We define $\mathcal{A}_E = sM - A + L_E C_E$ and accounting for the partitioning of E and C_E, we can express

$$\mathcal{A}_E = \left[\begin{array}{ccc} \mathcal{A}_{0,a} & \mathcal{L}_{0,b} & \mathcal{A}_{0,c} \\ \mathcal{A}_{1,a} & \mathcal{L}_{1,b} & \mathcal{A}_{1,c} \end{array}\right].$$

Here $\mathcal{L}_{0,b} = (sM_{0,b} - A_{0,b} + L_{0,E}C_{E,b}) \in \mathbb{R}^{(n-q)\times m}$ and $\mathcal{L}_{1,b} = (sM_{1,b} - A_{1,b} + L_{1,E}C_{E,b}) \in \mathbb{R}^{q\times m}$, where $M = \left[\begin{array}{ccc} M_{0,a} & M_{0,b} & M_{0,c} \\ M_{1,a} & M_{1,b} & M_{1,c} \end{array}\right]$ and $A = \left[\begin{array}{ccc} A_{0,a} & A_{0,b} & A_{0,c} \\ A_{1,a} & A_{1,b} & A_{1,c} \end{array}\right]$. This choice of $\mathcal{A}_E$ leads to

$$\mathcal{A}_\lambda = L_\lambda C_\lambda = \left[\begin{array}{ccc} L_{0,\lambda}C_{\lambda,a} & L_{0,\lambda}C_{\lambda,b} & L_{0,\lambda}C_{\lambda,c} \\ L_{1,\lambda}C_{\lambda,a} & L_{1,\lambda}C_{\lambda,b} & L_{1,\lambda}C_{\lambda,c} \end{array}\right].$$

The general idea is that the blocks $\mathcal{L}_{0,b}$ and $\mathcal{L}_{1,b}$ will be used to attenuate the impact of the unknown inputs on the e-variables. The matrix $\mathcal{A}_\lambda$ will be used to move the poles of the closed-loop error system, after achieving the desired level of unknown input attenuation, and hence $\mathcal{A}_\lambda$ provides us with extra degrees of freedom. We can now state the following theorem.

THEOREM 4.1

For a system $(M, A - LC, E, I)$ satisfying all the assumptions given in the preceding paragraphs, the following structure can be enforced on $G_{ew}(s = 0)$:

$$G_{ew}(s = 0) = I(sM - A + LC)^{-1}E|_{s=0} = \begin{bmatrix} 0 \\ G_b(s = 0) \\ 0 \end{bmatrix}, \tag{4.7}$$

if we have:

(a) $\mathcal{L}_{0,b}|_{s=0} G_b(s = 0) = 0$;

(b) $\ker \begin{bmatrix} \mathcal{A}_{0,a} + L_{0,\lambda}C_{\lambda,a} & \mathcal{A}_{0,c} + L_{0,\lambda}C_{\lambda,c} \\ \mathcal{A}_{1,a} + L_{1,\lambda}C_{\lambda,a} & \mathcal{A}_{1,c} + L_{1,\lambda}C_{\lambda,c} \end{bmatrix} |_{s=0} = \emptyset$;

(c) $\begin{bmatrix} L_{0,\lambda} \\ L_{1,\lambda} \end{bmatrix} C_{\lambda,b} = 0.$

(d) $\mathcal{L}_{1,b}|_{s=0} G_b(s = 0) = F.$

Proof. Pre-multiplying both sides of the expression $G_{ew}(s) = I\mathcal{A}^{-1}E$ by $\mathcal{A} = sM - A + LC$ yields the following set of linear equations:

$$\mathcal{A}G_{ew}(s) = E. \tag{4.8}$$

With the partitioning $G_{ew}(s) = \begin{bmatrix} G_a'(s) & G_b'(s) & G_c'(s) \end{bmatrix}'$, and developing the submatrix multiplications in the preceding equation the following sets of linear equations are obtained:

$$\underbrace{\begin{bmatrix} \mathcal{A}_{0,a} + L_{0,\lambda}C_{\lambda,a} & \mathcal{A}_{0,c} + L_{0,\lambda}C_{\lambda,c} \end{bmatrix}}_{\mathcal{B}_0} \underbrace{\begin{bmatrix} G_a(s) \\ G_c(s) \end{bmatrix}}_{G_0(s)} + (\mathcal{L}_{0,b} + L_{0,\lambda}C_{\lambda,b})\, G_b(s) = 0; \quad (4.9)$$

$$\underbrace{\begin{bmatrix} \mathcal{A}_{1,a} + L_{1,\lambda}C_{\lambda,a} & \mathcal{A}_{1,c} + L_{1,\lambda}C_{\lambda,c} \end{bmatrix}}_{\mathcal{B}_1} \underbrace{\begin{bmatrix} G_a(s) \\ G_c(s) \end{bmatrix}}_{G_0(s)} + (\mathcal{L}_{1,b} + L_{1,\lambda}C_{\lambda,b})\, G_b(s) = F, \quad (4.10)$$

where $\mathcal{B}_0 \in R^{(n-q)\times(n-m)}$ and $\mathcal{B}_1 \in R^{(q)\times(n-m)}$. We group (4.9) and (4.10) together to form:

$$\begin{bmatrix} \mathcal{B}_0 \\ \mathcal{B}_1 \end{bmatrix} G_0(s) + \begin{bmatrix} \mathcal{L}_{0,b} \\ \mathcal{L}_{1,b} \end{bmatrix} G_b(s) + \begin{bmatrix} L_{0,\lambda} \\ L_{1,\lambda} \end{bmatrix} C_{\lambda,b} G_b(s) = \begin{bmatrix} 0 \\ F \end{bmatrix} \quad (4.11)$$

Investigating conditions (a), (c) and (d), we notice that we need to evaluate (4.11) at $s = 0$ due to our restriction that the observer gain elements remain real.

Accounting for conditions (a), (c) and (d) from the theorem statement and evaluating

Equation (4.11) at $s = 0$ yields:

$$\begin{bmatrix} \mathcal{B}_0 \\ \mathcal{B}_1 \end{bmatrix} |_{s=0} G_0(s=0) = \begin{bmatrix} 0 \\ 0 \end{bmatrix}, \tag{4.12}$$

and from condition (b) we conclude that $G_0(s = 0) = 0$, implying that

$$G_{ew}(s=0) = \begin{bmatrix} 0 \\ G_b(s=0) \\ 0 \end{bmatrix}.$$

□

Discussion

Requirement (a) in the theorem statement can be satisfied if we set $\mathcal{L}_{0,b}|_{s=0} = (sM_{0,b} - A_{0,b} + L_{0,E}C_{E,b})|_{s=0} = 0$. This implies that we eliminate all the entries in this matrix and thus set $L_{0,E}C_{E,b} = A_{0,b}$. Interpreting this action graphically on the directed graph of $(M, A - LC, E, I)$ translates to cutting the forward paths from the measurement site to all the e-vertices that are not directly influenced by unknown inputs (i.e., the 0 block of E).

To obtain $\mathcal{L}_{1,b}$ we partition $F = \begin{bmatrix} F_R \\ F_Z \end{bmatrix}$ and correspondingly $\mathcal{L}_{1,b} = \begin{bmatrix} \mathcal{L}_R \\ \mathcal{L}_Z \end{bmatrix}$. The R subscript implies that the matrix is in $\mathbb{R}^{m\times m}$ and the Z subscript implies $\mathbb{R}^{(q-m)\times m}$. From condition (d) of Theorem 4.1 we have $\mathcal{L}_R|_{s=0}G_b(s = 0) = F_R$, and by defining the desired

level of attenuation for the elements of $G_b(s=0)$ we can find the elements of $\mathcal{L}_R|_{s=0}$ (note that $G_b(s)$ is invertible). To find $\mathcal{L}_Z|_{s=0}$ we use the relationship $\mathcal{L}_Z|_{s=0}G_b(s)|_{s=0} = F_Z$, and for F_R invertible we have $\mathcal{L}_Z|_{s=0} = F_Z F_R^{-1}\mathcal{L}_R|_{s=0}$.

Illustrative Example

We will investigate the 3-bus power system example we discussed at the beginning of this section. Let $C = \begin{bmatrix} 0 & 0 & 1 & 0 \\ 1 & 0 & 0 & 0 \end{bmatrix}$ and $E = \begin{bmatrix} 0 & 0 & \kappa_1 & \kappa_2 \end{bmatrix}'$, hence we have $m = 1$, $q = 2$, and $p = 2$. The structure of E is indicative of a line-flow perturbation (see Section 2.7.3). We split $\mathcal{A}$ up into

$$\mathcal{A}_E = \left[\begin{array}{cc|c|c} s & -1 & l_{11} & 0 \\ b_1+b_2 & s+d & -b_1+l_{21} & b_2 \\ \hline -b_1 & 0 & +b_1+b_3+l_{31} & -b_3 \\ -b_2 & 0 & -b_3+l_{41} & b_2+b_3 \end{array}\right], \text{ and } \mathcal{A}_\lambda = \left[\begin{array}{cc|c|c} l_{12} & 0 & 0 & 0 \\ l_{22} & 0 & 0 & 0 \\ \hline l_{32} & 0 & 0 & 0 \\ l_{42} & 0 & 0 & 0 \end{array}\right].$$

In order to satisfy condition (a) of Theorem 4.1 we set $\mathcal{L}_{0,b}|_{s=0} = 0$, by choosing $l_{11} = 0$ and $l_{21} = b_1$.

Testing condition (b) of Theorem 4.1, we construct

$$\begin{bmatrix} \mathcal{B}_0 \\ \mathcal{B}_1 \end{bmatrix} = \left[\begin{array}{ccc} s+l_{12} & -1 & 0 \\ b_1+b_2+l_{22} & s+d & b_2 \\ \hline -b_1+l_{32} & 0 & -b_3 \\ -b_2+l_{42} & 0 & b_2+b_3 \end{array}\right],$$

from which we see that the nullspace of the above matrix is empty at $s=0$ when: $l_{12} \neq 0$, $l_{22} \neq -b_1$, $l_{32} \neq b_1 - b_3$ in combination with $l_{42} \neq 2b_2 + b_3$; or $l_{12} \neq 0$, $l_{22} \neq -2b_2 - b_1$, $l_{32} \neq b_1 + b_3$ in combination with $l_{42} \neq -b_3$, as required. Thus we have placed modest restrictions on the values that L_λ can take.

We note that condition (c) of Theorem 4.1 is also satisfied and that $L_\lambda C_{\lambda,b} = 0$.

In order to complete the unknown-input attenuation design we need to find $\mathcal{L}_{1,b}|_{s=0}$. By Setting $G_b(s=0) = \frac{\kappa_1}{b_1+b_3+l_{31}}$ we deduce that $\mathcal{L}_R = b_1 + b_3 + l_{31}$ and that $\mathcal{L}_Z = \kappa_2\kappa_1^{-1}(b_1 + b_3 + l_{31})$. However, $\mathcal{L}_Z = -b_3 + l_{41}$, from which we can back out what we need l_{41} to be as a function of l_{31} (our design parameter used to manipulate $G_b(s=0)$).

Thus, in order to enforce $G_{ew}(s) = \begin{bmatrix} 0 & 0 & \frac{\kappa_1}{b_1+b_3+l_{31}} & 0 \end{bmatrix}$, we need to set $l_{11} = 0$, $l_{21} = b_1$, $l_{41} = \frac{b_1\kappa_2 + b_3(\kappa_1+\kappa_2) + \kappa_2 l_{31}}{\kappa_1}$ (note we did not require $s=0$, because we measured an algebraic variable). From this example we also note that we still have four degrees of freedom (l_{12}, l_{22}, l_{32} and l_{42}) to move the poles of $(M, A-LC)$, however, we have some restrictions on what these values can be.

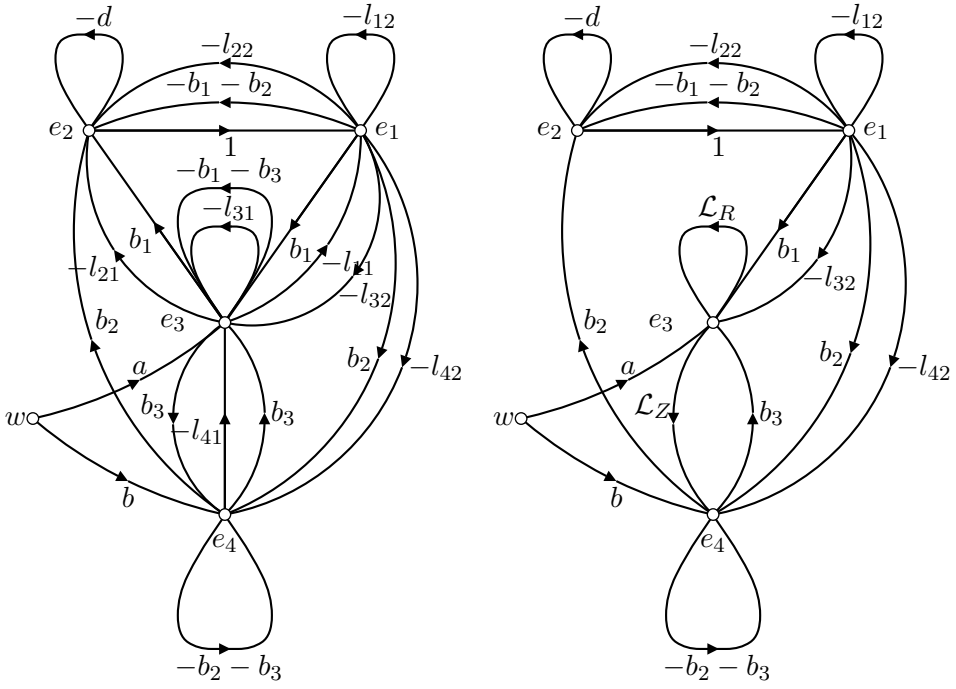

(a) Design Setup

(b) Designed Structured Error Dynamics

Figure 4.4: Graphical Observer Design with $C = \begin{bmatrix} 0 & 0 & 1 & 0 \\ 1 & 0 & 0 & 0 \end{bmatrix}$.

In Figure 4.4(a) the directed graph of $(M, A - LC, E, I)$ is shown before we assigned the values of L_E. In Figure 4.4(b) we show the directed graph of $(M, A - LC, E, I)$ after L_E was designed to achieve unknown-input attenuation. Notice that we cut the forward paths from e_3 to other e-vertices not directly influenced by w (i.e., forward paths from e_3 to e_1 and e_2). In this figure we show the high-gain arcs from e_3 to e_3, namely $\mathcal{L}_R$, and from e_3 to e_4, namely $\mathcal{L}_R$.

4.3 Measurement Placement, Type and Number

The different measurements that are available for observer design can be tested using this graphical-design approach. In this section we will discuss issues related to measurement placement, the type of measurements available for observer realization as well as the number of measurements necessary to achieve a designed level of w attenuation on the e-variables.

4.3.1 Measurement Placement

In this section we confine ourselves to only consider single measurement, single disturbance cases. We will investigate measurement placement on the three-bus power system shown in Figure 4.2(a), as well as the nine-bus power system example given in Figure 3.1.

Three-Bus Example

We investigate measurement placement of direct angle sensors. The unknown input is

assumed to be an unknown load change at bus 3 (i.e., $E = \begin{bmatrix} 0 & 0 & 0 & 1 \end{bmatrix}'$). The three possible sensor sites are at bus 1, 2 or 3. With the observer design we will aim to achieve a designed level of attenuation from the driving unknown input. Thus we want to be able to control all entries of $G_{ew}(s)$, as we discussed in Theorem 4.1.

Let us consider placing the angle measurement at bus 1. The directed graph depicting the observer design setup is shown in Figure 4.5(a). Following our design approach discussed in Section 4.2.2, we choose $L = \begin{bmatrix} 0 & (-b_1 - b_2) & b_1 & l_4 \end{bmatrix}'$ and the result of the design is shown in Figure 4.5(b). For this design, the transfer function matrix from w to e is found to be

$$G_{ew}(s) = \frac{\begin{bmatrix} 1 & s & \frac{b_3 s(d+s)}{b_2 b_3 + b_1(b_2+b_3)} & \frac{(b_1+b_3)s(d+s)}{(b_2 b_3 + b_1(b_2+b_3))} \end{bmatrix}'}{-b_2 + l_4 + s(d+s)}. \tag{4.13}$$

Using the final-value theorem we find the steady-state error response of the observer to a step input change, i.e., $G_{ew}(s=0) = \begin{bmatrix} \frac{1}{l_4 - b_2} & 0 & 0 & 0 \end{bmatrix}'$. By choosing l_4 to be large we can attenuate the effect of the unknown input to a desired level. We notice from $G_{ew}(s)$ in (4.13) that there are dynamics in the errors, and this is attributed to the use of a dynamic-variable measurement in the realization of this observer.

We notice from Figure 4.5(b) that the directed graph of the designed error dynamics has two cycles from e_4 to e_4 (i.e., closed paths in the graph: $e_4 \to e_2 \to e_1 \to e_4$ and $e_4 \to e_3 \to e_2 \to e_1 \to e_4$, ignoring self-cycles) and the shortest path consists of 3 hops.

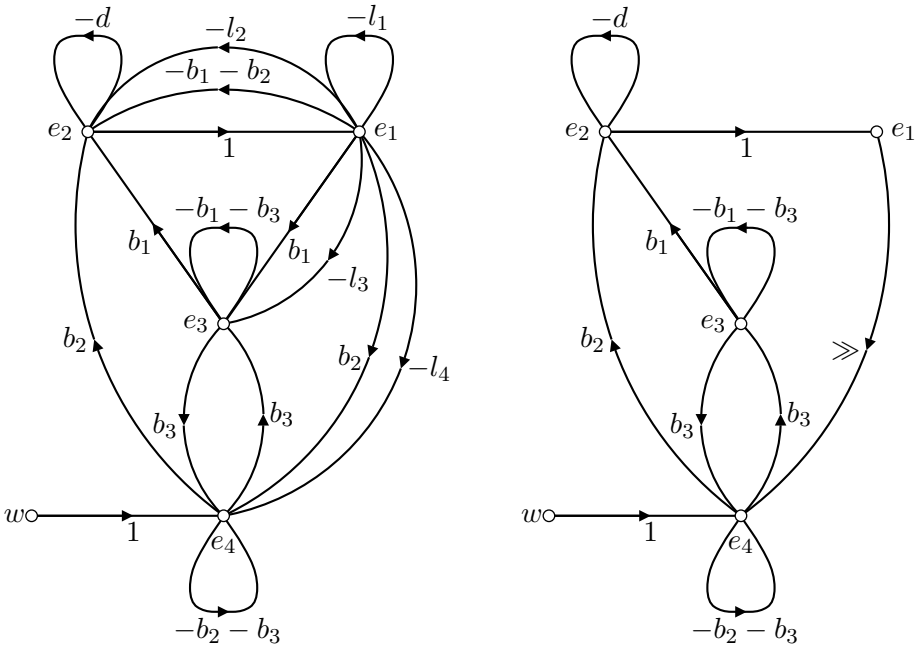

(a) Design Setup

(b) Designed Structured Error Dynamics

Figure 4.5: Graphical Observer Design with $C = \begin{bmatrix} 1 & 0 & 0 & 0 \end{bmatrix}$.

The case when we measure the angle at bus 2 (i.e., $C = \begin{bmatrix} 0 & 0 & 1 & 0 \end{bmatrix}$) has already been discussed. The directed-graph illustrating the design setup is shown in Figure 4.3(a), with the design result shown in Figure 4.3(b). From Figure 4.3(b), we notice that the designed directed graph of the error dynamics have three cycles from e_4 to e_4 (i.e., paths $e_4 \rightarrow e_2 \rightarrow e_1 \rightarrow e_4$, $e_4 \rightarrow e_2 \rightarrow e_1 \rightarrow e_3 \rightarrow e_4$, and $e_4 \rightarrow e_3 \rightarrow e_4$) and the shortest path consists of 2 hops.

Our last possible direct angle sensor site is bus 3, and for this case $C = \begin{bmatrix} 0 & 0 & 0 & 1 \end{bmatrix}$. The associated directed-graph design setup is shown in Figure 4.6(a). Following the graphical-observer design approach we obtain $L = \begin{bmatrix} 0 & b_2 & b_3 & l_4 \end{bmatrix}'$ and the design result is shown in Figure 4.6(b). We find the transfer function matrix from w to e to be

$$G_{ew}(s) = \begin{bmatrix} 0 & 0 & 0 & \frac{1}{b_2+b_3+l_4} \end{bmatrix}' \tag{4.14}$$

(note that s is absent here, because we use an algebraic-variable measurement in the observer realization). Analyzing the designed directed graph shown in Figure 4.6(b), we notice that there are no cycles going from e_4 to e_4, but only the self-cycle at e_4.

A designer might want to keep small the length of the shortest cycle, from (and to) the unknown input whose effect on the e-variables is to be attenuated, in the designed directed graph. However, in this thesis we will not investigate whether there is a link between keeping the cycles short and the performance of the observer.

Nine-Bus Example

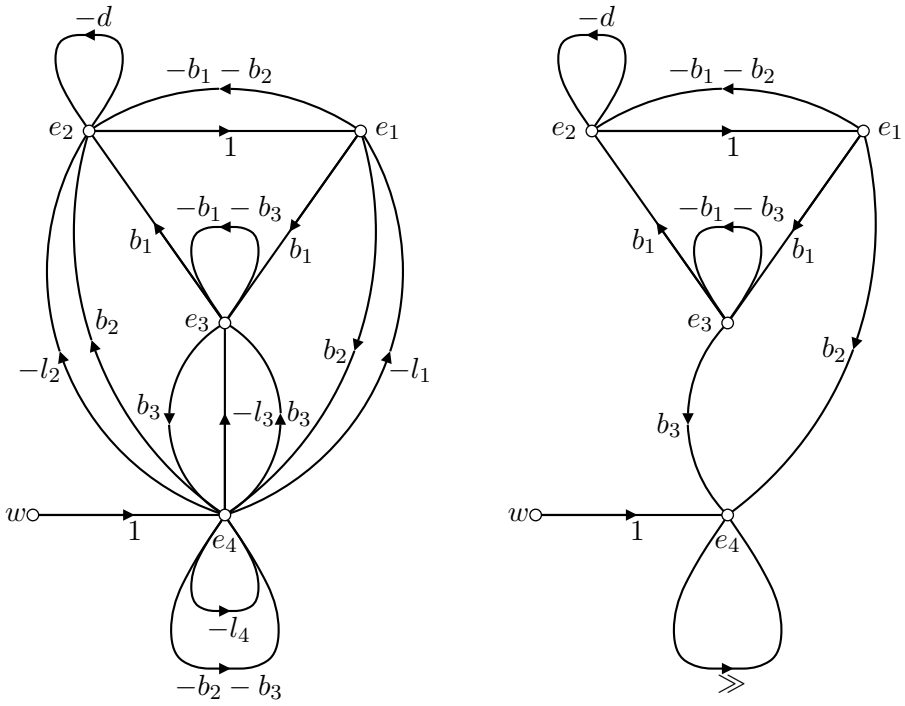

(a) Design Setup

(b) Designed Structured Error Dynamics

Figure 4.6: Graphical Observer Design with $C = \begin{bmatrix} 0 & 0 & 0 & 1 \end{bmatrix}$.

In this part we will demonstrate how we can design observers for the nine-bus power system shown in Figure 3.1. We will not attempt to draw the directed graph of this system, but will illustrate the design process using plots of the structure of the A and $A-LC$ matrices.

In this example we will compare the performance of two different observers. We assume that there is a single unknown input in the form of an unknown load change at bus 8. The first observer (abbreviated as 'Obs 1') uses an angle measurement taken at bus 4. The second observer ('Obs 2') uses an angle measurement taken at bus 8. From Figure 3.1 we notice that the measurement used in the realization of Obs 1 is far removed from the unknown input, and hence we anticipate that the shortest cycle in the directed graph of the designed, structured error dynamics will be longer than the shortest cycle in the designed directed graph of Obs 2.

Designing the observer gain for Obs 1 involves setting 5 gain elements in L (the rest of the entries will be zero). Four of these gain elements are indicated in Figure 4.7(a) and the fifth, L_{11}, is chosen large to create a high-gain path from $e_7(=\theta_4-\widehat{\theta}_4)$ to $e_{11}(=\theta_8-\widehat{\theta}_8)$. Thus we have eliminated (and we will not show this graphically) all forward arcs from e_7, and then inserted only one high-gain arc from e_7 directly to e_{11} (the e-vertex directly impacted by the unknown input).

Designing the observer gain of Obs 2 requires us to set three gain elements. In Figure 4.8(a) the structure of A for the nine-bus system is shown. In this figure we point out two gain elements that will feature in L. The third gain element, L_{11}, is chosen to be large in order to attenuate the effect of the unknown input. Gain elements L_{10} and L_{12} eliminate

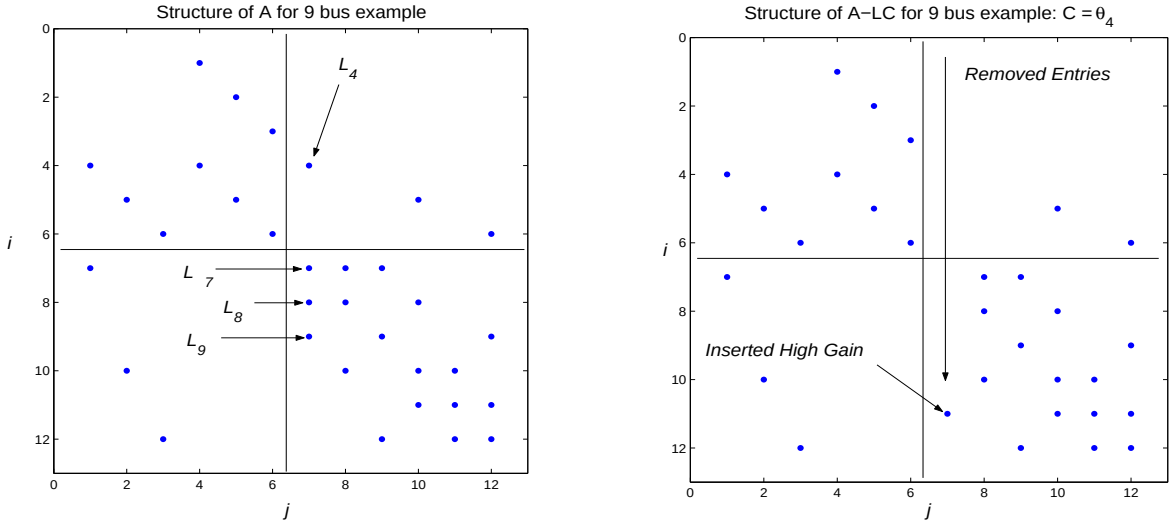

(a) Structure of A and nonzero elements of L

(b) Structure of $A - LC$

Figure 4.7: Observer 1 design steps.

transmission paths from e_{11} to any other vertices in the directed graph. For this designed observer there are no cycles from e_{11} to e_{11} (except the self-cycle at e_{11}).

In Figures 4.9(a) – 4.10(b), time responses of state estimates provided by both observers are compared to the variables of the actual system in response to an unknown load change at bus 8 ($2p.u.$ during $t \in [0.1s, 4s]$). We have introduced some parametric model uncertainty into the system model. We assumed that the parameters of the system are randomly perturbed by 10% (using a uniform distribution) around their associated nominal values. Nominal values were used for the realization of both observers.

From Figures 4.9(a) – 4.10(b) we note that both observers perform well. It appears as if Obs 2 performs marginally better than Obs 1. This observation coupled with the ease of

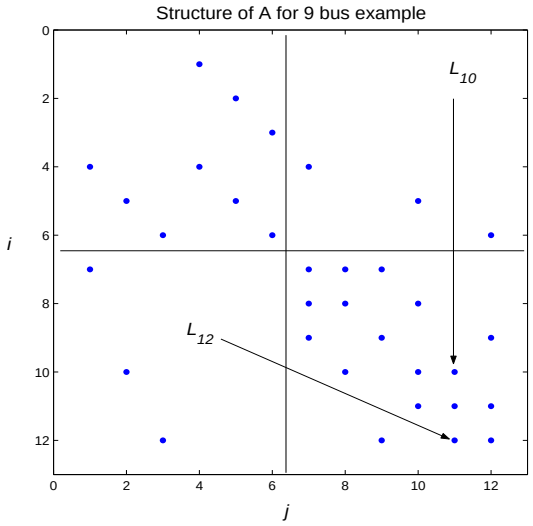

(a) Structure of A and nonzero elements of L

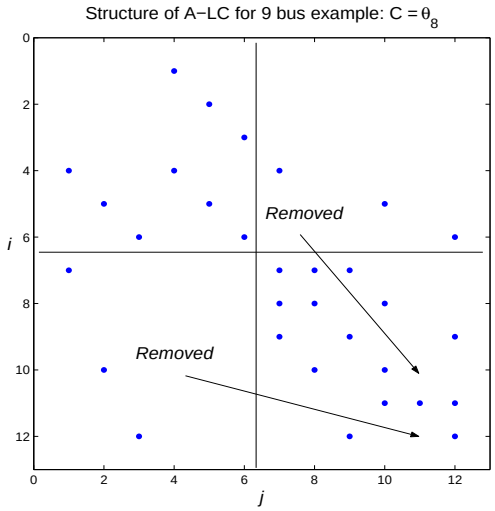

(b) Structure of $A - LC$

Figure 4.8: Observer 2 design steps.

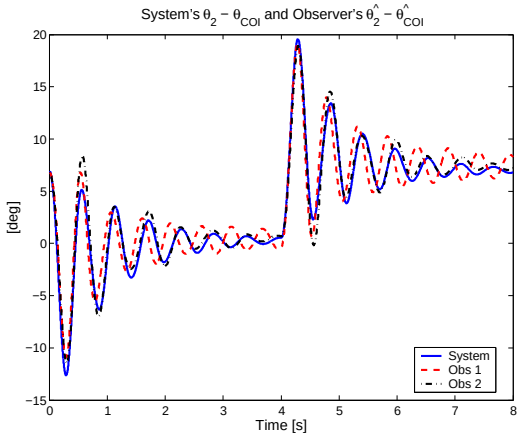

(a) $\theta_2 - \theta_{coi}$

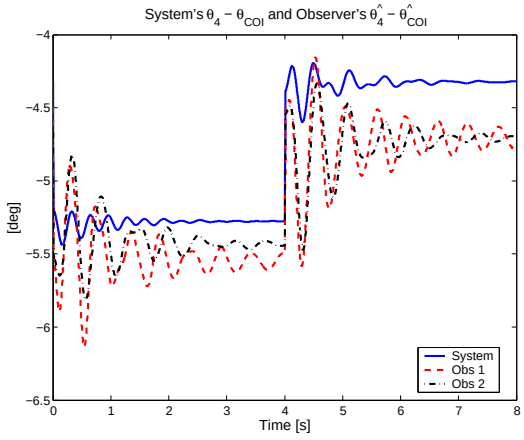

(b) $\theta_4 - \theta_{coi}$

Figure 4.9: Time plots of the system, and two observer evolutions in response to a $2p.u.$ unknown load change at bus 8 during $t \in [0.1s, 4s]$.

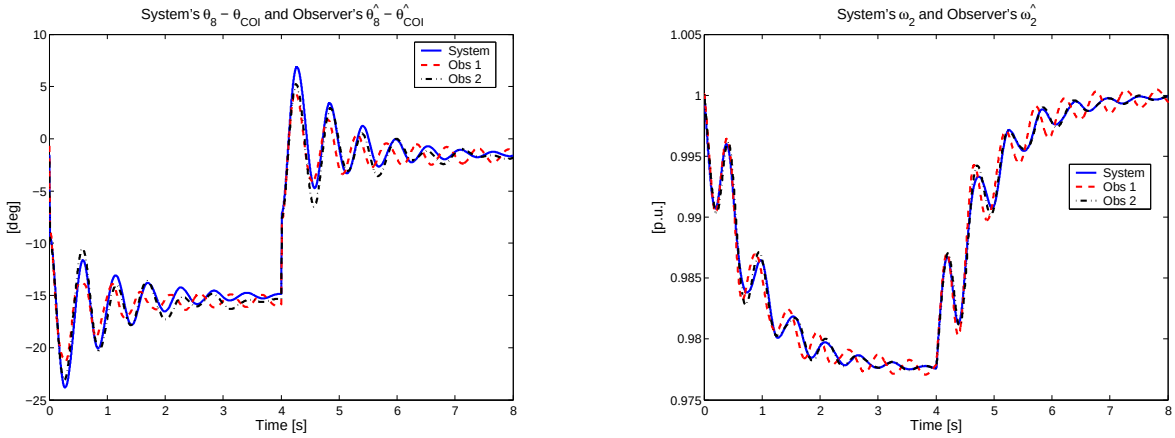

(a) $\theta_8 - \theta_{coi}$ (b) ω_2

Figure 4.10: Time plots of the system, and two observer evolutions in response to a $2p.u.$ unknown load change at bus 8 during $t \in [0.1s, 4s]$.

design associated with Obs 2 hints that it might be beneficial to have the measurement site in close proximity of the location of the unknown input.

4.3.2 Measurement Type

Let us expand our investigations and consider different types of measurements. In this section we will illustrate these types of investigations once again on our three-bus model, shown in Figure 4.2(a). The aim of this section is to illustrate how one would study the use of different types of measurements. We do not change the type of unknown input, and the type of measurements we have not considered yet are: machine speeds; angle differences (equivalent to power flow measurements on individual lines); and power flowing into the network at a particular bus.

We will not present an exhaustive study on the different types of measurements and their possible placements, but rather illustrate how similar studies can be approached.

Three-Bus Example

We start out with measuring the speed of the generator, i.e., $C = \begin{bmatrix} 0 & 1 & 0 & 0 \end{bmatrix}$. In Figure 4.11(a) we illustrate the directed graph for the design setup. Choosing $L = \begin{bmatrix} 1 & -d & 0 & l_4 \end{bmatrix}'$ we obtain the directed graph given in Figure 4.11(b). The transfer function matrix from w to e in this case is

$$G_{ew}(s) = \begin{bmatrix} 0 & \frac{1}{s+l_4} & \frac{b_3 s}{(s+l_4)(b_2b_3+b_1(b_2+b_3))} & \frac{(b_1+b_3)s}{(s+l_4)(b_2b_3+b_1(b_2+b_3))} \end{bmatrix}', \tag{4.15}$$

from which we notice that the system only has one pole that appears in $G_{ew}(s)$. WE know that we should expect two poles, thus we know that one pole and zero must have cancelled in all the three nonzero elements of $G_{ew}(s)$.

If we consider the the steady-state error associated with this observer in response to an unknown step input, we find that

$$G_{ew}(s) \longrightarrow \begin{bmatrix} 0 & \frac{1}{l_4} & 0 & 0 \end{bmatrix}' \text{ as } s \to 0. \tag{4.16}$$

Cutting the forward path from e_2 to e_1 introduces a row of zeros in the A matrix, and hence A drops rank and the resulting closed-loop error dynamics will have an additional eigenvalue at zero.

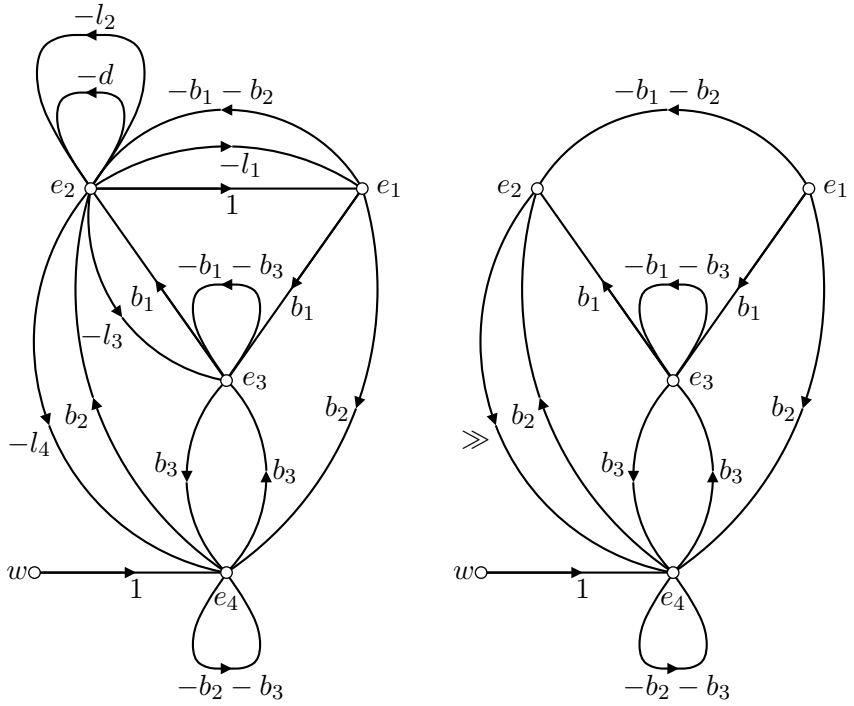

(a) Design Setup

(b) Designed Structured Error Dynamics

Figure 4.11: Graphical Observer Design with $C = \begin{bmatrix} 0 & 1 & 0 & 0 \end{bmatrix}$.

We now move on to investigating an angle difference measurement or a power flow measurement on a transmission line. The latter is a linear function of the angular difference across the line, hence a power flow measurement and its corresponding angle difference measurement are structurally equivalent. The angular difference measurement we investigate in Figure 4.12(a) is $\theta_1 - \theta_3$. We note that $C = \begin{bmatrix} 1 & 0 & -1 & 0 \end{bmatrix}$ violates our assumption in the buildup to Theorem 4.1 that $C_E = \begin{bmatrix} 0 & C_{\mathcal{L}} & 0 \end{bmatrix}$ where we assumed that $C_{\mathcal{L}}$ is square.

From Figure 4.12(a) it is not straightforward to decide which paths to cut. Performing a change of variables[1] so that $e_{new} = \begin{bmatrix} e_1 & e_2 & (e_1 - e_3) & e_4 \end{bmatrix}$ which modifies C to becomes $C_{new} = \begin{bmatrix} 0 & 0 & 1 & 0 \end{bmatrix}$, the matrix $\mathcal{A}(= sM - A + LC)$ is transformed to

$$\mathcal{A}_{new} = \left[\begin{array}{cc|c|c} s & 1 & -l_1 & 0 \\ -b_2 & s-d & -b_1 - l_2 & b_2 \\ -b_3 & 0 & b_1 + b_3 - l_3 & b_3 \\ \hline b_2 + b_3 & 0 & -b_3 - l_4 & -b_2 - b_3 \end{array}\right], \tag{4.17}$$

from which is clear that we want to choose $L = \begin{bmatrix} 0 & -b_1 & b_1 + b_3 & l_4 \end{bmatrix}'$. For this choice of L we obtain the the transfer function matrix from w to e to be

$$G_{ew}(s) = \begin{bmatrix} 0 & 0 & \frac{-1}{b_3 + l_4} & 0 \end{bmatrix}', \tag{4.18}$$

[1]The transformation matrix $T = \begin{bmatrix} 1 & 0 & 0 & 0 \\ 0 & 1 & 0 & 0 \\ 1 & 0 & -1 & 0 \\ 0 & 0 & 0 & 1 \end{bmatrix}$ is used and we have $e_{new} = T^{-1}e$ and $C_{new} = CT$.

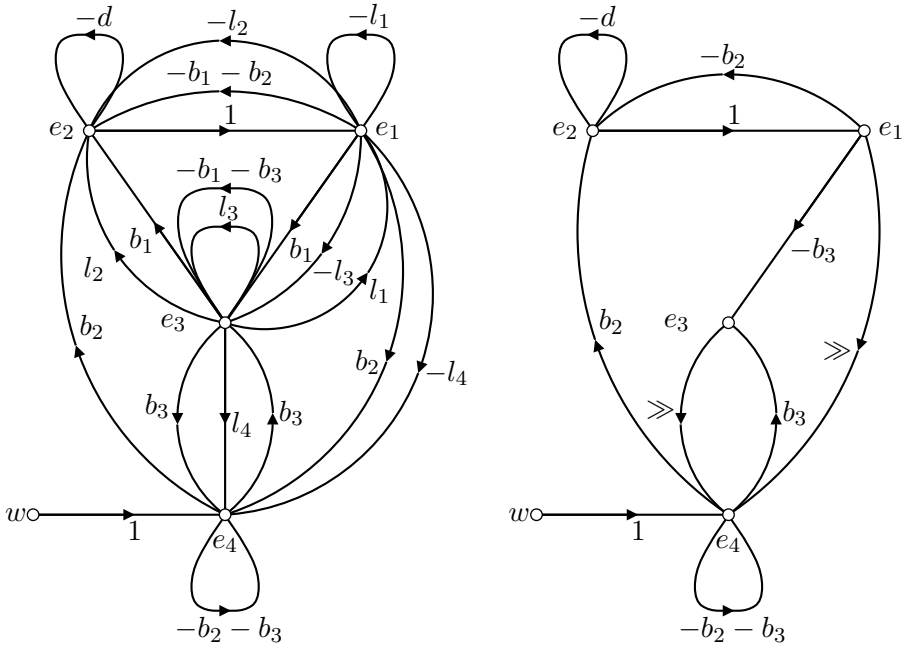

(a) Design Setup

(b) Designed Structured Error Dynamics

Figure 4.12: Graphical Observer Design with $C = \begin{bmatrix} 1 & 0 & -1 & 0 \end{bmatrix}$.

and in Figure 4.12(b) the designed directed graph for the current choice of L is shown.

The above choice of L is not the only choice that can yield a designed level of w-attenuation on e. For instance, suppose we change the internal-variables[2] such that $C_{new} = \begin{bmatrix} 1 & 0 & 0 & 0 \end{bmatrix}$

[2]The transformation matrix $T = \begin{bmatrix} 1 & 0 & 1 & 0 \\ 0 & 1 & 0 & 0 \\ 0 & 0 & 1 & 0 \\ 0 & 0 & 0 & 1 \end{bmatrix}$ is used.

and $e_{new} = \begin{bmatrix} (e_1 - e_3) & e_2 & e_3 & e_4 \end{bmatrix}$ and for this we find that

$$\mathcal{A}_{new} = \left[\begin{array}{c|ccc} s - l_1 & 1 & 0 & 0 \\ -b_1 - b_2 - l_2 & s - d & -b_2 & b_2 \\ b_1 - l_3 & 0 & -b_3 & b_3 \\ \hline b_2 - l_4 & 0 & b_2 + b_3 & -b_2 - b_3 \end{array}\right], \tag{4.19}$$

and following our design approach we choose $L = \begin{bmatrix} 0 & -b_1 - b_2 & b_1 & l_4 \end{bmatrix}'$ yielding

$$G_{ew}(s) = \begin{bmatrix} 0 & 0 & \frac{1}{b_2 - l_4} & \frac{1}{b_2 - l_4} \end{bmatrix}'. \tag{4.20}$$

We notice that even though we were not able to enforce the structure as given in Theorem 4.1, we still ended up with a desirable scenario of being able to manipulate the nonzero entries of $G_{ew}(s = 0)$ to a specified level by changing l_4. This positive outcome suggests that Theorem 4.1 should be revisited.

One interesting observation is that when we extract $\begin{bmatrix} \mathcal{B}_0 \\ \mathcal{B}_1 \end{bmatrix}$ from (4.17) we notice that its nullspace is nonempty when $s = 0$, but empty when $s \neq 0$. Extracting the same matrix from (4.19) we notice that its nullspace is nonempty for all s. This might be the reason why we can enforce the structure of Theorem 4.1 in (4.18) but not in (4.20).

Similar studies can be done for the angular difference measurements $\theta_1 - \theta_4$ and $\theta_2 - \theta_3$, but will not be shown here. From Figure 4.12(b) we notice that the graph structure looks similar

to the graph structure in 4.3(b). The only difference now is that we have two high-gain arcs — e_1 to e_4 and e_3 to e_4.

Measuring the power flow into the network at a particular bus can possibly provide a designer with a lot of dependent feedback arcs in the directed graph (number of arcs is a function of the number of transmission lines connected at the bus where the measurement is taken). Suppose, for our three-bus example, we measure the power flowing into the network at bus 1. We are thus measuring $P_{12}(\theta) + P_{13}(\theta) = \begin{bmatrix} b_1 + b_2 & 0 & -b_1 & -b_2 \end{bmatrix} \widetilde{x}$. This type of measurement is structurally equivalent to having $C = \begin{bmatrix} 2 & 0 & -1 & -1 \end{bmatrix}$. Using this structural equivalent measurement for observer design, we find the observer-design setup shown in Figure 4.13(a), and taking $L = \begin{bmatrix} 0 & -b_2 & -b_3 & l_4 \end{bmatrix}'$ results in the directed graph shown in Figure 4.13(b). The transfer function matrix from w to e for this design is

$$G_{ew}(s) = \begin{bmatrix} 0 & 0 & 0 & \frac{-1}{b_2+b_3-l_4} \end{bmatrix}'. \tag{4.21}$$

From Figure 4.13(b) we notice that the structure of the directed graph is similar to the directed graph shown in Figure 4.6(b). There are no cycles from e_4 to e_4 (excluding self-cycles). What we have done with our choice of L was to cut all the forward paths from e_4 and insert a self-gain arc at e_4.

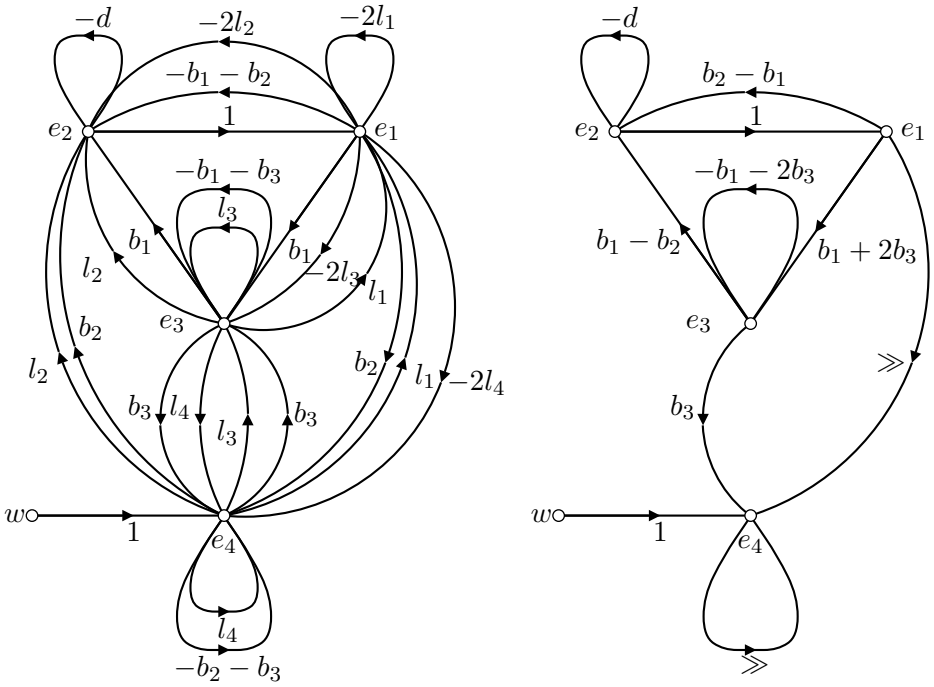

(a) Design Setup

(b) Designed Structured Error Dynamics

Figure 4.13: Graphical Observer Design with $C = \begin{bmatrix} 2 & 0 & -1 & -1 \end{bmatrix}$.

4.3.3 Number of Measurements

It is reasonable to ask whether we will be able to achieve a designed level of unknown-input attenuation with fewer measurements than the number of inputs. In [19], a similar type of question was addressed for a state-space model. The authors wanted to determine under what conditions (expressed in graph-theoretic terms) the fault detection and isolation problem could be solved. The fault detection and isolation problem has overlap with the problem of unknown-input attenuation, because a fault-detection filter needs to be insensitive to certain unknown inputs (viewed as disturbances), and sensitive to the remnant of the unknown inputs (i.e., the faults that we want to identify). The pertinent result from [19] is given by the following theorem, which deals with generic solvability of the FDI-problem.

LEMMA 4.2

[19] Consider a structurally observable system (A,B,C,D) and its associated directed graph $\mathbf{G}(\mathbf{V}, \mathbf{W})$*. The single observer-based triangular fault detection and isolation problem (i.e., the problem of attenuating all disturbances and identifying — but not necessarily isolating — all faults) is generically solvable with stability if and only if*

$$k = k_q + k_f$$

where: k *is the maximum number of unknown input to output vertex-disjoint paths in* $\mathbf{G}(\mathbf{V}, \mathbf{W})$*;*

k_q *is the maximum number of disturbance to output vertex-disjoint paths in* $\mathbf{G}(\mathbf{V}, \mathbf{W})$*; and*

k_f is the number of faults that need to be detected and isolated.

If we are only concerned with disturbance attenuation then $k_f = 0$, and we need $k = k_q$. Hence, in order to achieve 'ideal' disturbance attenuation we need at least as many measurements as there are disturbances, otherwise we would not be able to find vertex-disjoint paths.

In the buildup to Theorem 4.1 we confined our attention to the case where q (the number of e-vertices directly impacted by unknown inputs) is larger than or equal to m (the number of unknown inputs). We will consider the case when we have $q < m$ by hand of an example. Let us assume for the three-bus power system shown in Figure 4.2(a), we have

$$E = \begin{bmatrix} 0 & 0 & 0 \\ 0 & 0 & 0 \\ 1 & 0 & \kappa_1 \\ 0 & 1 & \kappa_2 \end{bmatrix}$$

and let us assume that

$$C = \begin{bmatrix} 1 & 0 & 0 & 0 \\ 0 & 0 & 1 & 0 \\ 0 & 0 & 0 & 1 \end{bmatrix}.$$

Clearly $q < m$, and the unknown-inputs are load changes at bus 2 and bus 3 as well as a line-flow change on the line between buses 2 and 3. We notice that we can not find vertex disjoint paths from the unknown inputs to the outputs of the system (M, A, E, C), and

applying Lemma 4.2 we might suspect that we would not be able to solve the unknown-input attenuation problem.

4.3.4 Illustrative Nine-Bus Example

Investigating the design of unknown-input attenuation observers is tricky when the measurements are overlapping. For instance, if one of our measurements is θ_i and another is $\theta_i - \theta_j$, then one cannot independently design the columns of L along the lines presented in the previous subsections. We will illustrate the subtleties by means of the following example.

We will investigate the nine-bus system shown in Figure 3.1. In this section we will compare the performance of two different observers. We assume that there are two unknown inputs: an unknown load change at bus 8; and a line perturbation going from bus 8 to bus 9 (we simulate a nearly complete line outage).

The first observer (abbreviated as 'Obs 1') uses an angle measurement taken at bus 4 in conjunction with an angular difference measurement between buses 4 and 5. The second observer ('Obs 2') uses angle measurements taken at buses 4 and 5. For both observers the measurement at bus 4 will be used to attenuate the effect of the possible line outage between buses 8 and 9. The second measurement of each observer will be used to attenuate the effect of the unknown-load change at bus 8.

Designing the observer gain for Obs 1 involves removing the entries in A by setting the

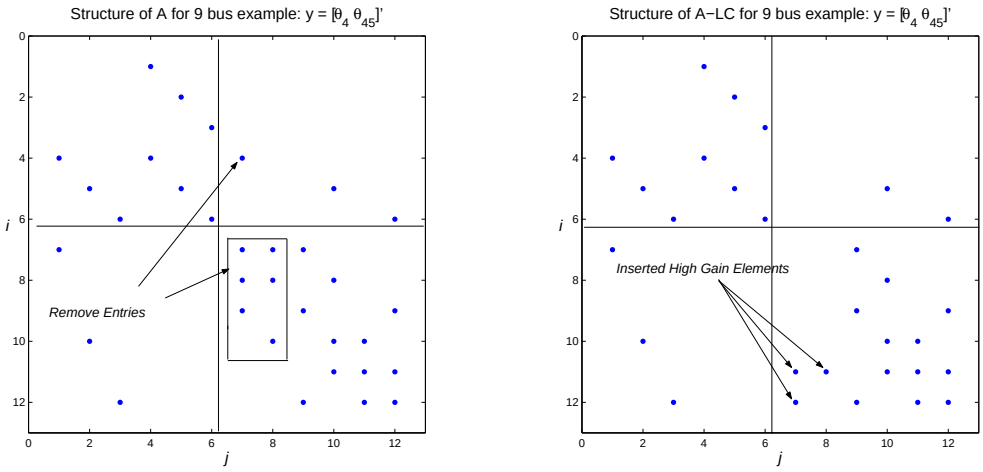

(a) Structure of A and nonzero elements of L

(b) Structure of $A - LC$

Figure 4.14: Observer 1 design steps.

first column of L (i.e., L_1) to $A_{:,i} - A_{:,j}$ and the second column of L (i.e., L_2) to $-A_{:,j}$, where i is an index associated with the angle at bus 4 and j corresponds to the angle at bus 5. In Figure 4.14(a), we illustrate what entries we want to remove. We then proceed to insert three high-gain elements in the $A - LC$ matrix as shown in Figure 4.14(b), by setting element g of L_1 to be large and element h of L_2 to the same large element. (Here g is the index that corresponds to the angle at bus 9 and h corresponds to the angle at bus 8.) Taking this action brings about the three high-gain elements as illustrated in Figure 4.14(b). We thus create high gain paths from: $e_7 = \theta_4 - \widehat{\theta}_4$ to $e_{11} = \theta_8 - \widehat{\theta}_8$; $e_7 = \theta_4 - \widehat{\theta}_4$ to $e_{12} = \theta_9 - \widehat{\theta}_9$; and $e_8 = \theta_5 - \widehat{\theta}_5$ to $e_{11} = \theta_8 - \widehat{\theta}_8$. We have thus eliminated all forward arcs from e_7 and e_8 from the original (M, A, E, I)-directed graph, and then inserted high-gain arcs (as indicated in Figure 4.14(b)) to the vertices e_{11} and e_{12} that are directly impacted by unknown inputs.

The design of Obs 2 is more straightforward: we set the first column of L to $L_1 = A_{:,i}$ and the second column of L to $L_2 = A_{:,j}$, with i and j as previously defined. We then proceed to insert the three required high-gain elements in the $A - LC$ matrix as shown in Figure 4.14(b), by setting element g of L_1 to be large and element h of L_1 to be the negative of the g element. We also set element h of L_2 to be large (and can be unrelated to the gains in L_1). Executing these steps, we enforce the same structure on $A - LC$ as in Figure 4.14(b).

In Figures 4.15(a) – 4.16(b) we illustrate how these two observers perform in tracking the state of the system in response to both unknown inputs occurring simultaneously. Even though we enforced the same structure on $A - LC$, Obs 1 fares worse than Obs 2. This performance degradation might be attributed to the overlapping measurements of Obs 1 (i.e., using θ_4 and $\theta_4 - \theta_5$ versus using θ_4 and θ_5). Thus caution should be exercised when overlapping measurements are used.

4.4 State Estimation of Large-Scale System: WSCC 179-Bus

The system under consideration in this section is a 179-bus aggregated version of the Western States Coordinating Council (WSCC) power system[3]. The one-line diagram of this system is shown in Figure 7.1[4]. There are a few discrepancies between this one-line diagram and the data of the model provided to us. These discrepancies do not impact the results of our studies adversely. The nature of these discrepancies are manifested as either a

[3]We would like to thank Professor A. G. Phadke at VPISU, Professor V. Vittal and Xiaoming Wang at Iowa State University for sharing the aggregated WSCC 179 bus model with us.

[4]A special thank you to Xiaoming Wang for providing us with this one-line diagram.

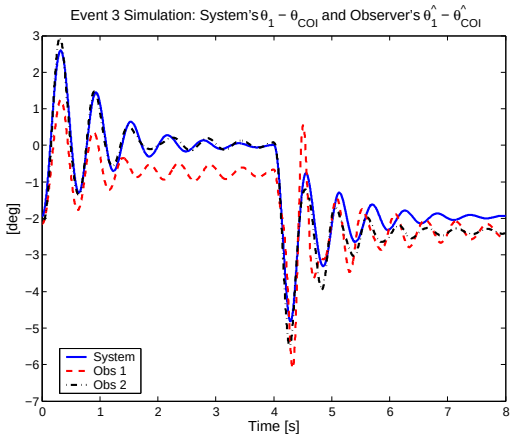

(a) $\theta_1 - \theta_{coi}$

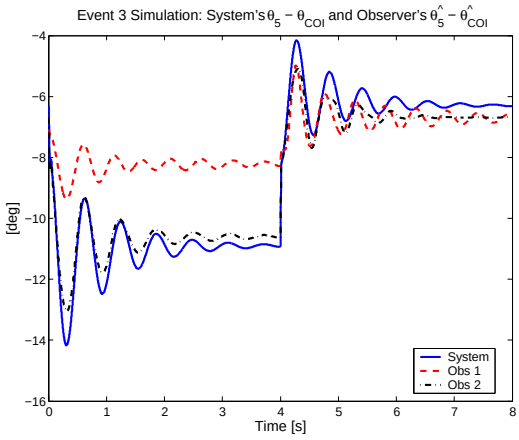

(b) $\theta_5 - \theta_{coi}$

Figure 4.15: Time plots of the system, and two observer evolutions in response to: an unknown load change at bus 8; and a line flow perturbation on the line directed from bus 8 to bus 9 during $t \in [0.1s, 4s]$.

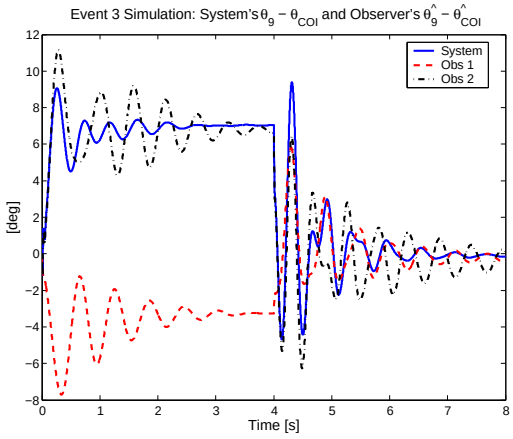

(a) $\theta_9 - \theta_{coi}$

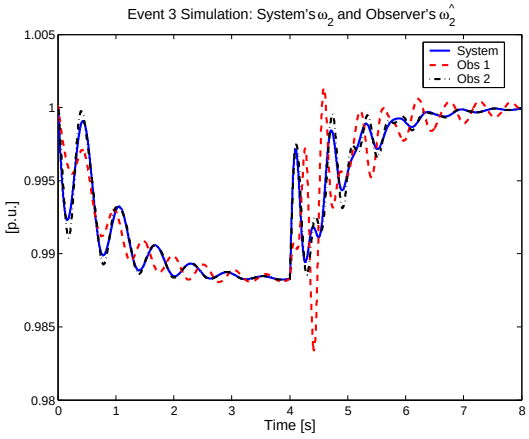

(b) ω_2

Figure 4.16: Time plots of the system, and two observer evolutions in response to: an unknown load change at bus 8; and a line flow perturbation on the line directed from bus 8 to bus 9 during $t \in [0.1s, 4s]$.

renumbering of network buses and order shuffling of local interconnections of non-generator buses.

In this section we will design a swing-motion observer for the uncontrolled system. We assume that none of the generators has any type of implemented controls (e.g., no governor controls). We assume that a generation change occurs at generator 30 in the form of a mechanical power pulse (amplitude of $1p.u.$ for 1 second starting at $t = 0.01s$). The angle measurement we will use is taken at bus 48. The perturbation is applied in the most northern part of the network, while we take our direct angle measurement in the southern part of the network. One can envision that the number of hops in the directed graph $(M, A-LC, E, I)$ from the measurement site to the e-vertex directly impacted by the unknown input will be very long.

We design the observer gain by setting L equal to the j^{th} column of A, where j is the index of the angle at bus 48 (the variable we are measuring). We then insert a high gain arc from e_j to e_i, where i is the index of the e-vertex directly impacted by the unknown input (i.e., $e_i = \omega_8 - \widehat{\omega}_8$, where ω_8 is the speed of the generator at bus 30).

In Figure 4.18 we show a select few time-plots of estimated angles, compared to the angles of the uncontrolled system, in response to the unknown (to the observer) mechanical power pulse occurring at generator 30. In this simulation we have introduced some parametric model uncertainty into the system model. We assumed that the parameters of the system are randomly perturbed by 10% (using a uniform distribution) around their associated nominal values. Nominal values were used for the realization of the observer. For this

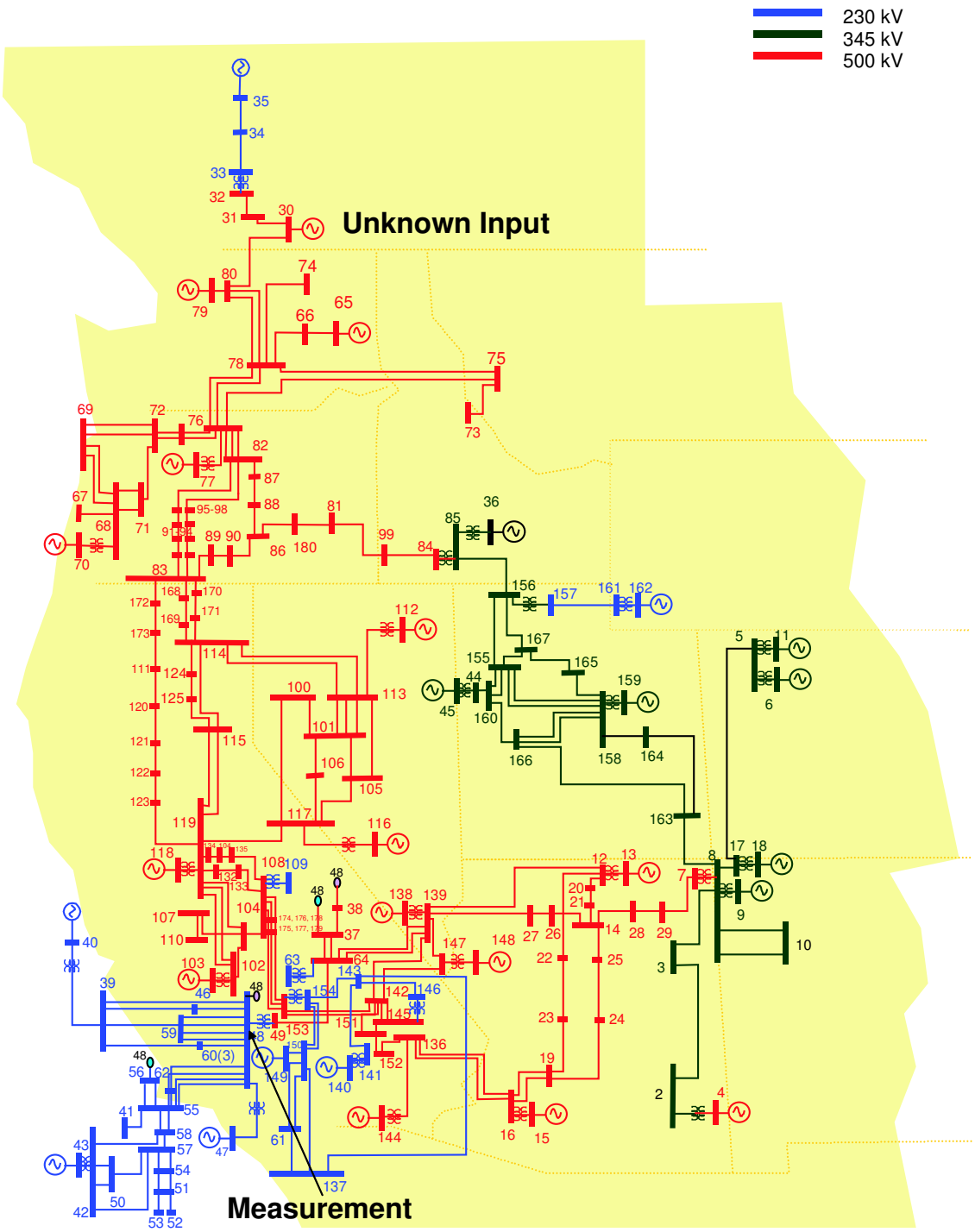

Figure 4.17: One-line diagram of an aggregated WSCC network. (Acknowledgement: A. G. Phadke, V. Vittal, X. Wang.)

simulation we assumed that the initial states of the system and the observer agreed. (This assumption was made in order to avoid solving the loadflow for the perturbed system before commencing our transient simulation.) The angles that we are displaying are $\theta - \widehat{\theta}_{coi}$ (where $\widehat{\theta}_{coi}$ is the estimated center of inertia movement for this system and $\theta - \widehat{\theta}_{coi}$ is the system angles relative to this estimated center of inertia movement) and $\widehat{\theta} - \widehat{\theta}_{coi}$ (observer).

The sample of plots in Figure 4.18 represent angles across the whole network. In Figure 4.18(a) we estimate the angle at bus 2, which is in the south-east part of the network. In Figure 4.18(b) we estimate the angle θ_{48} at the bus where our direct angle measurement is taken. In Figure 4.18(c) we show the estimate of the angle at bus 30, where the perturbation is applied. In Figure 4.18(d) we show the estimate of θ_{162}. All these plots illustrate that the observer does a very good job of tracking the angle-variables of the perturbed system in response to the unknown input step of P_{30}.

In Figure 4.19 a select few plots of generator speeds are shown. The sample plots are representative of the generator speeds across the network. We see from these plots that the observer adequately estimates the speed deviations of the generators. Note that the estimate of ω_8 appears very oscillatory (see Figure 4.19(b)), and this behavior is attributed to the high-gain arc we inserted in our design.

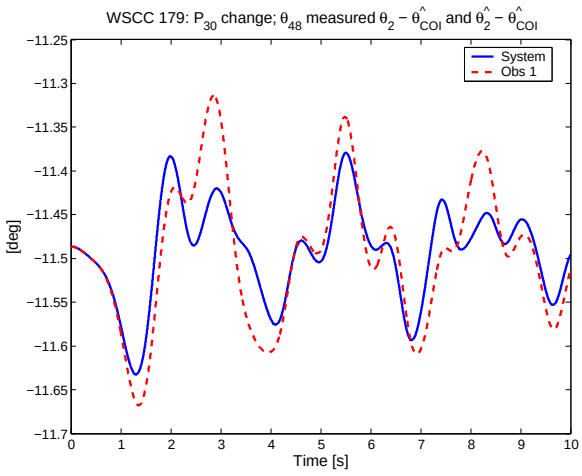

(a) $\theta_2 - \widehat{\theta}_{coi}$ versus $\widehat{\theta}_2 - \widehat{\theta}_{coi}$; P_{30} stepped

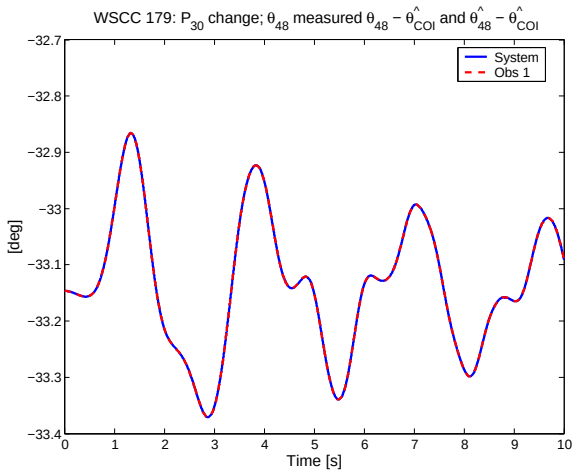

(b) $\theta_{48} - \widehat{\theta}_{coi}$ versus $\widehat{\theta}_{48} - \widehat{\theta}_{coi}$; P_{30} stepped; Measurement taken at bus 48

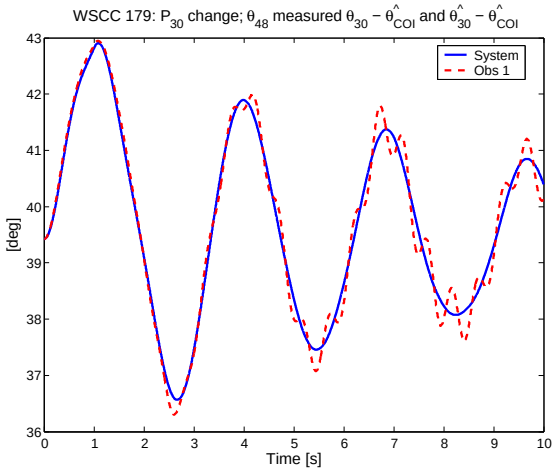

(c) $\theta_{30} - \widehat{\theta}_{coi}$ versus $\widehat{\theta}_{30} - \widehat{\theta}_{coi}$; P_{30} stepped

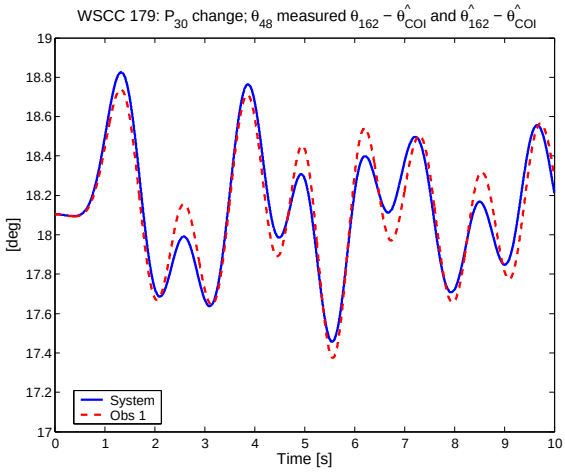

(d) $\theta_{83} - \widehat{\theta}_{coi}$ versus $\widehat{\theta}_{162} - \widehat{\theta}_{coi}$; P_{30} stepped

Figure 4.18: Time plots of selective angles in the network relative to the evolution of the estimated center-of-inertia movement of the system. During $t = 0.01s$ to $t = 1.01s$ the mechanical input power at bus 30 changed from its steady-state value.

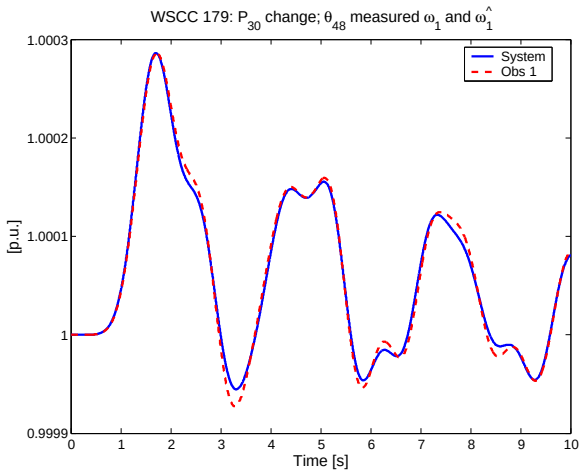

(a) ω_1 — Speed of generator at bus 4; P_{30} stepped

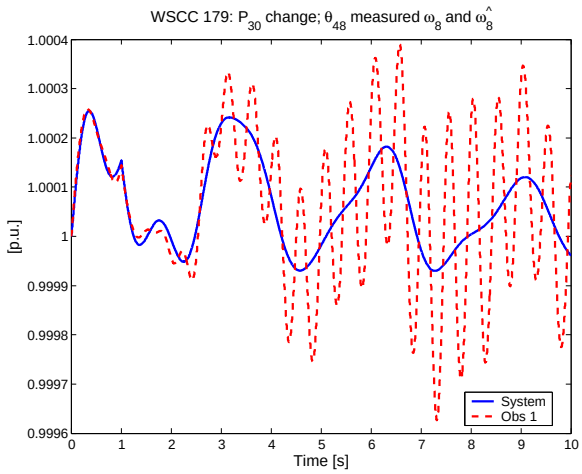

(b) ω_8 — Speed of generator at bus 30; P_{30} stepped

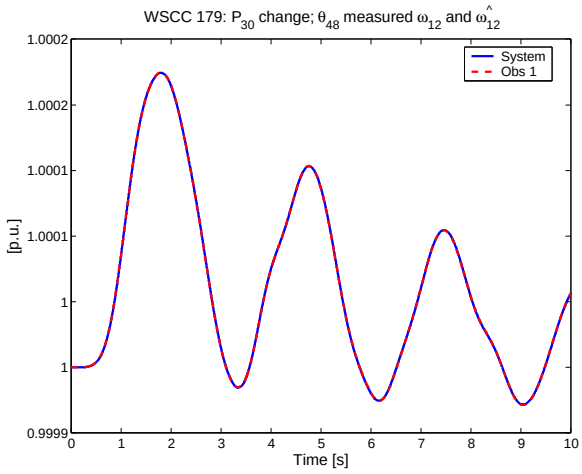

(c) ω_{12} — Speed of generator at bus 43; P_{30} stepped

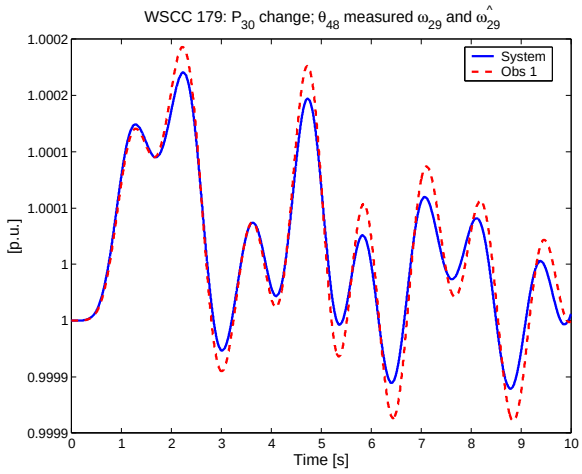

(d) ω_{29} — Speed of generator at bus 162; P_{30} stepped

Figure 4.19: Time plots of selective speeds of generators in the network. During $t = 0.01s$ to $t = 1.01s$ the mechanical input power at bus 30 changed from its steady-state value.

4.5 Conclusion

In Chapter 3 we investigated H_∞ filtering for DAE systems, and indicated that the design of these filters is very computationally intensive for large-scale systems. This motivated us to investigate an alternative design approach that relies on ideas of structured systems and their associated directed graphs. We introduced a novel graphically motivated observer-design approach and illustrated on small examples how one would address the impact of measurement placement, the number of measurements as well as the type of measurements on the observer design problem. This graphical design approach technique relies on knowledge of the network structure and on values that can be extracted from linearized models of the nonlinear swing model. This design approach is not computationally intensive, making it plausible for the realization of a linear-parameter-varying observers.

This graphical observer design technique is powerful for steady-state unknown input attenuation, but no guarantees on the stability of the filter are given. In Theorem 4.1 we did investigate the case where extra measurements can be used to change the eigenvalues of the $(M, A - LC)$ error system.

Thus if a mismatch in initial conditions between the observer and the plant is anticipated, and fast convergence of the error to zero is of importance, one would have to introduce extra degrees of freedom in order to move the eigenvalues of $(M, A - LC)$ such that the real parts of these eigenvalues are sufficiently negative.

We thus propose a dual design approach, where we first identify the unknown inputs, then

introduce (or use existing) measurements that can be used to achieve a desired level of unknown-input attenuation as described in this chapter. The second step will be to use more measurements that do not violate the conditions of Theorem 4.1 and use these for the sole purpose of moving the eigenvalues of $(M, A - LC)$ using an eigenstructure assignment technique.

Our work described in this chapter is still in the initial phases and more work is needed to address the issue of model uncertainty and robustness. In all the simulation showed in this chapter we did assume model uncertainty and the nominal values were used for observer design. Despite these moderate uncertainties the graphically designed observers did well. Another issue that need some further investigation is to quantify the link between the performance of an observer and the distance (in the directed graph of the structured system) between an unknown input and its canceling measurement.

In the next chapter we will focus on the graphical-observer design technique for linear structured systems and use it in the design of fault detection and isolation filters.

Chapter 5

Power System Monitors: Fault Detection and Isolation

In the previous chapter we investigated various observer design approaches for the swing model of a power system. The main purpose of this chapter is to illustrate the practical value of using these observers to create power system monitors.

One of the main points from the previous chapter was that for large-scale power systems it is computationally intensive to design full-order DAE observers using traditional design techniques, such as H_∞-filtering. We will use the graphical observer design technique introduced in Section 4.2.2 to design the monitors shown in this chapter.

In this chapter we will first consider the design of fault detection schemes on a small power system and then consider a large-scale system.

5.1 Model-Based Fault Detection and Isolation

Model-based FDI includes observer-based and parameter estimation approaches [17, 18]. FDI can be achieved by designing residual generators (realized using observers) that are sensitive to predefined faults and robust to predefined disturbances [14, 19]. For parameter estimation methods model parameters are tracked and changes in these parameters serve as the basis for detecting and isolating faults [18]. Model-based approaches are attractive in the power system setting, because power system models are well understood and considered to be quite accurate descriptions of the system.

In [20], a modular method for fast fault detection and classification in power systems is presented. Model-free and model-based fault detection approaches are discussed, and for the model-free case, signal processing and wavelet theory are used to create fast and sensitive fault indicators. For the model-based case the authors remark (and do not examine) that residual generation (RG) schemes can be used to generate fault indicators. The indicators can then be analyzed by standard, statistical hypothesis testing or artificial neural networks to create intelligent decision rules. The creation of intelligent decision rules falls outside the scope of this thesis, and investigations into generation of residuals as fault indicators in the power system context will be one of the contributions of this thesis.

Furthermore, in [20], the authors conduct a survey of fault-detection methods in the power system environment. They state that the problem of detecting high-impedance faults (i.e., line outages) is unresolved. They briefly mention different approaches explored, but the

survey is not extensive and might be a bit outdated.

In [21, 22] members of the Power Systems Engineering Research Center investigated a fault location algorithm applied to transmission networks using modeling, simulation, and limited field recorded data. The idea behind the algorithm is to match the recorded and simulated waveforms to determine the most probable fault location. The recorded waveforms are captured using digital relays. The simulated waveforms are obtained by running a short-circuit program using an accurate model of the system under consideration.

It is worthwhile pointing out that most of the fault detection and isolation literature in the power system context focuses on the three-phase-element level (i.e., it explores balanced and unbalanced faults), whereas in this thesis we will focus more on a higher level system description. Thus, the line faults that we will investigate will be of the balanced type.

In [17], a summary of current FDI techniques is given. The FDI field can be split into four groups: 1) Model-based techniques: This class includes quantitative methods (i.e., using system theory in order to design residual generators [14, 19], parameter estimation techniques, observer-based state estimation and parity space concepts [15]; 2) Qualitative and Artificial Intelligence methods: Methods mentioned are neural networks, fuzzy logic and decision neuro-fuzzy; 3) Knowledge-based methods; 4) Empirical and signal processing techniques (spectral analysis, parameter estimation methods using Auto Regressive Moving Average models).

In this thesis we will only consider model-based FDI methods. In the following few para-

graphs a subset of the earlier work on model-based FDI will be mentioned briefly.

Beard-Jones fault detection filters (BJDF) [14]: In 1971, Beard 1971 proposed the idea of replacing Hardware Redundancy with Analytical Redundancy. He developed filters that generate directional residuals for fault detection and isolation purposes. Jones (in 1973), Massoumnia, Willsky and Verghese (in 1989) redefined this approach in a geometric setting. Several papers have been devoted to the design of BJDF, and in [14] the authors state that the design problem is well understood for state space models.

Stochastic systems FDI [14]: Mehra and Peschon introduced a general procedure for FDI using innovations (or residuals) generated by a Kalman filter. In 1976, Willsky presented key concepts of analytic redundancy in model-based FDI with emphasis on stochastic systems and jump detection. One of the statistical approaches is the multiple model adaptive filter approach with multiple hypothesis testing on residuals generated by a bank of Kalman filters was developed by Willsky, Deyst and Crawford in 1974. Recent developments employ Principal Component Analysis (Martin, Morris and Zhang 1996 and [18]).

Parity relation approach for FDI [14]: This entails generating the residual (or parity vector), based upon consistency checking of the system input and output data over a time window (Mironovski 1978, 1980; Chow and Willsky 1984; Gertler 1998 [15]).

Parameter estimation approach for FDI [14]: Process fault diagnosis is achieved by tracking unmeasurable process parameters or state variables (as done by Isserman in 1984). System identification techniques are generally used.

Nonlinear dynamic systems FDI [14]: Two approaches are usually followed: (1) The model is linearized at an operating point. Robust techniques are applied to generate residuals. This approach works well if the linearization does not cause large mismatch between linear and nonlinear models and the system stays close to the operating point. (2) When these latter conditions are violated the FDI problem has to be tackled directly using nonlinear techniques.

Frequency domain design FDI [14]: An RG method based on the factorization of the system transfer matrix. H_∞ optimization and μ-synthesis techniques have been proposed to improve the robustness of the frequency RG approach.

In this thesis we will consider the implementation of residual generators (in which we use the observers developed in the previous chapter) in order to create fault detection and isolation (FDI) schemes.

5.1.1 FDI via Residual Generation

5.1.1.1 Brief Problem Description

The objective of robust FDI is to make a system robust to disturbances (subset of the unknown-inputs) while making it sensitive to the occurrence of predefined faults. Thus, for

the system

$$M\dot{x} = Ax + Bu + E_1 w + R_1 \psi, \tag{5.1}$$

$$y = Cx + Du + E_2 w + R_2 \psi, \tag{5.2}$$

faults ψ need to be identified while no false alarms should be recorded when disturbances w occur.

Fault detection filters are a special class of full-order observers and have the following form:

$$\begin{aligned} M\dot{\widehat{x}} &= (A - LC)\widehat{x} + (B - LD)u + Ly & (5.3)\\ \widehat{y} &= C\widehat{x} + Du & (5.4)\\ r &= Q(y - \widehat{y}) \\ &= QCe + QE_2 w + QR_2 \psi & (5.5) \end{aligned}$$

where L and Q are design matrices and r is the vector of residuals. The existence of Q relaxes the problem by providing the designer with extra degrees of freedom. Unknown-input attenuation and fault amplification are easier to achieve in this setting[1].

In [59], the authors state that the design freedom for Q and L is reflected by the number of independent outputs when employing a diagnostic observer as a residual generator. Generally it is assumed that the number of outputs is greater than the number of faults to be identified. The reasoning behind this assumption is that the dimension of the output

[1]Note that when $Q = I$ a BJDF will be realized.

measurements has to provide sufficient information for isolating multiple faults, as well as the additional freedom for characterizing the robustness of a diagnostic observer.

In [19] the generic solvability of the above FDI problem is investigated. The authors in [19] investigate LTI state space structured systems (i.e., the entries of the system matrices are either fixed zeros or free parameters) to which they associate a directed graph depicting paths from disturbances and faults to the system outputs. They then provide necessary and sufficient conditions under which the FDI problem has a solution for almost all values of the free parameters (see Lemma 4.2). These conditions are expressed in terms of input to output paths of the directed graph. Moreover, they state that if the maximum number of vertex-disjoint disturbance/fault to output paths is equal to the maximum number of vertex-disjoint disturbance to output paths plus the number of faults, then there exist an Q and an L such that $G_{rd}(s) = 0$ (for all s) and we can make $G_{rf}(s)$ upper triangular (which is desired for isolation purposes). Here $G_{rd}(s)$ is the multivariable transfer function matrix from disturbance to residuals, and $G_{rf}(s)$ is the transfer function matrix from faults to residuals. The authors do not address the design of such Q's and L's, and such design remains difficult with current techniques. Using the main result of this paper will enable a designer to place system measurements with greater effect in order to identify or reject particular faults and disturbances.

Eigenstructure assignment has been demonstrated [14] to be a viable design approach for observer-based residual generation for LTI models, and it appears that this design method has received the most attention in the past 20 years in the field of observer-based fault

detection and isolation. In [14], left eigenvectors of the observer (i.e., of $A-LC$) are assigned to be orthogonal to the disturbance distribution directions. Furthermore, the authors of [14] demonstrate that for a few instances where left eigenvector assignment does not work, partial right eigenvector assignment parallel to the disturbance distribution directions might be effective. Assignment of the eigenvectors is achieved by designing an appropriate L. Once these eigenvectors are assigned, these modes are blocked from propagating through to the residuals by designing an appropriate Q.

When a BJDF is realized, eigenstructure assignment is used to design the feedback gain matrix L in such a way that the output estimation error (i.e., the residual vector) has uni-directional characteristics associated with some known fault directions.

Fault detection investigations for descriptor systems have received less attention than LTI models [17, 49, 51]. In [51] the authors investigate robust fault detection for linear descriptor systems with only actuator faults and process disturbances. They present a new parametric eigenstructure assignment design approach where the residual is generated using a full-order, singular observer. The investigations here provide an alternative approach to this design problem.

5.1.1.2 Residual Generator Examples

We will study the nine-bus example shown in Figure 3.1. In all the simulations that we will present here, we will assume that there is some uncertainty in the model we are employing

when we realize observers. This uncertainty is modeled by randomly perturbing the model parameters by $\pm 10\%$, using a uniform distribution. In this thesis we will not consider the case of sensor failures or measurement disturbances, so that $R_2 = 0$ and $E_2 = 0$ and subsequently we drop the subscripts of E_1 and R_1 as well. Fault detection examples of this kind can be treated in a similar manner to the examples we present here. We will consider three fault detection cases:

Example 1

In the first case we assume that load changes at buses 5, 6 and 8 are faults that we want to identify. From [19] (see Lemma 4.2 for a discussion of the result in [19]) we know that we need at least three measurements in order to realize a fault detection filter. In Section 4.2.2 we illustrated how easily unknown-input observers for the system, with desired attenuation levels, can be realized by placing direct angle measurements at buses 5, 6, and 8 (i.e. at the buses directly impacted by the unknown inputs). The unknown-input observer design for this sketched scenario would involve cutting particular forward signal flow paths in the directed graph associated with the DAE system $(M, A - LC, E, I)$. We cut the paths from the e-vertices where the measurements are placed to all other e-vertices, except of the terminating (of a forward arc) e-vertex is directly affected by an unknown input w. This design philosophy assures that for our current example that the unknown inputs can only affect the e-vertices directly connected to the w-vertices. Thus, there will be a one-to-one mapping, thus $P_5 = w_1$ will affect only e_5, etc.. The final step in the design of the unknown-input observer would be to attenuate the w signals. This is achieved by choosing

the self-cycle gains at the e_5–, e_6–, and e_8–vertices to be large in order to achieve the desired levels of attenuation.

For the FDI-filter the design of the observer is similar, but the residuals need to indicate to us when an actual fault occurred. Thus in the last step, attenuation of the unknown-input signals (viewed as disturbances to the power system state-estimation monitor) will be modified to amplify the unknown inputs (now viewed as faults that we want to detect and isolate). The complete design approach is summarized as follows: repeat the step of cutting the forward signal flow paths in the directed graph of $(M, A - LC, R, C)$; then choose the self-cycle gains at the e_5–, e_6–, and e_8–vertices to be small in order to amplify the fault signals. From this design description it is evident that the transfer function from faults to residuals, $G_{rf}(s)$, will be diagonal for all s (assuming that the plant model is perfectly known). For our current example $G_{rf}(s) = 0.1I$, and this diagonal structure makes fault isolation and identification easy.

In Figure 5.1 time plots are shown of the residuals for the FDI-filter described above. In this particular simulation we assume that only P_8 occurs during the period $0.01s$ to $4.01s$. We expect that only $r_3(t)$ would significantly change during this event period, which is the case seen in Figure 5.1.

In Figure 5.2 time plots are shown of the residuals for the same FDI-filter, but for the scenario when all three faults occur simultaneously during the period $0.01s$ to $4.01s$. As expected, we see from Figure 5.2 that all three residual signals change in order to indicate that all three faults occurred simultaneously.

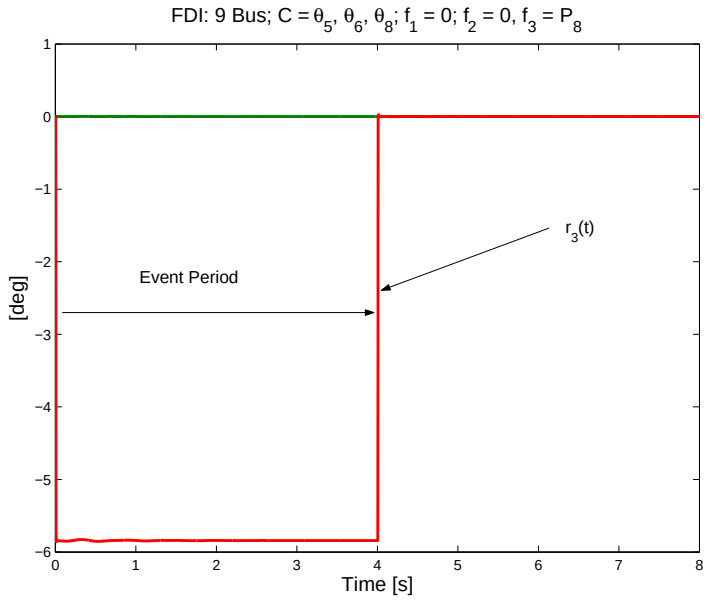

Figure 5.1: FDI example 1 for the nine-bus system. Faults: P_5, P_6, P_8; Measurements: θ_5, θ_6, θ_8. In this simulation only P_8 changed with $2p.u.$, during $0.01s$ and $4.01s$.

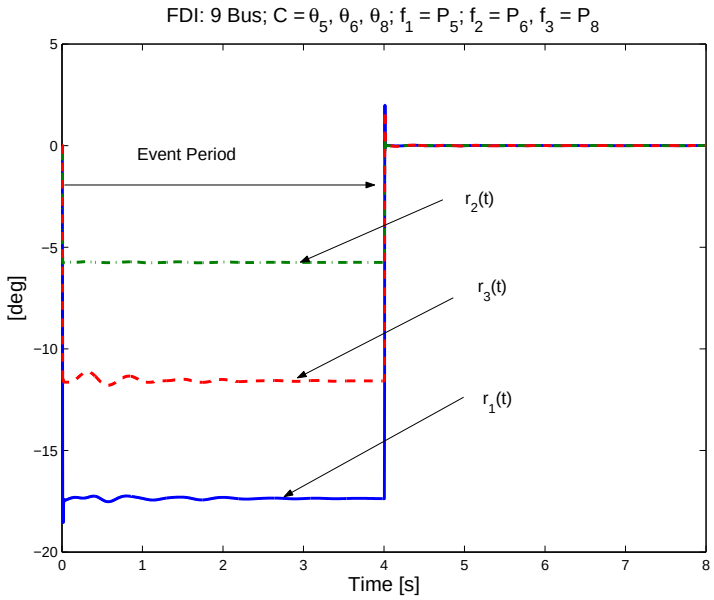

Figure 5.2: FDI example 1 for the nine-bus system. Faults: P_5, P_6, P_8; Measurements: θ_5, θ_6, θ_8. In this simulation all three faults occurred simultaneously (P_5 changed with $3p.u.$; P_6 changed with $1p.u.$; P_8 changed with $2p.u.$) between $0.01s$ and $4.01s$.

Example 2

Our second example presents us with a more challenging design. Suppose the nine-bus system (shown in Figure 3.1) is subjected to two possible faults: a line flow change due to a line outage between bus 8 and bus 9 (we will refer to it as f_1); and a load change at bus 8 (refer to as f_2). We assume that we have two direct angle measurements placed at bus 4 and bus 5. We want to associate f_1 with the angle measurement at bus 4 and f_2 with the angle measurement at bus 5. In Figure 5.3(a) the directed graph associated with the residual-generator filter design setup for the linear structured system $(M, A - LC, E, C)$ is shown. The vertices G_1, G_2, and G_3 are super nodes and each consists of two vertices associated with the angle and speed of the machines. A few feedback arcs, which are taken to be zero in the design, are omitted in this figure. These arcs are directed from the measurement locations (i.e., e_4 and e_5) to the generator super nodes. These omissions should not create confusion here.

The transfer function matrix from faults to residuals (i.e., $G_{rf}(s) = C(sM - A + LC)^{-1}E$) for the designed structured system shown in Figure 5.4(a) is obtained as

$$G_{rf}(s) = \begin{bmatrix} \frac{1}{3} & 0 \\ 0 & \frac{-1}{15} \end{bmatrix}. \tag{5.6}$$

This diagonal structure enables us to detect, isolate and identify simultaneous faults. The purpose of this example is to illustrate that we can achieve satisfactory fault detection and isolation by using measurements that are not placed in the vicinity of the faults. In our

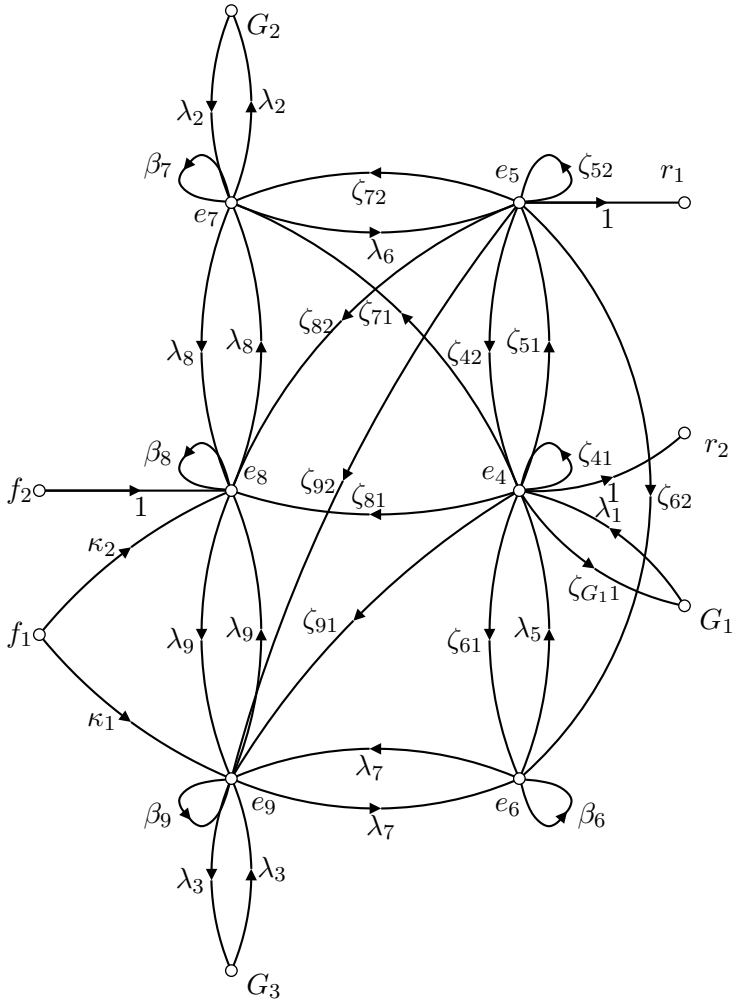

(a) Design Setup

Figure 5.3: Graphical Observer Design of a Fault Detection and Isolation Filter for the Nine-Bus System. $f_1 = P_8$, $f_2 = P_{89}$, $C = \{\theta_4, \theta_5\}$
Definitions: λ_h – edge weight of an element in A associated with line h of the power system. κ_1 and κ_2 are defined in Equation (2.37)
Unknowns for Figure (a): $\beta_6 = -\lambda_5 - \lambda_7$, $\beta_7 = -\lambda_2 - \lambda_8 - \lambda_6$, $\beta_8 = -\lambda_8 - \lambda_9$, $\beta_9 = -\lambda_3 - \lambda_7 - \lambda_9$, $\zeta_{G_1 2} = 0$, $\zeta_{G_2 2} = 0$, $\zeta_{G_3 2} = 0$, $\zeta_{G_1 1} = \lambda_1 - l_{11}$, $\zeta_{G_2 1} = 0$, $\zeta_{G_3 1} = 0$, $\zeta_{42} = \lambda_4 - l_{42}$, $\zeta_{52} = -\lambda_4 - \lambda_5 - l_{52}$, $\zeta_{51} = \lambda_4 - l_{51}$, $\zeta_{61} = \lambda_5 - l_{61}$, $\zeta_{92} = -l_{92}$, $\zeta_{71} = -l_{71}$, $_{81} = -l_{81}$, $\zeta_{91} = -l_{91}$, $\zeta_{72} = \lambda_6 - l_{72}$, $\zeta_{82} = -l_{82}$, $\zeta_{62} = -l_{62}$.

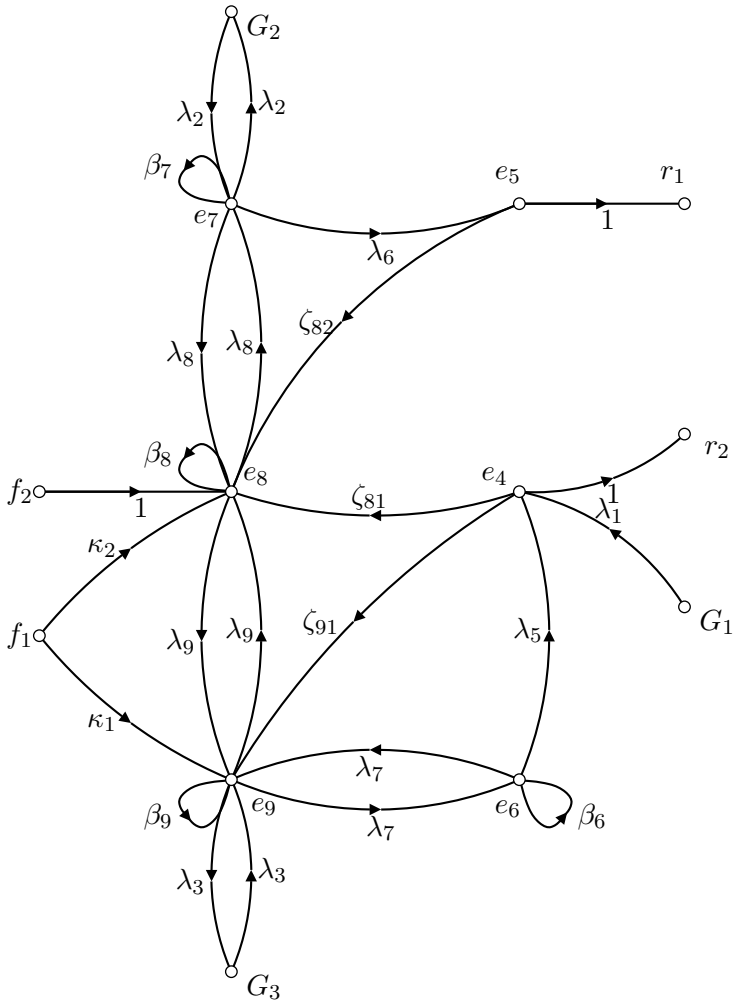

(a) Designed Structured Error Dynamics

Figure 5.4: Graphical Observer Design of a Fault Detection and Isolation Filter for the Nine-Bus System. $f_1 = P_8$, $f_2 = P_{89}$, $C = \{\theta_4, \theta_5\}$
Definitions: λ_h – edge weight of an element in A associated with line h of the power system. κ_1 and κ_2 are defined in Equation (2.37)
Unknowns: $\beta_6 = -\lambda_5 - \lambda_7$, $\beta_7 = -\lambda_2 - \lambda_8 - \lambda_6$, $\beta_8 = -\lambda_8 - \lambda_9$, $\beta_9 = -\lambda_3 - \lambda_7 - \lambda_9$, $\zeta_{G_1 2} = 0$, $\zeta_{G_2 2} = 0$, $\zeta_{G_3 2} = 0$, $\zeta_{G_1 1} = 0$, $\zeta_{G_2 1} = 0$, $\zeta_{G_3 1} = 0$, $\zeta_{42} = 0$, $\zeta_{52} = 0$, $\zeta_{51} = 0$, $\zeta_{61} = 0$, $\zeta_{92} = -l_{92}$, $\zeta_{71} = 0$, $_{81} = -l_{81}$, $\zeta_{91} = -l_{91}$, $\zeta_{72} = 0$, $\zeta_{82} = -l_{82}$, $\zeta_{62} = 0$.

previous example we placed our direct angle measurements at the buses impacted by the faults in order to yield a straightforward design problem. Note that we assumed some model uncertainty during our simulations, and that accounts for the discrepancies between what (5.6) suggests and the simulation results shown in Figures 5.5 – 5.7.

In the simulation results in Figure 5.5, where only f_1 occurred during the period $0.01s$ to $4.01s$, we show a few system states with their estimates as well as the residuals for the FDI-filter described above. We expect that only $r_1(t)$ (and $\widehat{\theta}_4 - \widehat{\theta}_{coi}$) would significantly change during this event period, which is what we see in the sub-figures of Figure 5.5.

In Figure 5.6, where only f_2 occurred during the period $0.01s$ to $4.01s$, we show a few system states with their estimates as well as the residuals for the above described FDI-filter. We expect that only $r_2(t)$ (and $\widehat{\theta}_5 - \widehat{\theta}_{coi}$) would significantly change during this event period, which is what we see in the sub-figures in Figure 5.6.

In Figure 5.7 simulation results are shown of a few system states with their estimates as well as the residuals for the above described FDI-filter, when both f_1 and f_2 occurred simultaneously. From the sub-figures of Figure 5.7 we see that both residuals changed significantly during the event period.

In the (c)-sub-figures of Figures 5.5 – 5.7 we illustrate that the FDI-filters provide us with good state estimates for θ_8 (and in fact for all states except θ_4 and θ_5 — our residuals), in addition to the residuals indicating when the faults occurred. This good state-tracking performance is attributed to level of disturbance attenuation we can achieve following our

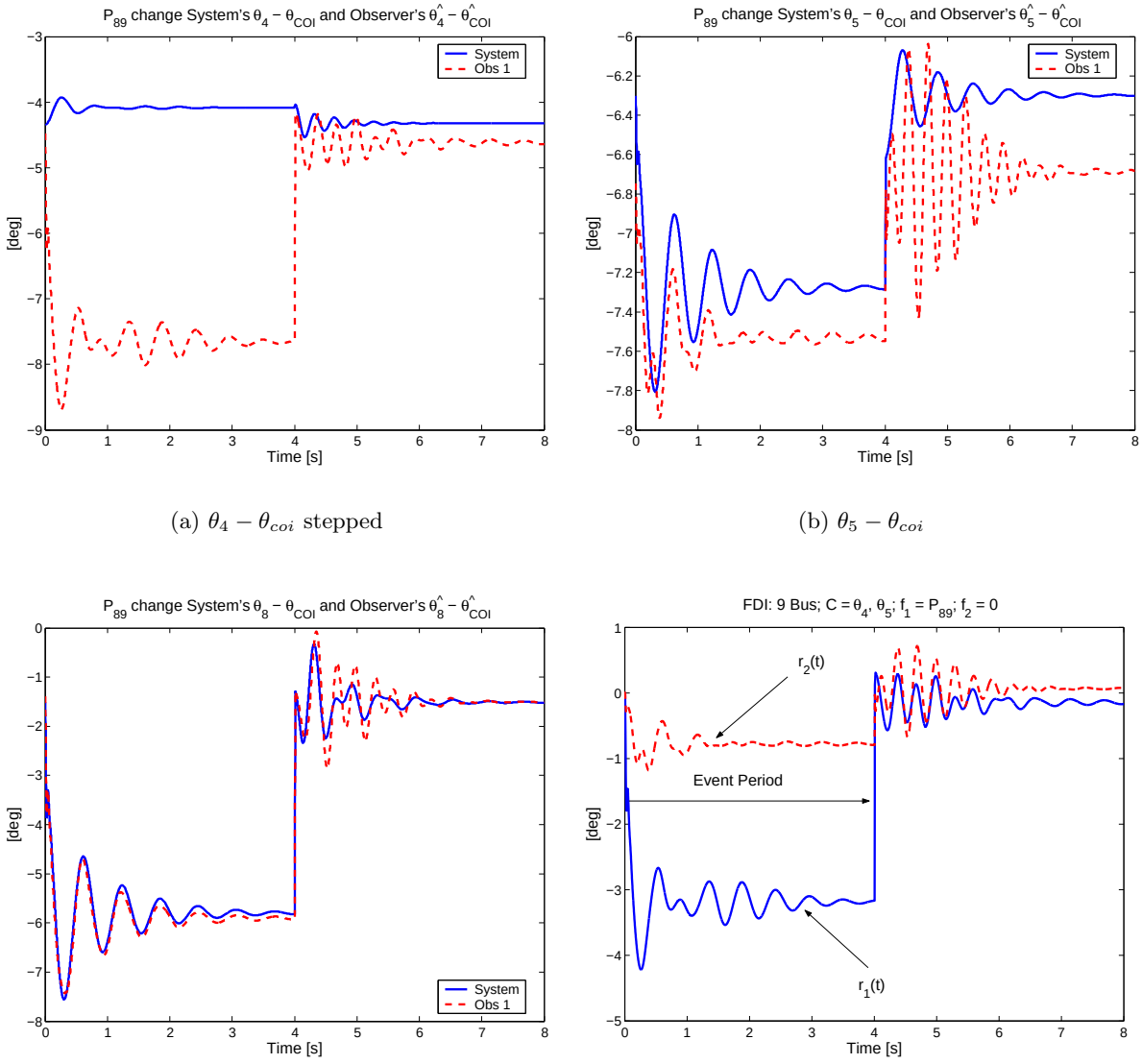

(a) $\theta_4 - \theta_{coi}$ stepped

(b) $\theta_5 - \theta_{coi}$

(c) $\theta_8 - \theta_{coi}$

(d) Residuals

Figure 5.5: FDI example 2 for the nine-bus system. Faults: P_{89}, P_8; Measurements: θ_4, θ_5. In this simulation only f_1 occurred during $0.01s$ and $4.01s$.

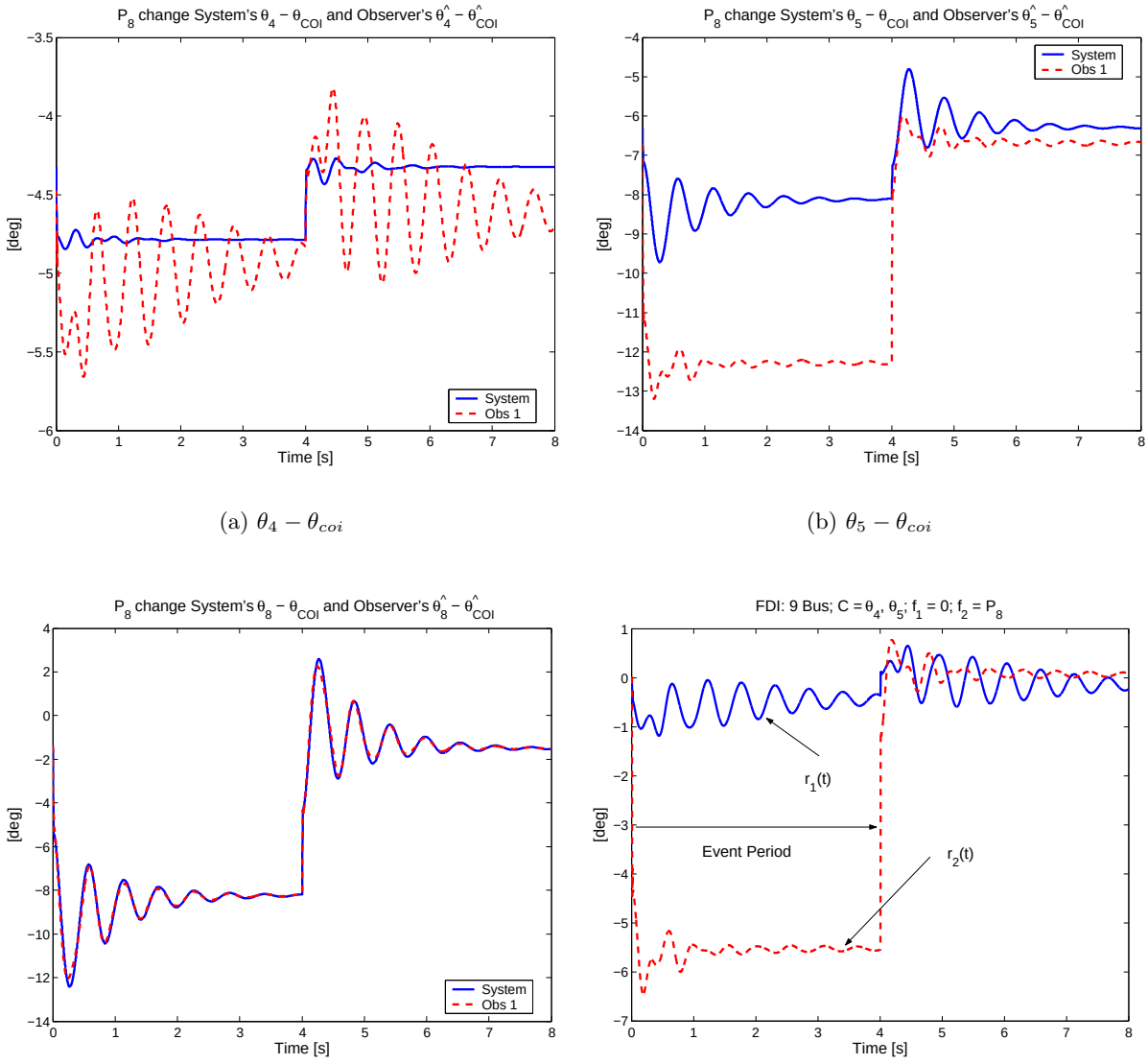

(a) $\theta_4 - \theta_{coi}$

(b) $\theta_5 - \theta_{coi}$

(c) $\theta_8 - \theta_{coi}$

(d) Residuals

Figure 5.6: FDI example 2 for the nine-bus system. Faults: P_{89}, P_8; Measurements: θ_4, θ_5. In this simulation only f_2 occurred between $0.01s$ and $4.01s$.

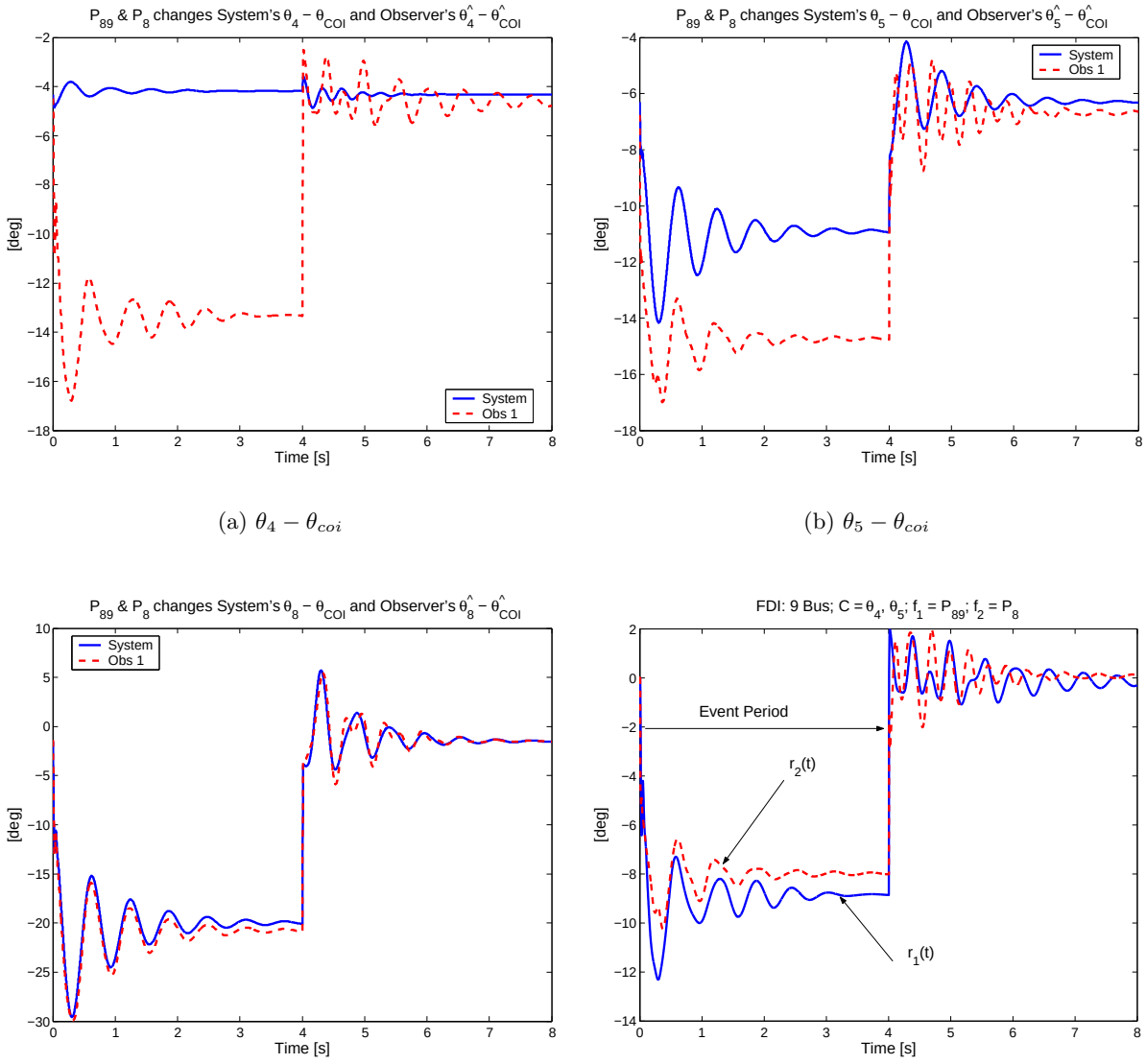

(a) $\theta_4 - \theta_{coi}$

(b) $\theta_5 - \theta_{coi}$

(c) $\theta_8 - \theta_{coi}$ stepped

(d) Residuals

Figure 5.7: FDI example 2 for the nine-bus system. Faults: P_{89}, P_8; Measurements: θ_4, θ_5. In this simulation both faults occurred simultaneously between $0.01s$ and $4.01s$.

graphical-observer design technique discussed in Section 4.2.2.

Example 3

The third case that we consider builds on the previous example. In particular, we add an additional disturbance, in the form of a mechanical input power change at generator 3. All the unknown inputs (i.e., faults and disturbance) occur in the same vicinity for this small example. The question we will ask is whether we will be able to solve the FDI-problem and attenuate this additional disturbance if we have an additional direct angle measurement at bus 7. We will answer the question by testing whether the result in [19] holds. We first draw the directed graph of the system $(M, A, [E \quad R], C)$. (We do not show this directed graph, and the interested reader can easily construct this graph.) From investigating this directed graph, we conclude that we cannot find three vertex-disjoint paths from the faults/disturbances to the system outputs as required by Lemma 4.2. Hence, we suspect that the FDI problem is not solvable for this system.

Moving this third measurement around, it becomes clear that only a direct angle measurement at bus 3 or a generator speed measurement at bus 3 can be used to attenuate this additional disturbance.

5.2 Fault Detection and Isolation for a Large-Scale System: WSCC 179-Bus System

The system under consideration in this section is the 179-bus aggregated version of the Western States Coordinating Council (WSCC) power system we introduced in Section 4.4.

In Figure 5.8 we illustrate on the WSCC 179-bus one-line diagram the fault, disturbance and measurement locations assumed for our example. We will assume that there are two faults and two disturbances. For each fault we chose a disturbance in close proximity, e.g., for the fault at bus 30 we chose a disturbance at bus 79, and for the fault at bus 40 we chose a disturbance at bus 43. We assume that we have direct angle measurements at buses 34, 59, 83 and 2 available for filter design. All the disturbances and faults are assumed to be in the form of mechanical power pulse perturbations. The unknown-input steps had the following amplitudes from $t = 0.01s$ to $t = 1.01s$: $\widetilde{P}_{30}$ – $0.5p.u.$; $\widetilde{P}_{40}$ – $1p.u.$; $\widetilde{P}_{43}$ – $-0.5p.u.$; and $\widetilde{P}_{79}$ – $1p.u.$.

In Figure 5.9 we show the residuals when all four unknown inputs (i.e., both faults and both disturbances) occur simultaneously. We notice that the residuals driven by the disturbances stay approximately zero and can be left out of the FDI-filter realization by choosing $Q = \begin{bmatrix} I_2 & 0 \end{bmatrix}$. From this figure we notice that $r_1(t)$ and $r_2(t)$ react during the event period. The amplifying gains used in the residual generator were not chosen very small in order to avoid numerical integration problems (attributed to large discontinuities when we want amplify the residual when the fault occurred). From this figure we note that we can identify

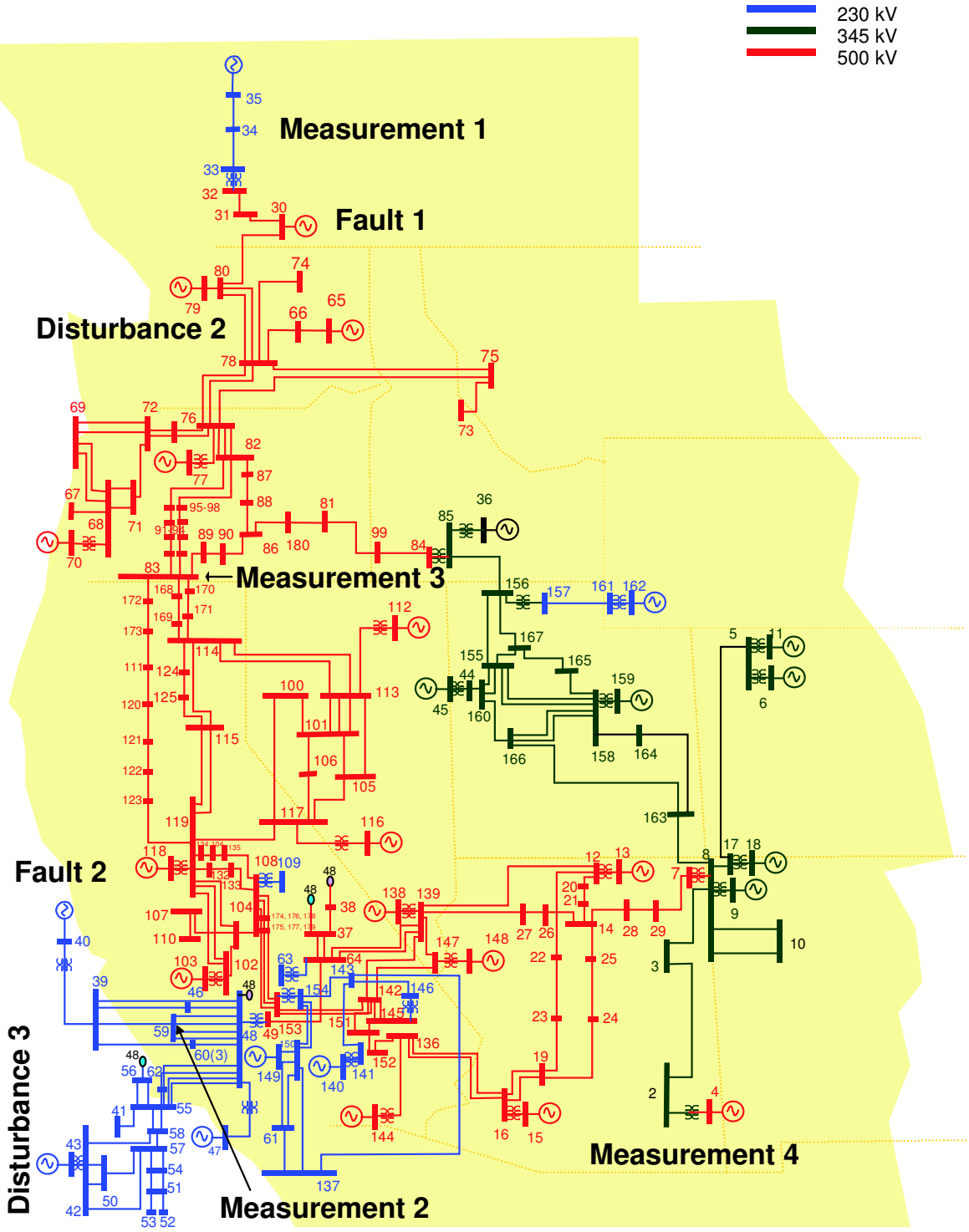

Figure 5.8: One-line diagram of an aggregated WSCC network, illustrating fault, disturbance and measurement locations.

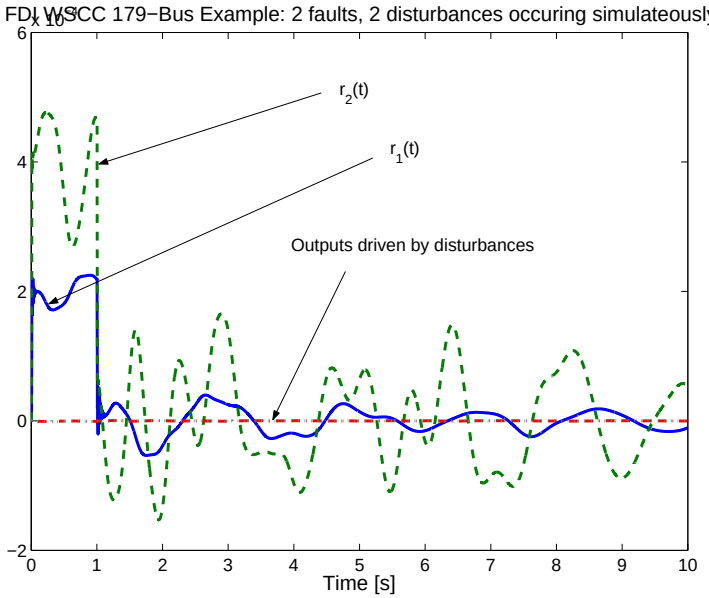

Figure 5.9: FDI example 1 for the WSCC 179-bus system. Faults: P_{30} and P_{40}; disturbances P_{79} and P_{43}; Measurements: θ_{34}, θ_{59}, θ_{83} and θ_2. In this simulation all four unknown-inputs occurred simultaneously between $0.01s$ and $1.01s$.

and isolate both faults that occur simultaneously.

5.3 Conclusions

In this chapter we discussed the fault detection and isolation problem using observers. We briefly surveyed the literature in the field, and then illustrated how we can design FDI-filters using our graphical observer design approach introduced in Chapter 4.

We found the graphical observer design to be very suited for the creation of fault detection and isolation filters for swing models of power systems. Following our design approach discussed in Section 4.2.2 and Theorem 4.1, we know that we can manipulate every element in

the transfer function from unknown-inputs to estimation errors (i.e., $G_{ew}(s)$) under certain conditions (that the swing models often meet). Under these conditions we can enforce a certain structure on $G_{ew}(s = 0)$ such that for a single unknown-input the observer using a certain single measurement, $G_{ew}(s = 0)$ will have all zero entries except for the one corresponding to the measurement used in the observer realization.

For state estimation purposes we made this non-zero element in $G_{ew}(s = 0)$ tend to zero by increasing a specific gain element, however for fault detection and isolation purposes we want to increase this element by lowering this same gain element. By doing so we will amplify the fault (unknown input) instead of attenuating its effect as in the state estimation case.

In this chapter we illustrated how to design residual generators, following the above approach, on a small-scale (i.e., 9 bus) and a large-scale (i.e., 179-bus WSCC) examples. This chapter concludes our investigations on power system monitors and we will now introduce novel controllers that can manipulate electromechanical movements of a power system in response to an electromechanical perturbation.

Part II

Decentralized Controllers for Electromechanical Waves in Power Networks

Chapter 6

Decentralized Electromechanical Wave Controllers

In this chapter we present a class of novel electromechanical wave controllers (EWC's), extending those introduced in [26, 60], and suited for decentralized deployment in a power network. Analogs of these controllers can be found in electromagnetic transmission line theory (e.g., matched impedances) and active vibration damping (e.g., energy absorbing controllers and vibration isolation).

We will focus on the control of electromechanical transients associated with the acceleration, deceleration, and stability of shaft dynamics of generators that are coupled through an electric power grid. The notion of electromechanical disturbances in power systems propagating as traveling waves first appeared in a paper by Semlyen in 1974 [23], which presented partial differential equations describing the idealized continuum limit of a swing-equation model. Cresap and Hauer [24] analyzed the Western Power System in 1981, in order to explain the emergence of a new swing mode. They conjectured that a distributed homogeneous string of generators can provide information about the low frequency modes of the system. The

simple wave equation they obtained was used to obtain the model frequencies, which they then reconciled with observed data of the actual system. More recently, electromechanical waves in power systems were similarly modeled by Thorp, Seyler and Phadke [25], as a way to understand angle observations from phasor measurement units in the field. These electromechanical waves are manifested in the mechanical shaft dynamics of electrically-coupled generators.

Accepting that electromechanical disturbances spread as traveling waves, one can design a controller to extinguish these transients in a manner analogous to impedance matching on transmission lines. In [26] and [60], we demonstrated that "zero-reflection" controllers (ZRC's) that enforce an impedance matching constraint at the boundary of the network effectively quench electromechanical traveling waves on the network. In [26] we also showed that this control strategy appears to be robust to wide variations in parameter values. In that work mostly regular grids of generators were considered. In this chapter we will extend these initial electromechanical wave control ideas and develop "zero-transmission" controllers (ZTC's), perturbation-quenching controllers (PQC's) and comment on placing ZRC's inside (as opposed to at the boundary) the network. At first these EWC will be introduced in the context of elementary (yet descriptive) swing models describing regular networks (such as a string of generators). We will also investigate the generalization of these EWC's to be applicable to more elaborate power system descriptions and their application to more general networks are to be covered in Chapter 7.

It is important to emphasize that the EWC approach to power system control design is very

different from traditional methods. Typical tuning of governor and power system stabilizer controls use linearized models and modal analysis [27]. Usually this is accomplished with a detailed model of the generator(s) to be tuned and a simplified representation for the remainder of the system. Hence, little spatial information is used in the design. In cases when a detailed representation over a wide geographical area is used, modal techniques are employed. One identifies critical modes of oscillations, and perhaps their mode shapes, and tunes the controller accordingly [27]. This approach is analogous to representing the dynamics as a superposition of standing waves rather than a traveling wave.

The damping controllers that are developed in this chapter have a similar structure to a damping controller Samuelsson proposed in [61]. The latter damping controller modulates active power injection at a load bus by using bus frequency as the controller input. Samuelson's and our damping controllers are the electromechanical equivalent of a dash-pot in a mechanical system or a resistor in a electric circuit. One of the differences between Samuelsson's damping controller and ours is the approach to designing the electromechanical 'impedance' (controller gain) of the controlled element. Samuelsson designs this impedance by using modal analysis and root locus design techniques, in order to increase the damping of a select few modes of the system [61, 62]. We, on the other hand, arrive at the gains of our damping controllers (ZRC's and PQC's) by thinking of a power network as a distributed 'electromechanical transmission line' (also referred to as a string-of-generators) in the one-dimensional case or as an 'electromechanical membrane' in the two-dimensional case. In [26] and [60], we designed the ZRC impedance to be equal to the electromechanical impedance of the string of generators, enforcing an impedance matching constraint resulting in zero

reflections.

Samuelsson suggests a means to practically realize one of his active power controllers by on-off control of a heating load (a field test of this controller is discussed in [61]). Interestingly, Japanese researchers have proposed and tested a similar type of superconducting magnetic energy storage (SMES) controller [63], where a more heuristic experimental approach was followed to derive an appropriate control law.

Samuelsson investigated the scenario where multiple damping controllers are used in order to damp extensive slow modes of the system [62]. He recognized that in order to achieve maximum damping for these modes the gains of these multiple damping controllers cannot be set arbitrarily large. He discussed the connection between maximum damping and impedance matching in the context of lumped parameter circuits, and used this analog as an explanation why the gains of the controllers cannot be set arbitrarily large. In the next chapter we will report our initial investigations into implementing multiple electromechanical wave controllers on general power networks. We point to how one can design appropriate controller gains without resorting to modal analysis and root locus design techniques.

In the following section the result of the electromechanical wave equation for swing power networks, as derived in [26], will be summarized. In Section 6.1.3 the insertion of a lumped electromechanical element connected in shunt between two 'electromechanical transmission lines' will be analyzed. In Section 6.2 electromechanical controllers are developed and tested on a string of generators.

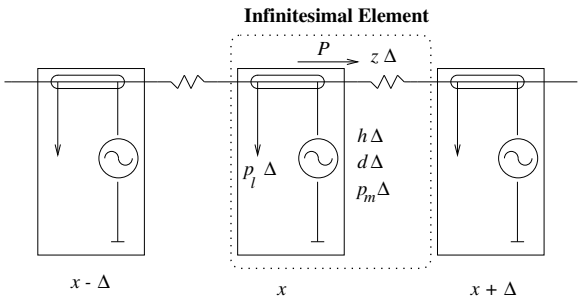

Figure 6.1: A link in a string of generators

6.1 Electromechanical Wave Theory

6.1.1 The Continuum Model

To develop a continuum swing model we start with a one-dimensional grid (string) of infinitesimal generators spaced infinitesimally apart. A single link in a chain of generators is highlighted in Figure 6.1, where x denotes spatial position. In this figure, the line impedance between generators is denoted by $z\Delta$, where Δ is the spatial distance separating neighboring generators and z is per-unit impedance per unit length. Similarly, the generator parameters are expressed as $h\Delta$, $d\Delta$ and $p_m\Delta$ respectively, where h is the inertia constant per unit length, d is the damping coefficient per unit length, and p_m is the mechanical input power per unit length. We assume a local load consuming real power $p_l\Delta$ and define $p_g = p_m - p_l$. In general z, h and d could be functions of position, but we shall focus on the case where these parameters are invariant with position. We neglect machine reactance, and also assume the voltage magnitude E is constant in space and time.

Writing $z^{-1} = g - jb$, the classical machine equation for the generator at position x can be

written as

$$\begin{aligned}\frac{2h\Delta}{\omega_s}\frac{\mathrm{d}^2\delta(x)}{\mathrm{d}t^2} &= p_g\Delta - d\Delta\frac{\mathrm{d}\delta(x)}{\mathrm{d}t} \\ &\quad -\frac{E^2b}{\Delta}\left(\sin(\delta(x)-\delta(x-\Delta))\right. \\ &\qquad \left. +\sin(\delta(x)-\delta(x+\Delta))\right) \\ &\quad -\frac{E^2g}{\Delta}\left(2-\cos(\delta(x)-\delta(x-\Delta))\right. \\ &\qquad \left. -\cos(\delta(x)-\delta(x+\Delta))\right) \end{aligned} \tag{6.1}$$

where ω_s is the nominal system frequency and δ is the machine angle relative to a frame rotating at ω_s. By taking the limit as $\Delta \to 0$ the paper [25] arrives at a nonlinear wave equation in δ. The controller we design in this paper is obtained from the simplified *linear* and undamped wave equation obtained under the assumptions $g = 0$ and $d = 0$. (However, the controller is tested in our simulations on lumped models for which both line conductance and machine damping are nonzero.) The simplified equation is identical to that in [23], and can be obtained as shown below.

By taking $g = 0$ and $d = 0$, the second and fourth terms on the right hand side of (6.1) disappear. Let P denote the power flow at x in the direction of increasing x. We find that in the limit as $\Delta \to 0$:

$$P = -E^2b\frac{\partial\delta}{\partial x} \tag{6.2}$$

because $\sin(\delta(x+\Delta)-\delta(x)) \approx \delta(x+\Delta)-\delta(x)$ for small Δ (assuming δ is continuous in x).

Let ω denote the deviation of machine speed from ω_s (so $\omega = \frac{d\delta}{dt}$). Then using (6.2) in equation (6.1) it is easily seen that in the limit the following partial differential equation results:

$$\frac{2h}{\omega_s}\frac{\partial \omega}{\partial t} = p_g - \frac{\partial P}{\partial x} \tag{6.3}$$

Differentiating (6.2) with respect to t, we get:

$$\frac{\partial P}{\partial t} = -E^2 b \frac{\partial \omega}{\partial x} \tag{6.4}$$

The pair of equations (6.3), (6.4) are analogous to the standard *telegrapher's equations* for electro*magnetic* waves on a transmission line, with P playing the role of line current and ω playing the role of voltage. From (6.2), (6.3) and (6.4), it is easy to obtain linear undamped wave equations for δ, ω, or P. For instance (6.3) and (6.2) together yield:

$$\frac{2h}{\omega_s}\frac{\partial^2 \delta}{\partial t^2} = p_g + E^2 b \frac{\partial^2 \delta}{\partial x^2}. \tag{6.5}$$

For two-dimensional grids, a similar derivation yields the same sorts of equations, but the parameters will have different units and the second derivative with respect to x is replaced by the Laplacian operator in two dimensions. For example, in two dimensions, h will correspond to inertia constant per unit area, and z will be per-unit impedance per unit length per unit cross-sectional width. However, in this thesis we will focus on the one-

dimensional wave equation and a practical power system will be seen as an interconnection of multiple one-dimensional lines.

6.1.2 One-Dimensional Wave Phenomena on a String-of-Generators

Equation (6.5) is a wave equation in the variable δ with characteristic velocity of propagation equal to

$$v = \sqrt{\left(\frac{\omega_s}{2h}\right)(E^2 b)}. \tag{6.6}$$

For purposes of illustrating wave phenomena in a string of generators, and to introduce an example on which we will later test different electromechanical controllers, we adapt a model presented in [25]. Specifically, we break the discrete ring system they considered, to form a string of 60 identical generators connected through identical transmission lines. (Note that in [26] we investigated a string of 64 instead of 60 generators.) With $\frac{2H}{\omega_s} = 1$, $E = 1p.u.$, $g = 1p.u.$ (line conductance), $d = 0.01p.u.$ (machine damping), and $b = 6p.u.$ ('negative' line susceptance) the classical machine equations describing this system in standard state space form are of the form (2.12). In the simulation that follows, the trivial loadflow solution is assumed.

The results of a simulation, where a power pulse perturbation was applied (amplitude $0.1p.u.$, $t_{begin} = 0.01s$, $t_{duration} = 0.5p.u.$, electrical energy injected $W = 0.05p.u.$) at generator 30, are shown in Figures 6.2 to 6.4. In Figure 6.2 the time evolution of successive

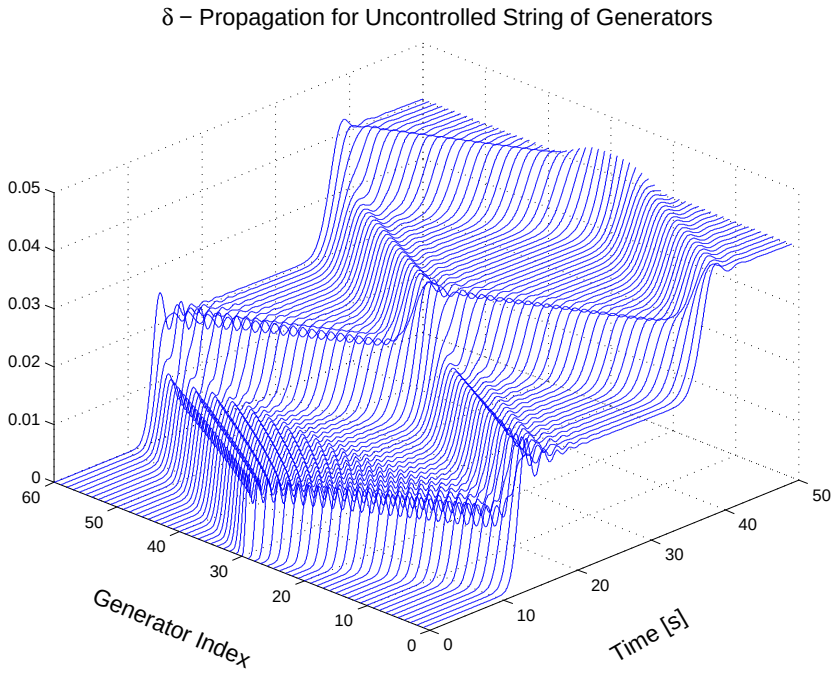

Figure 6.2: δ — wave propagation on an open-ended string of generators.

generator angles is shown. One can see the forward and reverse propagating waves and their (positive) reflections at the open-ended boundaries of the string of generators. One also notices the slow dispersion of the waves as they travel, which is due to the generator damping and the dissipative component of the line impedance.

In Figure 6.3 the deviational power flow on the transmission line sections between nodes s and t are shown. P_{st} is directional and defined as flowing from bus s to t.

In Figure 6.4 the angles of the generators at buses 30 and 60 are shown. The time it takes the electromechanical waves to travel down the line from bus 30 to 60 can be calculated as

$$t = \frac{x}{v} \approx \frac{30}{\sqrt{6}} = 12.25s, \tag{6.7}$$

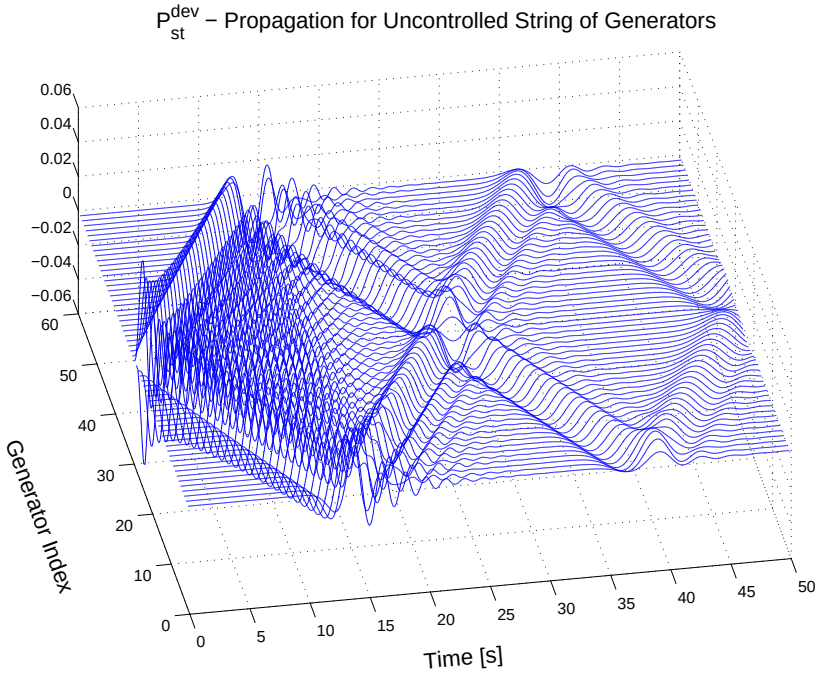

Figure 6.3: P_{st} — wave propagation on an open-ended string of generators.

which agrees well with the numerically calculated value of $12.33s$. (Note that the discrepancy can be due to the inclusion of line conductances during the simulation.)

We can calculate a wavelength associated with these wave-like swing motions. The wavelength λ is calculated as

$$\lambda = \frac{v}{f}, \tag{6.8}$$

where f is the frequency of the swing mode driving the wave-like propagation. Investigating the time-plots of ω and $\widetilde{P}$ (as well as executing a Fast Fourier Transform of ω_{60}) we find $f \approx 0.55Hz$. Using this value and the value for v we find that $\lambda = 4.4\Delta$. From standard electromagnetic textbooks we know that the discrete approximation (i.e., the nonlinear

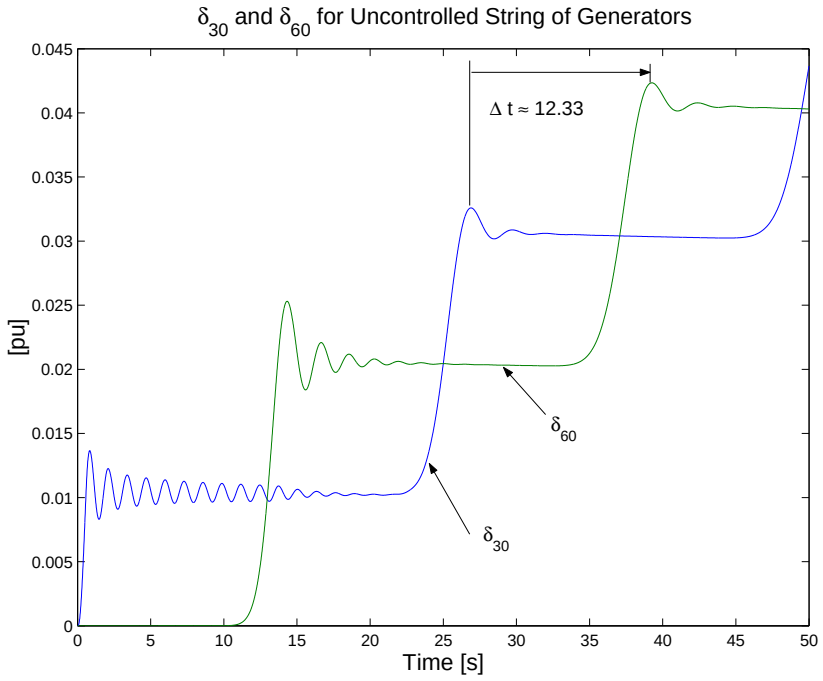

Figure 6.4: Plot of δ_{30} and δ_{60} showing the time taken to traverse from generator 30 to generator 60.

swing model) is a satisfactory replica of the continuum model (for low frequencies) when the discrete separation is much smaller than the wavelength. In this case this relation is smaller, but not substantially.

The traveling electro*mechanical* waves in this model are analogous to traveling electro*magnetic* waves on transmission lines. In the case of transmission lines, one considers traveling waves in terms of current and voltage, and one can describe the reflection using reflection coefficients based on the characteristic impedance of the line. Also, with proper termination, one can set the reflection coefficient to zero, which eliminates any reflection on the line. We propose to do the same with our string-of-generators example.

In the power system model, which exhibits electromechanical wave phenomena, we have

already seen that frequency and power flow are the variables that naturally play a similar role to voltage and current in the electromagnetic transmission line case. To find the characteristic impedance relating P and ω, consider forward traveling waves for both variables:

$$P^+ = P\left(t - \frac{x}{v}\right) = P(y) \tag{6.9}$$

$$\omega^+ = \omega\left(t - \frac{x}{v}\right) = \omega(y) \tag{6.10}$$

where v is the velocity of propagation. Substituting these into (6.4) gives

$$\frac{\partial P^+}{\partial y} = \frac{E^2 b}{v}\frac{\partial \omega^+}{\partial y}, \tag{6.11}$$

which leads to the solution

$$P^+ = \frac{E^2 b}{v}\omega^+. \tag{6.12}$$

This suggests that the forward traveling waves in power flow and frequency remain in constant proportion. The characteristic impedance, or proportionality constant, is defined by

$$C_o = \frac{\omega^+}{P^+} = \frac{v}{E^2 b} = \sqrt{\left(\frac{\omega_s}{2h}\right)\left(\frac{1}{E^2 b}\right)}. \tag{6.13}$$

At the ends of the string, the forward and reverse traveling waves must sum in a particular way to match the imposed boundary condition. If an end is open, i.e. power flow is equal to

zero, then the reverse traveling wave in power must be exactly the negative of the forward traveling wave, so that they sum to zero at the boundary. This situation corresponds to a negative reflection in power flow and a positive reflection in frequency (and angle). If the string of generators is terminated with a so-called "infinite bus" at which frequency is held constant, then the reverse traveling wave in frequency must be a negative reflection of the forward traveling wave. This corresponds to a negative reflection in frequency (and angle), and a positive reflection for power flow.

6.1.3 Inserting a Lumped Electromechanical Impedance Between Two Strings

In order to deal with more general power networks, it is instructive to consider the case depicted in Figure 6.5, where two different strings-of-generators are connected at $x = 0$. The string to the left has an electromechanical characteristic impedance of C_1, and the impedance of the string to the right is C_2. At $x = 0$ a lumped parameter electromechanical device is connected in shunt.

We assume that the electrical power P_c flowing into and the frequency ω_c across the lumped element are held in constant proportion,

$$\omega_c = CP_c. \tag{6.14}$$

An electromechanical element that maintains the above relationship is analogous to a re-

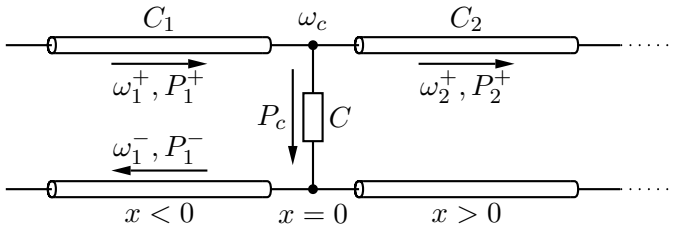

Figure 6.5: Connection of two different string-of-generators through a shunt lumped electromechanical element. ω_i^+ is the amplitude of the forward traveling frequency wave on the i^{th} string-of-generators and ω_1^- is the reverse traveling wave on string 1. The second string is infinitely long, hence no reverse traveling waves on string 2. The same convention holds for the power waveforms.

sistor in an electrical circuit, or a dash-pot in a mechanical system.

In this section, our aim is to define a reflection and transmission coefficient that will aid us in the development of different electromechanical wave controllers. Following an approach used in classical electromagnetic transmission line theory, we assume a time harmonic electromechanical wave excitation and can thus focus on the time-harmonic telegrapher's equations, which are ordinary differential equations in x for the phasors $\omega(x)$ and $P(x)$.

The solutions to the one-dimensional time-harmonic telegrapher's equations for the frequency waves are:

$$\omega_1(x) = \omega_1^+ e^{-jk_1 x} + \omega_1^- e^{jk_1 x}, \forall x \leq 0; \tag{6.15}$$

$$\omega_2(x) = \omega_2^+ e^{-jk_2 x}, \forall x \geq 0. \tag{6.16}$$

where k_1 and k_2 are the wave-numbers associated with string-of-generators 1 and 2 respectively; also ω_i^+ and ω_i^- are wave amplitudes of the forward and backwards traveling waves on the i^{th} string-of-generators. We assume that the string-of-generators for $x > 0$ is infinitely

long and that no backward traveling waves will exist, hence $\omega_2^- = 0$.

The solutions to the one dimensional time-harmonic telegrapher's equations for the electrical power waves are:

$$P_1(x) = P_1^+ e^{-jk_1 x} + P_1^- e^{jk_1 x} = \frac{\omega_1^+}{C_1} e^{-jk_1 x} - \frac{\omega_1^-}{C_1} e^{jk_1 x}, \tag{6.17}$$

$$P_2(x) = P_2^+ e^{-jk_2 x} = \frac{\omega_2^+}{C_2} e^{-jk_2 x}, \tag{6.18}$$

where we have used the fact $\frac{\omega_1^+}{P_1^+} = -\frac{\omega_1^-}{P_1^-} = C_1$.

Evaluating an electrical power balance at $x = 0$ (the electromagnetic equivalent is a current balance), we find that

$$\begin{aligned} P_c &= P_1(x=0) - P_2(x=0) \\ &= \frac{\omega_1^+}{C_1} - \frac{\omega_1^-}{C_1} - \frac{\omega_2^+}{C_2}. \end{aligned} \tag{6.19}$$

Furthermore, at $x = 0$ we know that $\omega_1(x=0) = \omega_2(x=0) = \omega_c$. Substituting $\omega_1^+ + \omega_1^-$ in place of ω_2^+ and ω_c in (6.19), we can calculate a reflection coefficient as

$$R_\omega = \frac{\omega_1^-}{\omega_1^+} = \frac{C_1^{-1} - C_2^{-1} - C^{-1}}{C_1^{-1} + C_2^{-1} + C^{-1}}. \tag{6.20}$$

Substituting ω_2^+ in place of ω_c in (6.19) and using (6.20), we can calculate a transmission

coefficient

$$T_\omega = \frac{\omega_2^+}{\omega_1^+} = \frac{2C_1^{-1}}{C_1^{-1}+C_2^{-1}+C^{-1}}. \tag{6.21}$$

There is a relationship between the reflection and transmission coefficients that can be obtained from the continuity constraint on the frequency waves at $x = 0$:

$$\omega_2^+ - \omega_1^- = \omega_1^+ \tag{6.22}$$

$$\Rightarrow T_\omega - R_\omega = 1. \tag{6.23}$$

The reflection and transmission coefficients are expressed for the frequency waves, and similar coefficients for the electrical power waves can be expressed in terms of the frequency waves' coefficients:

$$R_P = \frac{P_1^-}{P_1^+} = -R_\omega; \tag{6.24}$$

$$T_P = \frac{P_2^+}{P_1^+} = \frac{C_1}{C_2} T_\omega. \tag{6.25}$$

We can define an electrical power sink (or absorption) coefficient for the stationary con-

straint as:

$$S_P = \frac{P_c}{P_1^+} \tag{6.26}$$

$$= \frac{(1+R_\omega)C_1}{C} \tag{6.27}$$

$$= \frac{T_\omega C_1}{C} = \frac{2C^{-1}}{C_1^{-1}+C_2^{-1}+C^{-1}}. \tag{6.28}$$

Investigating the electrical power balance at $x = 0$ we have:

$$P_1(x=0) = P_2(x=0) + P_c \tag{6.29}$$

$$\Rightarrow P_1^+ + P_1^- = P_2^+ + P_c, \tag{6.30}$$

from which we find the relationship between T_P, R_P and S_P as,

$$T_P + S_P - R_P = 1. \tag{6.31}$$

The classic case addressed in electromagnetic transmission line theory deals with only one transmission line terminated in a load impedance C, so $C_2 = \infty$ in effect. For this case $R_\omega = \frac{C-C_1}{C+C_1}$ and $T_\omega = \frac{2C}{C+C_1}$. Matching the impedances by setting $C = C_1$ results in zero reflection. The part of the wave that is transmitted does not flow on any string (because none exists), but appears to flow on a virtual infinitely long string to the right of the constraint. For this matched impedance situation $S_P = 1$, and the maximum *electromechanical* power is transferred to the load.

Suppose now that string 1 is open ended at $x = 0$ (i.e., $C \to \infty$, in addition to $C_2 = \infty$, hence power flow equals zero). We find that $R_\omega = 1$ and $T_\omega = 2$ in this case. In the power system context, this implies that frequency (and angle) doubling will occur at the constraint, in conjunction with a negative reflection of power flow to yield zero power flow at the constraint point.

Now suppose this single string-of-generators is connected to an infinite bus at $x = 0$ (i.e., $C = 0$ and $C_2 = \infty$); we then compute $R_\omega = -1$, $T_\omega = 0$ and the frequency will remain constant at the constraint (i.e., $\omega_c = 0$).

6.2 Electromechanical Wave Controllers

Various types of electromechanical wave controllers can be realized by manipulating C, ω_c, or P_c. These control laws are motivated by the preceding electromechanical wave theory but will be implemented on discrete irregular power networks, where it might not be apparent that wave behavior exists. We will begin by looking at the zero-reflection controller discussed in [26] and [60], then move on to a zero-transmission controller and lastly investigate a perturbation-quenching controller.

6.2.1 Zero Reflection Control

We start off by recapping [26] and [60]. We confine our investigation to a single string (i.e., $C_2 = \infty$ in Figure 6.5). Terminating this string with $C = C_1$ would result in zero

reflections. In [26] it was shown how this impedance matching constraint can be achieved with a generator for the nonlinear discrete swing model. Moreover, by ensuring that the *deviation* in power flow from nominal into the end generator and the *deviation* in frequency from nominal of the end generator stay in the constant proportion C_1, the termination in a matched impedance can be enforced.

Given a simple swing equation model, the most natural control input is the mechanical power to the controlled generator. One could also consider controlling a local load power at the controlled generator bus, for instance using some flexible AC transmission system (FACTS) and/or SMES devices.

The control objective is to maintain the following relation:

$$\widetilde{P}_{end} = \frac{\omega_{end}}{C_1} \tag{6.32}$$

where $\widetilde{P}_{end}$ is the deviation from nominal in the line power flow $\overline{P}_{end}$ to the terminating generator. In [26] it was shown that a controller using the control law

$$\widetilde{P}_{g,end} \;=\; K(\widetilde{P}_{end} - \frac{\omega_{end}}{C_1}) - \widetilde{P}_{end} + D\omega \tag{6.33}$$

can approximately achieve this objective (where K is a gain, $\widetilde{P}_{g,end}$ is the deviation of $P_{g,end}$ from its nominal value $\overline{P}_{g,end}$). This control can be implemented if one possesses good estimates of the parameters C_1 and D, and good measurements of $\widetilde{P}_{end}$ and ω; otherwise, approximations to this control law (for instance omitting the term $D\omega$) can be considered.

Substituting (6.33) into the classical machine equation of the controlled generator, the dynamical equation becomes:

$$\frac{2H}{\omega_s}\frac{\mathrm{d}\omega_{end}}{\mathrm{d}t} = K\left(\widetilde{P}_{end} - \frac{\omega_{end}}{C_1}\right). \tag{6.34}$$

In [60] we showed that (6.32) can be achieved exactly, however the resulting control law required additional information (e.g. $\frac{\mathrm{d}\widetilde{P}_{end}}{\mathrm{d}t}$). From simulation, our example in [60] suggested that the performance enhancement between achieving (6.32) exactly versus approximately was small.

If the gain K can be chosen such that the generator dynamics are fast enough to track the incident wave, this controller will effectively eliminate reflections. If, due to physical limitations on $\widetilde{P}_{g,end}$, the dynamics cannot track the wave, then some reflection will occur. In the latter case, some other actuation will be required to meet the control objective (6.32). Choosing K too large might result in an overshoot of ω, inducing additional reflections.

We tested controller (6.33) on the 60-machine system introduced in the previous section. The controller is realized at machine 60, the gain is chosen to be $K = 2$, and it is assumed that measurements of frequency and electric power out of the generator are available. (Typically these measurements should be available on all machines.)

The results of simulations using the same initial disturbance described previously are shown in Figure 6.6. From this figure we see that the controller has eliminated the reflection observed without the controller (compare Figure 6.6 with Figure 6.2). The other end of the

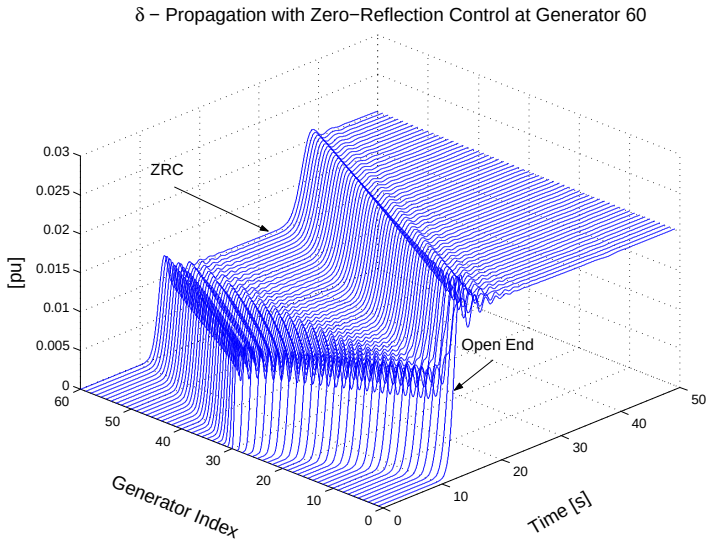

Figure 6.6: Angle wave propagation on a string-of-generators with a zero-reflection controller realized at the end generator.

string-of-generators remains open, and a reflection is observed at that end.

The controller works extremely well. If examined very closely, one can see that it does not completely eliminate reflections. Certainly there are a number of reasons why this is the case. The most obvious is that the wave equation model used to derive the controller is different from the lumped model governing the swing-motions of the string-of-generators. The former is distributed, linear, and neglects damping; the latter is discrete (in space) and contains nonlinearities. Furthermore, the controller objective is not achieved directly, but is implemented through an input into a generator. In Figure 6.7 we see that the waves of ω^+ and P^+ stay in constant proportion at the end generator, and conclude that the control objective is sufficiently met.

It is possible to realize a ZRC by controlling the power flowing into the lumped element

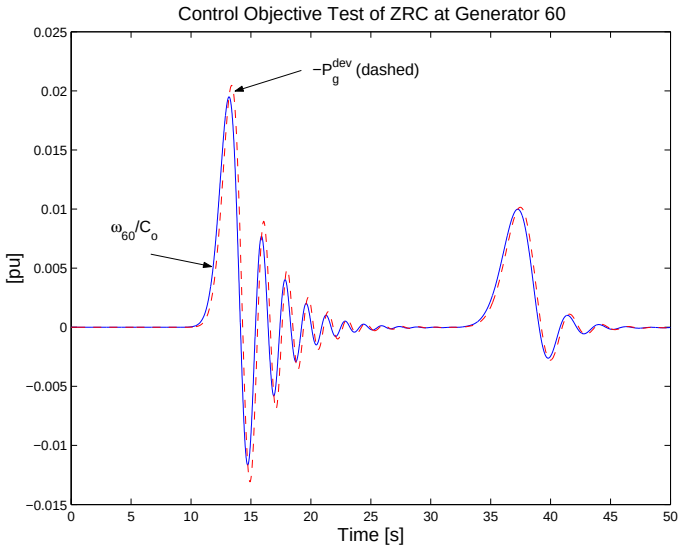

Figure 6.7: Control objective check at end generator (where a ZRC is realized).

directly. In the discrete power network this corresponds to controlling the deviational load power extraction at the bus. One possible approach is to set the deviational local load extraction to be equal to $\frac{\omega_{end}}{C_1}$. However, assuming the generator is absent at the end bus and hence only a local load extraction remains, it may be that ω_{end} will not be available. Samuelsson [61] advocates a similar control law and he has two approaches to deal with the issue of not having an ω readily available at the controlled load bus: lead filter the bus angle measurement at the controlled bus; or use the machine speed of the 'nearest' generator. Both of these approaches can present problems and for the second approach it might be difficult to gauge which machine is the closest.

Setting the controlled load extraction equal to $\frac{\omega_{end}}{C_1}$ presents us with a further predicament, that of using the appropriate mass $\frac{2h}{\omega_s}$ when calculating C_1. (Note that a load bus in the the swing model does not have an associated mass, because the swing models we study in

this thesis belongs to the class of Differential Algebraic Equation models.) Following an ad-hoc procedure we can use the mass of the 'nearest' generator, but it might be difficult to gauge which machine is the nearest. Not having the appropriate mass available does not influence the root-locus design technique that Samuelsson use to obtain the impedance of his controller [61].

A clear choice for our string-of-generators example is to use the machine speed at the adjacent generator. For this scenario the ZRC-Load control law takes the following form:

$$\widetilde{P}_{g,end} = -\frac{\omega_{end-1}}{C_1}. \tag{6.35}$$

We recognize the similarities between our ZRC and direct velocity (or force) feedback control used for damping control of active structures [64]. Such controllers absorb perturbation energy and are aptly named absorbing controllers. These energy absorbing controllers ensure that the closed-loop system is passive and as a result globally asymptotically stable [64]. The controller configuration belongs to the class of collocated controllers (i.e., the sensor and the actuator are located at the same location) [64], making it ideal for decentralized deployment. (Samuelsson also highlighted this point in [62], where he discussed his electromechanical damping controller that is realized at load buses and manipulates active power injection at the load.) Furthermore, the controller gain is only a function of local network parameters.

In Figure 6.8(a) we show the eigenvalues of the linearized system of the string-of-generators

with a ZRC implemented at generator 60. We can check whether this controller achieved maximum damping by linearizing this closed loop system at the current operating point. Furthermore, let us assume that the controller gain of $\frac{1}{C_1}$ is $\frac{1}{C}$, where C can be varied. Conducting a root-locus study for this feedback structure we increase the controller gain, $\frac{1}{C}$, from 0 to infinity. The result of this root-locus is shown in Figure 6.8(b). In Figure 6.8(c) we focus on the movement of one of the closed-loop eigenvalues when we increase the gain of the controller. Comparing Figure 6.8(b) with Figure 6.8(a) it is evident, from the envelope of the pole-zero movement that we achieve approximately maximum damping on all the modes when $C = C_1$. Thus, the turning point of the nose-curve plot shown in Figure 6.8(c) would correspond to when $C = C_1$. A more thorough stability analysis is warranted when one considers actuator limitations (such as ramp-rate limits) of the proposed controllers.

Energy Properties of Controllers

From Figure 6.6 we conclude that the perturbation energy has been *quenched*, and the system has settled at a new operating point. In the following two paragraphs, we will discuss the electrical and electromechanical energy balances associated with the system.

Electrical Energy Balance: We anticipate that the electrical energy we injected through the power pulse to be extracted by the zero-reflection controller. Integrating the control effort over time we find $\int \widetilde{P}_{g,end}\,\mathrm{d}t = -0.048 \approx -0.05[(p.u.)s]$, and the electrical energy injected into the system by means of a power pulse was $0.05[(p.u.)s]$. Thus, the electrical energy injected into the system is extracted by the ZRC, but this extraction is *distributed* in time. In addition, the amplitude of the control effort is equal to the amplitude of the impinging

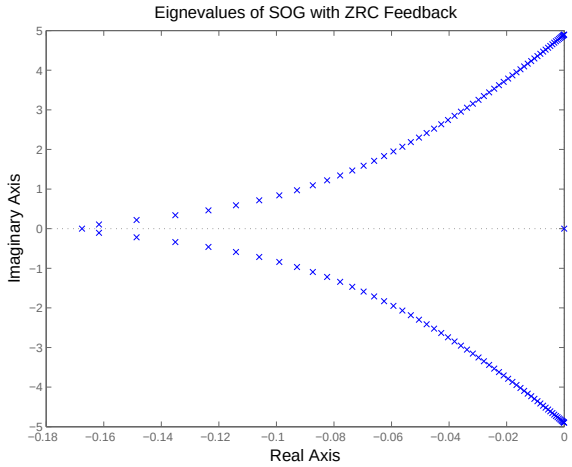

(a) Eigenvalue plot for the string-of-generators example with a ZRC at the end generator.

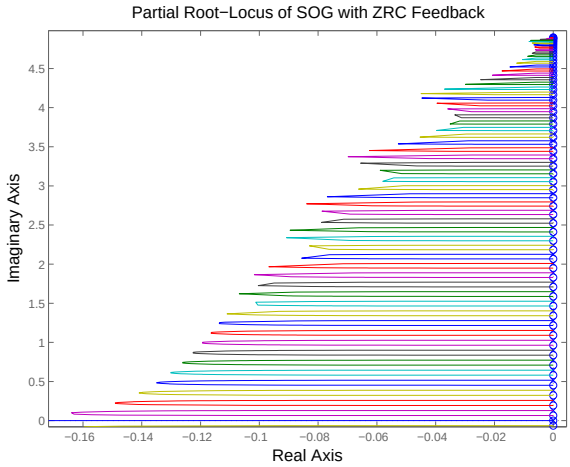

(b) Root locus plot of collocated controller at the end generator for the strings-of-generator example.

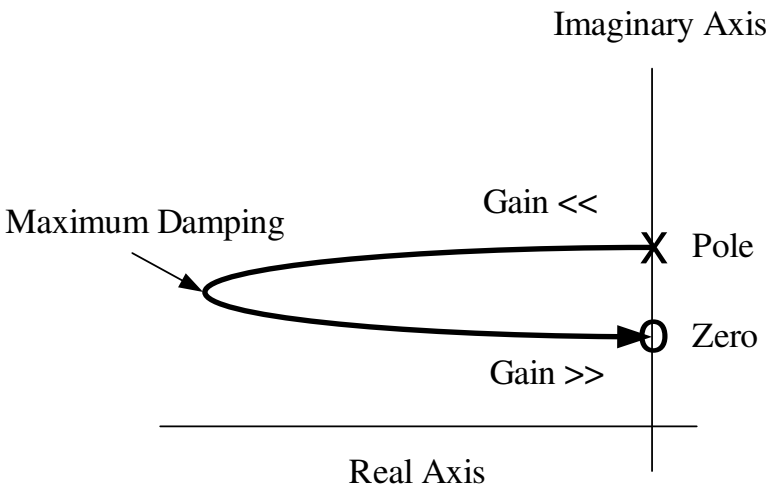

(c) Single eigenvalue movement when we modify the gain $\frac{1}{C}$ from small to large.

Figure 6.8: Eigenvalue plots for the linearized-ZRC closed loop system.

power wave, and has a maximum amplitude variation of 20% of the original perturbation pulse amplitude.

Electromechanical Energy Balance: From Figure 6.6, we notice that the angle differences across the edges are the same at the initial time instant and the final time instant, implying that the potential energy associated with angle differences across electrical transmission lines is unchanged between the initial and final times. The kinetic energy is similarly unchanged, because the generator speeds returned to synchronous. Hence the total work done on the system is zero. This constraint can be expressed in terms of the velocity of the center of inertia (*coi*) of the system:

$$\int_{t_0}^{t_f} (\widetilde{P}_{g,30} + \widetilde{P}_{g,60}) \omega_{coi} \, \mathrm{d}t = 0 \tag{6.36}$$

where $\omega_{coi} = \sum_{i=1}^{60} \frac{M_i}{M_{total}} \omega_i$. Evaluating the above integrals, we find that the electromechanical energy injected into the system is $\int \widetilde{P}_{g,30} \omega_{coi} \, \mathrm{d}t = 2.21 \times 10^{-5} p.u.$, and is approximately equal to the electromechanical energy absorbed by the ZRC, namely $|\int \widetilde{P}_{g,60} \omega_{coi} \, \mathrm{d}t| = 2.22 \times 10^{-5} p.u.$, confirming that the electromechanical perturbation was quenched. (For a discussion on energy function analysis in power systems, see [32].)

Another form of ZRC can be achieved at non-boundary buses. For the case depicted in Figure 6.5, if $C^{-1} = C_1^{-1} - C_2^{-1}$ it follows that $R_\omega = 0$ and $T_\omega = 1$. Such a controller can *shepherd* the whole impinging perturbation into a particular part of the network that is geared towards dealing with perturbations. Note, however, that for the scenario where $C_1 = C_2$, an infinite value of C results and the controller will be non-existent.

Two-Dimensional Example: L-shaped Grid of Generators

In [26] we also tested this control strategy on a 30-by-30 regular two-dimensional grid of generators, using the same generator and network impedance parameters as in the string-of-generators examples. By placing zero-reflection controllers on all generators located on the edges of the grid, one might expect that waves incident normally to the edges will not reflect, while waves not incident normally will propagate along the edge. This was indeed the case, as illustrated in [26]. Again, the controller works remarkably well; the initial disturbance travels to the edges of the grid and is essentially eliminated.

The objectives of the following example are three-fold. We want to illustrate how one can use these one-dimensional ZRC to control a two-dimensional grid of generators, and to show that the grid parameters need not be homogenous, and also show that the controllers only need local network information (making them ideal for decentralized control). We will thus examine an L-shaped grid with spatially varying parameters (first introduced in [26]). The parameters of each line and generator (only inertias) were randomly perturbed using a uniform distribution ranging from -90% to $+90\%$ of the corresponding nominal values.

The zero-reflection controllers on the boundaries of the grids are designed using only local characteristics of the grid. The controllers are designed to eliminate the normal component of the incident waves. Thus, only information about lines directed inward from the boundary are required for controller design. An initial machine angle displacement in the form of a two-dimensional Gaussian pulse was assumed and selected time shots of the time evolution due to this perturbation are shown in Figure 6.9. The time sequences of spatial plots shown

in this figure indicates how traveling waves traverse the non-uniform grid. The left-hand side of the time sequence plots correspond to the system response when no control was applied. The right-hand side plots correspond to the case when ZRC's were implemented on boundary generators. From these plots, it is evident that for the perturbed parameter systems, traveling wave phenomena are still evident, although the waves are non-smooth due to mismatched impedances inside the network. The general wave trend is visible and the deviations (due to parameter mismatches) are generally smaller than the traveling wavefront of the initial Gaussian angle disturbance.

This positive result on a system where the parameters varied significantly provide us with hope that we will be able to apply our EWC ideas to practical power systems.

6.2.2 Zero Transmission Control

Only being able to negate the electromechanical disturbance at the boundary of a network might expose heavily loaded parts of the network to a traveling electromechanical disturbance, making these parts prone to failures. This situation is not desirable and it might be beneficial for overall system stability and reliability if one is able to *confine* the disturbance to a local area and *quench* it locally. With this concept in mind, zero-transmission controllers (ZTC) will be developed in this section. (The analog of this concept in the mechanical vibration literature is vibration isolation.)

The premise of a ZTC is to negatively reflect the frequency and angle waveforms ($R_\omega =$

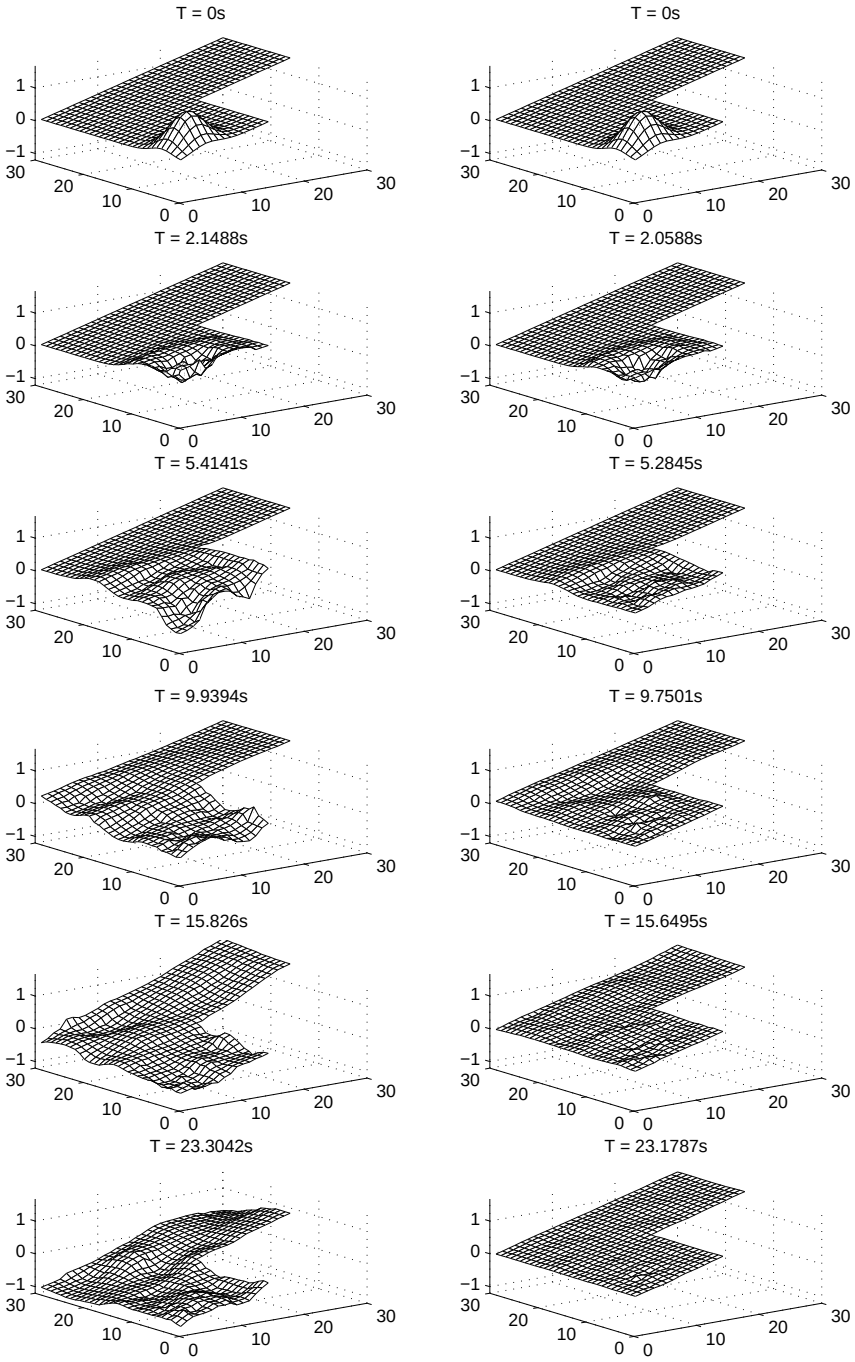

Figure 6.9: A sequence of snapshots of wave propagation in a 30x30 perturbed parameter L shaped grid of generators. Snapshots in lefthanded column correspond to the uncontrolled case and the snapshots in the righthanded column correspond to the ZRC case.

$-1 \Rightarrow T_\omega = 0$). In order to achieve zero transmission, the controlled generator should appear to have an electromechanical impedance $C = 0$. There are two ways to achieve this: by implementing a ZTC at a generator bus or a load bus.

When we implement the ZTC through a generator, it will have to appear as an 'infinite' bus when the waves hit the controlled (i.e. generator) bus. The controller will appear as an electromechanical short circuit and maximum deviational electrical power will flow into the controller. A conceivable ZTC control law can be obtained by replacing C_1 with $C = 0$ in the control law (6.33). However, the required control input power is infinite, which is not feasible. We can relax the requirement of having $R_\omega = -1$ and investigate the case where $R_\omega = -0.98$.

Implementing this control law at generator 50 for the string-of-generators example discussed above and applying the same power pulse perturbation at generator 30, we obtain the results shown in Figure 6.10. Note that when the forward traveling angle wave δ_1^+ encounters the ZTC at generator 50 (at approximately $8s$) it is reflected negatively, giving rise to δ_2^- traveling backward on the string. The backward traveling angle wave δ_1^- hits the open end of the string at roughly $12s$, and is positively reflected, giving rise to δ_2^+ traveling forward. Thus, it is evident that there are instances when the forward and backward traveling waves cancel one another. This *cancelling interference* of the angle waveforms can be beneficial to system operation.

From Figure 6.10, we note that after about $80s$ the waveform repeats (ignoring the small dispersion in the waveform due to nonzero line resistances). The controller does not ab-

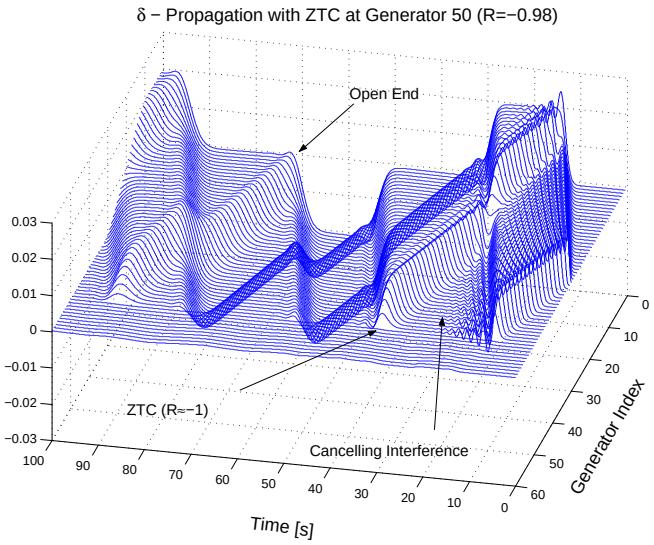

Figure 6.10: Angle wave propagation on a string-of-generators with a ZTC ($R_\omega = -0.98$) realized at generator 50.

sorb or inject any net electrical or electromechanical energy over this period. Moreover, integrating the control effort $\widetilde{P}_{g,50}$ over the cycle (i.e., from $t = 0$ to $t = 80s$) we find that the electrical energy injected into the system is very small (9.14×10^{-5}) compared to the perturbation energy injected (0.05). Thus, the injected energy (both electrical and electromechanical) due to the power pulse perturbation stays confined to the area between generators 1 and 50.

The negative reflection of ω is accompanied by a power doubling at the controlled bus; from Figure 6.11, we can see that the amplitude of the ZTC's control effort is twice the amplitude of the impinging power wave. Thus the amplitude of the ZTC's control effort shown in Figure 6.11 should be twice as large as the amplitude of the ZRC's control effort shown in Figure 6.7, which is easily verified.

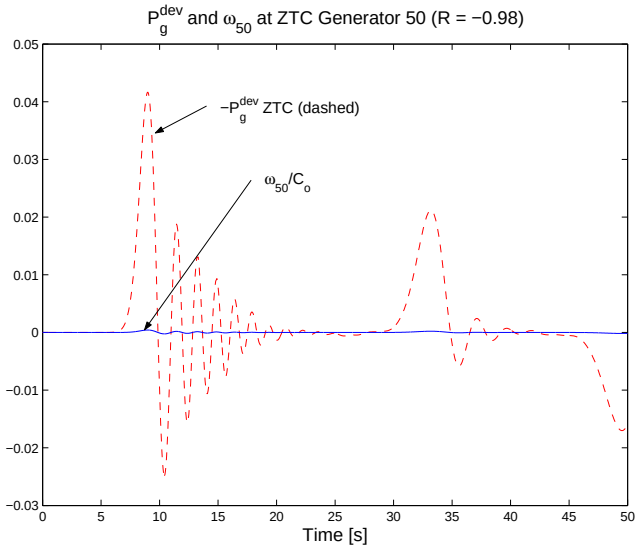

Figure 6.11: $\widetilde{P}_{g,50}$ and ω_{50} at generator 50 where a ZTC ($R_\omega = -0.98$) is realized.

In Figure 6.12 plots of ω_{50} and ω_{60} are shown. From this figure it is evident that not all of the incident wave (at generator 50) is reflected backwards; a small portion is transmitted to generator 60.

We can also realize a ZTC at a load bus by manipulating P_c instead of the bus frequency. For zero transmission we have $R_\omega = -1$ implying that $R_P = 1$ (from (6.24)) and $P_1^- = P_1^+$. By setting $C = 0$ in (6.28), we see that $S_P = 2$ implying that $P_c = 2P_1^+$ (i.e., power doubling). For this zero transmission scenario, we know that $P_c = P_1(x = 0) = P_1^+ + P_1^-$, and since $R_P = 1$ we have $P_c = 2P_1^+$. Translating this control requirement to the discrete nonlinear swing model, we note that all we need to maintain is $\widetilde{P}_{g,n} = -\widetilde{P}_{n-1,n}$. The controller throws the impinging wavefront back. This control law can be implemented at a load bus using a SMES device. In order to illustrate this point, we will remove the generator at bus 50 and realize a controlled load bus. Applying the same power pulse perturbation at generator 30,

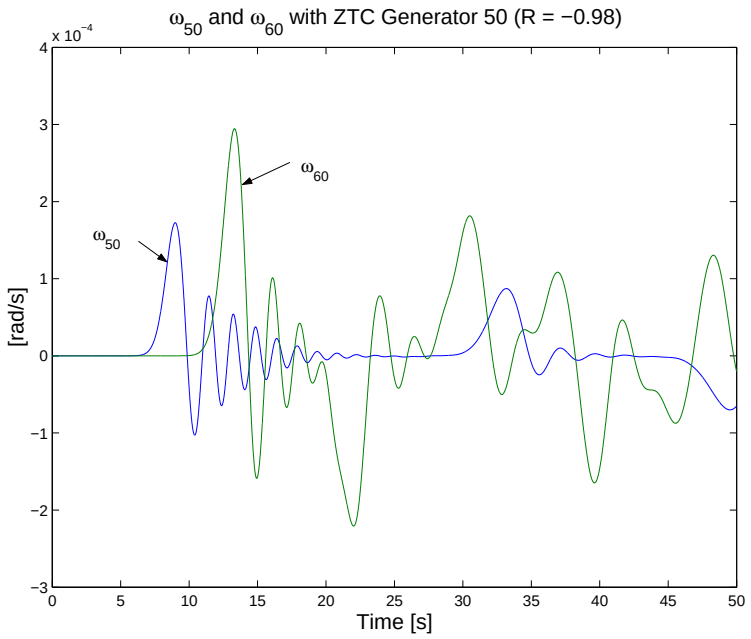

Figure 6.12: Plot of ω_{50} and ω_{60} showing that a small part of the wave does get transmitted.

we obtain the results shown in Figure 6.13.

6.2.3 Perturbation Quenching Control

As part of a *confining and quenching* strategy it will be helpful if we can extract electromechanical wave energy from the system at non-boundary buses. The purpose of this controller will be to absorb maximum incident electromechanical perturbation energy, thus limiting reflection and transmission of the incident wave.

The electromechanical power flowing into the lumped electromechanical element at $x = 0$

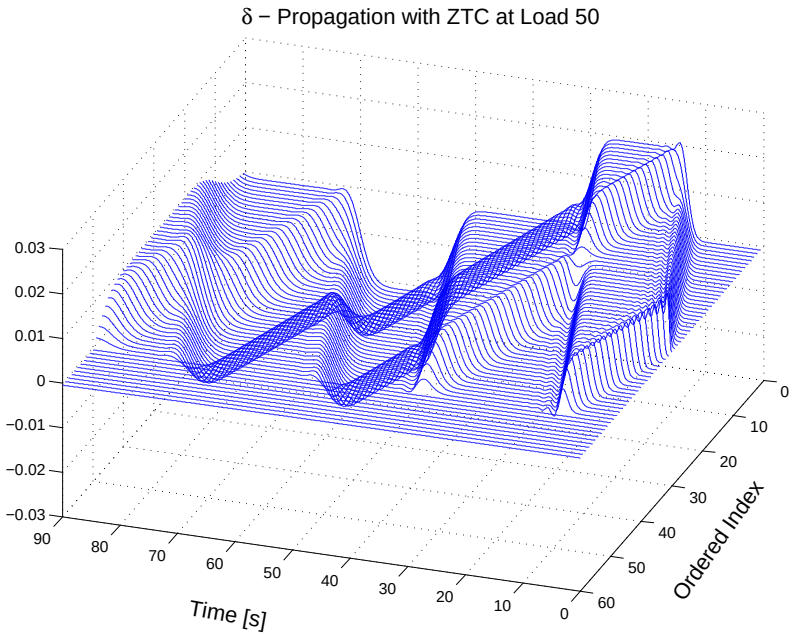

Figure 6.13: δ — wave propagation for a 60 bus string consisting of 59 identical generators and one load at bus 50 connected through identical transmission lines, with a ZTC implemented at bus 50. The reflection coefficient at bus 50 is $R_\omega = -1$.

(as shown in Figure 6.5) is

$$P_c\omega_c \quad = \quad \frac{\omega_c^2}{C_M} = \frac{(1+R_\omega)^2}{C_M}(\omega_1^+)^2, \tag{6.37}$$

where C_M is the impedance of the lumped element. Maximizing the incident electromechanical power (6.37) absorbed by the controller, we find that $C_M = (C_1^{-1} + C_2^{-1})^{-1}$, which is the parallel combination of the characteristic electromechanical impedances of the strings connected at $x = 0$.

We tested this controller on a modified 60-generator string-of-generators example. The original string was modified to form two different strings-of-generators connected at generator 50. The negative line susceptances of the transmission lines between generators

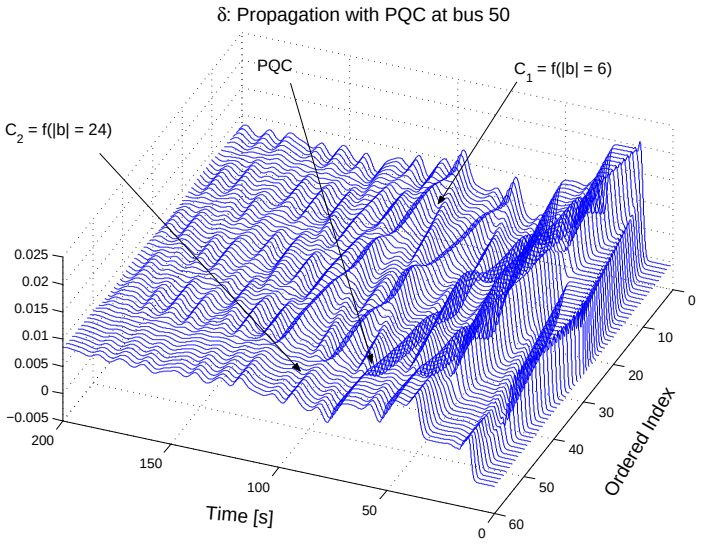

Figure 6.14: $\widetilde{\delta}$ evolution on two different strings-of-generators with a PQC realized at bus 50. String 1 (generators 1 through to 50) have $C_1 = f(|b| = 6)$, String 2 (generators 50 through to 60) have $C_2 = f(|b| = 24)$.

50 and 60 where changed from 6 $p.u.$ to 24 $p.u.$, while the rest of the parameters were kept the same as in the previous simulations. Figure 6.14 shows the result when simulating the previously discussed power pulse perturbation at generator 30. Comparing Figure 6.14 with Figure 6.2, we notice that electromechanical perturbation energy has been extracted from the system. We know that the perturbation electromechanical energy is $\int \widetilde{P}_{g,30}\omega_{coi}\,\mathrm{d}t = 2.21 \times 10^{-5} p.u.$ and the electromechanical energy delivered by the PQC controller is $\int \widetilde{P}_{g,50}\omega_{coi}\mathrm{d}t = -1.98 \times 10^{-5} p.u.$. Over the time interval shown in Figure 6.14, we notice that not all of the perturbation energy has been extracted, but a bulk of this energy is extracted within the first 60 seconds.

Writing an electromechanical power balance at $x = 0$ we can define an absorption coefficient associated with this controller. In studies dealing with noise and geophysics, absorption

coefficients are generally defined [65]. The absorption coefficient α in our case can be obtained via the following calculations:

$$P_1^+\omega_1^+ + P_1^-\omega_1^- + P_2^+\omega_2^+ + P_c\omega_c = 0 \tag{6.38}$$

$$\Rightarrow \frac{(\omega_1^+)^2}{C_1}(1 - R_\omega^2) + \frac{(\omega_1^+)^2}{C_2}T_\omega^2 + \frac{S_P T_\omega}{C_1 C}(\omega_1^+)^2 = 0; \tag{6.39}$$

$$\Rightarrow \alpha \triangleq \frac{S_P T_\omega}{C_1 C} = \frac{(T_\omega)^2}{C^2} = \frac{1-Rc^2}{C_1} - \frac{Tc^2}{C_2} \tag{6.40}$$

$$\Rightarrow \alpha = \frac{4C_2C}{(C_2C+C_1(C_2+C))^2}. \tag{6.41}$$

In [65], (where $C_1 = C_2$) the absorbtion coefficient (associated with a dashpot) was derived as $1 - R_\omega^2 - T_\omega^2$.

6.2.4 Transmission Doubling Control

Another possible EWC is to mimic an open circuit at $x = 0$. In this case $R_\omega = 1$ (angle doubling at $x = 0$), and from (6.23), we know that $T_\omega = 2$. We also note that for this case $R_P = -1$ and we will have cancelling interference of the electrical power waveforms for $x < 0$. In order to achieve this type of behavior we need to have $C = -C_2$, resulting in transmission doubling of the angles for $x > 0$; and from (6.31), $T_P = -S_P = \frac{2C_1}{C_2}$.

A possible benefit of this type of controller is that the electrical power waveform reflected back will subtract (and in the best case cancel) the incident electrical power waveform P_1^+. This might be beneficial if we are dealing with a heavily loaded string-of-generators, for which an increase of the electrical power waveform will result in a line trip. We will not

discuss this type of controller further in this thesis.

6.3 Electromechanical Wave Controllers Realized at Hub Nodes

Thus far, we investigated one-dimensional scenarios where we have, at most, two strings-of-generators connected at a shunt lumped electromechanical element. In this section we will investigate whether we can absorb maximum incident electromechanical power and limit transmission on certain lines by realizing an EWC at a hub node.

Due to the linear nature of the electromechanical wave equation, superposition holds, and for our present investigation we can confine our attention to the case where only one electromechanical wave (ω_1^+, P_1^+) is incident at the lumped element connected at the hub node. We will follow the same approach as depicted in Figure 6.5, but now we have $n-1$ infinitely long strings-of-generators that are connected in parallel for $x > 0$. For this system, the time-harmonic frequency solutions to the telegrapher's equations are given by:

$$\omega_1(x) = \omega_1^+ e^{-jk_1 x} + \omega_1^- e^{jk_1 x}, \forall x \leq 0; \tag{6.42}$$

$$\omega_i(x) = \omega_i^+ e^{-jk_i x}, \forall x \geq 0, \forall i \in [2, \cdots, n]; \tag{6.43}$$

where k_i is the wavenumber associated with string i and ω_i^+ is the frequency wave amplitude of the forward traveling wave on string i.

The electrical power waves that will flow on the string-of-generators after the wave is incident

at the stationary constraint are given by:

$$P_1(x) = \frac{\omega_1^+}{C_1} e^{-jk_1 x} - \frac{\omega_1^-}{C_1} e^{jk_1 x} \tag{6.44}$$

$$P_i(x) = \frac{\omega_i^+}{C_i} e^{-jk_i x}, \forall x \geq 0, \forall i \in [2, \cdots, n]. \tag{6.45}$$

We can easily obtain the reflection and transmission coefficient for the frequency waveforms, by replacing C_2 in (6.20) and (6.21) by the parallel combination of the electromechanical impedances of C_2 through to C_{n-1}, i.e., we replace C_2^{-1} with $\sum_{i=2}^{n-1} C_i^{-1}$ and obtain:

$$\begin{aligned} R_\omega &= \frac{C_1^{-1} - \sum_{i=2}^{n} C_i^{-1} - C^{-1}}{C_1^{-1} + \sum_{i=2}^{n} C_i^{-1} + C^{-1}} \\ &= \frac{C - C_1(1 + C\sum_{i=2}^{n} C_i^{-1})}{C + C_1(1 + C\sum_{i=2}^{n} C_i^{-1})}; \end{aligned} \tag{6.46}$$

$$T_\omega = \frac{2C_1^{-1}}{C_1^{-1} + \sum_{i=2}^{n} C_i^{-1} + C^{-1}}, \tag{6.47}$$

and once more we find $T_\omega - R_\omega = 1$.

Note that only one frequency transmission coefficient is defined. This result makes sense because at $x = 0$ we have $\omega_i^+ = (1 + R_\omega)\omega_1^+$, because of the continuity constraint on the frequency waves at $x = 0$.

The reflection and transmission coefficients of the electrical power waveforms can also be obtained to show that $R_P = -R_\omega$. Noticing that the electrical power splits up between the different strings-of-generators (the circuit analog is having resistors in parallel) yielding distinct transmission coefficients. The individual transmission coefficients can therefore be

expressed as follows:

$$\begin{aligned} T_P(k) &= \frac{(1-R_\omega)C_k^{-1}}{\sum_{i=2}^{n} C_i^{-1} + C^{-1}} \\ &= C_k^{-1} C_1 T_\omega, \end{aligned} \tag{6.48}$$

indicating how much electrical power is transmitted from string 1 to string k (where $2 \leq k \leq n-1$).

The fraction of incident electrical power that the lumped shunt electromechanical device sinks is given by $S_P = C^{-1}C_1T_\omega$, as shown previously.

6.3.1 Zero Reflection Control at Hub Nodes

As previously remarked, ZRC's can be realized at non-boundary buses inside the network. In this instance, we will manipulate $C^{-1} = C_1^{-1} - \sum_{i=2}^{n} C_i^{-1}$ to yield $R_\omega = 0$. The outcome is that $T_\omega = 1$, and thus the incoming electric power splits up in an analogous fashion to currents in paralleled resistors in an electrical circuit. Note that we do not have control over how these transmission powers split up. The electric power transmission coefficient for string k is given as $T_P(k) = \frac{C_1}{C_k}$.

6.3.2 Zero Transmission Control at Hub Nodes

Zero transmission controllers can also be implemented at hub nodes by either controlling the machine speed at the controlled bus or a local load extraction/injection. The electrical power transmission coefficient for string k is given by $T_P(k) = C_k^{-1}C_1T_\omega$, and can be minimized when we minimize T_ω. Hence, irrespective off what string transmission is to be limited, we still need to minimize T_ω. From (6.47) it can be seen that when $C = 0$ then $T_\omega \to 0$. Using the control law (6.33) with $C \to 0$, we can realize a ZTC at a generator bus. We know that requiring $C = 0$ would make the generator completely stiff and require an infinite mechanical input power to the generator to achieve this goal. By relaxing the requirement on R_ω to only be approximately equal to one, we can obtain a more reasonable control effort. This relaxation however, complicates matters slightly. Note that the realized ZTC described thus far is only sensitive to waves incident from $x < 0$, but in practice there might be more than one wave incident at $x = 0$. Thus, we will have to realize multiple control laws (that will be summed in the end), where each law will reflect each incoming wave 'completely' on the associated incoming line.

We can implement a ZTC by controlling the local load extraction/injection by taking the negative sum of the deviational electrical power flows on the edges into the controlled bus. However, the deviational flows on the edges where transmission is to be limited must be excluded from this summation. We will illustrate this law using Figure 6.15. Suppose we want to implement a ZTC at load bus n. Three directed edges are connected to n. The directed edges are denoted by (s, n), (n, t) and (n, l) where the first element in an edge

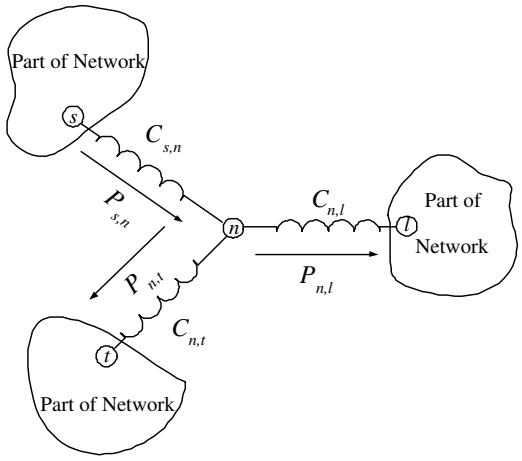

Figure 6.15: A link in a string of generators

2-tuple indicates the source node, and the second element the sink node. For this example the ZTC control law in order to limit transmission on (n, l) will be $\widetilde{P}_{g,n} = -\widetilde{P}_{s,n} + \widetilde{P}_{n,t}$. The control law to limit transmission on (n, t) and (s, n) will be $\widetilde{P}_{g,n} = \widetilde{P}_{n,l}$.

6.3.3 Perturbation Quenching Control at Hub Nodes

The results for the case presented in Section 6.2.3 easily extends to the more general case of having multiple lines in parallel for $x > 0$. In trying to find the controller that will ensure that maximum incident electromechanical power be absorbed we find that $C_M^{-1} = \sum_{i=1}^{i=n} C_i^{-1}$, which is the parallel combination of the electromechanical impedances of the strings connected to the controlled bus.

6.3.4 Some Thoughts on Control Strategies

In this chapter, we introduced a framework to devise control schemes that can manipulate electromechanical waves which travel on power networks. We are sure that there are many more control schemes one can think of that have not been developed, however, finding all the possible schemes is beyond the scope of this thesis. We do, however, want to suggest that we might be able to achieve maximum electrical power transfer to a particular line (say k) by controlling both C and C_k; or by manipulating electrical powers flowing on the lines. We will leave this question for future research.

6.4 Conclusion

In this chapter we discussed the notion of electromechanical wave theory. We investigated wave behavior on a discrete nonlinear swing model and verified that electromechanical wave theory seems plausible. We defined appropriate reflection, transmission and sink coefficients for the scenario where we have two strings-of-generators connected through a lumped shunt electromechanical element.

Different electromechanical wave controllers can be implemented by manipulating the electromechanical impedance of this lumped element. These controllers can be implemented in a decentralized fashion, and the controller gain/structure depend on local network parameters and topology. Electromechanical wave controllers can be realized using SMES or possible FACTS devices. Existing network generators can also be employed assuming

the mechanical input power to the generator can be manipulated fast enough. This is an idealized requirement and investigations into controlling the speed of the generator through the field excitation loop of the generator have been launched.

We conjecture that these decentralized electromechanical wave controllers can be configured in real-time, based on real-time measurements made elsewhere in the system (in order to assess which direction a perturbation waveform might be coming from). In order to achieve this a supervisory centralized level of control might be necessary, to assess the current topology of the network and configure the controllers accordingly. More work on the latter topic will yield fruitful integrated control schemes.

Chapter 7

Applications of EWC's to General Networks

In this chapter we will investigate whether the electromechanical wave controllers introduced in the previous chapter can be used to control general power networks. In this chapter the general model we will study is an aggregated version of the Western States Coordinated Council power network. Investigations similar in nature to those reported here have been reported in [66], where we studied a system based on the IEEE 118 bus loadflow test case.

In the second part of this chapter we focus on extending the ZRC developed for the simple swing model to more elaborate power system models. We will first extend our ZRC control law to the swing model with non-stiff voltage magnitudes and generators with nonzero source impedances. Thereafter, we will consider the two-axis model of a generator.

7.1 WSCC 179-Bus Aggregated Model

The system under consideration in this section is a 179-bus aggregated version of the Western States Coordinated Council (WSCC) power system already used in Chapter 4. A one-line diagram of this system is shown in Figure 7.1.

In Figure 7.2(a) we represent the geographical locations of the three-upper-voltage-level network buses of the full WSCC network (circa 1996)[1]. Figure 7.2(b) was obtained by incorporating the information contained in Figure 7.2(a)[2] with the aggregate model information associated with Figure 7.1.

In Chapter 6 we mainly focussed on all generator networks with regular grids (either one- or two-dimensional). In this section we want to investigate whether a general network such as the WSCC 179-bus model exhibits electromechanical wave behavior in response to an electromechanical perturbation. There is no reason that we should expect to see any behavior of the sort, but in [66] we illustrated wave behavior on a 118-bus system. We conjectured in [66] that one can view a general network as the interconnection of multiple strings-of-generators. This conjecture is partially inconsequential, because our aim is to illustrate how we can use wave-motivated control laws on a discrete (i.e., lumped parameter) sparse network where wave behavior might not be apparent.

The WSCC aggregated model has 29 generators and 150 non-generator buses. We might

[1]This work was completed by a graduated MEng student in our group, Paisarn Sonthikorn, in 2002.
[2]Geographical Information System Database created by P. Sonthikorn and E. Scholtz.

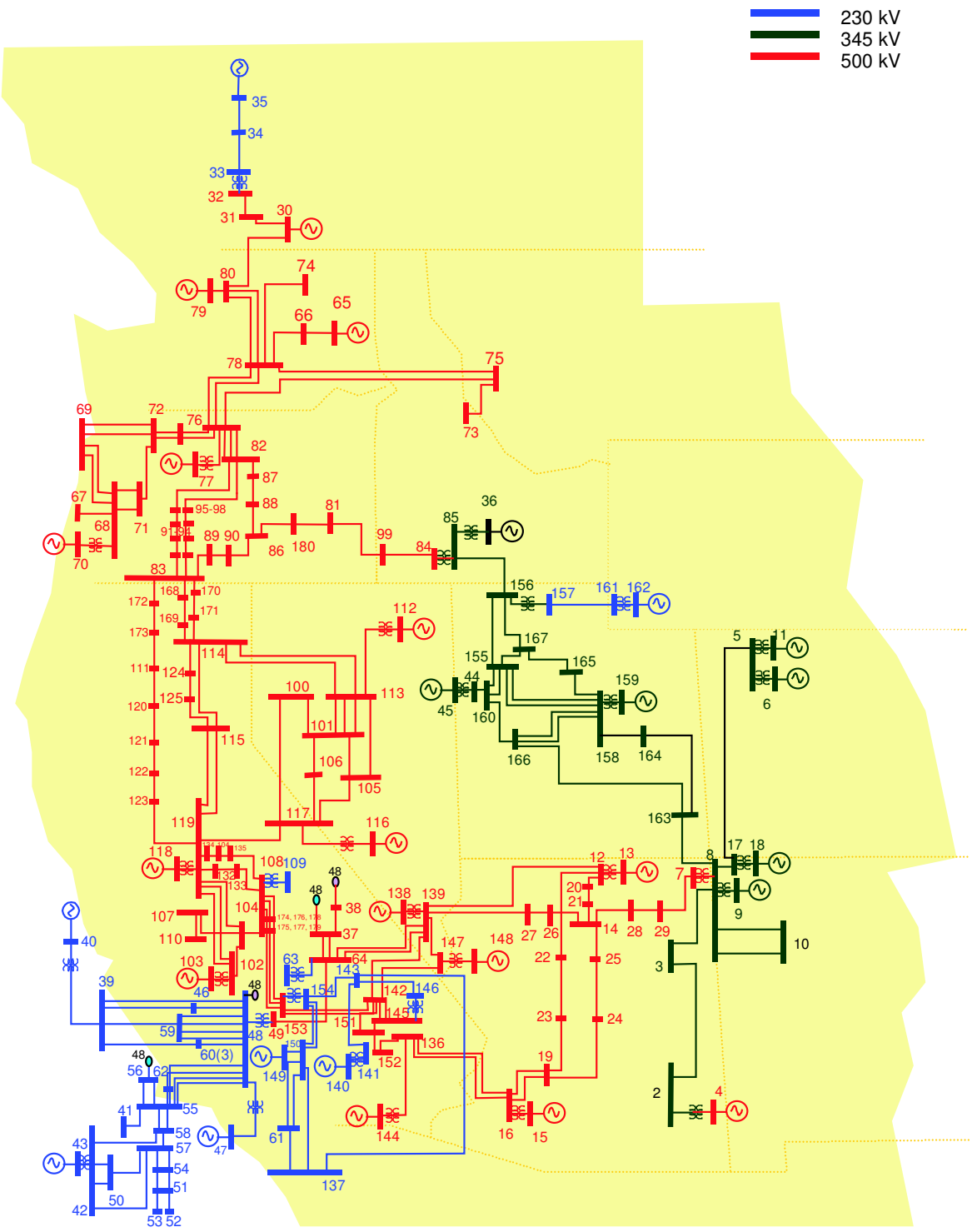

Figure 7.1: One-line diagram of an aggregated WSCC network.

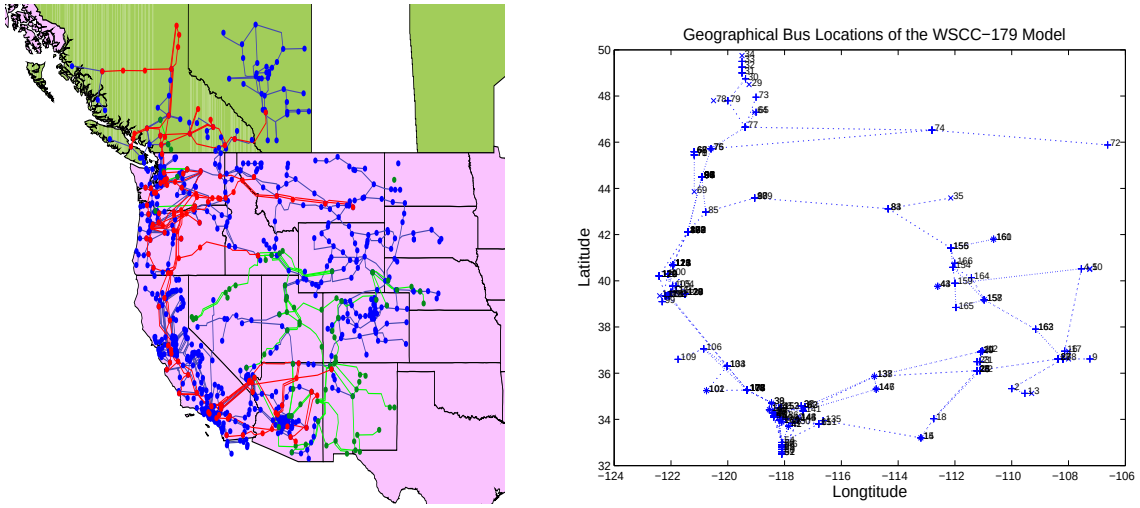

(a) WSCC upper three voltage levels

(b) WSCC 179-bus with geographical locations

Figure 7.2: Geographical locations of the WSCC-network buses.

anticipate that it will be difficult to spot wave phenomena due to the spare distribution of generators (hence mass) in the system.

In this section we make some simplifying assumptions. We assume that none of the generators has any type of implemented controls (e.g., no governor controls), and the only controllers that will be implemented are the EWC's that we will design. We will confine our attention to the simple swing model of the form (2.12) for which we assume that all voltage magnitudes at the buses are controlled tightly around the loadflow solution.

7.2 Uncontrolled Response

We start off by investigating the uncontrolled case. Let us assume that a power pulse perturbation (with amplitude $1p.u.$ and duration $1s$, resulting in a $100MJ$ energy injection, assuming a base of $100MW$) occurs at generator 30 (see top of Figure 7.1). We assume a nontrivial loadflow on the network, but will only illustrate deviational quantities of the variables in all subsequent figures.

In Figure 7.3 time evolutions of bus angles (machine and load angles) are shown, illustrating how the perturbation travels through the network. In order to make the spatial traveling effect more apparent, the original bus indices of Figure 7.1 were reordered according to the *geographical* distance from the perturbed bus. This reordered index was used in the creation of Figure 7.3, as seen on the y-axis, while the x-axis indicates time. From Figure 7.3 we see that the angles keep on increasing due to the electromechanical energy injected into the system.

The same information contained in the Figure 7.3 could also be displayed as a sequence of time-snap 'membrane' plots, as shown in Figure 7.4. The lightly dashed network graph shown in the xy plane forms a reference for the membrane. Vertical dashed lines are connected from this reference to the corresponding moving node of the membrane. The z-axis displacement reflects the bus angle displacements at the time the snap-shot was taken. The node and edge colors change in time in order to illustrate the time evolution of the variables $\widetilde{\delta}$ and $\widetilde{P}_{st}$ respectively. (Note that the flows on the edges have certain associated

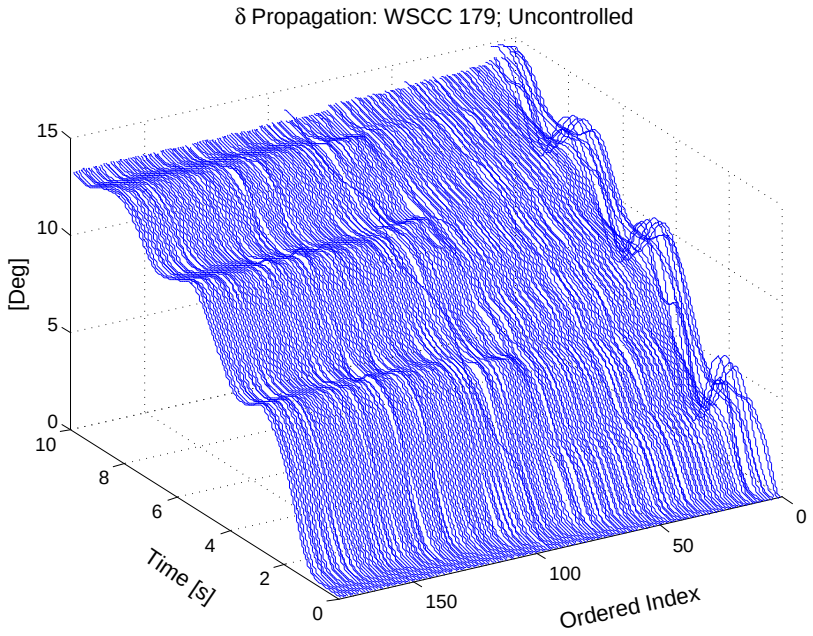

Figure 7.3: $\widetilde{\delta}$ wave propagation on the WSCC network with no controls implemented.

directions, as defined when F is constructed for the network.) Dark blue indicates the most negative value and bright red the maximum positive value. The color scheme we use is based on the 'JET' color scheme of Matlab. The color range for the node evolutions in the plots shown in Figure 7.4, Figure 7.9 and Figure 7.15 are assumed to be the same (the maximum positive deflection 15° and the most negative deflection value is taken as $-4°$).

We can calculate the wavelength associated with this traveling perturbation, but in order to do so we need the swing frequency associated with this traveling perturbation as well as the wave velocity. We calculate the 'velocity' by noting the time difference between the start times of angle responses associated with bus 81 and bus 2 in response to the applied perturbation. Using this information we calculate $v \approx \frac{1246.5km}{0.53s} \approx 2360km.s^{-1}$, which agrees with a figure of $2500km.s^{-1}$ mentioned by Cresap and Hauer in [24]. We identify the swing

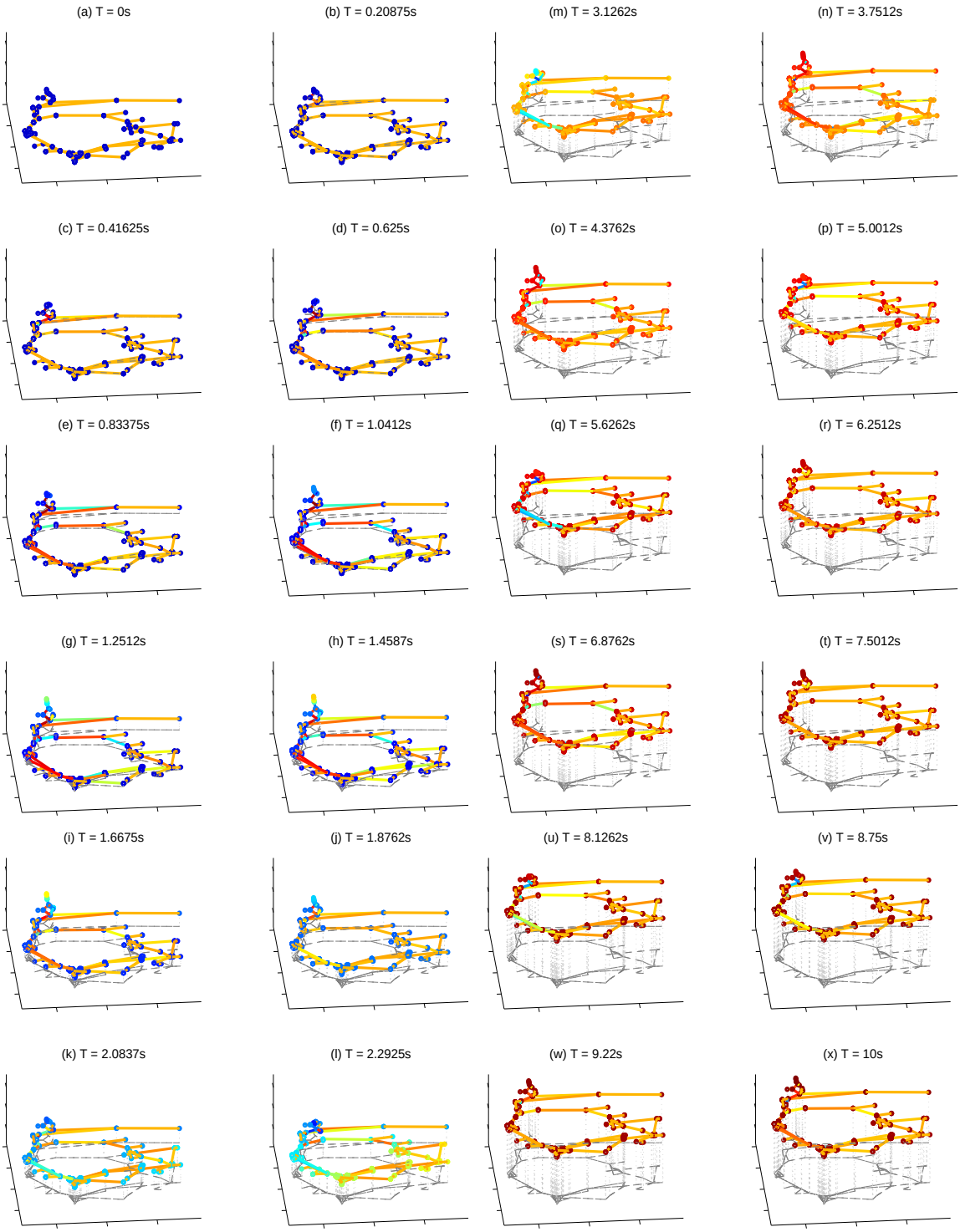

Figure 7.4: Time snap membrane plots for the WSCC 179-bus uncontrolled case. The vertical movement of the nodes indicate the evolution of the bus angles. The lightly dashed network graph in the xy plane serves as a reference for the moving membrane.

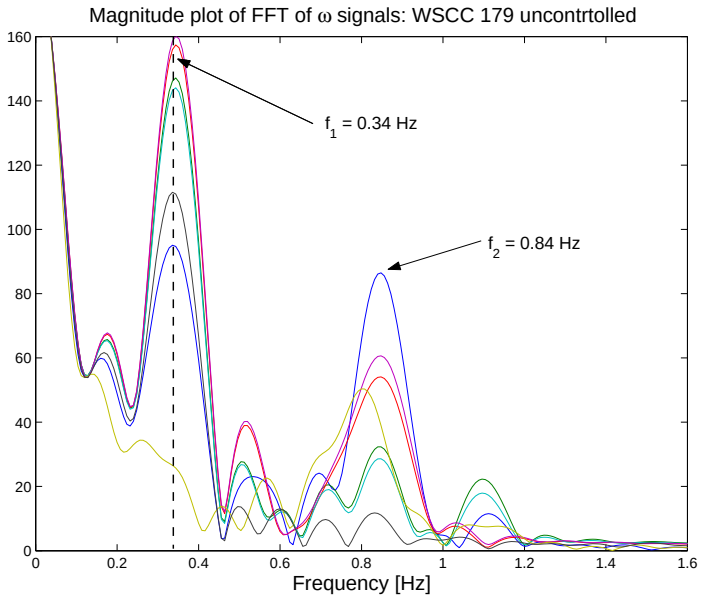

Figure 7.5: Magnitude plot of Fast Fourier Transforms of a few generator-speed signals.

frequency by executing Fast Fourier Transforms of a few generator-speed signals, and in Figure 7.5 we show a magnitude plot of these Fast Fourier Transforms. From this figure we observe two peaks at $0.34Hz$ and at $0.84Hz$. In [24] the authors mention frequencies of $0.2Hz$ and $0.33Hz$. Using the first frequency peak in Figure 7.5 we calculate the wavelength to be roughly $6940km$ (4340 $miles$).

7.2.1 Estimation of Electromechanical Waves Using Observers

In this section we illustrate that using our observer framework, developed in the first part of this thesis, we can estimate a traveling wave on the network. Let us recall our state-estimation example shown in Section 4.4. In this example we assumed a mechanical input power pulse at bus 30 and measured the direct angle at bus 48. Thus we have the perturba-

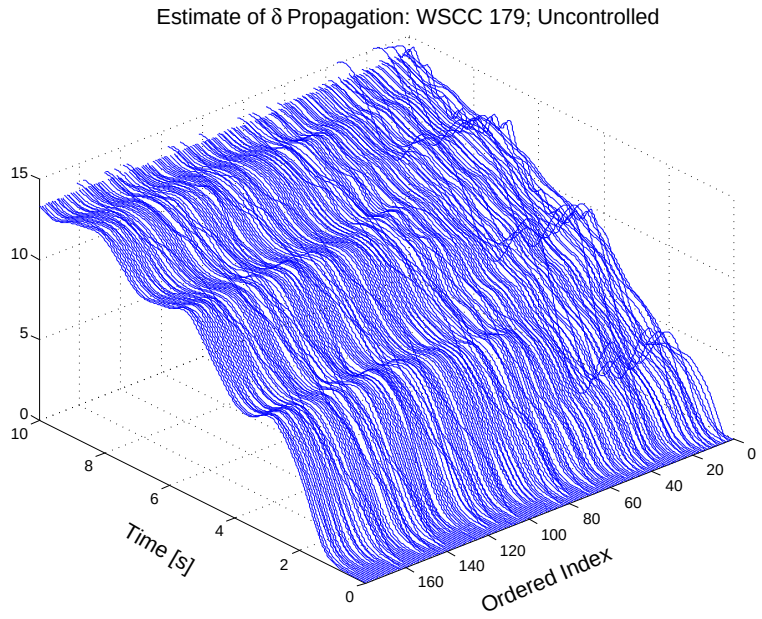

Figure 7.6: Estimate of $\widetilde{\delta}$ wave propagation on the WSCC network with no controls implemented.

tion in the north and the measurement in the south. In Figure 4.18 a select few estimated angles are compared to real angles. If we create a waterfall plot of all the angles (ordered according to the geographical distance away from the perturbation impact), we obtain Figure 7.6. Comparing Figure 7.6 with Figure 7.3, we can not distinguish between the actual state and the estimated state. It appears as if the quality of our estimations is not impacted by the separation between our measurement site and the perturbation location.

7.3 Quenching Control Strategy

In order to combat the continuing movement of the system's center-of-inertia (as illustrated in Figure 7.3), the injected electromechanical perturbation energy needs to be extracted

from the system. The goal of the ensuing investigation is to establish whether the injected energy can be extracted by utilizing a few ZRC's placed at the extremities of the network. There are numerous possible control strategies/placements/numbers of these controllers that we can investigate, but this section is not intended to be of an exhaustive nature, and will merely serve as an illustration of how these EWC's can be employed to control general power networks.

We place three ZRC's at the boundary of the WSCC network in an arbitrary fashion. In Figure 7.7 the locations of the ZRC's are indicated with white squares. These controller are designed in a straightforward manner. The control laws for these ZRC's are of the form (6.33). The characteristic impedance used in the realization of a ZRC is calculated using only local information, i.e., the mass of the generator used as the actuator and the susceptance of the branch connected to this controlled generator bus. Note that the system has non-uniform parameters and we are not saying that calculating the above 'characteristic impedance' will yield maximum quenching of the perturbation, but rather that this provides us with more than adequate quenching control as can be seen in Figure 7.8.

In Figure 7.8 time evolutions of the bus angles are shown, illustrating how the perturbation traverses the network. Once again we have the same bus reordering as was described in the previous section. In this plot we notice that the deviational angles settle, because the perturbation energy is absorbed by the boundary ZRC's. The corresponding membrane plots are shown in Figure 7.9, from which we observe that the system settled at a new operating point. From these plots it is also evident that the waves reach the boundaries of

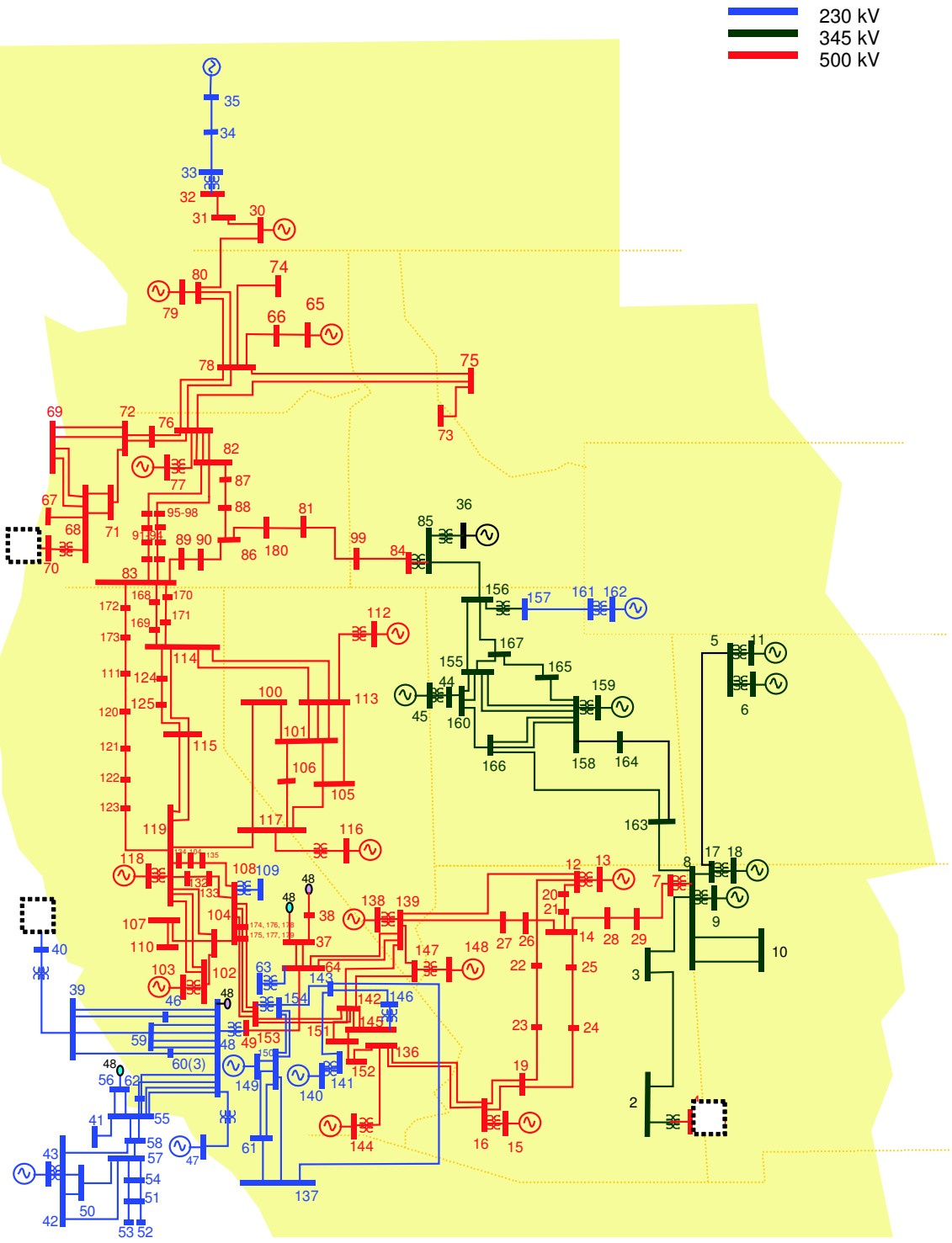

Figure 7.7: Quenching control strategy setup.

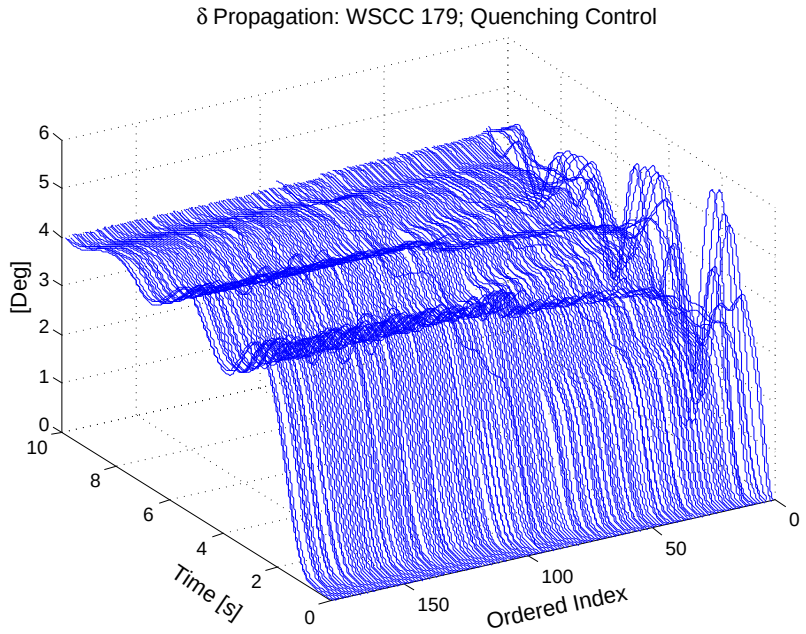

Figure 7.8: $\widetilde{\delta}$ wave propagation on the network for the quenching control strategy.

the grid, where the injected perturbation energy is absorbed by the ZRC's (whose locations are indicated by squares in the sub-figures of Figure 7.9).

Control Effort

An important question that we need to ask is whether or not we are setting unrealistic goals for the ZRC's. Figure 7.10 sheds some light on this issue. We notice from this figure that the control effort for the investigated simulation is divided comparably between the three controllers. Thus all controllers work equally hard to absorb the perturbation energy. Importantly we again notice that the control effort is distributed over time, and the peak demand on the controllers is not excessive, compared to the original perturbation amplitude. For instance, the peak amplitude of the control effort of generator 70 (located nearest to where the perturbation was applied, hence it reacts first) is about 30% of the perturba-

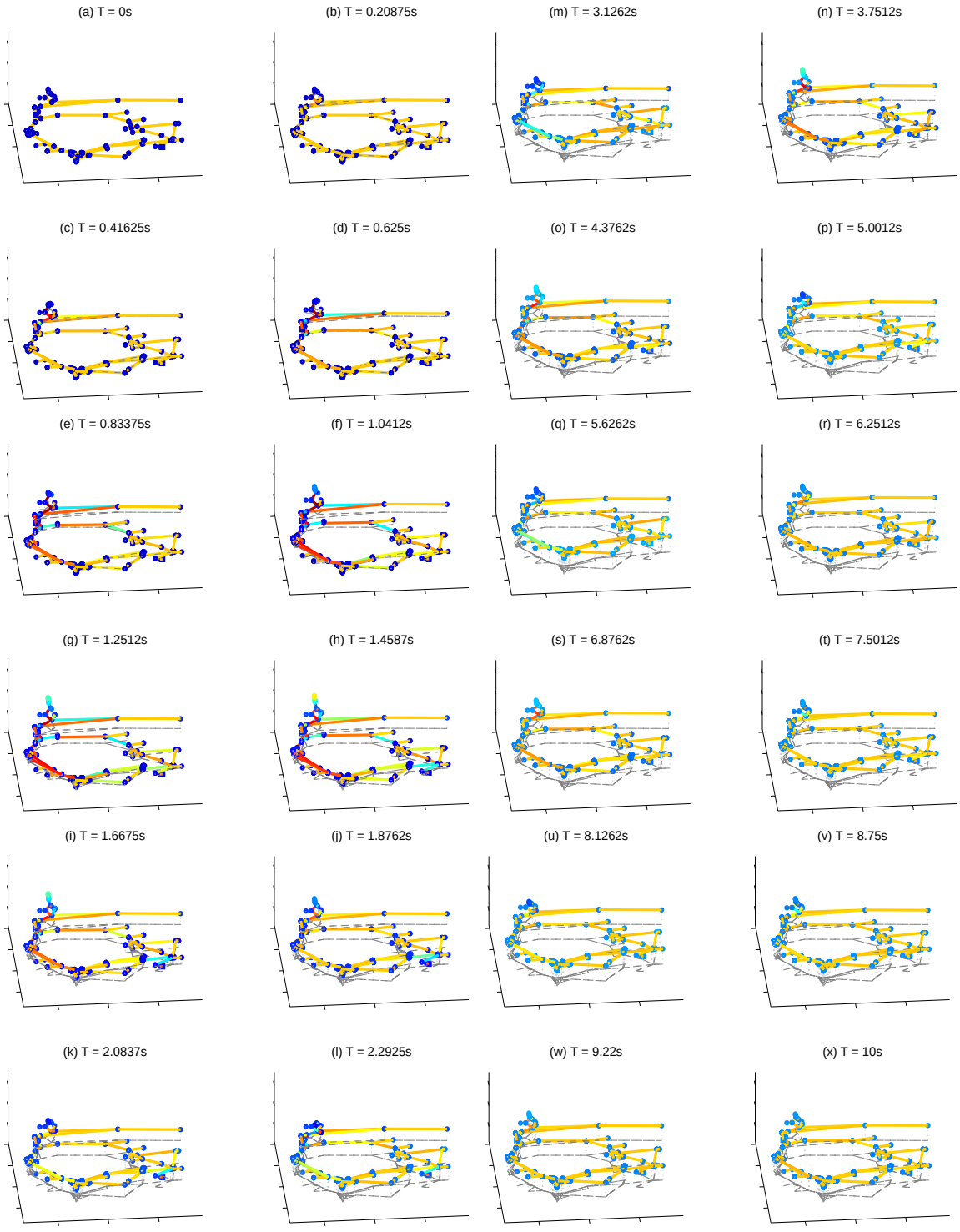

Figure 7.9: Time snap membrane plots for the WSCC 179-bus quenching controlled case. The vertical movement of the nodes indicate the evolution of the bus angles. The lightly dashed network graph in the xy plane serves as a reference for the moving membrane.

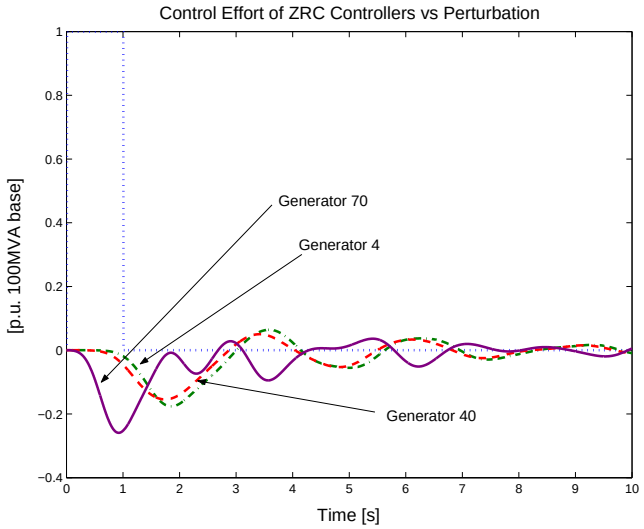

Figure 7.10: Control effort associated with the quenching control strategy.

tion amplitude (assuming a $100MVA$ base, this works out to be $30MW$, which compares favorably to the $1200MW$ supplied by this generator in steady-state to the system).

From Figure 7.10 it appears as if the generator at bus 70 works the hardest in quenching the perturbation. We can quantify this by evaluating the electromechanical energy injected into the network at each of the controlled buses as follows:

$$E_{em,i} = \int_0^{t_{fin}} \omega_{coi} \widetilde{P}_{g,i}(\tau) d\tau, \tag{7.1}$$

using this we find: $E_{em,4} = -3.4 \times 10^{-3}$; $E_{em,40} = -4.0 \times 10^{-3}$; $E_{em,70} = -8.6 \times 10^{-3}$. Summing up these numbers, the electromechanical energy that was extracted equals 16.0×10^{-3}, which is smaller than the injected energy of 26×10^{-3}. The difference between these two numbers is attributed to network losses.

In order to help us understand the sizing of the actuators, it is instructive to investigate

the electrical energy injected into the network, i.e.,

$$E_{e,i} = \int_0^{t_{fin}} \widetilde{P}_{g,i}(\tau) d\tau, \tag{7.2}$$

using this we find: $E_{e,4} = -0.1909$; $E_{e,40} = -0.1844$; $E_{e,70} = -0.3041$. Summing these numbers, the electrical energy extracted equals -0.6794. This is smaller than the injected energy of 1. The difference is attributed to the system not having settled yet. Thus we see that the ZRC at bus 70 needed to absorb roughly $30MJ$ when the perturbation was $100MJ$.

Note that if more ZRC's had been used, the effort required of each would have been correspondingly smaller.

Control Scheme Performance in Response to Different Perturbations

A natural question to ask is whether the proposed control setup will be able to deal with other perturbations in an effective manner. In this section we will keep the same control setup but investigate two different power pulse perturbations.

First let us assume that a power pulse perturbation (of similar magnitudes as previously) occurs at generator 43 (see the bottom left corner of Figure 7.1). The performance of the control scheme in response to this perturbation is illustrated by the plots in Figures 7.11(a) and 7.11(b). In Figure 7.11(a) we see that the system settles at a new operating point in a similar fashion as in Figure 7.8. The ordered index in Figure 7.11(a) differs from the ordered index in Figure 7.8; the former is ordered according to the distance away from bus

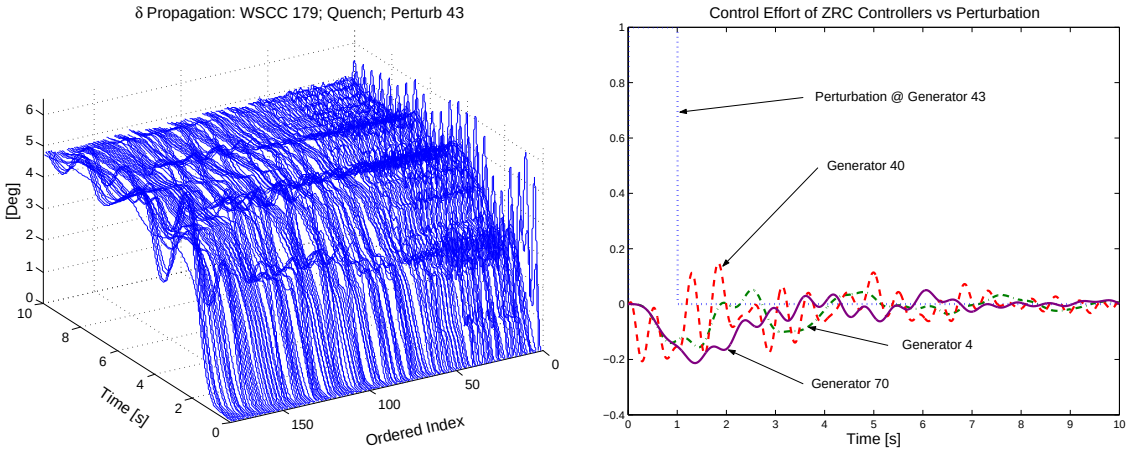

(a) $\widetilde{\delta}$ Propagation (b) Control Effort

Figure 7.11: Confining control study when the perturbation occurs at bus 43.

43 while the latter uses the distance away from bus 30. The control effort shown in Figure 7.11(b) is of the same order of magnitude as that shown in Figure 7.10.

In the second case we will assume a power pulse perturbation occurs at the generator located at bus 112 (see the middle of Figure 7.1). The performance of the control scheme in response to this perturbation is illustrated by the plots in Figures 7.12(a) and 7.12(b). Once more we see in Figure 7.12(a) that the system settles at a new operating point in a similar fashion as in Figures 7.8 and 7.11(a). The ordering associated with the ordered index (y-axis) in Figure 7.12(a) differs from the orderings associated with the two sets of ordered indices (i.e., tow different y-axis) in Figure 7.8 and Figure 7.11(a). For Figure 7.12(a) the indices were ordered according to the distance away from bus 112. The control effort shown in Figure 7.12(b) is of the same order of magnitude as those shown in Figures 7.10 and 7.11(b).

What we can conclude from these studies is that the application of ZRC's at fixed locations

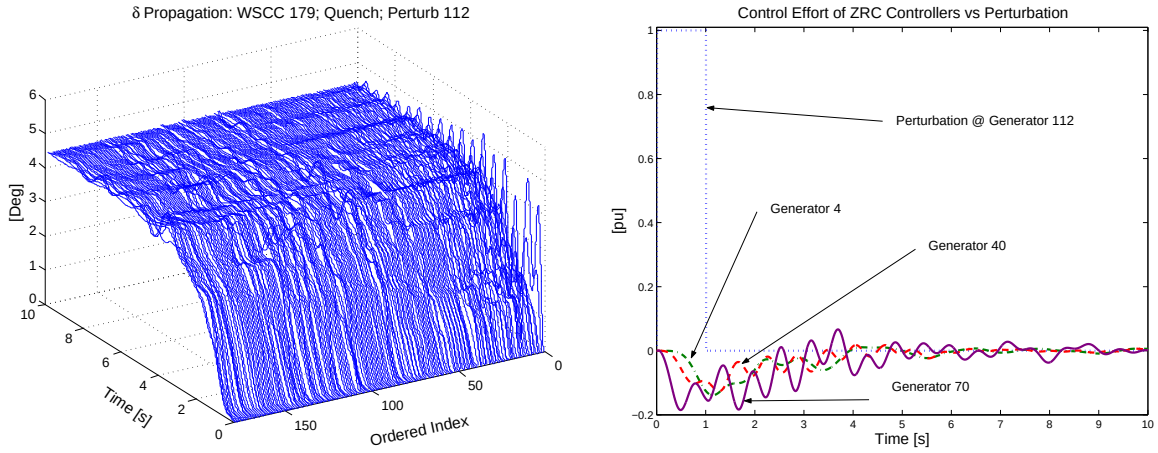

(a) $\widetilde{\delta}$ Propagation (b) Control Effort

Figure 7.12: Confining control study when the perturbation occurs at bus 111.

appears to handle different input perturbations with comparable efficiency.

7.4 Confining and Quenching Control Strategy

Suppose we want to confine and quench the power pulse perturbation occurring at bus 30 by isolating the lower left corner of the network and absorbing the injected perturbation energy in the rest of the network (see Figure 7.13, where the dashed boundary marks the region to be isolated). In order to achieve our goal we place ZTC's at the locations indicated by the white diamonds in Figure 7.13, and ZRC's in at the locations indicated by the white squares.

The ZRC's are designed as we described in Section 7.3. The design steps associated with realizing ZTC's at non-generator buses, with multiple lines connected to the bus, are dis-

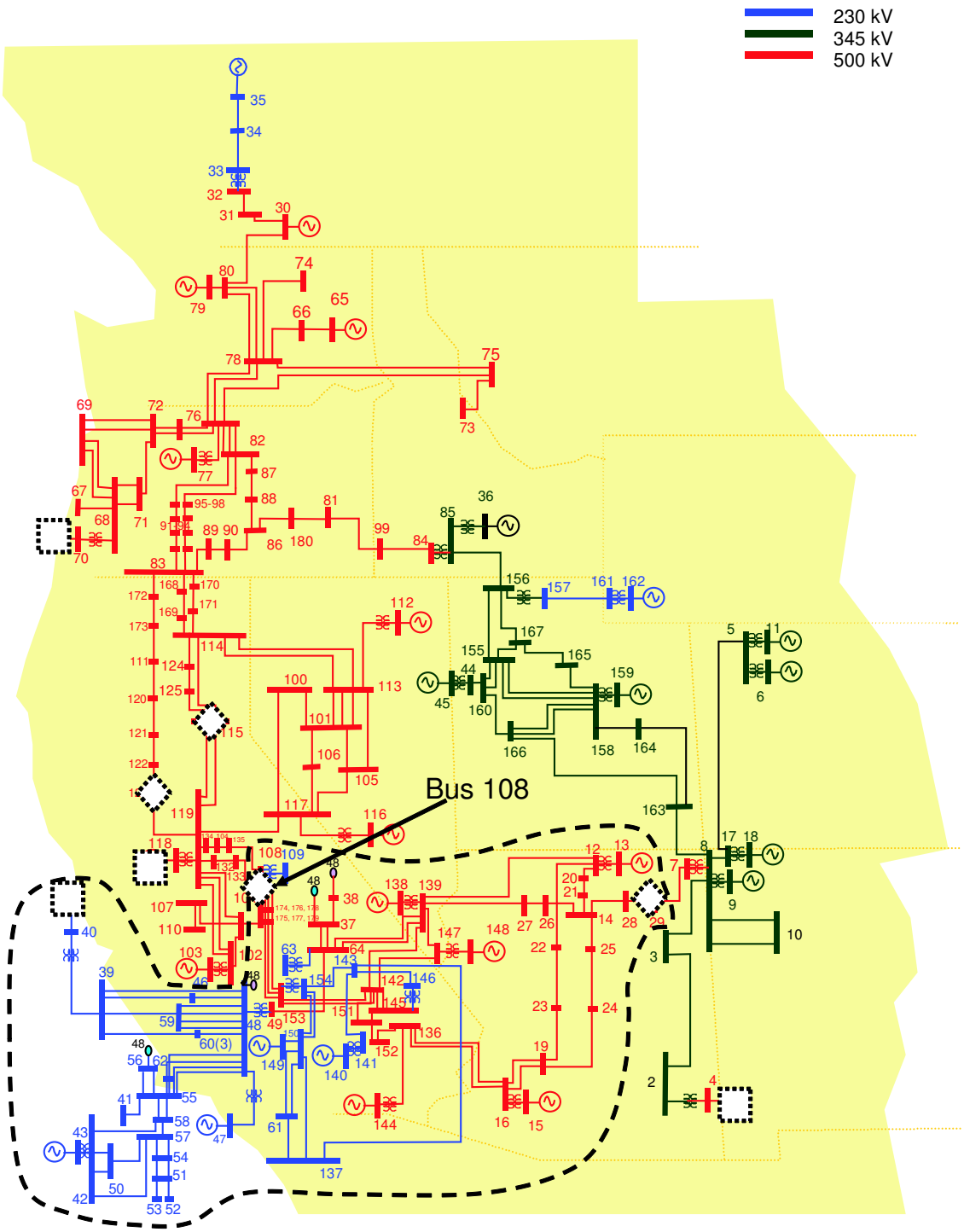

Figure 7.13: Confining and quenching control setup. (White diamonds — ZTC's; White squares — ZRC's).

cussed in Section 6.3.2. We modify the active power we inject at the controlled bus in order to reflect the impinging wave backwards. For instance, the ZTC law at bus 108 is realized as follows:

$$\widetilde{P}_{g,108} = -\widetilde{P}_{135,108} - \widetilde{P}_{133,108} - \widetilde{P}_{104,108}, \tag{7.3}$$

where buses 104, 109, 133, 135, 153, 174 and 175 are connected to bus 108 through branches. $\widetilde{P}_{i,j}$ is the deviational power flowing from bus i to bus j on the branch directed from bus i to bus j. We note that in (7.3), we do not include the deviational power flows on the lines that transmission of the perturbation is to be limited.

In Figure 7.14 we see that there are sections of the network that are not exposed to the perturbation. The time-snap membrane plots in Figure 7.15 provide an alternative view of the results shown in Figure 7.14. From these figures it is clear that we do a satisfactory job isolating the lower left part of the network from this perturbation.

This isolation scheme comes at a premium, as is seen when we analyze the control effort of the ZTC's given in Figure 7.16(b). We observe from Figure 7.16(a) that the quenching of the perturbation is left to mainly two controllers. From Figure 7.14 it appears as if the quenching controllers have a tougher time to quench the perturbation. Significant oscillations are still visible at 10 seconds.

In Figure 7.16 the control efforts of the various controllers are shown. Evaluating (7.1) for each controller we find: $E_{em,29} = 22.1 \times 10^{-3}$; $E_{em,4} = -6.5 \times 10^{-5}$; $E_{em,40} = -1.3 \times 10^{-6}$;

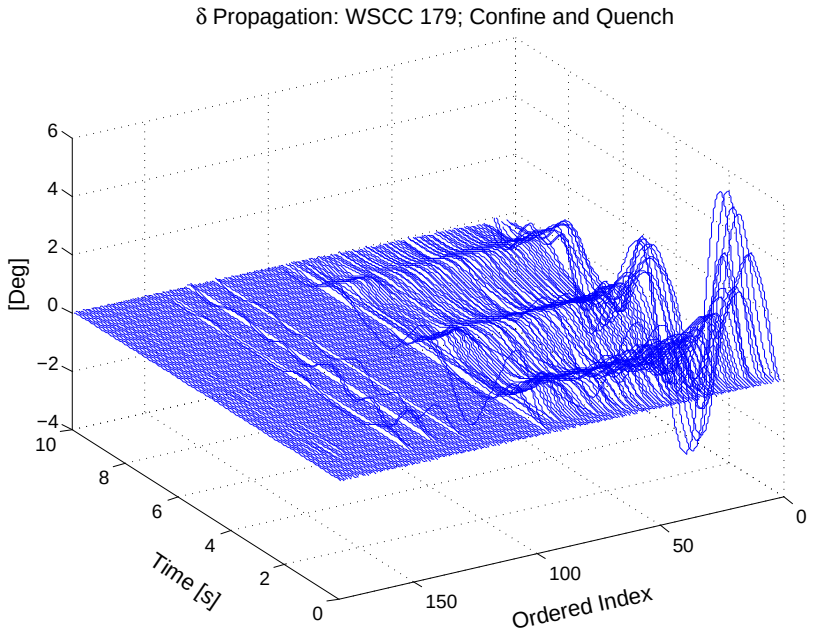

Figure 7.14: $\widetilde{\delta}$ wave propagation on the network for the confining and quenching strategy.

$E_{em,70} = -14.8\times10^{-3}$; $E_{em,118} = -10.8\times10^{-3}$; $E_{em,108} = 12.4\times10^{-3}$; $E_{em,28} = 2.0\times10^{-3}$; $E_{em,129} = 4.6\times10^{-6}$; $E_{em,131} = 7.2\times10^{-6}$; and summing up these numbers we find there is a 10.9×10^{-3} positive amount of energy unaccounted for. Part of this unaccounted energy is attributed to network losses. The remnant can be explained by observing that the system has not completely settled. From these numbers and Figure 7.16 it is evident that the ZRC's at buses 4 and 40 can be eliminated.

7.5 Conclusion

In this chapter we used different types of Electromechanical Wave Controllers (EWC's) that we developed in Chapter 6 to create various control schemes, that we tested on a 179-bus

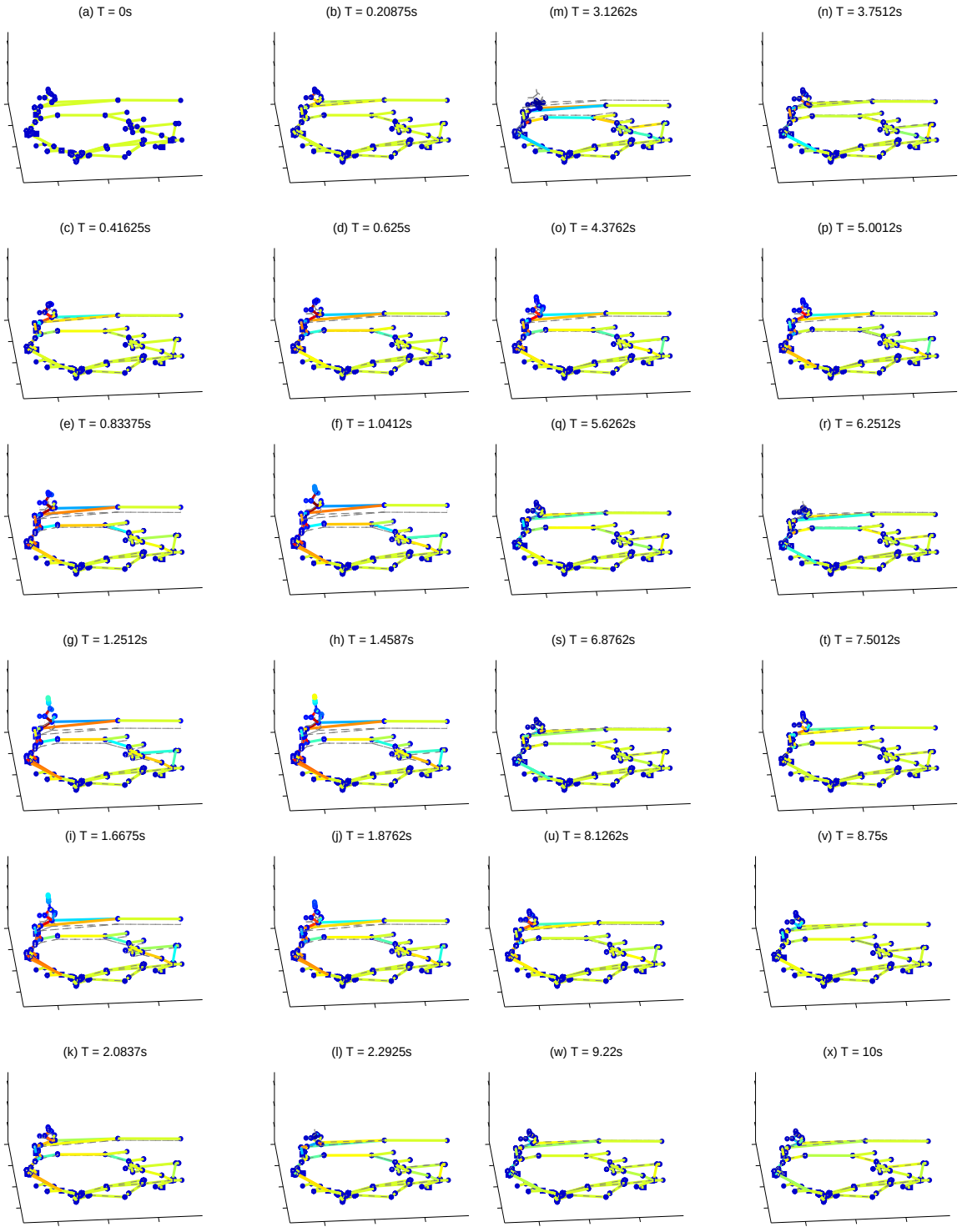

Figure 7.15: Time snap membrane plots for the WSCC 179-bus confining and quenching controlled case. The lightly dashed network graph in the xy plane serves as a reference for the moving membrane.

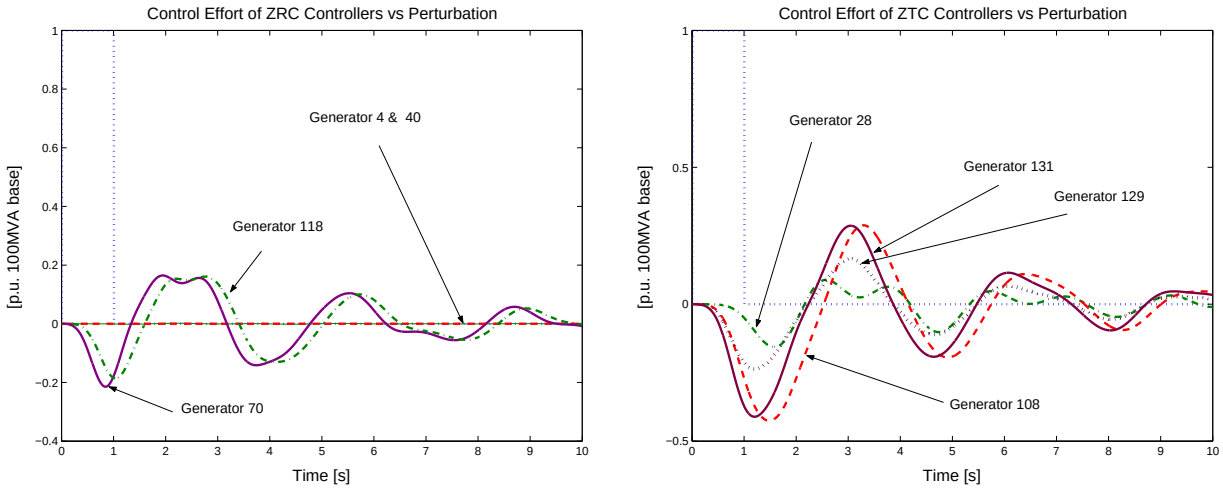

(a) Control Effort: Quenching

(b) Control Effort: Confining

Figure 7.16: Control effort associated with the realization of the confining and quenching strategy.

aggregated WSCC system. We focused on the swing dynamics of this WSCC system, and assumed that no other controls were implemented.

We investigated the uncontrolled case, where we applied a perturbation in the northern part of the network and watched it spread through this sparse network. We calculated the wavelength of the perturbation wave obtained from our simulation of this discrete lumped nonlinear swing model. The values we calculated for the wave velocity and wave frequency agree with values of these variables mentioned in [24].

In this chapter we also illustrated how we can use our observer framework developed in the first part of this thesis to estimate traveling perturbation waves. This illustration does not hint towards the numerous possibilities of having monitors that can detect and identify perturbations, estimate the state of the system and then in real-time configure controllers

(such as our EWC's). However, it does tie the two parts together.

In this chapter we also investigated two different control strategies that were realized using the EWC's we devised in Chapter 6. First, we investigated a quenching control strategy realized using three ZRC's that we placed in an arbitrarily fashion. We found that these three controllers did an adequate job in quenching the applied perturbation.

Second, we realized a confining and quenching control strategy. With this example we illustrated that we can isolate the south-western part of the network from the northern-applied perturbation. We needed multiple ZTC's in order to guarantee reasonable control efforts.

One issue that is still unresolved is, whether the required ramp rates of the control efforts shown in this chapter are plausible when we use existing power equipment. We did illustrate that the magnitudes of the control efforts do not seem unreasonable, but no conclusion can be drawn regarding the ramp rates as of yet.

In Appendix C initial ideas pertaining to a ZRC realization through the voltage loop of a generator (using its Automatic Voltage Regulator) are presented. We anticipate that controlling a generator in this fashion, that we might be able to achieve the desired ramp rates. However, this AVR-control strategy might have a control-effort magnitude limit. This limit can be bypassed by using multiple controllers, hence distributing the control effort. At this point in time we believe that SMES devices are the easiest to implement as actuators in our EWC's.

Chapter 8

Conclusions and Future Work

In this thesis we covered mainly two topics: power system monitors; and decentralized controllers for electromechanical waves in power networks. Our contributions reported in this thesis are to the following fields: power system modeling, power system state estimation, observer design for Differential Algebraic Equation (DAE) systems, observer design for fault detection and isolation filters for these DAE systems, application of fault detection and isolation schemes to power networks, investigation into an integrated temporal and spatial view (i.e., wave view) of the swing dynamics of a power system, and control of power networks by manipulating electromechanical waves (i.e., swing motions) of a power network.

In this chapter a brief summary of the work discussed in the various chapters will be given. We will also highlight the lessons we learned and the contributions we made, before pointing to future research possibilities.

8.1 Summary and Conclusions

In Chapter 1 we stated the aim of this thesis and related our work to existing literature as well as indicated some of the contributions of this thesis.

In Chapter 2 we introduced swing dynamic models from the well established field of power system modeling. As a minor contribution we extended the work presented in [67], where the powerflow equations of a network (active and reactive power), and the directed line-flows in the power network are expressed using matrix-vector equations. These equations account for the network topology more clearly. This formulation helps us to form a better wide-area view of a power system's swing motion behavior in response to faults/disturbances. In this chapter we also spent some time discussing the type of disturbances that a power system might experience. The types of disturbances are not exhaustive, and we decided to concentrate on only a few of them.

In the first part of this thesis we focused on the design of power system monitors. Chapters 3 and 4 were concerned with various topics associated with model-based observers, which form the building blocks of power system monitors. The monitors we investigated in this thesis are swing-state estimators of the system, and fault-detection-and-isolation filters. Chapters 3 and 4 were mainly concerned with the creation of state-estimation monitors in the presence of unknown inputs (i.e., unknown electromechanical perturbations such as load or generation changes as well as line-flow perturbations).

Model-based observers make up for the non-redundancy of sensors in space (because of their

isolated and scattered deployment) and/or in time (because of limitations on their sampling rate). We use model-based observers as the core of our power system monitors, and the quality of such a monitor is only as good as the designed observer. Thus, a significant amount of time was spent in this thesis to investigate different observer design techniques that can be used for the design of full-order observers for the DAE model of a power system's swing dynamics.

In Chapter 3 different possible nonlinear observers were investigated (for instance we extended the novel Arcak-Kokotović observer introduced in [45] and studied it in the power system context). We discussed and illustrated that in order to design a global stabilizing observer gain for the nonlinear observer-error dynamical system of the swing model, we needed an extensive measurement set (e.g., measuring all the load bus angles); however, in this thesis we wanted to confine our attention to cases where we have a limited set of sensors available for observer design. (We also concluded that the novel Arcak-Kokotović observer, where the nonlinear terms featured in the error DAE model can be cancelled, also required an extensive measurement set. The benefit of using this observer was not clear to us for the case where we only use a limited set of sensors.) Hence, we chose a full-order nonlinear DAE observer (originally proposed in [7]) that yields local asymptotically stable local error dynamics. This observer is the intuitive nonlinear extension of the standard linear state-space observer, and uses the nonlinear model of the system plus a linear correction term that is proportional to the discrepancy between the system measurements and the observer's estimate of these measurements. The gain matrix of this linear term is designed using a linear synthesis technique. In Chapter 3 we also showed that the nonlinear error dynamical

system can be written as a linear parameter varying (LPV) error dynamical system, where the varying parameters are the observer's estimate of the internal variables of the system x. Essentially, a linear synthesis technique is used to design observer gains, possibly on-line, along the trajectory of the observer's estimate of x. This approach appears attractive for power systems, seeing that linearized models of power systems are often computed on-line during contingency studies. However, this approach can be very computationally intensive depending on the linear synthesis method employed.

One important contribution we made to DAE observer design is illustrating that by using the original DAE model (as compared to a collapsed state-space model) during the observer design process, we had extra degrees of freedom (as compared to state-space observer design) for unknown-input attenuation.

A significant part of Chapter 3 was devoted to H_∞ filtering for DAE systems in the presence of measurement corruption signals. The case of robust H_∞ filtering design in the presence of model uncertainty, using the Linear Matrix Inequality (LMI) framework, is discussed in Appendix B. We incorporated parametric model uncertainty in the mass matrix (the matrix that pre-multiplies $\dot{x}$) into our investigations, and in doing so we extended the work reported in [52, 68]. We concluded Chapter 3 by observing that H_∞ filtering for DAE models of large-scale power networks is currently very computationally expensive, eliminating LMI-based H_∞ filter design as a possibility for the on-line realization of an observer with an LPV error system. This prompted us to investigate the observer design technique reported in Chapter 4.

The novel graphical observer design technique introduced in Chapter 4 employs ideas from the theory of linear structured systems. For these systems, directed graphs can be constructed that depict signal flow paths from unknown inputs to internal variables to outputs. Investigations such as number-and-type of measurements were graphically investigated on small-scale examples. The lessons learned from these investigations were used to create state estimators for larger systems, which performed superior to the H_∞ filters designed in Chapter 3 for the same systems. This graphical observer design method is attractive for application to larger-scale systems, because the design relies on setting most values in the observer gain matrix to be equal to values extracted from the system matrices, except for very specific high-gain arcs.

This graphical design approach relies on knowledge of the network topology and the values that can be extracted from linearized models of the nominal nonlinear swing model. This design approach is not computationally intensive, making it plausible for the realization of an observer with an LPV error system. The expensive part in the on-line realization of this observer will be the linearization step around the observer's estimate of x. Once we have this linearized system, the observer gain is designed by extracting specific values from the linearized matrices.

We found this graphical observer design technique to be very powerful during the design of monitors (which we assume to be stable) that can achieve a *desired* level of steady-state unknown-input attenuation. However, this design approach does not provide us with any guarantees on the stability of the filter. In Theorem 4.1 we did investigate the case where

extra measurements can be used to change the eigenvalues of the error dynamical system to ensure stability of the filter.

If a mismatch in initial conditions between the observer and the system is anticipated, and fast convergence of the error to zero is of importance, one would have to introduce extra degrees of freedom during the design process in order to move the eigenvalues of the error system $(M, A - LC)$, such that the real part of these eigenvalues are sufficiently large negative numbers.

We propose a dual design approach, where we first identify the unknown inputs whose effect on the errors we want to attenuate, then we introduce (or use existing) measurements that can be used to achieve a *desired* level of unknown-input attenuation as described in Chapter 4. The second step is to use extra measurements that do not violate the conditions of Theorem 4.1, and employ them for the sole purpose of moving the eigenvalues of $(M, A-LC)$ by using an eigenstructure assignment technique. Eigenstructure assignment techniques are generally considered to be suited for large-scale system design. Eigenstructure assignment techniques for state-space and DAE systems exist in the literature. However, it appears from the literature that eigenstructure assignment designs have mainly focused on the dual problem of observer design (i.e., state-feedback control). Note that if we are only concerned about moving the eigenvalues of the error system, and we are certain that we will not negatively influence our unknown-input attenuation design, we can use a pole placement technique for a new modified collapsed state-space system.

More measurements, due to cheap and easy deployment of measurement devices, might

enhance our estimator's performance, by providing us with more degrees of freedom to attenuate identified unknown inputs as well as being able to move the eigenvalues of the error dynamical system. A large set of measurements also holds potential benefits for fault detection, isolation and identification.

The relative ease of designing observers using the graphical observer design method simplified the task of creating fault-detection-and-isolation filters for swing models of power systems, as illustrated in Chapter 5. This chapter illustrates how to design residual generators (i.e., fault-detection-and-isolation filters) for various combinations of different types of faults and in the presence of disturbances, using a small-scale and a large-scale example. Following our design approach discussed in Section 4.2.2 and Theorem 4.1, we know that we can manipulate every element in the transfer function from unknown-inputs to estimation errors (i.e., $G_{ew}(s)$) under certain conditions (which the swing models generally meet). Under these conditions we can enforce a certain structure on $G_{ew}(s = 0)$ (where $s = 0$ indicates steady state properties). For example, we can design $G_{ew}(s = 0)$ to have all zero entries except for one, which corresponds to the measurement used in the observer realization, for the case when we have a single unknown input and a specific type of single measurement. For state estimation purposes we make this non-zero element in $G_{ew}(s = 0)$ tend to zero by increasing a specific gain element. However, for fault detection and isolation purposes we want to increase this element by lowering this same gain element. By doing so we amplify the fault we want to detect instead of attenuating its effect as in the state estimation case.

In Chapter 5 we illustrated how to design residual generators, following the above approach,

on a small-scale (i.e., 9-bus) and a large-scale (i.e., 179-bus) examples. This chapter concluded our investigations into power system monitors and we then moved on to introduce our novel controllers that can manipulate electromechanical movements of a power system in response to an electromechanical perturbation.

The second part of this thesis concentrated on the development and application of decentralized controllers of electromechanical transients in power networks. We believe that the spatio-temporal dynamics of electromechanical systems (such as the swing model of a power network) are important because of the vast geographical areas these networks span. Consequently we developed an integrated wave point of view to study the transients associated with the occurrence of electromechanical perturbations. Previous researchers used such a viewpoint to study and explain various power system analysis questions, whereas in our work we use this wave view to devise controllers that we apply to the lumped, discrete, nonlinear swing model.

In Chapter 6 we used this notion of electromechanical waves traveling in power networks to develop an electromechanical strings-of-generators theory (along the same lines as electro*magnetic* transmission line theory). Furthermore, we developed control strategies for decentralized control of these electromechanical waves, drawing on prototype controllers found in electromagnetic transmission line theory (e.g., matched-impedance terminations) and active vibration damping (e.g., energy-absorbing controllers and vibration isolators). These decentralized "Electromechanical Wave Controllers" (EWC's) belong to the class of collocated controllers (i.e., controllers with input and output located at the same point in

space), and include controllers that can achieve zero reflection or zero transmission of a traveling electromechanical perturbation at certain spatial points of the network. In Chapter 6 we mainly studied homogeneous all-generator networks in order to formulate and test our ideas in a controlled environment. The structure of EWC's is not novel to the power system community, and Samuelsson proposed a similar structured damping controller that modulates active power injection at a load bus by using bus frequency as the controller input [61]. The difference between his and our damping controller is the manner in which the controller gain is obtained. (Samuelsson uses root locus design and we use our wave point of view). One of our contributions to the field of power system damping and control is our investigation into the energy properties and control effort of our EWC's, for which we noticed that our damping controllers would quench perturbation energy with modest time-distributed control efforts. Our zero-transmission controllers on the other hand would not quench the perturbation, but rather redirect the energy of the perturbation.

The actuators we envision are existing power equipment such as generators, active loads, SMES devices and flywheels. From our studies we concluded that the peak demand on an actuator might be modest (this is a function of the perturbation magnitude), but the required ramp rate of the control effort still needs to be related to current capabilities of existing power equipment.

In Chapter 7 we applied EWC's to a 179-bus aggregated model of the Western States Coordinating Council's network. This sparse power network has more load buses than generators. We first investigated whether the simulation of the classical model associated

with this general network yields swing motions that can be interpreted as electromechanical waves. We then realized a quenching control scheme where a limited number of zero-reflection controllers are placed at the boundary of the network. We successfully illustrated that these few controllers were able to absorb the injected perturbation energy adequately. The peak demand of the control effort for this specific example was found to be roughly 25% of the peak amplitude of the perturbation pulse, and roughly 2% of the steady-state power delivered by the controlled generator. In the case of larger disturbances, these three ZRC's would have to work harder, pushing the machines to their limits. However, we were ambitious in our choice of only three controllers for the 179-bus system, and operators would most likely want to share the burden among more controllers. A confining and quenching control strategy for the same perturbation was satisfactorily investigated for the same WSCC system.

In Chapter 7 we also tied the two thesis topics together by showing how we can estimate a traveling electromechanical perturbation using our observer framework developed in the first part of this thesis. This elementary illustration hints at the possibilities of having monitors that can detect and identify perturbations, estimate the state of the system and then in real-time configure controllers (such as our EWC's). We are very optimistic about such integrated monitoring and control schemes, and will elaborate more on this in the section pointing to future research possibilities.

8.2 Future Work

In this thesis various topics were addressed and in the previous section we highlighted several of our contributions of this thesis. However, as is the case with research, some new interesting questions arose. These questions and other interesting problems are left for future research.

8.2.1 Power System Monitors

The observer framework developed in Chapters 3 and 4 was done using the DAE swing model of a power system. The next foreseeable extension of our work would be to move beyond the swing model and investigate a DAE model where generators are represented by the two-axis model (possibly with Automatic Voltage Regulators included) and to incorporate bus-voltage magnitudes and reactive power flow.

We are optimistic that the time invested in arriving at the graphical observer design method was well spent. We envision that using this design method for DAE two-axis power system models will enable us to yield insight into monitoring of real-world networks, making our approach and ideas more tangible for power system operators.

A deeper understanding into the workings of the graphical design method might also be fruitful. The issue of observer robustness in the presence of parametric model uncertainty for the graphically designed observers has not been addressed in this thesis. However, in all the simulations shown in Chapters 4 and 5 we assumed that there was some model

uncertainty and we used nominal values during observer design. Despite these moderate uncertainties we introduced, the graphically designed observers performed well.

Another issue that needs some further investigation is to quantify the possible link between the performance of an observer and the distance (as measured in the directed graph of the structured system) between an unknown input and its cancelling measurement. If this length is large in the directed graph, this might correspond to a large geographical separation between these sites. We might discover that this distance should be small for good performance. For instance in Section 4.3.1 we showed by means of a nine-bus example that a monitor where this distance was short performed better when compared to another monitor where this distance was longer.

The case of measurement faults has not been investigated during our fault detection and isolation studies. Investigations into how we can use these type of fault detection filters in the identification of bad data, and use these filters as an aid to traditional power system static state estimators, might be interesting.

Lastly we can state more generally that more work is required to assess the capabilities and uses of our monitors in system-wide monitoring and control (e.g., protective relaying) of power systems, especially in a deregulated environment.

8.2.2 Decentralized Electromechanical Wave Controllers

The next step in our controller studies will be to move beyond the swing model. As part of this extension we already initiated investigations into whether wave phenomena for ω and P hold when more elaborate power system models (e.g., where generators are represented by two-axis models) are used. These studies are not reported in this thesis and they are of a numerical nature.

Another part of our investigation that warrants more investigation is whether we would be able to use generators as actuators by controlling them through the voltage loop using the Automatic Voltage Regulator of the generator. Following this approach will yield insight into the relationship between our proposed EWC's and currently employed Power System Stabilizers. Some of the points to clarify are the similarities and differences between the damping controllers proposed in this thesis and the damping controllers proposed by Samuelsson, as well as the relation of these collocated controllers to notions of passivity.

We would also like to suggest more study on the placement of controllers. Currently controllers are placed by studying the topology of the network and considering the aim of the control strategy.

A further question that seems interesting to investigate and potentially important for the future is the idea of controller reconfiguration in real-time by having an overlying supervisory control level.

8.2.3 An Integrated Monitoring and Control Framework

The power-system monitors and controllers developed in this thesis can be integrated to form an integrated on-line monitoring and control system. A possible approach might be to use FDI filters to detect power-system perturbations, then isolate and identify them in order to gauge the magnitudes of these perturbations. Having this information available, operators can then configure in real-time a desired EWC constellation (e.g., a quenching or a confining and quenching control strategy). The information regarding the magnitudes of the perturbations will enable system operators to configure the appropriate number and type of controllers in order to distribute the cumulative control effort of the EWC's across the network. We envision that multiple controller sites may exist across the network, to be configured (as zero-reflection or zero-transmission controllers) in real time and switched in to operation as needed.

Our power system state estimation monitors can further be used in a parameter estimation scheme that estimate those parameters that feature in the controller gain calculation (e.g., the controlled generator mass and impedances of the transmission lines connected to the controlled generator bus). One such parameter estimation scheme, which uses the outputs of multiple parallel-running observers and the measurements of the system to estimate the parameters, was investigated as a possible fault-detection and identification scheme in [16].

Appendix A

Linear Matrix Inequalities

It has been shown in recent years that Linear Matrix Inequalities (LMI's) can be used to approach control problems that appear hard if not impossible to solve in an analytical fashion [55]. An LMI is an expression of the form $Q(z) = Q_0 + z_1 Q_1 + \cdots + z_m Q_m > 0$ where $z = (z_1, \cdots, z_m)$ is a vector of m real numbers refered to as 'decision variables'. $Q_0, \cdots, Q_m$ are real symmetric matrices belonging to $R^{n \times n}$. LMI's are interesting because the LMI $Q(z) > 0$ defines a convex constraint on z.

Many optimization problems in control, identification and signal processing can be formulated (or reformulated) using LMIs. The cost function associated with the LMI formulated problem is convex and well-proven convex optimization techniques can be used to solve the problem. There are three generic problems related to the study of LMI's [55]:

- Feasibility Problem: Test whether there exists a solution z to the problem $Q(z) > 0$. The LMI is feasible if such an z exists, otherwise it is called infeasible.
- Optimization Problem: This problem involves the optimization of a scalar cost function $J(z)$ that is subject to an LMI constraint $Q(z) > 0$.

- Generalized Eigenvalue Problem: The objective of this problem is to minimize a real scalar λ, subject to

$$\begin{cases} \lambda Q(z) - R(z) > 0 \\ Q(z) > 0 \\ R(z) > 0 \end{cases}$$

In [55, 54] numerical methods used to solve LMI problems efficiently are discussed. Such discussions fall outside the scope of this thesis and the interested reader is referred to these references. The LMI Control Toolbox in Matlab [56] is used to solve the LMI problems formulated in this thesis.

The following two lemmas (taken from [54]) come in handy when one investigates LMI problems (for instance then conversion of a Linear Matrix Inequality to its associated Algebraic Riccati Equation).

LEMMA A.1

Schur Complement for Strict Inequality: *[54] The matrix inequality, with R_{11} and R_{22} symmetric,*

$$R(z) = \begin{bmatrix} R_{11} & R_{12} \\ R_{12}' & R_{22} \end{bmatrix} > 0$$

holds if and only if

$$R_{22} > 0,$$

$$R_{11} - R_{12} R_{22}^{-1} R_{12}' > 0.$$

LEMMA A.2

Schur Complement for Nonstrict Inequality: *[54] The matrix inequality, with* R_{11} *and* R_{22} *symmetric,*

$$R(z) = \begin{bmatrix} R_{11} & R_{12} \\ R'_{12} & R_{22} \end{bmatrix} \geq 0$$

holds if and only if

$$R_{22} \geq 0,$$

$$R_{11} - R_{12}R_{22}^{\dagger}R'_{12} \geq 0,$$

$$R_{12}(I - R_{22}R_{22}^{\dagger}) = 0,$$

where $R_{22}^{\dagger}$ *denotes the Moore-Penrose inverse of* R_{22}*.*

Appendix B

Robust H_∞ Estimation

In Section 2.6 we discussed possible uncertain parameters in our swing models. This parametric model uncertainty has not been accounted for during the observer design stage, and we will do so at this juncture. In this section we will illustrate how one can design estimation filters utilizing theory from robust control. This framework provides the designer with an avenue to include model uncertainty and make the obtained filter robust to such uncertainties. State-space observer design will not be investigated in this section, because the collapsed state-space swing model does not have the structure-preserving properties of the DAE model, making it more challenging to investigate the effect of parametric model uncertainty.

In [52] the robust H_∞ filtering problem for a state-space model with parametric uncertainty and state delay is considered. In [68] the stabilization problem for a descriptor system with parametric uncertainty (in all the matrices except M) was studied. The results reported in this section join the work done in the latter two papers, but also extend it by considering the scenario of having uncertainty in M.

As a recap, the uncertain DAE swing model can be written as:

$$(\overline{M} - \widetilde{M})\dot{\widetilde{x}} = (\overline{A} + \widetilde{A})\widetilde{x} + Ew, \tag{B.1}$$

$$\widetilde{y} = (C + \widetilde{C})\widetilde{x}, \tag{B.2}$$

$$\widetilde{z} = Q\widetilde{x}, \tag{B.3}$$

where the minus sign in front of $\widetilde{M}$ was chosen for convenience and should not create confusion. In (B.1) we also assumed that $\widetilde{u} = 0$, and in (B.2) we assumed that $v = 0$.

It can be shown for the swing model that the uncertain time-varying matrices $\widetilde{M}$, $\widetilde{A}$ and $\widetilde{C}$ can be written in the following forms:

$$\begin{bmatrix} \widetilde{A} \\ \widetilde{C} \end{bmatrix} = \begin{bmatrix} S_1 \\ S_2 \end{bmatrix} \Delta T_1, \tag{B.4}$$

$$\widetilde{M} = S_m \Delta_m T_m, \tag{B.5}$$

where $\Delta'\Delta \leq I$ and $\Delta_m'\Delta_m \leq I$. This type of uncertainty formulation is also considered in [52, 68].

Making this formulation more concrete we find that S_1, S_2 and T_1 are:

$$S_1 = \begin{bmatrix} S_b & S_g & S_d & 0 \end{bmatrix} \tag{B.6}$$

$$S_2 = \begin{bmatrix} 0 & 0 & 0 & S_c \end{bmatrix} \tag{B.7}$$

$$T_1 = \begin{bmatrix} T_b' & T_g' & T_d' & T_c' \end{bmatrix}' \tag{B.8}$$

$$\Delta = \mathrm{diag}(\Delta_b, \Delta_g, \Delta_d, \Delta_c) \tag{B.9}$$

The submatrices forming part of S_1, S_2 and T_1 are calculated as:

$$\sum_{h=1}^{n_e} \widetilde{A}_b = S_b \Delta_b T_b = \underbrace{\begin{bmatrix} 0 \\ I_n \end{bmatrix}}_{S_b} F \mathcal{B} \rho_b \, \Delta_b \, F' \underbrace{\begin{bmatrix} I_{ng} & 0 & 0 \\ 0 & 0 & I_{nl} \end{bmatrix}}_{T_b} \tag{B.10}$$

$$\sum_{h=1}^{n_e} \widetilde{A}_g = S_g \Delta_g T_g = \underbrace{\begin{bmatrix} 0 \\ I_n \end{bmatrix}}_{S_g} |F| \mathcal{G} \rho_g \, \Delta_g \, F' \underbrace{\begin{bmatrix} I_{ng} & 0 & 0 \\ 0 & 0 & I_{nl} \end{bmatrix}}_{T_g} \tag{B.11}$$

$$\widetilde{A}_d = S_d \Delta_d T_d = \underbrace{\begin{bmatrix} 0 \\ I_{ng} \\ 0 \end{bmatrix}}_{S_d} \rho_d D_g \, \Delta_d \underbrace{\begin{bmatrix} 0 & I_{ng} & 0 \end{bmatrix}}_{T_d} \tag{B.12}$$

$$\widetilde{C} = S_c \Delta_c T_c = \rho_c \Delta_c C. \tag{B.13}$$

Similarly we can find S_m and T_m as:

$$\widetilde{M} \;=\; S_m \Delta_m T_m = \underbrace{\begin{bmatrix} 0 \\ I_{ng} \\ 0 \end{bmatrix}}_{S_m} \rho_m M_g \, \Delta_m \underbrace{\begin{bmatrix} 0 & I_{ng} & 0 \end{bmatrix}}_{T_m} \tag{B.14}$$

Before we prove a lemma that is concerned with the asymptotic stability of the system given by (B.1) and (B.3), we list the following lemma that will be invoked in appendix.

LEMMA B.1

Let $\mathcal{D}$, $\mathcal{S}$, $\mathcal{F}$ be real matrices of appropriate dimensions with $\mathcal{F}$ satisfying $\mathcal{F}'\mathcal{F} \leq 0$. Then for any scalar $\epsilon > 0$ and vectors τ and $\upsilon \in \mathbb{R}^n$ the following holds:

$$2\tau'\mathcal{D}\mathcal{F}\mathcal{S}\upsilon \leq \epsilon^{-1}\tau'\mathcal{D}\mathcal{D}'\tau + \epsilon\upsilon'\mathcal{S}'\mathcal{S}\upsilon.$$

We will now prove the lemma that is concerned with the asymptotic stability of the system given by (B.1) and (B.3).

LEMMA B.2

System (B.1), (B.3) is asymptotic stable and $\|z\|_2^2 < \gamma^2\|w\|_2^2$ under zero-initial conditions

for any non-zero w, if there exist scalars $\epsilon_1 > 0$ and $\epsilon_2 > 0$ and matrix X such that

$$\overline{M}'X = X'\overline{M} \geq 0 \tag{B.15}$$

$$\left[\begin{array}{cc|ccc} \Xi & 0 & X'S_1 & X'S_m & X'E \\ 0 & \epsilon_2 T_m'T_m & 0 & 0 & 0 \\ \hline S_1'X & 0 & -\epsilon_1 I & 0 & 0 \\ S_m'X & 0 & 0 & -\epsilon_2 I & 0 \\ E'X & 0 & 0 & 0 & -\gamma^2 I \end{array}\right] < 0, \tag{B.16}$$

$$\Xi = \overline{A}'X + X'\overline{A} + Q'Q + \epsilon_1 T_1'T_1, \tag{B.17}$$

where S_1, T_1, S_m and T_m are as defined earlier.

Proof. We will first establish asymptotic stability of the system (B.1), (B.3) under the conditions of the lemma with $w = 0$. Let us consider the Lyapunov function candidate $\mathcal{V} = \widetilde{x}'\overline{M}X\widetilde{x}$ (see [44] for an exposition on Lyapunov theory for DAE systems) and its time derivative,

$$\dot{\mathcal{V}} = \widetilde{x}'(\overline{A}'X + X'\overline{A} + \widetilde{A}'X + X'\widetilde{A})\widetilde{x} + 2\widetilde{x}'X'\widetilde{M}\dot{\widetilde{x}}, \tag{B.18}$$

where we can rewrite the last term as

$$2\widetilde{x}'X'\widetilde{M}\dot{\widetilde{x}} = 2\widetilde{x}'X'S_m\Delta T_m\dot{\widetilde{x}}. \tag{B.19}$$

Using Lemma B.1 we can bound (B.19) as follows,

$$2\widetilde{x}'X'S_m\Delta T_m\dot{\widetilde{x}} \;\leq\; \epsilon_2^{-1}\widetilde{x}'X'S_mS_m'X\widetilde{x} + \epsilon_2\dot{\widetilde{x}}'T_m'T_m\dot{\widetilde{x}}, \tag{B.20}$$

where this inequality will hold for any $\epsilon_2 > 0$.

Using (B.4) we can rewrite $(\widetilde{A}'X + X'\widetilde{A})$ as

$$(\widetilde{A}'X + X'\widetilde{A}) = (S_1\Delta T_1)'X + X'(S_1\Delta T_1), \tag{B.21}$$

which we can bound using the following identity taken from [68].

LEMMA B.3

[68] For any matrices K_1, K_2, K_3 of appropriate dimensions with $K_2 > 0$ the following inequality holds

$$K_1'K_3 + K_3'K_1 \leq K_1'K_2K_1 + K_3'K_2^{-1}K_3.$$

Choosing $K_1 = S_1'X$, $K_2 = \epsilon_1^{-1}I$ and $K_3 = \Delta T_1$ we can bound (B.21) as follows,

$$\begin{aligned}(S_1\Delta T_1)'X + X'(S_1\Delta T_1) \;&\leq\; \epsilon_1^{-1}X'S_1S_1'X + \epsilon_1T_1'\Delta'\Delta T_1 &\text{(B.22)}\\ &\leq \epsilon_1^{-1}X'S_1S_1'X + \epsilon_1T_1'T_1, &\text{(B.23)}\end{aligned}$$

where the last inequality follows from having $\Delta'\Delta \leq I$.

Incorporating the inequalities (B.20) and (B.23) into (B.18) we find,

$$\dot{\mathcal{V}} \leq \begin{pmatrix} \widetilde{x} \\ \dot{\widetilde{x}} \end{pmatrix}' \underbrace{\begin{bmatrix} \Lambda & 0 \\ 0 & \epsilon_2 T_m' T_m \end{bmatrix}}_{\Omega_1} \begin{pmatrix} \widetilde{x} \\ \dot{\widetilde{x}} \end{pmatrix}, \tag{B.24}$$

$$\Lambda = \overline{A}'X + X'\overline{A} + \epsilon_1^{-1} X' S_1 S_1' X + \epsilon_1 T_1' T_1 + \epsilon_2^{-1} X' S_m S_m' X \tag{B.25}$$

We can show that Ω_1 in (B.24) is equivalent to

$$\Omega_1 \equiv \left[\begin{array}{ccc|c} \overline{A}'X + X'\overline{A} + \epsilon_1 T_1' T_1 & 0 & & X'S_1 \quad X'S_m \\ 0 & \epsilon_2 T_m' T_m & & 0 \quad 0 \\ \hline S_1' X & 0 & & -\epsilon_1 I \quad 0 \\ S_m' X & 0 & & 0 \quad \epsilon_2 I \end{array}\right], \tag{B.26}$$

by using the Schur complement (see Appendix A).

Investigating the lemma statement we note that $\Omega_1 < 0$. Thus, $\mathcal{V}$ is positive semi-definite and $\dot{\mathcal{V}}$ is negative definite, implying that $\mathcal{V}$ is a valid Lyapunov function and that system (B.1) is asymptotic stable.

Let us now consider the case where $w \neq 0$, and the system is under zero initial conditions. If system (B.1) – (B.3) is dissipative with respect to the supply function $\gamma^2 w'w - y'y$ for any quadratic function $\mathcal{V} = \widetilde{x}\overline{M}' X \widetilde{x}$, then from [55] we know that $\dot{\mathcal{V}}$ should be less than or equal to the supply function. This is the condition that we need to check given our current

theorem statement. Thus, let us define J as follows

$$J = z'z - \gamma^2 w'w + \dot{\mathcal{V}}, \tag{B.27}$$

where $\dot{\mathcal{V}}$ is given by (B.18) with the additional term $2\widetilde{x}X'Ew$ (due to the nonzero input) added to the righthand side.

Thus, we can easily show that

$$\dot{\mathcal{V}} \leq \begin{pmatrix} \widetilde{x} \\ \dot{\widetilde{x}} \\ w \end{pmatrix}' \begin{bmatrix} \Omega & \begin{bmatrix} X'E \\ 0 \end{bmatrix} \\ \begin{bmatrix} E'X & 0 \end{bmatrix} & 0 \end{bmatrix} \begin{pmatrix} \widetilde{x} \\ \dot{\widetilde{x}} \\ w \end{pmatrix}, \tag{B.28}$$

from which it follows

$$J \leq \begin{pmatrix} \widetilde{x} \\ \dot{\widetilde{x}} \\ w \end{pmatrix}' \underbrace{\left[\begin{array}{cc|c} \Lambda + Q'Q & 0 & X'E \\ 0 & \epsilon_2 T_m' T_m & 0 \\ \hline E'X & 0 & -\gamma^2 \end{array}\right]}_{\Omega_2} \begin{pmatrix} \widetilde{x} \\ \dot{\widetilde{x}} \\ w \end{pmatrix}. \tag{B.29}$$

And we can now show by using Schur complements that Ω_2 is equivalent to

$$\Omega_2 \equiv \left[\begin{array}{cc|ccc} \Xi & 0 & X'S_1 & X'S_m & X'E \\ 0 & \epsilon_2 T_m' T_m & 0 & 0 & 0 \\ \hline S_1'X & 0 & -\epsilon_1 I & 0 & 0 \\ S_m'X & 0 & 0 & -\epsilon_2 I & 0 \\ E'X & 0 & 0 & 0 & -\gamma^2 I \end{array}\right],$$

where Ξ is given in (B.17). From LMI (B.16) in the theorem statement we see that $J < 0$ hence, the system is dissipative and $\|z\|_2^2 \leq \gamma^2 \|w\|_2^2$. □

Let us suppose that we want to realize an observer for system (B.1), (B.2) of the form

$$\overline{M}\widetilde{\widehat{x}} = (\overline{A} - L\overline{C})\widetilde{\widehat{x}} + Ly, \tag{B.31}$$

from which we obtain the following associated error dynamical system:

$$\overline{M}\dot{e} = (\overline{A} - L\overline{C})e + Ew + \widetilde{M}\dot{\widetilde{x}} + (\widetilde{A} - L\widetilde{C})\widetilde{x}. \tag{B.32}$$

From (B.32) we notice that the actual state and the error dynamics are not independent, and we have to consider them together in order to design a robust stable observer.

THEOREM B.4

The robust H_∞ filtering problem is solvable for the stable uncertain system given in (B.1) –

(B.3) if there exist scalars $\epsilon_1 > 0$, $\epsilon_2 > 0$ and matrices X_a, X_b and Y such that the following LMIs hold:

$$\overline{M}' X_a = X_a' \overline{M} \geq 0 \tag{B.33}$$

$$\overline{M}' X_b = X_b' \overline{M} \geq 0 \tag{B.34}$$

$$\Gamma = \left[\begin{array}{cc|ccc} \Gamma_{11} & 0 & \Gamma_{13} & \Gamma_{14} & \Gamma_{15} \\ 0 & \Gamma_{22} & 0 & 0 & 0 \\ \hline \Gamma_{13}' & 0 & -\epsilon_1 I & 0 & 0 \\ \Gamma_{14}' & 0 & 0 & -\epsilon_2 I & 0 \\ \Gamma_{15}' & 0 & 0 & 0 & -\gamma^2 I \end{array}\right] < 0 \tag{B.35}$$

$$\Gamma_{11} = \left[\begin{array}{cc} \overline{A}' X_a + X_a' \overline{A} + \epsilon_1 T_1' T_1 & 0 \\ 0 & \overline{A}' X_b + X_b' \overline{A} + Y' \overline{C} + \overline{C}' Y + C_e' C_e \end{array}\right] \tag{B.36}$$

$$\Gamma_{22} = \left[\begin{array}{cc} \epsilon_2 T_m' T_m & 0 \\ 0 & 0 \end{array}\right] \tag{B.37}$$

$$\Gamma_{13} = \left[\begin{array}{c} X_a' S_1 \\ X_b' S_1 + Y S_2 \end{array}\right] \tag{B.38}$$

$$\Gamma_{14} = \left[\begin{array}{c} X_a' S_m \\ X_b' S_m \end{array}\right] \tag{B.39}$$

$$\Gamma_{15} = \left[\begin{array}{c} X_a' E \\ X_b' E \end{array}\right] \tag{B.40}$$

where $Y' = -X_b' L$. A suitable H_∞ observer will be of the form (B.31).

Proof. Let us concatenate the dynamical equations of the uncertain system and the error dynamics associated with the observer to form the following system:

$$\underbrace{\begin{bmatrix} \overline{M} & 0 \\ 0 & \overline{M} \end{bmatrix}}_{\overline{\mathcal{M}}} \begin{pmatrix} \dot{\widetilde{x}} \\ \dot{e} \end{pmatrix} = \underbrace{\begin{bmatrix} \overline{A} & 0 \\ 0 & \overline{A} - L\overline{C} \end{bmatrix}}_{\overline{\mathcal{A}}_c} \underbrace{\begin{pmatrix} \widetilde{x} \\ e \end{pmatrix}}_{\eta} + \underbrace{\begin{bmatrix} \widetilde{A} & 0 \\ \widetilde{A} - L\widetilde{C} & 0 \end{bmatrix}}_{\widetilde{\mathcal{A}}_c} \begin{pmatrix} \widetilde{x} \\ e \end{pmatrix} + \underbrace{\begin{bmatrix} \widetilde{M} & 0 \\ \widetilde{M} & 0 \end{bmatrix}}_{\widetilde{\mathcal{M}}} \begin{pmatrix} \dot{\widetilde{x}} \\ \dot{e} \end{pmatrix} + \underbrace{\begin{bmatrix} E \\ E \end{bmatrix}}_{\mathcal{E}} w \tag{B.41}$$

$$e = \mathcal{C}_e \eta \tag{B.42}$$

The uncertain matrices $\widetilde{\mathcal{A}}_c$ and $\widetilde{\mathcal{M}}$ are respectively equivalent to:

$$\widetilde{\mathcal{A}}_c = \underbrace{\begin{bmatrix} S_1 \\ S_1 - LS_2 \end{bmatrix}}_{\mathcal{S}_1} \Delta \underbrace{\begin{bmatrix} T_1 & 0 \end{bmatrix}}_{\mathcal{T}_1}; \tag{B.43}$$

$$\text{and } \widetilde{\mathcal{M}} = \underbrace{\begin{bmatrix} S_m \\ S_m \end{bmatrix}}_{\mathcal{S}_m} \Delta_m \underbrace{\begin{bmatrix} T_m & 0 \end{bmatrix}}_{\mathcal{T}_m}. \tag{B.44}$$

We still have that $\Delta'\Delta < I$ and $\Delta_m'\Delta_m < I$.

Defining $\mathcal{X} = \text{diag}(X_a, X_b)$ and $\mathcal{Y} = \text{diag}(0, Y)$ we can show that Γ is equal to

$$\Gamma \equiv \left[\begin{array}{cc|ccc} \Xi & 0 & \mathcal{X}'\mathcal{S}_1 & \mathcal{X}'\mathcal{S}_m & \mathcal{X}'\mathcal{E} \\ 0 & \epsilon_2\mathcal{T}_m'\mathcal{T}_m & 0 & 0 & 0 \\ \hline \mathcal{S}_1'\mathcal{X} & 0 & -\epsilon_1 I & 0 & 0 \\ \mathcal{S}_m'\mathcal{X} & 0 & 0 & -\epsilon_2 I & 0 \\ \mathcal{E}'\mathcal{X} & 0 & 0 & 0 & -\gamma^2 I \end{array}\right] \tag{B.45}$$

$$\text{where } \Xi = \overline{\mathcal{A}}_c'\mathcal{X} + \mathcal{X}'\overline{\mathcal{A}}_c + \mathcal{C}_e'\mathcal{C}_e + \epsilon_1\mathcal{T}_1'\mathcal{T}_1 \tag{B.46}$$

From this equivalence and the fact that $\Gamma < 0$ from the theorem statement we see that we can apply Lemma B.2, which completes the proof. □

At this juncture we will not illustrate with an example. We can demonstrate the feasibility of this LMI problem on a small system, similar to what was done in [52]. In [52] the authors did not minimize γ^2, but rather chose a value and then computed a feasible solution for their example. From preliminary investigations on a small example we found that trying to minimize γ^2 we ran into feasibility problems.

Appendix C

Towards Implementing an EWC through an AVR

This write up highlights some of the issues involved toward implementing an EWC through the voltage loop of a generator using the Automatic Voltage Regulator (AVR). We will mainly focus on realizing a ZRC for a string-of-generators example and we will only investigate the simple swing model.

In this write up we assume that the external mechanical-torque input to the generator can not be manipulated as well as that an external active-load extraction at the controlled bus is non-existent. Thus the only variable that can be used to achieve control is to modify the electrical power output of the generator.

Let us start with the swing model with no source impedance. For simplicity we assume that the voltage magnitudes are constant for all time. The dynamical equations of the end

generator is:

$$\dot{\delta} = \omega \tag{C.1}$$

$$\frac{2H}{\omega_s}\dot{\omega} = P_m + P_{end}, \tag{C.2}$$

where P_{end} is the power that flow into the final generator. Only ω is expressed as a deviational variable, and in steady state we have that $\overline{P}_m = -\overline{P}_{end}$.

Following our approach in [60] we enforce $\widetilde{P}_{end} = \frac{\omega}{C_o}$ by substituting this relationship into (C.2) (where we now assume that $\widetilde{P}_m = 0$, which is not the case in [60]), from which we find that the dynamical equations of the end generator change to:

$$\dot{\delta} = \omega \tag{C.3}$$

$$\frac{2H}{\omega_s}\dot{\omega} = \frac{\omega}{C_o} \tag{C.4}$$

and we see that there is a positive eigenvalue associated with this closed loop system. Thus the end generator will go unstable and we can thus not achieve a ZRC at this end generator by manipulating the electrical power output of this generator.

Alternatively, if we follow our approach in [26] the right hand side of (C.2) is equal to $K(\widetilde{P}_{end} - \frac{\omega}{C_o})$, and from this equivalence we obtain what $\widetilde{P}_m$ should be to achieve the control objective. In our current investigation we assume that $\widetilde{P}_m = 0$. Evaluating the LHS

equivalence we have:

$$\widetilde{P}_{end} = K(\widetilde{P}_{end} - \frac{\omega}{C_o}) \tag{C.5}$$

$$\rightarrow (K-1)\widetilde{P}_{end} = K\frac{\omega}{C_o} \tag{C.6}$$

where we see that (C.6) is consistent with our objective $\widetilde{P}_{end} = \frac{\omega}{C_o}$ only in the limit as K becomes large. Making $\widetilde{P}_{end}$ the subject of (C.6) and substituting it into the right hand side of (C.2) we find:

$$\dot{\delta} = \omega \tag{C.7}$$

$$\frac{2H}{\omega_s}\dot{\omega} = \frac{K}{(K-1)}\frac{\omega}{C_o} \tag{C.8}$$

and if $0 < K < 1$ then the eigenvalue $\frac{K}{\frac{2H}{\omega_s}(K-1)C_o}$ will be in the LHP. Thus we have contradicting aims: first we want K to be very large, second we want $0 < K < 1$.

What note that both (C.4) and (C.8) do not have any driving terms and the dynamic evolution of ω will be attributed to a nonzero initial condition of ω (which is taken to be zero).

New approach

We relax our aim of trying to control the impinging wave at the end generator and rather focus on controlling the impinging wave at the second to last generator (refer to it as generator 1 henceforth). From our previous studies we know that if the power a local active

load extraction at generator 1 is equal to $\frac{\omega_1}{C_o}$ then there will be no wave reflections at the bus of generator 1 and the end generator will absorb the wave energy. We will use the end generator to provide us with this load extraction/injection, and hence we have $\widetilde{P}_e = -\frac{\omega_1}{C_o}$. Substituting this into the dynamical equations of the last two generators we obtain:

$$\dot{\delta}_1 = \omega_1 \tag{C.9}$$

$$\dot{\delta} = \omega \tag{C.10}$$

$$\frac{2H}{\omega_s}\dot{\omega}_1 = \widetilde{P}_{end} - \frac{\omega_1}{C_o} \tag{C.11}$$

$$\frac{2H}{\omega_s}\dot{\omega} = \frac{\omega_1}{C_o} \tag{C.12}$$

This control scheme works and we are able to absorb the wave energy similar to the case where we manipulated the mechanical input power to the last generator.

Adding Voltages and Source Impedances

Next, we assume that the generator has a source impedance and we will distinguish between δ (machine angle) and θ (bus angle). We model voltage magnitudes on the network as well. In Figure C.1 we show the last two generators in the string of generators for this kind of power system model.

From the preceding paragraphs we have realized that we will not be able to achieve ZRC at the end generator bus, but rather that we want to manipulate the output power of this generator in order to achieve zero reflection control at the second-to-last generator bus.

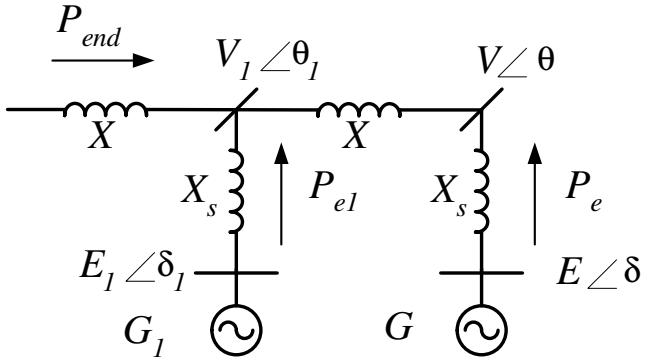

Figure C.1: Last two generators in our string-of-generators example, where generators have source impedances.

We can achieve ZRC at the bus of generator 1, if we can guarantee that the power supplied to the network bus of generator 1 is

$$\widetilde{P}_e + \widetilde{P}_{e1} \;=\; -\frac{\dot{\theta}_1}{C_o}, \tag{C.13}$$

where $\dot{\theta}_1$ is the bus frequency at the second-to-last generator. We can simplify matters by assuming that $\dot{\theta}_1 \approx \omega_1$, because we will not manipulate $\widetilde{P}_{e1}$. Ideally we want $\widetilde{P}_{e1} \approx 0$.

Assuming that we achieve this objective of having $\widetilde{P}_e = -\frac{\omega_1}{C_o} - \widetilde{P}_{e1}$ and substituting this

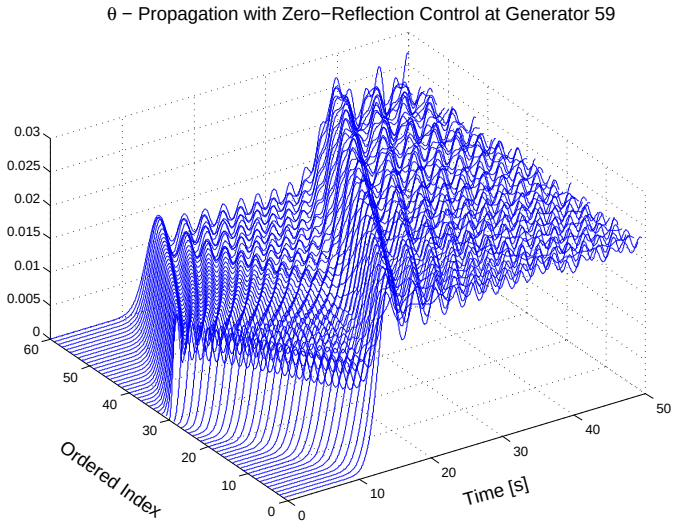

Figure C.2: θ-Propagation on the string of generators, with generator impedances included ($X_s = \frac{X}{4}$).

objective into the electromechanical differential equations of the last generator we obtain

$$\dot{\delta}_1 = \omega_1 \tag{C.14}$$

$$\dot{\delta} = \omega \tag{C.15}$$

$$\frac{2H}{\omega_s}\dot{\omega}_1 = -\widetilde{P}_{e1} \tag{C.16}$$

$$\frac{2H}{\omega_s}\dot{\omega} = \frac{\omega_1}{C_o} + \widetilde{P}_{e1} \tag{C.17}$$

$$0 = \widetilde{P}_{end} + \widetilde{P}_e + \widetilde{P}_{e1} = \widetilde{P}_{end} - \frac{\omega_1}{C_o}. \tag{C.18}$$

From C.18 we notice that we indeed satisfy the zero-reflection control objective at bus 1.

This control scheme does an adequate job as illustrated in Figure C.2.

The deviational-electric power out of the end generator is expressed as

$$\widetilde{P}_{elec} = \frac{EV}{X'_d}\sin(\delta - \theta) - \overline{P}_{elec} \tag{C.19}$$

where E is the voltage behind machine reactance and V is the voltage magnitude at the network bus. If we extrapolate to the two-axis model and control the last generator through the AVR then we would essentially modulate V (the terminal voltage of the generator) as wells as δ. We will not test such an implementation at this point in time, and leave it for future research.

Bibliography

[1] U.S.-Canada Power System Outage Task Force, "Final report on the August 14, 2003 blackout in the United States and Canada: Causes and recommendations," Technical Report, U.S. Department of Energy, April 2004.

[2] A. Monticelli, *State Estimation in Electric Power Systems*. Kluwer Academic Publishers, 1999.

[3] P. Rousseaux, T. V. Cutsem, and T. D. Liacco, "Whither dynamic state estimation?," *Electric Power and Energy Systems*, vol. 12, no. 2, pp. 104–116, 1990.

[4] K.-R. Shih and S.-J. Huang, "Application of a robust algorithm for dynamic state estimation of a power system," *IEEE Transactions on Power Systems*, vol. 17, pp. 141–147, February 2002.

[5] A. Debs and R. Larson, "A dynamic estimator for tracking the state of a power system," *IEEE Transactions on Power Apparatus*, vol. 89, no. 7, pp. 1670–1688, 1970.

[6] M. D. C. Filho, J. Glover, and A. L. da Silva, "State estimators with forecasting capability," *Proc. of the 11th PSCC, Avignon, France*, vol. II, pp. 689–695.

[7] E. Scholtz, P. Sonthikorn, G. C. Verghese, and B. C. Lesieutre, "Observers for swing-state estimation of power systems," *North American Power Symposium 2002*, October 2002.

[8] I. Stolz, "Observers and graphic displays for the swing motions of a power system," Master's thesis, Technical University of Berlin (research done at MIT), October 1994.

[9] J. Chang, G. Taranto, and J. Chow, "Dynamic state estimation in power system using a gain-scheduled nonlinear observer," *Proceedings of the 4th IEEE Conference on Control Applications*, pp. 221–226, 1995.

[10] H. Modir and R. A. Schlueter, "A dynamic state estimator for dynamic security assessment," *IEEE Transactions on Power Apparatus and Systems*, vol. 100, pp. 4644–4652, November 1981.

[11] H. Modir and R. A. Schlueter, "A dynamic state estimator for power system dynamic security assessment," *Automatica*, vol. 20, pp. 189–200, March 1984.

[12] A. G. Phadke, "Hidden failures in protection systems," *Power Systems and Communications Infrastructure for the Future*, September 2002.

[13] Q. Ding and A. Abur, "An improved measurement placement method against loss of multiple measurements and branches," *IEEE Power Engineering Society Winter Meeting*, vol. 1, pp. 234–237, January 2002.

[14] J. Chen and R. J. Patton, *Robust Model-Based Fault Diagnosis For Dynamic Systems*. Asian Studies in Computer and Information Science, Kluwer Academic Publishers, 1999.

[15] J. Gertler, *Fault Detection and Diagnosis in Engineering Systems*. New York: Marcel Dekker, 1998.

[16] E. Scholtz, "Parameter estimation for singular systems via multiple observers." Research Qualifying Exam Report, MIT EECS, May 2003.

[17] R. J. Patton, P. M. Frank, and R. N. Clark, eds., *Issues of Fault Diagnosis for Dynamic Systems*. Springer Verlag, 2000.

[18] L. H. Chiang, E. L. Russell, and R. D. Braatz, *Fault Detection and Diagnosis in Industrial Systems*. Springer Verlag, 2001.

[19] C. Commault, J.-M. Dion, O. Sename, and R. Motyeian, "Observer-based fault detection and isolation for structured systems," *IEEE Transactions on Automatic Control*, vol. 47, no. 12, pp. 2074–2079, 2002.

[20] F. N. Chowdhury and J. L. Aravena, "A modular methodology for fast fault detection and classification in power systems," *IEEE Transactions on Control System Technology*, vol. 6, pp. 623–634, September 1998.

[21] M. Kezunovic, S. Luo, Z. Galijasevic, and D. Ristanovic, "Accurate fault location in transmission networks using modeling, simulation and limited field recorded data," PSERC Publication 02-44, Power System Engineering Research Center, November 2002.

[22] M. Kezunovic, S. Luo, and D. R. Sevcik, "A novel method for transmission network fault location using genetic algorithms and sparse field recordings," *IEEE Power Engineering Society Summer Meeting*, pp. 1101–1106, July 2002.

[23] A. Semlyen, "Analysis of disturbance propagation in power systems based on a homogeneous dynamic model," *IEEE Transactions on Power Apparatus and Systems*, vol. 93, no. 2, pp. 676–684, 1974.

[24] R. L. Cresap and J. F. Hauer, "Emergence of a new swing mode in the western power system," *IEEE Transactions on Power Apparatus and Systems*, vol. 100, no. 4, pp. 2037–2045, 1981.

[25] J. S. Thorp, C. E. Seyler, and A. G. Phadke, "Electromechanical wave propagation in large electric power systems," *IEEE Transactions on Circuits and Systems-I: Fundamental Theory and Applications*, vol. 45, pp. 614–622, June 1998.

[26] B. C. Lesieutre, E. Scholtz, and G. C. Verghese, "A zero-reflection controller for electromechanical disturbances in power networks," *Power System Computation Conference, Seville Spain*, June 2002.

[27] P. Kundur, *Power System Stability and Control*. EPRI Power System Engineering Series, McGraw-Hill, 1994.

[28] P. Anderson and A. Fouad, *Power System Control and Stability*. IEEE Press Power System Engineering Series, IEEE New York: IEEE Press, 1994.

[29] A. Bergen, *Power systems analysis*. Englewood Cliffs, N.J. : Prentice-Hall, 1986.

[30] E. W. Kimbark, *Power System Stability: Elements of Stability Calculations*, vol. 1. NY, NY: IEEE Press, 1995.

[31] M. Ilić and J. Zaborsky, *Dynamics and Control of Large Electric Power Systems*. John Wiley and Sons, 2000.

[32] P. W. Sauer and M. A. Pai, *Power System Dynamics and Stability*. Prentice Hall Inc., 1998.

[33] P. C. Muller, "Descriptor systems: Analysis and control design," *SACTA*, vol. 3, no. 3, pp. 181–195, 2000.

[34] B. Ayazifar, *Graph Spectra and Modal Dynamics of Oscillatory Networks*. PhD thesis, Massachusetts Institute of Technology, 2002.

[35] G. C. Verghese, B. C. Lévy, and T. Kailath, "A generalized state-space for singular systems," *IEEE Transactions on Automatic Control*, vol. 26, pp. 811–831, August 1981.

[36] L. Dai, *Singular Control Systems*. Lecture Notes in Control and Information Sciences, Springer-Verlag, 1989.

[37] D. L. Chu and V. Mehrmann, "Disturbance decoupled observer design for descriptor systems," *Systems and Control Letters*, vol. 38, pp. 37–48, September 1999.

[38] J.-M. Dion, C. Commault, and J. van der Woude, "Generic properties and control of linear structured systems: a survey," *Automatica*, vol. 39, p. 1125 1144, 2003.

[39] E. A. Misawa, *Nonlinear State Estimation Using Sliding Observers*. PhD thesis, Department of Mechanical Engineering, Massachusetts Institute of Technology, 1988.

[40] R. Rajamani, "Observers for lipschitz nonlinear systems," *IEEE Transactions on Automatic Control*, vol. 43, no. 3, pp. 397–401, 1998.

[41] A. Megrteski, "6.243j: Dynamics of nonlinear systems." 2003.

[42] A. Packard and M. Kantner, "Gain scheduling the lpv way," in *Proceedings of the 35th Conference on Decision and Control, Kobe, Japan*, pp. 3938–3941, December 1996.

[43] J. Y. Ishihara and M. H. Terra, "Impulse controllability and observability of rectangular descriptor systems," *IEEE Transactions on Automatic Control*, vol. 46, pp. 991–994, June 2001.

[44] J. Y. Ishihara and M. H. Terra, "On the Lyapanov theorem for singular systems," *IEEE Transactions on Automatic Control*, vol. 47, pp. 1926–1930, November 2002.

[45] M. Arcak and P. Kokotović, "Nonlinear observers: A circle criterion design and robustness analysis," *Automatica*, vol. 37, pp. 1923–1930, 2001.

[46] M. Arcak and P. Kokotović, "Observer-based control of systems with slope-restricted nonlinearities," *IEEE Transactions on Automatic Control*, vol. 46, pp. 1–5, 2001.

[47] M. Arcak and P. Kokotović, "Feasibility conditions for circle criterion designs," *Systems and Control Letters*, vol. 42, pp. 405–412, 2001.

[48] M. Hou and P. C. Muller, "Observer design for descriptor systems," *IEEE Transactions on Automatic Control*, vol. 44, no. 1, pp. 164–168, 1999.

[49] D. N. Shields, "Observer design and detection for nonlinear descriptor systems," *International Journal of Control*, vol. 67, no. 2, pp. 153–168, 1997.

[50] S. Xu, J. Lam, and Y. Zou, "H_∞ filtering for singular systems," *IEEE Transactions on Automatic Control*, vol. 48, no. 12, pp. 2217–2222, 2003.

[51] G. R. Duan, D. Howe, and R. J. Patton, "Robust fault detection in descriptor linear systems via generalized unknown input observers," *International Journal of Systems Science*, vol. 33, no. 5, pp. 369–377, 2002.

[52] S. Xu and P. van Dooren, "Robust H_∞ filtering for a class of non-linear systems with state delay and parameter uncertainty," *International Journal of Control*, vol. 75, no. 10, pp. 766–774, 2002.

[53] R. S. Mangoubi, *Robust Estimation and Failure Detection: A Concise Treatment*. Springer, 1998.

[54] S. Boyd, L. E. Ghaoui, E. Feron, and V. Balakrishnan, *Linear Matrix Inequalities in System and Control Theory*. SIAM, 1994.

[55] C. Scherer and S. Weiland, "Linear matrix inequalities in control." Course Notes for the Dutch Institute of Systems and Controls (Delft University of Technology and Eindhoven University of Technology), October 2000.

[56] P. Gahinet, A. Nemirovski, A. J. Laub, and M. Chilali, *LMI toolbox*. Mathworks.

[57] K. J. Reinschke and G. Wiedemann, "Digraph characterization of structural controllability for linear descriptor systems," *Linear Algebra and its Applications*, vol. 266, no. 1, pp. 199–217, 1997.

[58] K. J. Reinschke, *Multivariable control :a graph-theoretic approach*. Springer Verlag, 1988.

[59] R. J. Patton and J. Chen, "On eigenstructure assignment for robust fault diagnosis," *International Journal of Robust and Nonlinear Control*, vol. 10, pp. 1193–1208, 2000.

[60] B. Lesieutre, E. Scholtz, and G. Verghese, "Impedance matching controllers to extinguish electromechanical waves in power networks," *IEEE Conference on Control Applications, Glasgow, Scotland*, September 2002.

[61] O. Samuelsson, *Power System Damping — Structural Aspects of Controlling Active Power*. PhD thesis, Department of Industrial Electrical Engineering and Automation, Lund University, 1997.

[62] O. Samuelsson, "Load modulation at two locations for damping of electro-mechanical oscillations in a multimachine system," *Power Engineering Society Summer Meeting*, vol. 3, pp. 1912–1917, July 2000.

[63] H. Fujita, M. Goto, and Y. Kito, "Improvement of dynamic stability in a multimachine power system via smes with active power modulation controlled by frequency deviation," *Electrical Engineering in Japan*, vol. 115, no. 2, pp. 32–45, 1995.

[64] A. Preumont, *Vibration Control of Active Structures*. Kluwer Academic Publishers, 1997.

[65] S.-Y. Lee and J. C. D. Mote, "Traveling wave dynamics in a translating string coupled to stationary constraints: Energy transfer and mode localization," *Journal of Sound and Vibration*, vol. 212, no. 1, pp. 1–22, 1998.

[66] E. Scholtz, B. C. Lesieutre, and G. C. Verghese, "Decentralized controllers for electromechanical waves in power networks," *North American Power Symposium – Idaho*, August 2004.

[67] C. L. DeMarco and J. Wassner, "A generalized eigenvalue perturbation approach to coherency," *Proceedings of the 4th IEEE Conference on Control Applications*, pp. 611–617, 1995.

[68] S. Xu, P. van Dooren, R. Stefan, and J. Lam, "Robust stability and stabilization for singular systems with state delay and parameter uncertainty," *IEEE Transactions on Automatic Control*, vol. 47, no. 7, pp. 1122–1128, 2002.